Effects of Sensorimotor Perturbations on Balance Performance and Electrocortical Dynamics

By

Steven M. Peterson

A dissertation submitted in partial fulfillment
of the requirements for the degree of
Doctor of Philosophy
(Biomedical Engineering)
in the University of Michigan
2018

Doctoral Committee:

Associate Professor Cynthia Chestek, Co-Chair
Professor Daniel P. Ferris, University of Florida, Co-Chair
Assistant Professor Sean Meehan, University of Waterloo
Associate Professor William Stacey

Steven M. Peterson
stepeter@umich.edu
ORCID iD: 0000-0003-0782-5788

Acknowledgments

The research for this dissertation was sponsored by a graduate research fellowship from the National Science Foundation (grant number: DGE 1256260) and by the Army Research Laboratory under Cooperative Agreement Number W911NF-10-2-0022 (Cognition and Neuroergonomics Collaborative Technology Alliance).

So much of this dissertation would not have been possible without the support and assistance of several other people. I would like to acknowledge the help of my ever-supportive partner, Alexandra. Thank you for always believing in me. I would also like to thank my entire committee, especially Dan for helping me become the scientist I am today. In addition, I would like to thank my friends and colleagues in the Human Neuromechanics Lab and in journal club as well as my family. Finally, I would like to acknowledge all of the subjects that gave their time to help these experiments happen.

Preface

Chapters 2-6 were written as separate manuscripts, so each can be read as a separate work.

Table of Contents

List of Tables

List of Figures

Abstract

Humans must frequently adapt their posture to prevent loss of balance. Such balance control requires complex, precisely-timed coordination among sensory input, neural processing, and motor output. Despite its importance, our current understanding of cortical involvement during balance control remains limited by traditional neuroimaging methods, which are stationary and have poor time resolution. High-density electroencephalography (EEG), combined with independent component analysis, has become a promising tool for recording cortical dynamics during balance perturbations due to its portability and high temporal resolution. Additionally, recent improvements in immersive virtual reality headsets may provide new rehabilitative paradigms, but the effects of virtual reality on balance and cortical function remain poorly understood. In my first study, I recorded high-density EEG from healthy, young adult subjects as they walked along a beam with and without virtual reality high heights exposure. While virtual high heights did induce stress, the use of virtual reality during the task increased performance errors and EEG measures of cognitive loading compared to real-world viewing without a headset. In my second study, I collected high-density EEG from healthy young adults as they walked along a treadmill-mounted balance beam to determine the effect of a transient visual perturbation on training in virtual reality. Subjects in the perturbations group improved comparably to those that trained without virtual reality, indicating that the perturbation helped subjects overcome the negative effects of virtual reality on motor learning. The perturbation primarily elicited a cognitive change. In my third study, healthy, young adult EEG was recorded during physical pull and visual rotation perturbations to tandem walking and tandem standing. I

found similar electrocortical patterns for both perturbation types, but different cortical areas were involved for each. In my fourth study, I used a phantom head to validate EEG connectivity methods based on Granger causality in a real-world environment. In general, connectivity measures could determine the underlying connections, but many were susceptible to high-frequency false positives. Using data from my third study, my fifth study analyzed corticomuscular connectivity patterns following sensorimotor balance perturbations. I found strong occipito-parietal connections regardless of perturbation type, along with evidence of direct muscular control from the supplementary motor area during the standing perturbation response. Taken together, the work presented in this dissertation greatly expands upon the current knowledge of cortical processing during sensorimotor balance perturbations and the effect of such perturbations on short-term motor learning, providing multiple avenues for future exploration.

Chapter 1: Introduction

Real-world Neuroimaging using EEG

In everyday life, humans must constantly adjust their posture to avoid losing their balance. These adjustments necessitate precisely-timed coordination among sensory input, neural processing, and motor control (Macpherson & Horak, 2012). Dual-tasking research has demonstrated the importance of human supraspinal centers for maintaining balance during both walking and standing (Rankin, Woollacott, Shumway-Cook, & Brown, 2000; Woollacott & Shumway-Cook, 2002). Despite the importance of such supraspinal areas, the current understanding of real-world human cortical activity in response to balance perturbations remains limited (Varghese, McIlroy, & Barnett-Cowan, Perturbation-evoked potentials: Significance and application in balance control research, 2017). Traditional neuroimaging techniques, such as functional magnetic resonance imaging (fMRI) and functional near-infrared spectroscopy (fNIRS), are restricted by low temporal resolution and stationary recordings.

High-density EEG has become a promising method for noninvasively assessing cortical activity in mobile settings such as balance control. This is primarily due to its portability and high temporal resolution (Gramann, Ferris, Gwin, & Makeig, 2014; Gramann, et al., 2011). High temporal resolution is useful for capturing the quick cortical responses during perturbed balance. EEG has traditionally been confined by artifact contamination and low spatial resolution (Urigüen & Garcia-Zapirain, 2015). However, blind-source separation using independent component analysis, which finds sources with minimal statistical independence, can be used to

separate out cortical activity from artifacts, minimizing artifact contamination while boosting spatial resolution (Gwin, Gramann, Makeig, & Ferris, 2010; Makeig, Bell, Jung, & Sejnowski, 1996). In addition, the sources from independent component analysis can be used to make inferences about specific cortical areas as opposed to choosing specific electrodes which will be influenced by volume conduction from the head (Brunner, Billinger, Seeber, Mullen, & Makeig, 2016).

Virtual Reality Training

Virtual reality has become a popular training tool because it can expose users to unique sensory environments and training scenarios (Adamovich, Fluet, Tunik, & Merians, 2009). Virtual reality can immerse a user in a virtual world (Sanchez-Vives & Slater, 2005) and has been used in clinical scenarios such as reducing the sensation of pain for patients with burn injuries (Hoffman, et al., 2008; Hoffman, et al., 2014). Virtual reality can also improve gait speed and stability (Darekar, McFadyen, Lamontagne, & Fung, 2015; Mirelman, et al., 2011), and it is frequently used for rehabilitation of mobility and balance control (Darekar, McFadyen, Lamontagne, & Fung, 2015; Booth, Masud, Connell, & Bath-Hextall, 2013; Corbetta, Imeri, & Gatti, 2015; Palacios-Navarro, Albiol-Pérez, & García-Magariño García, 2016). However, many of these studies display virtual environments on a screen, which does not move with the user and allows the user to look away. Recent commercially available virtual reality head-mounted displays may provide more effective immersion, leading to new virtual experiences.

Despite the potential of such immersive experiences, studies have found that virtual reality head-mounted displays worsen gait performance and balance control compared to real-world viewing (Epure, et al., 2014; Robert, Ballaz, & Lemay, 2016). Of the studies that used fully immersive virtual reality head-mounted displays and measured gait stability, all reported worsened stability

when using a virtual reality head-mounted display (Epure, et al., 2014; Robert, Ballaz, & Lemay, 2016; Lott, Bisson, Lajoie, McComas, & Sveistrup, 2003; Kelly, Riecke, Loomis, & Beall, 2008; Kawamura & Kijima, 2016; Soffel, Zank, & Kunz, 2016; Calogiuri, et al., 2017). We did not find any study reporting that training with virtual reality head-mounted displays was as good as or better than real-world training. There is a need to overcome the negative effects of immersive virtual reality on balance training in order to provide novel experiences equivalent with real world training.

Sensory Perturbations

One way to potentially boost balance training is by perturbing the sensory information needed during balance control. This idea relies on the specificity of learning hypothesis, which states that humans performing a task only utilize the optimal sources of information. These optimal sources of information can shift during a task when useful sensory information becomes impaired (Assländer & Peterka, 2014). Such shifts can be induced by altering vision, either by prism goggles (Fortis, Goedert, & Barrett, 2011; Martin, Keating, Goodkin, Bastian, & Thach, 1996) or in virtual reality (Wright, 2014; Chiarovano, et al., 2015), but the effects are usually temporary. In contrast, repeated exposure to sensory perturbations can lead to improvements in motor performance (Luu, et al., 2017a). In a similar manner, repeated visual perturbations during balance may boost short-term motor learning.

In addition to enhancing balance training, sensory perturbations can also yield insight into cortical sensorimotor integration during balance control. In particular, visual manipulations can have substantially affect EEG dynamics and balance performance because of conflict among visual, vestibular, and proprioceptive sensory systems. Understanding the role of vision during balance control is important because over-reliance on vision can lead to falls in older adults

(Franz J. R., Francis, Allen, O'Connor, & Thelen, 2015). Blindfolded walking in healthy adults can alter electrocortical dynamics in somatosensory areas, which are involved in sensorimotor integration (Oliveira, Schlink, Hairston, König, & Ferris, 2017a). Similarly, rotating prism goggles worsen mediolateral stability because of unreliable visual input (Cauquil, Bessou, Dupui, & Bessou, 1998). Sensory perturbations may also be advantageous for EEG experiments because they do not induce consistent motion artifact tied to the event of interest, which occurs during walking (Kline, Huang, Snyder, & Ferris, 2015).

Connectivity

Along with individual analysis of cortical areas, effective connectivity analysis investigates how these cortical areas interact with each other. Connectivity analysis has been used to characterize cortical networks during different tasks (Lau, Gwin, & Ferris, 2014) and to identify potential cortical impairments (Xu, et al., 2014). Multiple cortical areas appear active during balance control (Sipp, Gwin, Makeig, & Ferris, 2013; Slobounov, Cao, Jaiswal, & Newell, 2009), making such an analysis relevant. However, many different measures can be used for connectivity estimation, with no real-world validation on ground-truth signals of how well these measures perform when exposed to volume conduction and head motion (Blinowska, 2011). Many connectivity measures are based on Granger causality, which assumes that one channel (Channel A) causes activity in another channel (Channel B) if A provides past information that helps with predicting B (Granger, 1969). This principle has been extended to multichannel data with multivariate autoregressive models, which fit the EEG data by predicting the next value in time using a linear combination of past values (Harrison, Penny, & Friston, 2003). Connectivity estimation can be performed on either channel data or independent components, but component data can be less susceptible to motion artifact and volume conduction (Brunner, Billinger,

Seeber, Mullen, & Makeig, 2016; Snyder, Kline, Huang, & Ferris, 2015). Despite the advantages of performing connectivity estimation on independent components, combining multi-subject results into group-level connectivity estimation remains an open problem when using independent components. This is because independent component analysis is primarily data-driven. While this is usually advantageous, it becomes a liability for connectivity analysis because the locations of independent components vary across subjects, making it challenging to combine them into a group-level result. There is a need to accurately perform group-level connectivity analyses, ideally by balancing group-level and subject-specific information.

Dissertation Contributions

The goals of this dissertation are to quantify the electrocortical effects of sensory perturbations during balance and to determine if such perturbations can improve balance learning during immersive virtual reality headset use. In chapter 2, I investigated the immersive effects of virtual reality high heights exposure during overground beam-walking on healthy young adults, as measured by heart rate variability, electrodermal activity, reaction time, and electrocortical dynamics. My results highlighted the negative behavioral and cortical effects of virtual reality. In chapter 3, I analyzed the effect of brief field-of-view rotations in virtual reality on healthy young adults as they learned a balance beam walking task. I used the number of step-offs per minutes on the beam to measure performance, demonstrating that the negative effects of immersive virtual reality use can be minimized. EEG activity was recorded to determine the cortical effects caused by perturbations training. In chapter 4, I quantified the similarities and differences between different sensorimotor perturbations to balance while healthy young adults performed tandem walking and tandem standing. I recorded EEG, lower leg electromyography (EMG), and motion capture. In chapter 5, I used a phantom head embedded with known signals to validate

multiple EEG connectivity estimators under real-world volume conduction and head motion conditions. In chapter 6, I developed a novel group-level technique to quantify differences in effective connectivity due to sensorimotor perturbations. I recorded EEG and EMG, finding evidence of corticomuscular connectivity during the perturbation response. This dissertation increases our understanding of cortical dynamics during perturbed sensorimotor input and how such perturbations can be leveraged to enhance motor learning.

Chapter 2: Effects of Virtual Reality High Heights Exposure during Beam-walking on Physiological Stress and Cognitive Loading[1]

Abstract

Virtual reality has been increasingly used in research on balance rehabilitation because it provides robust and novel sensory experiences in controlled environments. We studied 19 healthy young subjects performing a balance beam walking task in two virtual reality conditions and with unaltered view (15 minutes each) to determine if virtual reality high heights exposure induced stress. We recorded number of steps off the beam, heart rate, electrodermal activity, response time to an auditory cue, and high-density electroencephalography (EEG). We hypothesized that virtual high heights exposure would increase measures of physiological stress compared to unaltered viewing at low heights. We found that the virtual high height condition increased heart rate variability and heart rate frequency power relative to virtual low heights. Virtual reality use resulted in increased number of step-offs, heart rate, electrodermal activity, and response time compared to the unaltered viewing at low heights condition. Our results indicated that virtual reality decreased dynamic balance performance and increased physical and cognitive loading compared to unaltered viewing at low heights. In virtual reality, we found significant decreases in source-localized EEG peak amplitude relative to unaltered viewing in the anterior cingulate, which is considered important in sensing loss of balance. Our findings indicate that virtual reality provides realistic experiences that can induce physiological stress in

[1] This chapter has been previously published in *PLoS One* (Peterson, Furuichi, & Ferris, 2018).

humans during dynamic balance tasks, but virtual reality use impairs physical and cognitive performance during balance.

Introduction

Humans regularly perform activities of daily living and tasks of mobility that require maintenance of dynamic balance. With human aging, balance control can deteriorate (Kanekar & Aruin, 2014), leading to falls and other serious consequences (Sterling, O'Connor, & Bonadies, 2001). In addition, falls can induce a fear of falling again, potentially leading to a loss of independence (Lach, 2005).

Balance training often reduces the risk of falling (Carter, Kannus, & Khan, 2001; Kannus, Sievänen, Palvanen, Järvinen, & Parkkari, 2005), even more than basic walking tasks (Sherrington, et al., 2008). Balance training equipment varies widely from wobble boards (Ogaya, Ikezoe, Soda, & Ichihashi, 2011) to complex balance systems (Ibrahim, Mattar, & Elhafez, 2016). Because integrating balance training into everyday activities reduces falls (Clemson, et al., 2012), virtual reality has been used to motivate users to perform challenging balance tasks in realistic scenarios (Duque, et al., 2013; Kalron, Fonkatz, Frid, Baransi, & Achiron, 2016). Dynamic training in virtual reality has improved walking speed for Parkinson's patients (Mirelman, et al., 2011) and walking stability for stroke patients (Darekar, McFadyen, Lamontagne, & Fung, 2015). However, many studies project virtual environments onto a screen, which does not move with the user and allows the user to look away (Booth, Masud, Connell, & Bath-Hextall, 2013; Corbetta, Imeri, & Gatti, 2015). Virtual reality presented using a head-mounted display may provide more effective immersion.

To test the realism of a head-mounted display virtual environment during dynamic balance, we exposed subjects to high heights in virtual reality while walking on a balance beam. High heights anxiety is both prevalent (Huppert, Grill, & Brandt, 2013) and measurably affects dynamic and static stability (Carpenter, Frank, & Silcher, 1999; Schniepp, et al., 2014). Human physiological stress levels increase at higher heights and do not noticeably differ across age groups (Brown, Polych, & Doan, 2006). Immersive virtual reality can provide a cognitive sense of presence where the user feels that they are in a real environment (Sanchez-Vives & Slater, 2005; Gonzalez-Franco & Lanier, 2017). Virtual reality heights exposure is comparable to real-world heights exposure (Emmelkamp, Bruynzeel, Drost, & van der Mast, 2001), with virtual high heights increasing measures of fear and altering standing posture dynamics (Seinfeld, et al., 2015; Cleworth, Horslen, & Carpenter, 2012). In addition, presence during virtual heights exposure can be enhanced by having subjects stand with their feet on a ledge raised only a few centimeters off the ground (Meehan, Insko, Whitton, & Brooks, 2002). Given these results, virtual high heights should alter stress levels during a dynamic locomotor task.

Despite advances in physiological recording methods, stress remains challenging to quantify. Cortisol level is considered one of the best standards for stress detection because cortisol is generated by the hypothalamus-pituitary-adrenal axis directly in response to stress, but measuring cortisol from blood or urine is invasive. Salivary cortisol, while non-invasive, has less fine time resolution than blood cortisol, creating a time lag between stress and cortisol levels (Hellhammer, Wüst, & Kudielka, 2009). Heart rate variability is affected by both parasympathetic and sympathetic activity, which vary based on stress levels (Thayer, Ahs, Fredrikson, Sollers, & Wager, 2012). It has been generally thought that stress induces less heart rate variability (Boesch, et al., 2014; Clays, et al., 2011), but results are conflicting and likely

depend on the paradigm and stressor used (Schlink, et al., 2017). Electrodermal activity may also indicate stress, as it is affected by sympathetic activity (Critchley, 2002). Electrodermal activity contains a tonic (slow) and phasic (fast) component (Lim, et al., 1997), with increased phasic activity relating to increases in stress (Reinhardt, Schmahl, Wüst, & Bohus, 2012; Giromini, et al., 2016). Other ways to quantify stress include cognitive task performance (Munoz, Sliwinski, Scott, & Hofer, 2015) and EEG activity (Schlink, et al., 2017). Our primary outcome measures of stress were electrodermal activity and heart rate variability because of their direct connections to sympathetic and parasympathetic responses and the ease of recording them during a dynamic balance task.

In addition to stress, we wanted to quantify the physical and cognitive effects of virtual reality use. A head-mounted display moves with the user, which may be advantageous for dynamic balance training compared to screen displays, but immersive virtual reality may induce motion sickness. Motion sickness varies greatly across people and virtual reality setups (Kolasinski, 1995), so it is important to limit and quantify its effects. To estimate cognitive loading, we measured response time to an auditory stimulus (Regenbogen, et al., 2012; Sabri, et al., 2014). We also wanted to know where a potential change in cognitive load was occurring in the brain. For this, we used EEG source localization, which has revealed areas of the brain involved during balance beam walking (Sipp, Gwin, Makeig, & Ferris, 2013). This added complexity helped us determine which cognitive centers were most affected by virtual reality use during beam-walking. EEG has been used before to measure cognitive response to stimuli in virtual reality (González-Franco, Peck, Rodríguez-Fornells, & Slater, 2014).

The purpose of this study was to determine if high height exposure in virtual reality induced stress and if virtual reality use affected physical and cognitive performance during a dynamic

balance-beam walking task. Our hypotheses were: 1) subjects' stress would increase at a high virtual height compared to a low virtual height, as measured by increases in heart rate variability and electrodermal activity, and 2) virtual reality use during beam-walking would increase cognitive load compared to no virtual reality use during the task, as measured by increased response time to an auditory stimulus and decreases in EEG event-related activity peak amplitude. We included a virtual reality low height condition, which matched the beam height of the unaltered view low height condition, for this second comparison. We found that high virtual heights induced stress, and virtual reality use at low heights increased cognitive loading compared to beam-walking without the headset, confirming both hypotheses.

Materials and Methods

Subjects

Nineteen healthy subjects participated in the study (10 male, age 23±4 years old (mean±SD)). All subjects identified themselves as right hand and right foot dominant. Subjects were screened for any orthopedic, cardiac, or neurological conditions and injuries. Any subjects indicating they experienced acrophobia (fear of heights) were excluded from the study because we wanted all subjects to be able to complete the full experiment. All subjects gave written informed consent. The protocol was approved by the University of Michigan Institutional Review Board for the protection of human subjects.

Prior to the main experiment session, we screened subjects for motion sickness in virtual reality. Subjects stood in place while wearing the headset (Oculus Rift DK2, Oculus VR, Irvine, CA) for 5 minutes. Subjects moved around a virtual environment using body gestures tracked by a Microsoft Kinect V2 (Microsoft, Redmond, WA). We intentionally included this disconnect

between real and virtual movements to be more disorienting than the experiment. Subjects were allowed to participate in the main experiment if both the experimenter and subject agreed that the subject did not exhibit any symptoms of motion sickness. Two subjects exhibited symptoms of motion sickness and did not perform the experiment; 19 subjects passed this screening process.

Experiment Setup

We tested subjects on a 3.8 cm-wide by 2.5 cm-tall by 3.05 meter-long wooden balance beam, similar to previous studies (Domingo & Ferris, 2009; Domingo & Ferris, 2010). We attached the beam to a non-skid surface to prevent it from slipping. Subjects walked the entire length of the beam in one direction, referred to as a beam pass. After completing a beam pass, subjects walked over-ground back to their starting position. Subjects walked heel-to-toe with their arms crossed over their chest. We did not make subjects follow a specific gait speed to avoid any effects from attending to this speed. We demonstrated a desired pacing of 0.22 m/s and informed the subject if he or she was walking too fast or too slow. We chose this speed based on previous beam-walking experiments (Sipp, Gwin, Makeig, & Ferris, 2013; Domingo & Ferris, 2009). We also instructed subjects to look at their feet while balancing in all 3 conditions.

Subjects performed the same physical beam-walking task under 3 viewing conditions: unaltered view low, virtual reality low, and virtual reality high. Unaltered view low involved normal viewing without virtual reality. For virtual reality low and virtual reality high, subjects wore the Oculus virtual reality headset. Subjects viewed themselves 2.5 cm off the ground in virtual reality low, which agreed with the real-world balance-beam height, and 15 meters off the ground in virtual reality high (Figure 2-1). To enhance the effects in the virtual reality high condition, subjects “fell” 15 meters in the virtual environment when they stepped off the beam. Both virtual reality conditions contained a virtual beam that was aligned with the physical beam. In all 3

conditions, subjects performed the same balance task on the physical beam. Subjects took 10 minute breaks between each condition. We randomized the order of the virtual reality conditions, but all subjects performed the unaltered view low condition second to spread out virtual reality use during the experimental session.

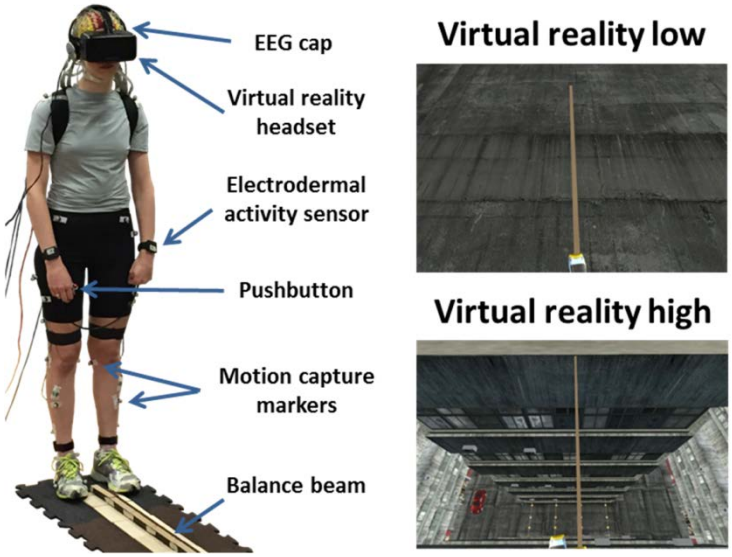

Figure 2-1: Subject setup and virtual reality views. Typical subject setup is shown (left). All subjects walked on the same physical beam for all three conditions. In both virtual reality conditions, subjects saw a virtual beam that aligned with the physical beam. In virtual reality low, the virtual beam was the same height off the ground as in unaltered view low (top right), while the virtual beam was 15 meters off the ground in virtual reality high (bottom right).

The virtual environment was rendered using Unity 5 software (Unity Technologies, San Francisco, CA) and included a virtual avatar controlled by the Microsoft Kinect. This computer used a NVIDIA Titan X graphics card (NVIDIA, Santa Clara, CA) to avoid slow-downs in the virtual reality presentation. Because humans more reliably perceive heights when they have a body in virtual reality (Gutekunst, et al., 2014), each subject had a virtual avatar. This avatar mimicked the subject's movements in the virtual environment, using the Kinect tracking with the 'Kinect v2 Examples with MS-SDK' Unity package. We did not have the Kinect control the

avatar's arms, hands, and toes because the Kinect could not reliably track them during the experiment. Because the Kinect can only reliably track a user that faces it, subjects made beam passes in one direction and walked over-ground in the other direction. Each condition ended after 15 minutes of forward beam passes. We choose a fixed time instead of a fixed number of passes so that subjects were not encouraged to walk faster.

Performance & Physiological Measures

While beam-walking, subjects wore several sensors to measure physiological and cognitive activity. To determine gait events, we placed 30 reflective motion capture markers placed on the feet and legs of each subject, sampled at 100 Hz (Vicon, Los Angeles, CA). A wearable device (Empatica E4) was placed on both wrists to record electrodermal activity (Empatica, Milan, Italy). We recorded from both wrists to average out any unreliable activity (Picard, Fedor, & Ayzenberg, 2015). Figure 2-1 shows a representative subject during testing. Subjects also completed surveys after the experiment ended to assess motion sickness in virtual reality (Motion Sickness Assessment Questionnaire (Gianaros, Muth, Mordkoff, Levine, & Stern, 2001)) and high heights apprehension (Heights Interpretation Questionnaire (Steinman & Teachman, 2011)).

We analyzed beam-walking performance using motion capture markers at each foot. Marker traces were cleaned in Vicon Nexus and further processed in Visual3D (C-Motion, Germantown, MD). We implemented a similar algorithm as Zeni et al. to find gait events and manually inspected each trial to ensure accuracy (Zeni, Richards, & Higginson, 2008). We quantified balance performance by determining the number of times balance was lost divided by the total time spent on the beam. This metric is known as failures per minute and has previously assessed beam-walking performance (Domingo & Ferris, 2009; Domingo & Ferris, 2010). By including

the total time spent on the beam, faster walkers are not rewarded more than slower walkers for making fewer mistakes. In addition, we recorded the number of beam passes for each condition. We also estimated beam-walking speed by calculating the time subjects were on the beam and using the total number of passes as an estimate of distance.

We recorded heart rate via an electrode taped over the sternum. We reduced line noise using the Cleanline EEGLAB plugin and bandpass filtered between 5 and 20 Hz. Kubios HRV software found the R-peaks, which correspond to heartbeats (Tarvainen, Niskanen, Lipponen, Ranta-Aho, & Karjalainen, 2014). We manually adjusted incorrectly labelled peaks. We determined heart rate variability as the standard deviation of the heart rate time series. We calculated heart rate frequency power by taking the fast Fourier transform power spectrum of the inter-beat intervals and determining the percent of total power not in the 0.04-0.15 Hz range. Kubios calculated all heart rate and heart rate variability metrics based on guidelines in the field (Malik, 1996).

Electrodermal activity data was processed using Ledalab (Benedek & Kaernbach, 2010a; Benedek & Kaernbach, 2010b), which uses deconvolution to separate the tonic and phasic components of the signal. We ran deconvolution with the default parameters. Electrodermal activity responses were calculated as differences in the deconvoluted phasic signal greater than 0.05μS (Schmidt & Walach, 2000). We averaged responses across each condition and normalized by condition duration in minutes.

While beam-walking, subjects were instructed to listen for an auditory tone and press a pushbutton upon hearing the tone. We designed this secondary task to be simple because balance performance may worsen if it is too challenging (Howell, Osternig, & Chou, 2016; Woollacott & Shumway-Cook, 2002). Tones were spaced randomly 7-9 seconds apart, consistent with previous

research (Lawrence & Barry, 2010). We recorded the time subjects took to respond to the tone as an estimator of cognitive load during the beam-walking task. Increased cognitive load during beam-walking would be accompanied by decreased attention to the auditory tone task, resulting in increased response times.

Auxiliary Experiment

To determine if any differences found in our measures were caused by simply wearing the headset, we performed an auxiliary experiment on 20 subjects (10 male, age 24±5 years old (mean±SD)). Four subjects participated in both the main and auxiliary experiments, but on separate days. All subjects gave written informed consent, and the protocol was approved by the University of Michigan Institutional Review Board for the protection of human subjects. Subjects performed 4 randomized 5-minute blocks of sitting and standing, both with and without the headset. Subjects were asked to stand and sit up straight while staring at a fixation cross displayed at eye level. We recorded the same electrodermal activity, response time, and heart rate metrics as the main experiment.

Fatigue Assessment

Because we were concerned about fatigue, we quantified changes in failures per minute, heart rate, and response time during each condition. We chose these measures because they estimate motor performance, physical exertion, and cognitive loading, each of which can be affected by fatigue. We calculated percent change as the difference between the last and first 3 minutes of each condition, all divided by the first 3 minutes and converted to a percent. We divided the difference by the first 3 minutes because we wanted to see how each measure changed relative to its initial value during the first 3 minutes. If fatigue was present, we would expect to see a large percent change from the first 3 minutes to the last 3 minutes.

EEG Data

In addition to response time, we recorded EEG to determine if specific brain areas showed increases in cognitive load during beam-walking. By comparing peak EEG activity following the tone, we can determine changes in electrocortical activity across conditions. Because an increase in cognitive loading during the main task likely results in less focus on the secondary task, we would expect a corresponding decrease in event-related peak amplitude (Gentili, et al., 2014; Neelon, Williams, & Garell, 2006). We performed independent components analysis (ICA) to find brain source activity from the channel data (Makeig, Bell, Jung, & Sejnowski, 1996). We used ICA because event-related potentials show distinct activity from compact sources in the brain (Makeig S. , 2002). Unlike response time, EEG with source localization provides insight into cognitive loading differences in specific brain areas. We recorded EEG using a 136-channel BioSemi Active II system (BioSemi, Amsterdam, NL), sampled at 512 Hz. The EEG AD-box and battery were placed in a backpack worn by the subject (Kline, Poggensee, & Ferris, 2014).

EEG data was processed using custom scripts in EEGLAB (Delorme & Makeig, 2004). We high-pass filtered the data at 1 Hz and removed noisy channels (Kline, Huang, Snyder, & Ferris, 2015; Oliveira, Schlink, Hairston, König, & Ferris, 2017a). We removed 12±8 bad channels (mean±SD) and interpolated them to maintain a consistent montage across the head. We ran AMICA 15 on the data (Palmer, Kreutz-Delgado, & Makeig, 2006; Palmer, Makeig, Kreutz-Delgado, & Rao, 2008), using principal component analysis to reduce down to 100 principal components prior to ICA. This was less than the minimum number of channels remaining following bad channel removal (102 channels), ensuring that the data sent into ICA remained full rank.

After obtaining independent components, we fit the ICA scalp maps to equivalent current dipoles using DIPFIT2 (Oostenveld & Oostendorp, 2002). Independent components with residual variance <15% were retained for further analysis. We manually rejected independent components with non-brain activity, using power spectra and dipole location. We manually rejected 17±4 dipoles and retained 7±3 (mean±SD) cortical dipoles per subject. Brain dipoles were grouped using k-means clustering, using weights of 10, 2, and 1 for dipole location, power spectra, and scalp maps, respectively.

We grouped the 178 total dipoles into 11 clusters. We retained 8 clusters containing dipoles from more than half (>9) the total subjects (Figure 2-2): anterior parietal (12 subjects, 17 dipoles), left sensorimotor (11 subjects, 17 dipoles), right frontal (11 subjects, 14 dipoles), anterior cingulate (15 subjects, 27 dipoles), medial occipital (11 subjects, 13 dipoles), supplementary motor area (14 subjects, 21 dipoles), left posterior parietal (12 subjects, 13 dipoles), and right sensorimotor (13 subjects, 16 dipoles). We epoched the data from -300 to 800 ms around the auditory tone presentation, subtracted average activity across each epoch, and rejected epochs with amplitude outside ±75 μV to remove excessive artifact. We removed 1±1 trials for unaltered view low and 2±3 for virtual reality low, resulting in 102±4 trials for unaltered view low and 102±10 trials for virtual reality low (mean±SD). We only analyzed auditory events occurring while subjects were on the beam. We then calculated event-related potential activity time-locked to the auditory stimulus onset for each cluster. Auditory tone onset was set at time 0. We subtracted out 300 ms of average activity preceding the stimulus as baseline activity.

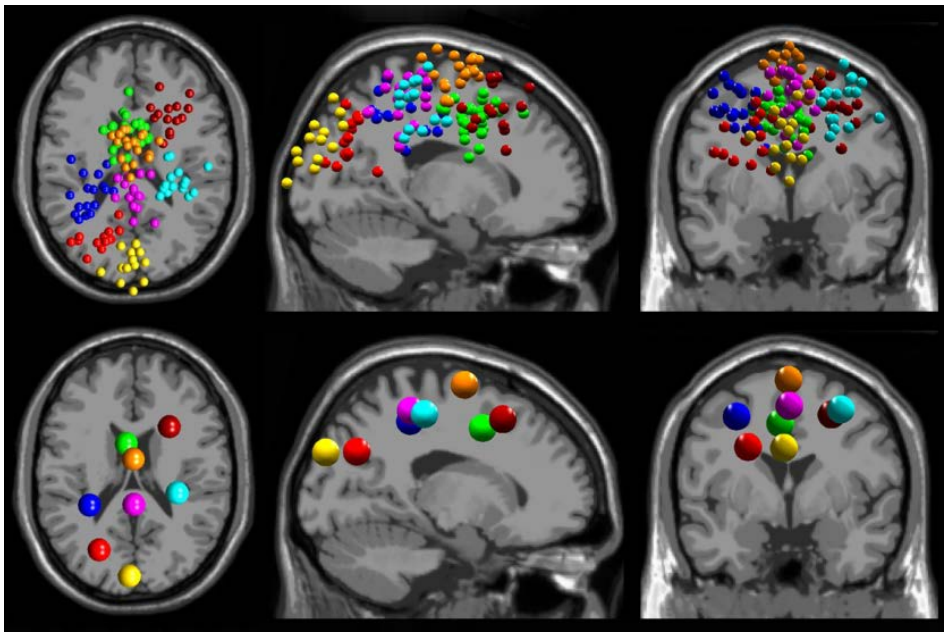

Figure 2-2: EEG source localization results. EEG source localization results are shown for the 8 cortical clusters found across all subjects (n=19). Dipole locations (top) and cluster centroids (bottom) are shown in transverse, sagittal, and coronal views (left to right). We found clusters in anterior parietal (purple), left sensorimotor (blue), right frontal (maroon), anterior cingulate (green), medial occipital (yellow), supplementary motor area (orange), left posterior parietal (red), and right sensorimotor (cyan).

Statistical Analyses

For main experiment mean physiological and behavioral data, we used non-parametric Friedman and Wilcoxon signed-rank tests due to non-normal data. We were not interested in comparing unaltered view low and virtual reality high due to difficulty interpreting any differences between these two conditions. We used Bonferroni correction for multiple comparisons, except for electrodermal activity, failures per minute, heart rate, and response time because these were planned, a priori comparisons. For the auxiliary experiment and fatigue comparison of percent change, differences across conditions were determined using non-parametric Friedman and post-hoc Wilcoxon signed-rank tests with Bonferroni correction for multiple comparisons. Non-EEG statistical analyses were performed using SPSS Statistics 22 (IBM SPSS Statistics 22.0, Armonk,

NY, United States). For EEG event-related activity, we used EEGLAB permutation statistics with 8000 permutations to calculate pairwise comparisons and false discovery rate to correct for multiple comparisons (Luck, 2014). Significance was determined to be less than 0.05 for all statistical tests.

Results

Survey Results

Subjects did not experience substantial motion sickness from participating in the study. Results from the motion sickness survey are shown in Table 2-1, using a normalized percentage scale (0-100%). 0% suggests motion sickness was completely absent during testing, while 100% indicates motion sickness was fully present across all subjects. Questions are also grouped into subsections referencing different factors of motion sickness. All subsection scores were less than 25% across subjects, with a score of 5.8% for feeling nauseous. We were primarily concerned with adverse effects from nausea and dizziness, but subjects reported minimal effects from these areas. Also, subjects scored 15.1%±14.9% (mean±SD) on the Heights Interpretation Questionnaire, with 0% indicating no high heights apprehension.

Table 2-1: Motion Sickness Assessment Results

Feeling nauseous	5.8% (7.5%)
Feeling dizzy	12.0% (9.8%)
Feeling sweaty	21.3% (22.0%)
Feeling tired	20.2% (14.9%)
Total	14.2% (10.3%)

Mean motion sickness assessment scores are shown normalized from 0-100%, with standard deviation in parentheses (n=19). The motion sickness assessment contains four subsections to analyze four factors of motion sickness: gastrointestinal (feeling nauseous), central (feeling dizzy), peripheral (feeling sweaty), and sopite (feeling tired).

Physiological and Behavioral Measures

We found significant increases in heart rate variability and heart rate frequency power in virtual reality high compared to virtual reality low ($p=0.015$ and $p=0.006$, respectively), as shown in Table 2-2. Both heart rate variability and heart rate frequency power did not significantly differ between unaltered view low and virtual reality low ($p=1.0$ and $p=0.108$). Electrodermal activity did not significantly differ between virtual reality conditions ($p=0.738$), but did significantly increase in virtual reality low compared to unaltered view low ($p=0.009$).

Table 2-2: Behavioral and Physiological Measures

	Measure Value			P Value	
Measure	UVL	VRL	VRH	UVL|VRL	VRL|VRH
Heart Rate Variability (beats/min)	6.6 (1.5)	7.0 (1.6)	8.3 (2.4)	1.00	0.02*
Heart Rate Frequency Power (%)	45.6 (12.5)	51.8 (15.2)	58.9 (14.0)	0.11	<0.01*
Electrodermal Activity (counts/min)	8.2 (11.7)	15.1 (14.7)	13.7 (11.0)	<0.01*	0.74
Failures per Minute (counts/min)	7.1 (2.5)	26.1 (4.9)	24.8 (5.6)	<0.01*	1.00
Heart Rate (beats/min)	92.0 (7.9)	97.0 (8.7)	97.1 (10.6)	<0.01*	1.00
Response Time (s)	0.76 (0.25)	0.88 (0.25)	0.94 (0.27)	0.02*	0.10
Number of Beam Passes	43.0 (15.7)	26.6 (9.4)	24.7 (7.6)	<0.01*	0.38
Estimated Gait Speed (m/s)	0.18 (0.07)	0.13 (0.04)	0.13 (0.04)	0.03*	1.00

Mean behavioral and physiological measures are shown for unaltered view low (UVL), virtual reality low (VRL) and virtual reality high (VRH), with standard deviation in parentheses (n=19 for each condition). The first 3 measures assessed stress induction. The other measures assessed cognitive and physical performance. All measures shown had significant Friedman test results across conditions. Pairwise comparison p-values are shown, with asterisks denoting significant differences ($p<0.05$). We only made two comparisons: 1) unaltered view low vs. virtual reality low and 2) virtual reality low vs. virtual reality high.

Subjects' heart rate and response time significantly increased in virtual reality low compared to unaltered view low ($p<0.001$ and $p=0.018$, respectively), indicating increased physical and cognitive exertion in virtual reality. We found no significant differences in heart rate ($p=1.0$) and response time ($p=0.103$) between virtual reality conditions.

Subjects' balance performance significantly worsened in virtual reality low compared to unaltered view low (Table 2-2), as measured by failures per minute ($p=1.0$). There was no significant difference between virtual reality conditions ($p=0.343$). In addition, subjects performed significantly more beam passes in unaltered view low compared to virtual reality low ($p<0.001$), likely because fewer step-offs occurred. We found no significant differences in beam passes between virtual reality conditions ($p=0.378$). Subjects also beam-walked significantly faster in unaltered view low compared to virtual reality low ($p=0.027$). We found no significant difference in gait speed between virtual reality conditions ($p=1.0$). Gait speeds for all groups were lower than our desired speed of 0.22 m/s, potentially due to the difficulty of the beam-walking task.

Auxiliary Experiment Results

Our auxiliary experiment found few significant differences, and none of these differences appear to occur from wearing the virtual reality headset (Table 2-3). We only found significant effects for heart rate and heart rate variability ($p<0.001$ and $p=0.006$). Heart rate increased when standing with the headset on and off compared to sitting with the headset on ($p=0.004$ and $p<0.001$) and sitting with the headset off ($p=0.022$ and $p=0.007$). Comparisons within standing conditions and within sitting conditions had non-significant p-values ($p=1.0$), suggesting that heart rate significantly changes due to alterations in physical task performance (sitting vs. standing), not from wearing the headset. While heart rate variability significantly differed across conditions, we did not find any significant pairwise comparisons. Sitting with the headset on decreased heart rate variability compared to standing with the headset off, but was not significant ($p=0.061$). This difference may be caused by sitting vs. standing and has the opposite trend compared to the main experimental results. Electrodermal activity, response time, and heart rate

frequency power did not significantly differ across conditions. Our auxiliary study of headset effects indicates that the significant differences found during beam-walking are likely not caused by just wearing the headset.

Table 2-3: Sitting/standing experiment results.

Measure	Sit Headset Off	Sit Headset On	Stand Headset Off	Stand Headset On
Heart Rate Variability (beats/min)	4.9 (1.5)	4.5 (1.7)	6.0 (1.5)	5.6 (2.0)
Heart Rate Frequency Power (%)	60.2 (15.5)	59.7 (15.9)	54.6 (16.5)	50.8 (14.4)
Electrodermal Activity (counts/min)	4.5 (9.9)	2.8 (5.3)	8.1 (12.7)	6.9 (10.1)
Heart Rate (beats/min)	72.7 (10.5)*	70.7 (10.2)*	88.4 (14.5)†	86.0 (13.1)†
Response Time (s)	0.63 (0.14)	0.66 (0.14)	0.62 (0.11)	0.66 (0.13)

* significantly different from standing conditions

† significantly different from sitting conditions

Mean physiological results are shown for the auxiliary headset experiment, with standard deviation in parentheses (n=20). Pairwise significance was determined following a significant Friedman test ($p<0.05$). Heart rate and heart rate variability had significant Friedman test results, with significant pairwise differences in heart rate found between sitting and standing. No other significant differences were found.

Fatigue Assessment Results

We found significant differences across conditions related to fatigue for heart rate and failures per minute, but not for response time (Figure 2-3). Subjects' percent change in failures per minute significantly increased in virtual reality compared to unaltered view low ($p=0.004$), suggesting that virtual reality impaired motor acquisition. Percent change in failures per minute did not significantly differ between virtual reality conditions ($p=0.703$). Heart rate percent

change did not significantly differ between virtual reality low and unaltered view low (p=0.489). Heart rate percent change significantly increased in virtual reality high compared to virtual reality low (p=0.021), which may have been induced by stress from virtual high heights. Response time percent change did not significantly differ between unaltered view low and virtual reality low (1.0) and between virtual reality conditions (1.0), suggesting that subjects did not experience significantly different cognitive fatigue across conditions.

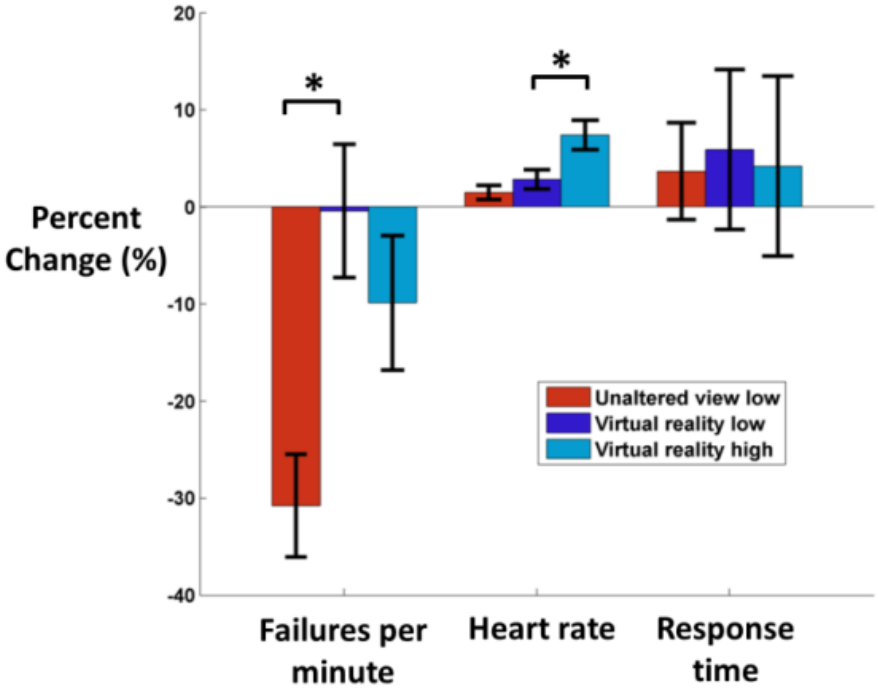

Figure 2-3: Percent change in failures per minute, heart rate, and response time. To assess fatigue effects, we calculated the percent change (mean±SE) between the first and last 3 minutes of each condition (n=19). Failures per minute, heart rate, and response time are shown for unaltered view low (red), virtual reality low (dark blue), and virtual reality high (light blue). Negative percent change indicates that the value in the final 3 minutes decreased compared to the first 3 minutes. Failures per minute percent change significantly decreased in unaltered view low compared to virtual reality low. Heart rate percent change significantly increased in virtual reality high compared to virtual reality low. No other comparisons were significant between 1) unaltered view low vs. virtual reality low and 2) virtual reality low vs. virtual reality high.

EEG Data

We found significant differences in EEG event-related activity following the tone for the anterior cingulate cluster only (Figure 2-4). Because response time significantly differed between unaltered view low and virtual reality high but not between virtual reality conditions, we only compared EEG activity between unaltered view low and virtual reality low. In the anterior cingulate, virtual reality low peak activity significantly increased from 500-600 ms after the tone compared to unaltered view low. We were not concerned about motion artifact in the EEG recordings due to time-locking to a cognitive event and the slow gait speeds during the task (Table 2-2).

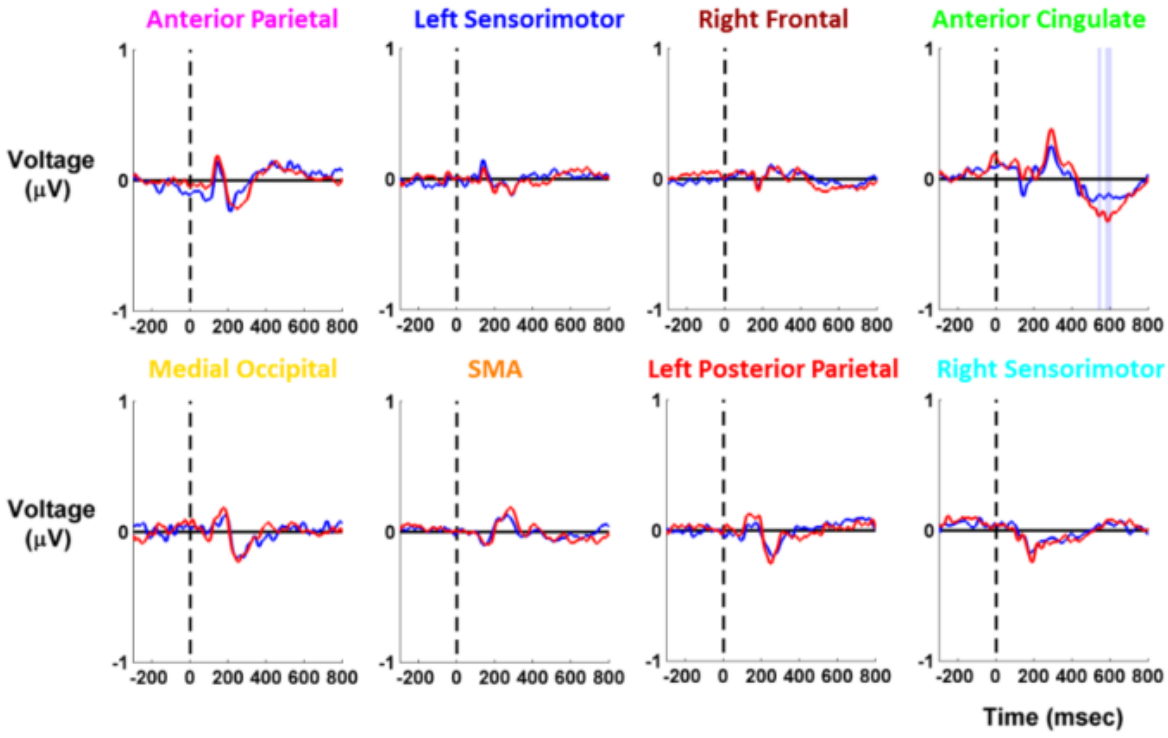

Figure 2-4: EEG event-related activity for cortical clusters. EEG event-related activity is shown for each cortical cluster (n=19), with unaltered view low in red and virtual reality low in blue. Tone presentation occurred at 0 ms, preceded by 300 ms of baseline activity. We analyzed 800 ms following the tone presentation. Shading reflects the condition with significantly higher amplitude (red for unaltered view low, blue for virtual reality low). We found significant differences in the anterior cingulate cluster only.

Discussion

We found that heart rate variability indicated increased stress at virtual high heights, which agreed with our first hypothesis. Subjects' response time also significantly increased in virtual reality low compared to unaltered view low, but this difference was not due to fatigue. Significantly decreased EEG event-related peak activity in anterior parietal and anterior cingulate areas further corroborated our response time findings, confirming our second hypothesis.

We also found increased heart rate variability during virtual high heights exposure compared to low virtual heights exposure (Table 2-2). Increased heart rate variability during stress runs contrary to some studies (Clays, et al., 2011; Boesch, et al., 2014), but agrees with a recent study using an acute stressor (Schlink, et al., 2017). Such a discrepancy may arise from the paradigm that induced stress. In addition, a faster heart rate makes it more difficult to have high heart rate variability because there would be less time in a heartbeat cycle for variation in timing (McCraty & Shaffer, 2015). Heart rate variability significantly increased in virtual reality high compared to virtual reality low, despite both conditions having similar heart rates.

Another measure of stress, heart rate frequency power, was also greater during virtual high heights exposure compared with virtual low heights exposure (Table 2-2). Heart rate frequency power focused on the percent of total power at all frequencies except 0.04-0.15 Hz. This excluded band contains a mix of sympathetic and parasympathetic responses (Thayer, Ahs, Fredrikson, Sollers, & Wager, 2012). The frequency power in this band decreased with high heights exposure, despite an increased heart rate in virtual reality. This suggests that the 0.04-0.15 Hz frequency band primarily measured parasympathetic response during the task, which significantly decreased with virtual high heights exposure. It is worth noting that

parasympathetic changes can occur rapidly (milliseconds) compared to the sympathetic response (seconds) (Thayer, Hansen, & Johnsen, 2010). The sympathetic response may have been masked by increased physical exertion. While many studies focus on the high frequency power band (0.15-0.4 Hz) or on the ratio of low to high frequency power (Mellman, Knorr, Pigeon, Leiter, & Akay, 2004; Hjortskov, et al., 2004), a decrease in low frequency power with stress has also been documented (Clays, et al., 2011).

While both heart rate variability metrics supported our hypothesis that stress was induced during virtual high heights exposure, electrodermal activity was primarily affected by physical exertion, instead of stress (Table 2-2). Electrodermal activity only measures the sympathetic response and has been shown to increase under both stress and physical loading (Poh, Swenson, & Picard, 2010). Our findings contrast with stationary studies that have found decreased electrodermal activity in virtual reality (Cleworth, Horslen, & Carpenter, 2012; Simeonov, Hsiao, Dotson, & Ammons, 2005). This suggests that physical exertion primarily affected electrodermal activity. This is an important consideration for future experiments and highlights the challenges of quantifying stress, particularly during paradigms with high physical exertion. While we presented the phasic results of electrodermal activity here, we found similar results for the slower tonic component as well.

Subjects performed worse on the beam-walking task in virtual reality, based on failures per minute (Table 2-2). In addition, we found that subjects significantly lowered their failures per minute in unaltered view low viewing compared to virtual reality low (Figure 2-3). This indicates that both motor performance and motor acquisition were impaired by virtual reality use. Virtual reality use has been shown to worsen balance performance, with comparable stability to

being blindfolded (Horlings, et al., 2009; Akizuki, et al., 2005). Subjects may have had difficulty adapting to virtual reality, reflected by increased physical and cognitive exertion.

The cognitive load of the subjects was greater during virtual reality use than during the unaltered view low condition, as measured by significantly increased response time in virtual reality low (Table 2-2). Significantly decreased EEG peak amplitude also indicated increased cognitive loading in the anterior cingulate cluster during virtual reality use (Figure 2-4). Similar decreases in event-related activity have been seen for this type of secondary auditory task when subjects performed a more challenging cognitive task (Shaw, et al., 2018). The anterior cingulate is important for maintaining balance (Sipp, Gwin, Makeig, & Ferris, 2013) as it is thought to perform error-detection (Wolpert, Goodbody, & Husain, 1998; Gehring & Knight, 2000). Bogost et al. also found that the activity of the anterior cingulate and somatosensory area weakened during a reactive balance task when performing a challenging secondary task (Bogost, Burgos, Little, Woollacott, & Dalton, 2016). Dual-task interference during balance also reduces activity in sensorimotor and sensory areas in parietal cortex (Little & Woollacott, 2015). Other studies have found strong EEG activity in these regions during balance control with eyes open (Sipp, Gwin, Makeig, & Ferris, 2013; Slobounov, Cao, Jaiswal, & Newell, 2009) and eyes closed (Hülsdünker, Mierau, & Strüder, 2015). Increased cognitive loading in the anterior cingulate may affect error detection while balancing, which may help explain why balance performance significantly worsened during virtual reality viewing.

While virtual reality induces realistic stress during virtual high height exposure, virtual reality headsets leave something to be desired during postural control. Low latency and limited field of view may have affected balance performance. The latency of the headset was 60 frames per second, but the movement generated by the Kinect was approximately 30 frames per second,

which was likely noticeable to the user. In addition, the Kinect may not have provided ideal body tracking, which could break a subject's sense of presence in virtual reality. Such breaks in presence can alter cognitive processing (Padrao, Gonzalez-Franco, Sanchez-Vives, Slater, & Rodriguez-Fornells, 2016) and may have affected how realistic the virtual reality high heights experience felt to each subject. The headset also had a 110 degree field of view. In contrast, humans have at least a 180 degree field of view (Walker, Hall, & Hurst, 1976), and peripheral vision plays a primary role in worsen postural control (Amblard & Carblanc, 1980; Assaiante, Marchand, & Amblard, 1989). However, virtual reality can still impair stability even when controlling for latency and field of view (Kelly, Riecke, Loomis, & Beall, 2008). Virtual reality headsets continue to improve, and other options such as augmented reality may improve balance without the limitations of virtual reality headsets. This experiment establishes useful measures for assessing future virtual reality headsets in a dynamic setting.

Conclusions

Dynamic virtual reality exposure to high heights induces stress, indicating that this setup could provide realistic scenarios during dynamic balance training. However, technological limitations of virtual reality headsets currently limit the efficacy of balancing with a virtual reality headset. Balance performance, physical exertion, and cognitive loading provided a comprehensive quantification of how virtual reality use affects healthy young adults. Virtual reality technology needs to facilitate comparable balance to real world use before assisting patients with a fear of falling. Virtual reality technology will continue to develop, and we expect that future virtual reality headsets will achieve comparable results to balancing without a headset on.

Chapter 3: Transient Visual Perturbations Boost Short-term Balance Learning in Virtual Reality by Modulating Electrocortical Activity[2]

Abstract

Immersive virtual reality can expose humans to novel training and sensory environments, but motor training with virtual reality has not been able to improve motor performance as much as motor training in real world conditions. An advantage of immersive virtual reality that has not been fully leveraged is that it can introduce transient visual perturbations on top of the visual environment being displayed. The goal of this study was to determine if transient visual perturbations introduced in immersive virtual reality modify electrocortical activity and behavioral outcomes in human subjects practicing a novel balancing task during walking. We studied 3 groups of healthy young adults (5 male and 5 female for each) while they learned a balance beam walking task for 30 minutes under different conditions. Two groups trained while wearing a virtual reality headset, and one of those groups also had half-second visual rotation perturbations lasting ~10% of the training time. The third group trained without virtual reality. We recorded high-density electroencephalography (EEG) and movement kinematics. We hypothesized that virtual reality training with perturbations would increase electrocortical activity and improve balance performance compared to virtual reality training without perturbations. Our results confirmed the hypothesis. Brief visual perturbations induced increased theta spectral power and decreased alpha spectral power in parietal and occipital regions, and improved balance performance in post-testing. Our findings indicate that transient visual

[2] This chapter has been previously published in *Journal of Neurophysiology* (Peterson, Rios, & Ferris, 2018).

perturbations during immersive virtual reality training can boost short-term motor learning by inducing a cognitive change, minimizing the negative effects of virtual reality on motor training.

Introduction:

Virtual reality has become a popular paradigm for training due to its ability to expose users to novel training and sensory environments (Adamovich, Fluet, Tunik, & Merians, 2009). Virtual reality use can make a user feel present in a virtual world (Sanchez-Vives & Slater, 2005) and improve clinical scenarios such as the sensing of pain in patients with burns (Hoffman, et al., 2014; Hoffman, et al., 2008). Virtual reality has also been shown to improve walking speed and gait stability (Darekar, McFadyen, Lamontagne, & Fung, 2015; Mirelman, et al., 2011), leading to its use in rehabilitation of mobility and balance control (Booth, Masud, Connell, & Bath-Hextall, 2013; Darekar, McFadyen, Lamontagne, & Fung, 2015). Recently, affordable virtual reality head-mounted displays have been able to provide unprecedented immersion into novel virtual experiences. These new headsets have driven interest in adapting virtual reality further into other clinical and research settings.

Despite the promise of such immersive experiences, virtual reality head-mounted displays have been shown to decrease gait performance compared to unaltered viewing (Epure, et al., 2014; Robert, Ballaz, & Lemay, 2016). Numerous studies have examined the possibility of using virtual reality for improving rehabilitation and gait (Booth, Masud, Connell, & Bath-Hextall, 2013; Corbetta, Imeri, & Gatti, 2015; Darekar, McFadyen, Lamontagne, & Fung, 2015; Palacios-Navarro, Albiol-Pérez, & García-Magariño García, 2016), but few studies used head-mounted displays to provide fully immersive virtual reality. Among those that have measured gait stability, all reported worsened stability when subjects used the virtual reality head-mounted display (Calogiuri, et al., 2017; Epure, et al., 2014; Kawamura & Kijima, 2016; Kelly, Riecke,

Loomis, & Beall, 2008; Lott, Bisson, Lajoie, McComas, & Sveistrup, 2003; Robert, Ballaz, & Lemay, 2016; Soffel, Zank, & Kunz, 2016). Two studies have found improvements in timed-up and go performance in stroke patients when trained in virtual reality compared to conventional training (Jung, Yu, & Kang, 2012; Kang, Kim, Chung, & Hwang, 2012), but the head-mounted displays for these studies were similar to spectacles placed away from the eyes, providing users with peripheral vision. Another study found improved step length and walking speed in stroke patients when performing obstacle walking in immersive virtual reality (Jaffe, Brown, Pierson-Carey, Buckley, & Lew, 2004). This comparison may be influenced by the control group performing overground walking while the virtual reality group performed treadmill walking. We could find no studies in the literature that found that training with virtual reality head-mounted displays was as good as or better than training in real world conditions. Despite these limitations, virtual reality head-mounted displays are the best available solution for controlling a user's entire field of view while walking. There is a need to overcome the effects of impaired performance training in immersive virtual reality in order to provide novel experiences equivalent to real world training.

One potential way to improve balance training outcomes is to perturb the sensory input required for balance control. This partly relies on the specificity of learning hypothesis, where humans use the optimal sources of information during the task. These optimal sources of sensory information can dynamically change based on sensory perturbations (Assländer & Peterka, 2014), such as less emphasis on proprioception during balance when vision is available and reliable (Bernier, Chua, & Franks, 2005; Proteau, Marteniuk, & Lévesque, 1992). Transient perturbations of optical flow during stance in healthy adults have been shown to increase EEG parietal theta power. Studies have used virtual reality to expose subjects to visual rotations up to 45° (Wright,

2014; Chiarovano, et al., 2015), similar to prism goggle studies (Martin, Keating, Goodkin, Bastian, & Thach, 1996; Fortis, Goedert, & Barrett, 2011). However, such effects are usually temporary. In contrast, repeated exposure to visuomotor perturbations during lower limb cursor control has been shown to reduce tracking errors and decreases response time (Luu, et al., 2017a). Using the control over the user's visual field provided by a virtual reality head-mounted display, it may be possible to provide similar repeated perturbations during dynamic balance to the user's visual input, leading to improved short-term motor learning.

The purpose of this study was to determine if a transient visual perturbation, presented as visual rotations in virtual reality, can boost motor training outcomes and potentially overcome the negative effects of immersive virtual reality. We studied young health subjects performing short-term motor training on a balance beam (Domingo & Ferris, 2009; Domingo & Ferris, 2010). We used a virtual reality headset to present brief visual perturbations. We chose visual perturbations because they induce large effects on mediolateral stability (Franz J. R., Francis, Allen, & Thelen, 2016), making them relevant to a beam-walking task. We compared these results to virtual reality without perturbations and unaltered viewing without virtual reality (i.e. real world conditions) to determine if the sensory perturbation boosted short-term motor learning and overcome the negative training effects from virtual reality. We hypothesized that brief visual perturbations in virtual reality would significantly improve balance performance compared to virtual reality training without perturbations. To provide insight into the neural mechanisms for changes in balance performance, we used high-density electroencephalography (EEG) with independent component analysis (ICA) and source localization (Makeig, Bell, Jung, & Sejnowski, 1996; Sipp, Gwin, Makeig, & Ferris, 2013). We hypothesized that EEG theta spectral power in parietal and occipital sensorimotor integration areas would increase following

perturbation onset due to conflicting visuomotor information and impaired visual working memory.

Materials and Methods:

Subjects

We recruited 32 healthy, young adults for this study. All subjects identified themselves as right hand and right foot dominant, with normal or corrected vision. We screened subjects for any orthopedic, cardiac, or neurological conditions and injuries. All subjects provided written informed consent. Our protocol was approved by the University of Michigan Health Sciences and Behavioral Sciences Institutional Review Board for the protection of human subjects.

Before each experiment, we screened subjects for motion sickness in virtual reality. Subjects stood in place during a 5 minute activity while wearing a virtual reality headset (Oculus Rift DK2, Oculus virtual reality, Irvine, CA). Subjects walked and jumped around a virtual environment using body gestures tracked by a Microsoft Kinect v2 (Microsoft, Redmond, WA). We intentionally included a disconnect between real and virtual movements to be more disorienting than our main testing protocol. Subjects participated in the main experiment if both the subject and experimenter agreed that they did not exhibit any symptoms of motion sickness. Two potential subjects exhibited motion sickness symptoms and did not perform the experiment; 30 subjects passed this screening (15 males and 15 females, age 22.6±4.5 years (mean±SD)).

Experiment Design

Subjects walked at a fixed speed of 0.22 m/s on a 2.5 cm wide by 2.5 cm tall treadmill-mounted balance beam, similar to previous studies (Domingo & Ferris, 2009; Sipp, Gwin, Makeig, & Ferris, 2013). We based this speed on pilot data we recorded at a range of walking speeds. The

0.22 m/s speed was the lowest speed setting on the treadmill. We placed subjects in a body-support harness for safety, with extended support straps to increase unrestricted mediolateral movement. All subjects performed 30 minutes of training, separated into three 10-minute trials. Subjects also performed a 3 minute pretest before training and 3 minute posttest after training. Subjects took breaks as needed between training trials, with a 5-minute break between the end of training and the posttest. While beam-walking, subjects crossed their arms and walked heel-to-toe, with their feet along the direction of the beam. We gave subjects specific instruction to look straight ahead and to avoid looking at their feet. If subjects stepped off while on the beam, they were instructed to step off the beam with both feet and walk on the treadmill for approximately 5 seconds. When on the balance beam, subjects were instructed to only move their hips side-to-side to balance, avoiding rotations across their body's longitudinal axis. Our instructions followed previous studies (Domingo & Ferris, 2009; Domingo & Ferris, 2010).

We randomly assigned subjects to one of three groups during training: 1) virtual reality with perturbations, 2) virtual reality without perturbations, and 3) unaltered view. Each group had 10 subjects, with equal numbers of males and females. Subjects in all groups performed the same physical beam-walking task. Group 1 subjects wore a virtual reality headset with a webcam (Logitech C930e, Logitech, Lausanne, Switzerland) mounted underneath the front, providing the subject a passthrough view of what was in front of them. For this group, the webcam view rotated 20° clockwise or counterclockwise for 0.5 sec when both feet were placed on the beam, referred to as a visual perturbation. We used brief perturbations because continuous feedback can lead to dependency on the feedback used, leading to less general learning (Schmidt R. A., 1991; Schmidt, Young, Swinnen, & Shapiro, 1989). We added a random delay (up to 1 sec) to this visual perturbation to make it more difficult to anticipate. We rendered the virtual environment

with Unity 5 software (Unity Technologies, San Francisco, CA) using a NVIDIA Titan X graphics card (NVIDIA, Santa Clara, CA) to avoid slow-downs in the virtual reality presentation. Group 2 subjects wore the same virtual reality headset and webcam, but without any visual perturbations. Group 3 subjects had unaltered vision (no virtual reality headset). We included groups 2 and 3 to establish the negative effects of our virtual reality setup without perturbations on balance performance without a virtual reality headset. All groups performed the pretest and posttest with unaltered vision. Figure 3-1 shows the setup for a subject in one of the virtual reality groups, along with example visual perturbations in each direction.

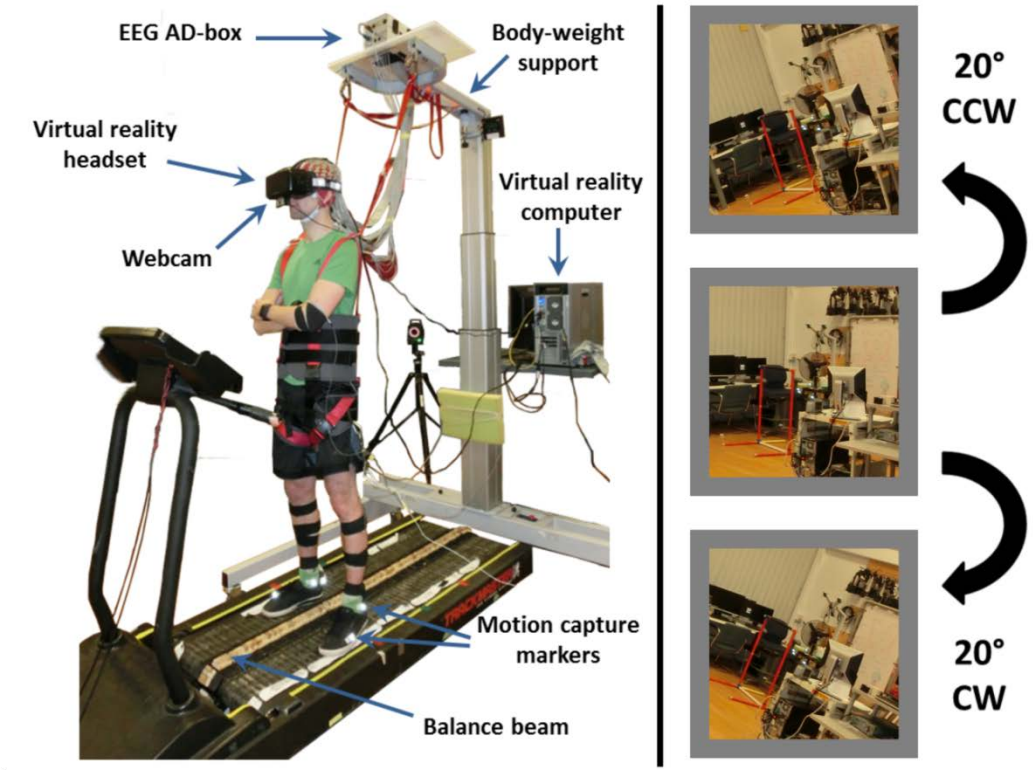

Figure 3-1: Subject setup and example visual perturbations. Typical subject setup for the virtual reality groups is shown (left). All 4 groups walked on the same physical beam. For the virtual reality training with perturbations group, each subject's field of view in virtual reality was randomly rotated 20° counterclockwise (CCW; top right) or clockwise (CW; bottom right). The perturbation rotations are shown on an example image similar to the subject's view during the experiment (right). Perturbations lasted for 0.5 sec and only occurred when subjects placed both feet on the balance beam.

Performance and Physiological Measures

We recorded motion capture at the feet, sacrum, neck, and head using 16 reflective markers (Vicon, Los Angeles, CA) sampled at 100 Hz. We recorded EEG using a 136-channel BioSemi ActiView II system (BioSemi, Amsterdam, NL) sampled at 512 Hz. We placed one external electrode on the sternum to record heart rate, three external electrodes around the eyes to record eye movements, two external electrodes on the neck to record neck electromyography, and two external electrodes on each mastoid. EEG electrode locations were measured using a Zebris ELPOS digitizer (Zebris Medical GmbH, Isny, Germany). We placed the AD-box and battery upside-down on top of the body-weight support to maximize the reach of the cables, fastening the wires to the body-weight support to avoid wires pulling out of the AD-box. We programmed different key presses on the virtual reality keyboard to correspond with the visual perturbation onset and termination, using Windows Input Simulator. This keyboard input was recorded and synchronized with the EEG data using Lab Streaming Layer (Delorme, et al., 2011). We used a 0.5 Hz square pulse to synchronize the motion capture and EEG data. We also measured skin conductance using wrist sensors (Empatica E4, Empatica, Milan, Italy), as a proxy for sympathetic activity. Subjects in the virtual reality groups filled out surveys for motion sickness (Motion Sickness Assessment Questionnaire (Gianaros, Muth, Mordkoff, Levine, & Stern, 2001)) and presence (Witmer & Singer Presence Questionnaire (Witmer & Singer, 1998) and Slater-Usoh-Steed Questionnaire (Slater, Usoh, & Steed, 1994)) after performing the experiment.

To assess behavioral performance, we recorded the number of times each subject stepped off the beam and the total time spent on the beam. We combined these measures into failures per minute, computed as the number of step-offs divided by the total time spent on the beam in minutes (Domingo & Ferris, 2009; Domingo & Ferris, 2010). Failures per minute decrease when

subjects spend more time on the beam and have fewer step-offs. To assess pretest-to-posttest changes in performance, we calculated the percent change in failures per minute as the posttest value minus the pretest, divided by the pretest value and multiplied by 100. A negative percent change in testing performance indicated that a subject's balance performance improved in the posttest compared to the pretest. We also calculated failures per minute during training to determine if balance performance differed across groups during training. Based on our beam-walking performance results, we concentrated further analysis solely on the two virtual reality groups, which reduced confounding factors in our comparisons.

We used mean heart rate and electrodermal activity to assess physical exertion across groups during training. Electrodermal activity measures sympathetic activity, making it a good indicator of physical exertion (Critchley, 2002). We processed heart rate data during training using the Cleanline EEGLAB plugin (Mullen T. R., 2014) and bandpass filtering between 5 and 20 Hz. Kubios HRV software determined the R-peaks, which correspond to heartbeats (Tarvainen, Niskanen, Lipponen, Ranta-Aho, & Karjalainen, 2014). We manually adjusted incorrectly labeled R-peaks and used the mean heart rate calculated by Kubios. We processed the electrodermal activity using deconvolution in Ledalab to separate out the transient component of the signal (Benedek & Kaernbach, 2010a; Benedek & Kaernbach, 2010b). We ran deconvolution using default parameters. We counted the differences in the deconvoluted transient signal greater than 0.05 μS (Schmidt & Walach, 2000) during training, divided by the duration of training in minutes.

Motion capture marker trajectories were cleaned in Vicon Nexus and further processed in Visual3D (C-Motion, Germantown, MD). We low-pass filtered the data at 6 Hz and determined foot contacts by finding the peaks and troughs of the foot markers in the anterior/posterior

direction of movement on the treadmill (Zeni, Richards, & Higginson, 2008). We manually adjusted incorrectly labeled foot contacts. We determined whether the foot contact was on or off the beam by manually thresholding the foot marker data in the mediolateral direction of movement. The beam location varied slightly for each subject, necessitating a manual threshold. In addition to foot contacts, we calculated the mediolateral standard deviation of markers at the head and sacrum as a measure of movement variability. For both markers, we calculated the average standard deviation during training, along with the percent change in standard deviation from the first to last 3 minutes of training. We also calculated the percent change in standard deviation from pretest to posttest. We only used marker values from when the subject was on the balance beam for calculating standard deviation.

EEG Data & Analysis

EEG data were processed using custom scripts in EEGLAB (Delorme & Makeig, 2004). Our complete EEG processing pipeline can be seen in Figure 3-2. We downsampled the data to 256 Hz, high pass-filtered the EEG data at 1 Hz, and merged all conditions, referencing all channels to a common median reference to reduce the impact of potential outlier channels. We used Cleanline to reduce 60 Hz electrical noise. We rejected channels that had an abnormally high standard deviation from all other electrodes, had a kurtosis above five standard deviations, or were uncorrelated with other channels for more than 1% of the time (Kline, Huang, Snyder, & Ferris, 2015; Oliveira, Schlink, Hairston, König, & Ferris, 2017a). Including the five eye and neck muscle external channels, we retained 116 channels on average (range: 100-127).

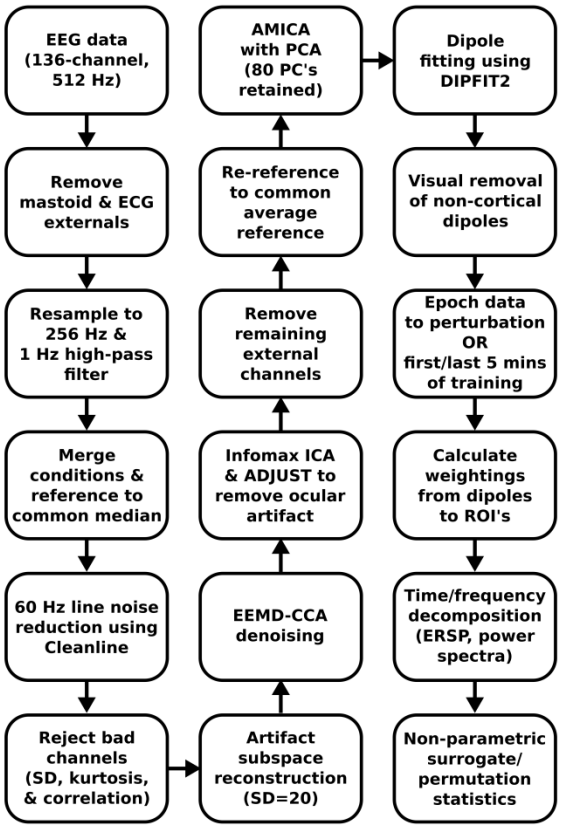

Figure 3-2: EEG processing flow chart. A flowchart of the EEG processing pipeline is shown, including all pre-processing and cleaning methods. All methods were performed in EEGLAB using custom Matlab scripts.

Following channel rejection, we used multiple denoising procedures to reduce prominent artifacts in the data. First, we used artifact subspace reconstruction (Mullen, et al., 2015) with a standard deviation of 20 to remove large artifacts. Next, we developed high-frequency denoising method based on two emerging signal processing methods: ensemble empirical mode decomposition (EEMD) (Wu & Huang, 2009) and canonical correlation analysis (CCA) (Hotelling, 1936), which have been combined before (Roy, Shukla, Shukla, & Rawat, 2017). Our EEMD-CCA method performed selective low-pass filtering, specifically targeting large high-frequency activity with low autocorrelation such as muscle activity and line noise. With EMDLAB (Al-Subari, et al., 2015), we used EEMD to find the high-frequency content of each

channel, called the first intrinsic mode function (IMF1) (Huang, et al., 1998). Compared to standard filters, EEMD filtering is data-driven and does not assume the data is stationary. In our data, IMF1 mostly contained high frequencies above 40 Hz. We assumed that IMF1 primarily contained non-brain activity, such as line noise and muscle artifact. This assumption aligns with previous uses of EEMD denoising where IMF1 is completely removed as artifact (Boudraa & Cexus, 2007; Safieddine, et al., 2012). Instead of completely removing it, we ran CCA on IMF1 and a copy of IMF1 time-lagged by one data point (Friman, Borga, Lundberg, & Knutsson, 2002). We did this to separate out sources of activity based on autocorrelation, where muscle activity is expected to have low autocorrelation (Chen, He, & Peng, 2014). Then we applied a threshold to remove large CCA components based on interquartile range. We removed all CCA components from IMF1 whose variance exceeded the median interquartile range of IMF1. This targets high-frequency data that is well-clustered by CCA, similar to previous EEG methods to reduce muscle artifact (Bai, et al., 2016; Safieddine, et al., 2012). The data rank is not altered by removing CCA components because they are only removed from the first IMF of the signal, similar to typical frequency filtering. We have included pseudocode for this method in Figure 3-3 to facilitate reproducibility. After EEMD-CCA denoising, we ran extended Infomax ICA (Lee, Girolami, & Sejnowski, 1999) and used the ADJUST plugin to automatically remove eye artifacts (Mognon, Jovicich, Bruzzone, & Buiatti, 2011). Our data included external channels around the eyes to potentially improve eye artifact removal. We then removed the external channels from the data.

```
%Run ensemble empirical mode decomposition (EEMD) to get first intrinsic mode
%function (IMF1)
for all EEG channels
    run EEMD using EMDLAB (set number of modes = 2 to get IMF1 and a residual)

%Run canonical correlation analysis (CCA)
run CCA on IMF1 and a copy time-shifted ahead by one data point

%Calculate interquartile ranges (IQRs) and remove high-varying CCA components
IQR_IMF1_median =the median IQR of IMF1 channels
IQR_comps =the IQR for each CCA component
find which IQR_comps >IQR_IMF1_median and remove these components from IMF1
add the resulting IMF1 to the residual from EEMD to get the denoised EEG data
```

Figure 3-3: EEMD-CCA pseudocode. The computational steps used to perform high-frequency denoising using a combined EEMD-CCA approach are described.

We re-referenced the remaining channels to a common average and interpolated the rejected channels to maintain a consistent montage across the head. Next, we ran adaptive mixture of independent components analysis (AMICA 15) (Palmer, Kreutz-Delgado, & Makeig, 2006; Palmer, Makeig, Kreutz-Delgado, & Rao, 2008), using principal components analysis to reduce down to 80 principal components prior to keep the data at full rank. AMICA also rejected unlikely data frames.

Following ICA, we performed dipole fitting (DIPFIT2) and retained dipoles explaining greater than 85% of the scalp variance (Oostenveld & Oostendorp, 2002). We removed non-cortical independent components based on visual inspection of power spectrum and dipole location. We then combined the remaining dipoles for each group (67 for virtual reality training with perturbations and 63 for virtual reality training without perturbations) and projected each dipole measure into predefined regions of interest (Bigdely-Shamlo, Mullen, Kreutz-Delgado, &

Makeig, 2013). We split the brain into 11 general regions of interest according to the LONI LPBA40 atlas (Shattuck, et al., 2008): left/right occipital, left/right parietal, left/right frontal, left/right fusiform, left/right temporal and cingulate (Figure 3-4). We excluded results from temporal and fusiform regions because few dipoles were located in these areas. Instead of weighting each dipole measure in a region equally, measure projection performs a weighted average based on each dipole's location within a region, using a three-dimensional Gaussian (14.2 mm full-width half-maximum) to spatially smear each dipole. We chose this method so that we compared the same predefined regions between two groups of subjects.

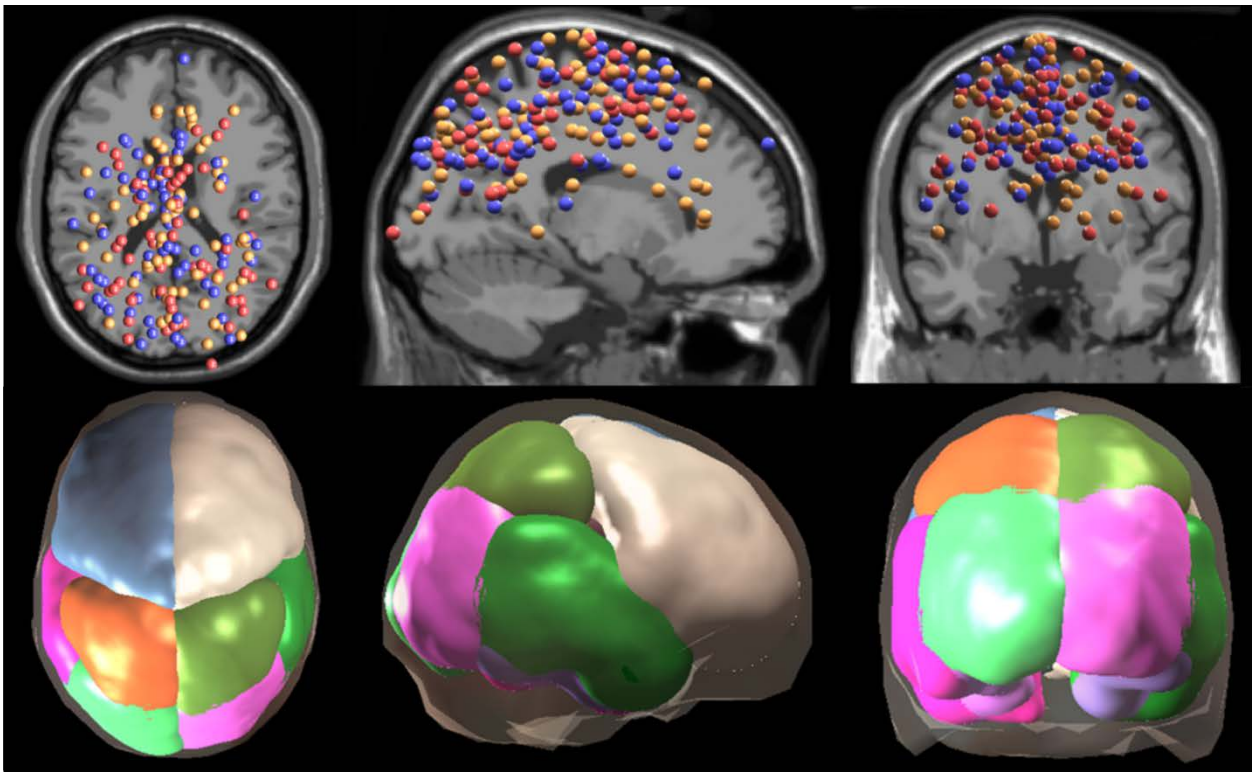

Figure 3-4: EEG source localization and regions of interest. EEG source localization are shown in blue for virtual reality training with perturbations, red for virtual reality training without perturbations training, and orange for unaltered view (n=10 for each group). Dipole locations (top) and regions of interest (bottom) are shown in transverse, sagittal, and coronal views (left to right). We retained 7 regions of interest: left frontal (blue), right frontal (tan), left parietal (orange), right parietal (olive green), left occipital (light green), right occipital (purple), and cingulate (pink; shown in small head plots).

For each region of interest, dipole weights are normalized to 1 for creating weighted averages of measures. Prior to normalization, weights sum to 1 for each dipole. We summed up the unnormalized weights as an estimate of dipole density in each region of interest (Bigdely-Shamlo, Mullen, Kreutz-Delgado, & Makeig, 2013). For virtual reality training with perturbations, dipole density at each region was: 14.5 (left frontal), 6.4 (right frontal), 3.7 (left parietal), 4.7 (right parietal), 4.7 (left occipital), 2.9 (right occipital), and 3.7 (cingulate). For virtual reality training without perturbations, dipole density at each region was: 9.7 (left frontal), 7.4 (right frontal), 6.0 (left parietal), 6.1 (right parietal), 3.6 (left occipital), 4.9 (right occipital), and 1.5 (cingulate).

To assess perturbation-evoked electrocortical activity, we computed time-frequency activity for the virtual reality training with perturbations group (n=10) averaged across epochs, known as event-related spectral perturbation (ERSP) plots. We split the EEG data during training into epochs of -0.5 to 1.5 sec, with visual perturbation onset at 0 sec. We separated epochs by direction of the perturbation, resulting in 121±18 clockwise and 103±17 counterclockwise epochs for each subject (mean±SD). We took the median instead of the mean across trials to avoid any single trial from disproportionately affecting the resulting ERSP. Average baseline activity from -0.5 to 0 sec before perturbation onset was subtracted out. We computed the ERSP for each dipole in the virtual reality training with perturbations group and projected this to the 7 regions of interest.

We compared electrocortical differences between virtual reality groups using spectral power during the first and last 5 minutes of training (referred to as early training and late training, respectively). For each 5 minute period, we only analyzed spectral power while subjects were on the beam. The power spectra for each dipole were projected to the 7 regions of interest, using the

same measure projection weights as the ERSPs. Because differences in total power could be attributed to inter-subject recording and processing differences, we normalized all 4 conditions (virtual reality with perturbations early/late and virtual reality without perturbations early/late) to their common average total power.

While motion artifact is a concern when collecting EEG activity (Castermans, Duvinage, Cheron, & Dutoit, 2014; Kline, Huang, Snyder, & Ferris, 2015; Snyder, Kline, Huang, & Ferris, 2015), we mitigated the effects of motion artifact by having subjects walk at a slow speed (0.22 m/s) and analyzing visual perturbation events, where any head motion would be delayed after the stimulus presentation. Based on prior studies analyzing motion artifact during human walking (Kline, Huang, Snyder, & Ferris, 2015; Nathan & Contreras-Vidal, 2015; Snyder, Kline, Huang, & Ferris, 2015), any effects of head motion on EEG results should have been negligible. To verify this, we computed the average sacrum and head mediolateral marker motion from our motion capture data, time-locked to the visual perturbation. These trajectories were baseline-subtracted to the 1.5 seconds preceding the perturbation onset. Due to the way we ran the experiment, we presented perturbations to all 3 groups during training, except that the virtual reality perturbations group had a 20° rotation while the virtual reality perturbations group had a 0° rotation (pseudo-perturbation) and the unaltered view group was not wearing the headset. This gives us a similar event to compare motion capture displacement across groups to determine what sacrum and head displacement was caused by the 20° perturbation for the virtual reality perturbations group.

Statistical Analysis

We performed behavioral performance statistical tests across all groups using ANOVA and pairwise t-tests with Bonferroni correction ($p<0.05$). These statistical tests were performed using

R (R Core Team, 2017). In addition, we tested if the failures per minute during the pretest and posttest were stable, to ensure that the performance improvement values we calculated were accurate. We used the heel strikes on and off the beam to create a "running total" failures per minute metric across each 3-minute condition. We normalized each subject's data by subtracting out the mean and dividing by the standard deviation to reduce inter-subject variability within groups. For each group and pre/post trial, we then took the average "running total" and performed an augmented Dickey-Fuller test using R, which tests if data is stationary over time by assuming that the data is not stationary (null hypothesis).

For EEG ERSPs, time-frequency activity was bootstrapped 200 times to determine significance ($p<0.05$). We used dipoles in each region with normalized weights above 0.05 to create the bootstrap distribution, so only the dipoles that noticeably contributed to a region were used. Non-significant differences were set to 0. Because amount of time on the beam varied across subjects, we randomly selected 85 half-second time bins on the beam for each subject from the last 5 minutes of training. Similar to the ERSPs, each time bin was projected to a region and normalized to average total power. We averaged these projected power spectra into predefined frequency bands: delta (1-4 Hz), theta (4-8 Hz), alpha (8-13 Hz), beta (13-30 Hz), and gamma (30-50 Hz). We used 3x2 non-parametric ANOVA's with 2000 permutations to test for main effects of group (virtual reality with perturbations vs. virtual reality without perturbations vs. unaltered viewing) and training (early vs. late) on the power spectra results. Further pairwise comparisons were performed using a Wilcoxon rank-sum test ($p<0.05$) (Gibbons & Chakraborti, 2011), with false discovery rate correction for multiple comparisons.

Results:

Beam-walking Performance

The percent change in beam-walking performance varied considerably across groups ($F(2,27)=14.2$, $p=6.10e-5$, ANOVA) (Table 3-1). Subjects improved significantly less during virtual reality training without perturbations compared to virtual reality training with perturbations ($t(27)=4.50$, $p=3.50e-4$, paired t-test with Bonferroni correction) and training with unaltered view ($t(27)=4.73$, $p=1.90e-4$, paired t-test with Bonferroni correction). There was more than a four-fold increase in beam-walking performance increases with virtual reality training with perturbations (mean 42%, SD 17%) compared to virtual reality training without perturbations (mean 9%, SD 20%). We found no significant difference in beam-walking performance improvement between unaltered view and virtual reality training with perturbations ($t(27)=0.23$, $p=1.0$, paired t-test with Bonferroni correction). In addition, we found significant results for the augmented Dickey-Fuller test for all groups and pre/post trials ($p<0.02$), indicating that pretest and posttest failures per minute can be reasonably assumed to be stationary for all 3 groups.

We also found that the number of errors made during the entire training period differed across groups ($F(2,27)=14.69$, $p=4.802e-5$, ANOVA) (Table 3-1). Subjects made significantly fewer errors during training with unaltered view compared to virtual reality training with perturbations ($t(27)=4.70$, $p=2.10e-4$, paired t-test with Bonferroni correction) and virtual reality training without perturbations ($t(27)=4.69$, $p=2.10e-4$, paired t-test with Bonferroni correction). We found no significant difference between virtual reality conditions ($t(27)=0.002$, $p=1.0$, paired t-test with Bonferroni correction).

Table 3-1: Training failures per minute and percent change

Measure	VR with perturbations	VR without perturbations	Unaltered view
Testing failures change (%)	-42.4% (16.7%)	-9.1% (20.4%)*	-44.2% (12.5%)
Training failures (min^{-1})	32.6 (9.3)	32.6 (10.0)	14.9 (5.7)*

Average percent change in failures per minute from pretest to posttest are shown for the 3 viewing groups (A), with standard error bars (n=10 for each group). Negative percent change indicates that subjects improved balance performance in posttest compared to pretest. Asterisk denotes significantly less percent change in the virtual reality training without perturbations group compared to the other 3 conditions. Average failures per minute during training are shown with standard error bars (B). Asterisk denotes significantly fewer training failures per minute during training with unaltered view compared to the other 3 conditions. Significant pairwise comparisons were performed using post-hoc t-test with Bonferroni correction following significant ANOVA ($p<0.05$ for both).

Behavioral & Physiological Measures

We found no substantive differences in the gross physiological measures compared across groups (Table 3-2). There were no significant differences between virtual reality groups for motion sickness ($F(1,18)=0.064$, $p=0.803$, ANOVA) and both of the presence assessments ($F(1,18)=0.005$, $p=0.942$, ANOVA and $F(1,18)=0.055$, $p=0.817$, ANOVA, respectively). In addition, heart rate and electrodermal activity during training was not significantly different across groups ($F(2,27)=0.053$, $p=0.949$, ANOVA and $F(2,27)=0.085$, $p=0.919$, ANOVA) .

Table 3-2: Surveys and physiological measures during training

Measure	VR with perturbations	VR without perturbations	Unaltered view
Motion Sickness	24.3% (17.3%)	22.2% (19.6%)	-
Presence #1 (WS)	64.9% (8.7%)	65.2% (9.6%)	-
Presence #2 (SUS)	55.2% (18.1%)	57.0% (16.1%)	-
Heart Rate (beats/min)	105.15 (18.74)	104.98 (9.02)	103.29 (12.99)
Electrodermal Activity (counts/min)	42.76 (9.42)	41.73 (17.62)	40.03 (16.45)

Average values for motion sickness (Motion Sickness Assessment Questionnaire) and presence questionnaires, along with average heart rate and electrodermal activity during training for both virtual reality groups and unaltered view (n=10 for each group). Standard deviation is in parentheses. Presence #1 refers to Witmer & Singer Presence Questionnaire and presence #2 refers to Slater-Usoh-Steed Questionnaire. We found no significant differences across groups for these measures (ANOVA $p>0.05$).

Head and sacrum motion variability were mostly similar between virtual reality groups, but head motion significantly increased with perturbations training (Table 3-3). Percent change in head marker standard deviation significantly differed across groups ($F(2,26)=5.441$, $p=0.011$, ANOVA), with significantly increased percent change during virtual reality training with perturbations compared to training with unaltered view ($t(26)=0.807$, $p=0.012$, paired t-test with Bonferroni correction) but not compared to virtual reality training without perturbations ($t(26)=2.401$, $p=0.071$, paired t-test with Bonferroni correction). The perturbations increased head movement as training progresses. We checked the correlation between performance improvement and the magnitude of change in head movement during training across groups. We found a nonsignificant correlation of 0.32 ($p=0.094$), which suggests that larger changes in head motion during training may lead to increased performance improvement, but more subjects

would likely be needed to establish a significant correlation. The percent change in head marker standard deviation from pretest to posttest ($F(2,26)=0.504$, $p=0.610$, ANOVA) did not significantly differ across groups ($F(1,18)=0.126$, $p=0.727$, ANOVA). The overall average head marker standard deviation during training was significantly different across groups ($F(2,26)=3.965$, $p=0.031$, ANOVA), with significantly increased head motion during training during unaltered view compared to virtual reality training with perturbations ($t(26)=2.570$, $p=0.049$, paired t-test with Bonferroni correction) but not compared to virtual reality training without perturbations ($t(26)=2.332$, $p=0.083$, paired t-test with Bonferroni correction). No other significant differences were found. For the sacrum marker, we found no significant differences in percent change during training ($F(2,26)=2.462$, $p=0.105$, ANOVA), percent change during testing ($F(2,26)=1.570$, $p=0.226$, ANOVA), and overall average during training ($F(2,26)=2.471$, $p=0.104$, ANOVA). Overall, we found few non-cognitive differences between virtual reality groups.

Table 3-3: Motion Capture Marker Standard Deviation

	Measure	VR with perturbations	VR without perturbations	Unaltered view
Head marker	Train (% change)*	16.1% (19.7%)	-0.9% (6.4%)	-6.8% (18.2%)
	Test (% change)	2.7% (29.1%)	-5.3% (22.8%)	6.8% (28.3%)
	Train (cm)	5.8 (1.1)	6.0 (0.8)	7.4 (2.1)
Sacrum marker	Train (% change)	3.9% (8.7%)	0.7% (9.5%)	-5.7% (10.3%)
	Test (% change)	-8.5% (20.4%)	6.7% (28.0%)	-8.2% (15.8%)
	Train (cm)	5.1 (0.8)	5.2 (0.8)	4.5 (0.6)

Average values for head and sacrum markers standard deviation during training along with percent change during training and testing for both virtual reality groups and unaltered view (n=10 for each group). Standard deviation is in parentheses. Head marker percent change during training significantly differed between groups, denoted with an asterisk (post-hoc t-test with Bonferroni correction following significant ANOVA; $p<0.05$). We found no other significant differences.

EEG during Perturbations

Parietal and occipital areas showed the strongest EEG activity immediately following perturbation onset and termination (Figure 3-5). We found synchronization in delta (1-4 Hz), theta (4-8 Hz) and alpha (8-13 Hz) EEG bands. The parietal and occipital synchronization was followed by beta (13-30 Hz) desynchronization. There was similar time-frequency activity for each perturbation direction across all regions. The cingulate region showed delta and theta synchronization after perturbation onset, followed by delta, alpha, and gamma (30-50 Hz) synchronization after perturbation termination. Frontal areas showed little activity, except for delta synchronization in the right frontal area during clockwise perturbations.

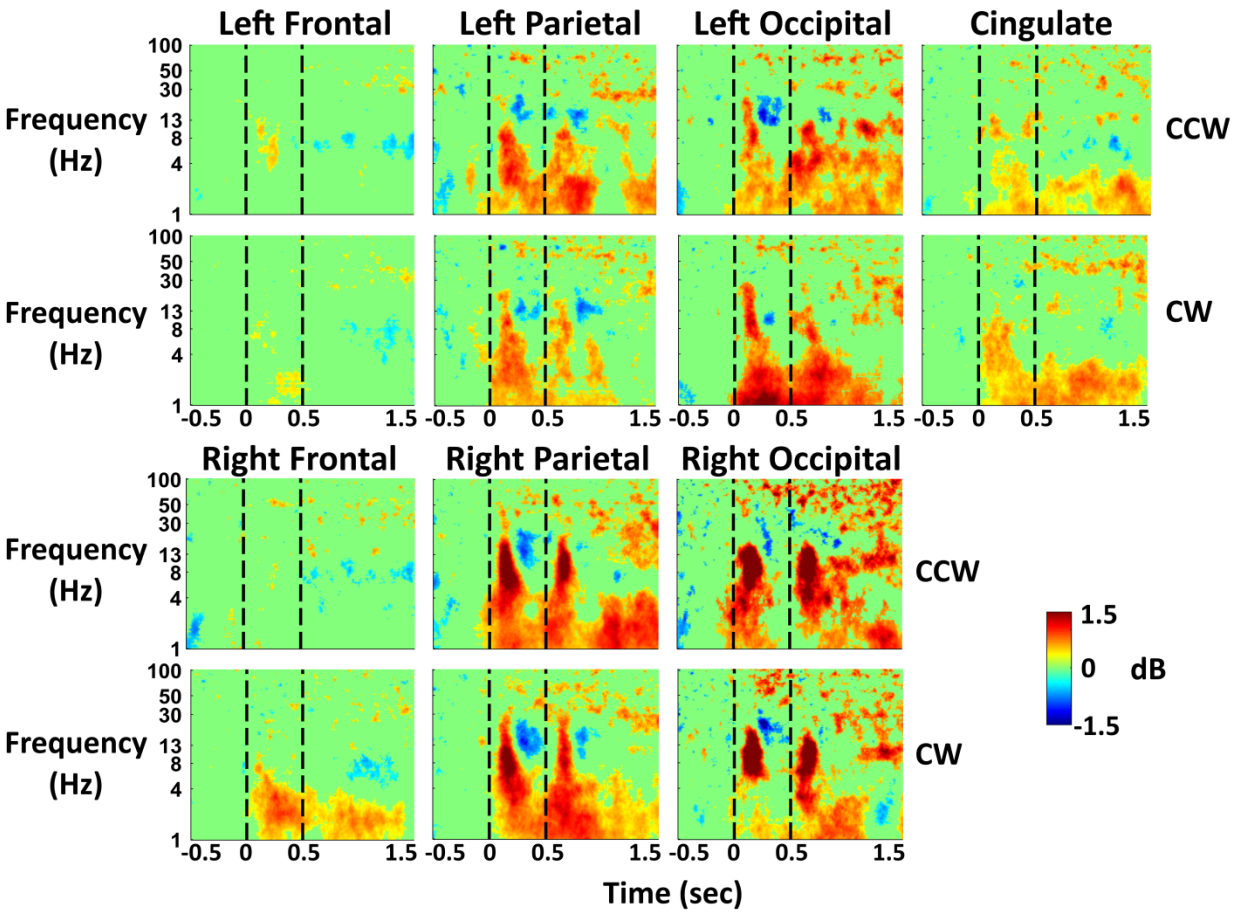

Figure 3-5: ERSP plots for virtual reality perturbation. EEG ERSPs are shown for the 7 regions of interest for averaged perturbation activity during training in the virtual reality training with perturbations group (n=10). Perturbation onset occurs at 0 sec, with perturbation termination at 0.5 sec. Perturbations were split based on counterclockwise (CCW) or clockwise (CW) rotation. Non-significant ERSP power was set to 0 (bootstrap statistics; $p>0.05$). We subtracted out the spectral power during the 0.5 sec before perturbation onset as baseline activity.

Power Spectra between Conditions

We found increased theta spectral power during virtual reality with perturbations training across multiple cortical regions compared to the virtual reality without perturbations and unaltered view training groups (Figure 3-6). Theta power was significantly increased during virtual reality with perturbations compared to the other two conditions in left/right frontal, left/right occipital, and cingulate regions (pairwise $p<0.002$ for all). These significant differences were maintained for both early and late training, except for a non-significant difference in the left frontal region

between early virtual reality with perturbations training and early unaltered view training (p=0.075). Left occipital also had significantly decreased theta power during late training compared to early training (perturbations: p=0.009; no perturbations: p=0.001; unaltered view: p=0.006).

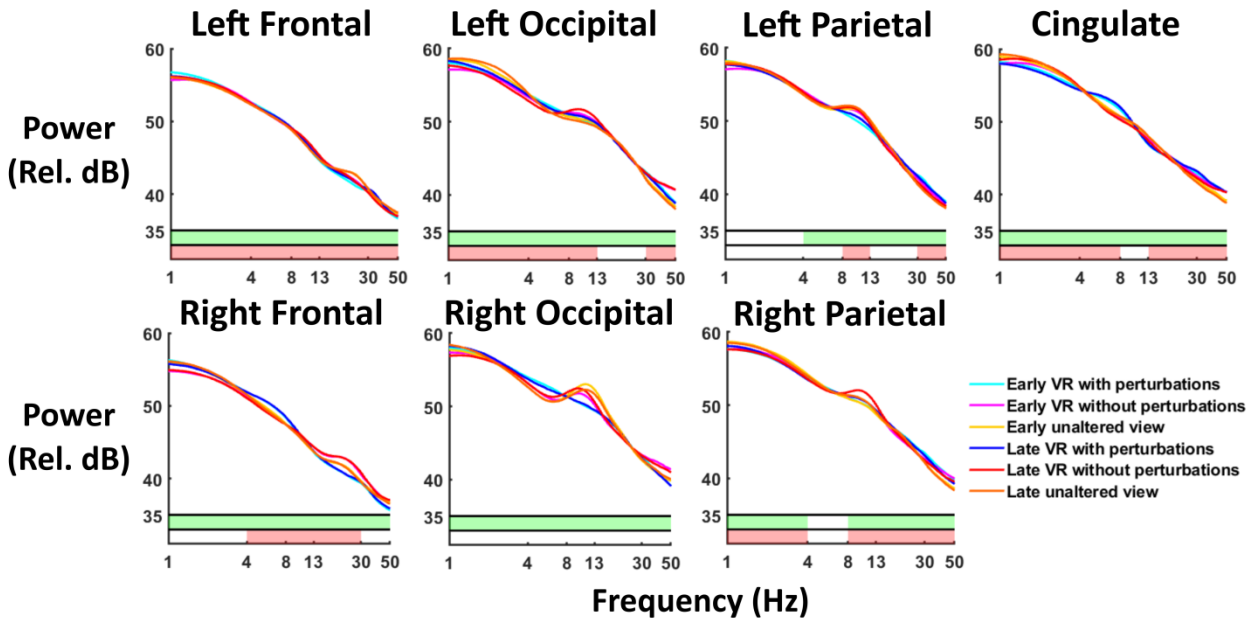

Figure 3-6: Spectral power across groups. Average EEG spectral power is shown for the 7 regions of interest during the first (early) and last (late) 5 minutes of training for both virtual reality training groups and the unaltered view group (n=10 for each group). Average spectral power is shown for virtual reality with perturbations during early (cyan) and late (blue) training. For virtual reality without perturbations, early training is shown in magenta with late training in red. Early training with unaltered view is shown in yellow, with late training in orange. We plotted across frequencies from 1-50 Hz. Shaded areas at the bottom denote significant differences in spectral power between groups, as compared across 85 randomly selected time bins for each subject using non-parametric 3x2 ANOVA comparisons using permutation statistics. Green shading corresponds to a significant main effect of group (virtual reality with perturbation vs. virtual reality without perturbation vs. unaltered viewing). Red shading corresponds to a significant main effect of training (early vs. late).

Alpha spectral power primarily decreased during perturbations training and also increased as training progressed for all 3 groups. Compared to virtual reality without perturbations training, alpha power decreased during virtual reality with perturbations and unaltered view training in

left frontal, left occipital, and right parietal (pairwise $p<0.001$ for all). This alpha power decrease occurred for both early and late training. Alpha power also significantly decreased during virtual reality with perturbations training compared to virtual reality training without perturbations in right occipital and left parietal for both early and late training (pairwise $p<0.001$ for all). In contrast, alpha power significantly increased in the cingulate region during late virtual reality training without perturbations compared with late training for both other groups (pairwise $p<0.001$ for both). In addition, alpha power significantly increased from early to late training for all 3 groups in left occipital and left/right parietal (pairwise $p<0.003$ for all).

We found differences in beta and gamma spectral across groups across most cortical regions. Gamma power was significantly decreased during virtual reality with perturbations training in left and right occipital areas compared to virtual reality without perturbations training (pairwise $p<0.001$ for all). This significant difference persisted through early and late training. The virtual reality with perturbations group also showed significant gamma power increases in left/right parietal and cingulate regions compared to the other two groups for both early and late training (pairwise $p<0.003$ for all). Beta power was significantly decreased in right frontal during virtual reality training with perturbations compared to both other groups (pairwise $p<0.001$ for all). We also found significantly decreased gamma power in left/right parietal regions during late training compared to early training for all 3 groups (pairwise $p<0.003$ for all).

Perturbation-evoked Body and Head Displacement

In our comparison of head and sacrum mediolateral displacement following perturbation onset, we found large, slow deviations preceding the perturbation onset for the virtual reality with perturbations group (Figure 3-7). Similar activity was also seen in the virtual reality without perturbations and unaltered viewing groups, suggesting that the deviations seen were primarily

due to movements while balancing. For virtual reality with perturbations, subjects received a 20° rotation perturbation, while the other two groups received a 0° pseudo-perturbation. The perturbation onset for all groups occurred shortly after subjects had both feet on the beam, which may explain why similar head and sacrum displacements were seen for both groups. In addition, we found nearly identical head and sacrum displacements during early and late training for all groups. This suggests that the visual perturbation did not induce consistent head motion artifact in our EEG results.

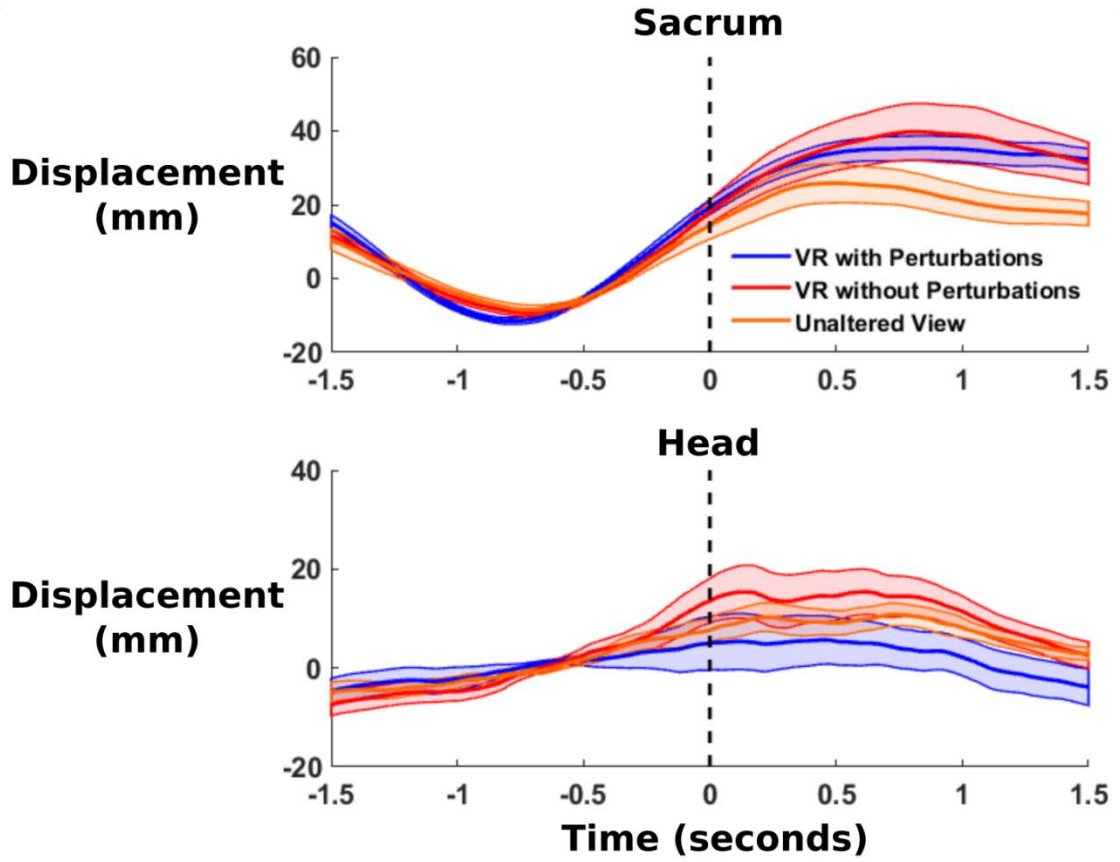

Figure 3-7: Perturbation-evoked head and sacrum motion. Average mediolateral motion capture marker trajectories are shown from the sacrum (top) and head (bottom) during training for virtual reality with perturbations (blue), virtual reality without perturbations (red), and unaltered view (orange), time-locked to the perturbation onset (n=10 for each group). In the case of the virtual reality without perturbations group, a pseudo-perturbation of 0° was performed. Motion capture trajectories were baseline subtracted to the 1.5 seconds preceding perturbation onset.

Discussion:

Virtual reality training with perturbations resulted in equivalent pretest-to-posttest improvement compared to unaltered viewing without virtual reality. Performance improvement in both groups were significantly increased compared to virtual reality training without perturbations, indicating that the visual rotation perturbations helped subjects overcome the negative effects of virtual reality. Similar training errors and physiological results between virtual reality groups indicated that the perturbations primarily induced a cognitive change. We found strong perturbation-evoked parietal and occipital activity, as hypothesized, but hardly any noticeable tuning based on perturbation direction. Subjects training in virtual reality with perturbations showed increased theta power in the cingulate, occipital, and frontal cortical regions compared to unaltered viewing and virtual reality training without perturbations. Perturbations training also decreased alpha power across multiple cortical regions compared to virtual reality training without perturbations. One interpretation of these findings is that our visual perturbations primed cortical areas to facilitate short-term motor learning equivalent to training without immersive virtual reality.

Behavioral & Physiological Measures

We found similar beam-walking improvement between virtual reality training with perturbations and unaltered viewing, indicating that the brief visual perturbations helped subjects overcome the negative effects of virtual reality. Both virtual reality training with perturbations and unaltered viewing showed significantly improved performance compared with virtual reality without perturbations. Increased improvement during perturbations training agrees with similar research using unexpected mechanical perturbations during walking to improve balance control (Kurz, et al., 2016). Comparing the two virtual reality groups, we found no evidence that the perturbation

affects the quantity of training errors, subjects' experience of virtual reality, or physical exertion. While the perturbation may induce similar sensorimotor adaptation as prism glasses (Nemanich & Earhart, 2015), the resulting improvement is not likely an after-effect and likely reflects changes in short-term motor learning. Based on the average perturbations during training (224), perturbations occurred approximately every 8 seconds during training. Each perturbation lasts one half-second, leaving subjects in an unperturbed view for ~93.8% of training. Long-lasting improvements might occur because of repeated exposure to the perturbation (Bastian, 2008; Krakauer, Ghez, & Ghilardi, 2005) with randomly presented perturbations in clockwise and counterclockwise directions to avoid directional dependencies. Repeatedly adapting to shifting visual input can improve subjects' ability to adapt to novel visual perturbations (Welch, Bridgeman, Anand, & Browman, 1993). Such adaptive generalization, also called learning to learn, has been seen during upper-limb movements (Seidler, 2004; Shadmehr & Moussavi, 2000) and gait training (Batson, et al., 2011; Mulavara, Cohen, & Bloomberg, 2009), with the anterior cingulate thought to be involved (Seidler, 2010). Similar virtual reality visual perturbations have improved responses to falls in older adults (Parijat, Lockhart, & Liu, 2015), although our paradigm induced more catastrophic errors whenever a perturbation occurred. Previous research has shown the importance of catastrophic errors, such as step-offs or falls, for improving stability (Domingo & Ferris, 2009).

In addition to differences in beam-walking improvement, perturbation training increased mediolateral head motion variability as training progressed compared to the unaltered viewing groups. Control of the head during stance perturbations is initiated by proprioceptive and vestibular signals (Allum, Gresty, Keshner, & Shupert, 1997; Héroux, Law, Fitzpatrick, & Blouin, 2015). This increase in head movement may reflect alterations in sensory processing of

the visual perturbation during training. However, this large increase in head movement during training does not translate to increased head movement from pretest to posttest. It is interesting to note that the unaltered view group had higher head motion variability than the virtual reality conditions during training and that increased change in head motion during training appeared to be potentially related to increased balance performance improvement. This may reflect the importance of training head motion during balance beam walking. We primarily found cognitive differences due to the visual perturbations, agreeing with visuomotor perturbation research during upper-limb movements (Anglin, Sugiyama, & Liew, 2017).

EEG Differences

EEG showed robust time-frequency activity during perturbation onset and termination in the parietal and occipital areas. Unpredictable perturbations during stance induce large EEG event-related potentials (Adkin, Quant, Maki, & McIlroy, 2006), with decreased amplitude when attention is diverted to a secondary task (Quant, Adkin, Staines, Maki, & McIlroy, 2004). We saw little activity in frontal areas in response to visual perturbations whereas frontal areas typically have large responses to mechanical perturbations (Maki & McIlroy, 2007; Mihara, Miyai, Hatakenaka, Kubota, & Sakoda, 2008). The exception to this was right frontal delta synchronization to the clockwise perturbations only. Our delta band results must be interpreted cautiously due to the close proximity of delta band to our high-pass filtering frequency of 1 Hz. In occipital and parietal areas, we found similar theta, alpha, and beta synchronization following perturbation onset and termination, which matches previous research (Varghese, et al., 2014). The beta desynchronization following this activity aligns with research indicating that beta desynchronization occurs when stability is important (Bruijn, Van Dieën, & Daffertshofer, 2015). While no differences in perturbation direction were found, we noticed larger magnitude

responses in right parietal and occipital areas, which may reflect increased right hemisphere involvement in position sensing (Iandolo, et al., 2018). Also, theta and alpha synchronization occurred in the cingulate region only during perturbation onset. Several studies suggest that the anterior cingulate functions as an error monitor (Anguera, Seidler, & Gehring, 2009; Carter, et al., 1998; Kerns, 2004; Miltner, et al., 2003), and our results showing increased activity during visuomotor conflict appear to support this claim. We also found increased gamma activity in occipital, parietal, and cingulate regions following perturbation onset and termination, which may indicate increased cognitive processing during instability (Slobounov, Cao, Jaiswal, & Newell, 2009; Sipp, Gwin, Makeig, & Ferris, 2013).

Power spectral analysis revealed significantly increased theta power for the virtual reality with perturbations group in frontal, occipital, and cingulate regions, likely related to differences in sensorimotor processing. Increased theta power is consistent with Slobounov et al., which found theta activity located in the anterior cingulate (Slobounov, Cao, Jaiswal, & Newell, 2009). Balance beam walking increases frontal theta power compared to walking on a treadmill (Sipp, Gwin, Makeig, & Ferris, 2013). Increased theta power also corresponds to more challenging balance tasks (Hülsdünker, Mierau, & Strüder, 2015; Youssofzadeh, Zanotto, Wong-Lin, Agrawal, & Prasad, 2016). Our increase in theta power may indicate improved sensorimotor processing during balancing and may be of interest for future studies with motor training interventions.

We also found wide-spread decreases in alpha power for the virtual reality perturbations group compared to virtual reality training without perturbations, likely indicating more active cortical processing. The unaltered view group also had significant decreases in alpha power in multiple regions compared to virtual reality training without perturbations, suggesting that alpha power

reflects impaired cortical processing due to virtual reality use. Regions with significantly decreased alpha power also showed significantly higher alpha power during late training compared to early training. This may indicate decreased mental engagement towards the end of training. Alpha activity decreases when walking compared to standing (Presacco, Goodman, Forrester, & Contreras-Vidal, 2011; Youssofzadeh, Zanotto, Wong-Lin, Agrawal, & Prasad, 2016), when walking in interactive virtual reality compared to walking while viewing a black screen (Wagner, Solis-Escalante, Scherer, Neuper, & Müller-Putz, 2014), and when walking with closed-loop brain-computer interface control of a virtual avatar compared to no closed-loop control (Luu, Nakagome, He, & Contreras-Vidal, 2017b). Centro-parietal alpha suppression has also been associated with improved stance stability (Del Percio, et al., 2007). Increased alpha power has been found in high fall-risk older adults compared to a low fall-risk group during perturbed balance (Chang, Yang, Yang, & Chern, 2016), showing similarity with our results where the subjects with improved balance showed reduced alpha power.

We also found significant differences in beta and gamma power across multiple regions, suggesting differences in active cortical processing during training (Başar, Başar-Eroglu, Karakaş, & Schürmann, 2001). Beta power decreased in the right frontal region during perturbations training compared to the other 2 groups, agreeing with research showing decreased beta power under more challenging balance conditions (Bruijn, Van Dieën, & Daffertshofer, 2015). This reinforces the idea that the perturbations may induce a greater challenge to stability than training without them. Perturbations training also increased parietal gamma power, which may indicate greater instability (Slobounov, Cao, Jaiswal, & Newell, 2009). The significant decrease in parietal gamma power from early to late training may indicate improved stability for all groups as a result of training. Yet, gamma power results should be interpreted with caution

due to the possible presence of neck muscle contamination, especially in the occipital regions. Fortunately, EEG differences across groups are not likely influenced by perturbation-induced artifacts based on similar mediolateral head movements around the perturbation onset (Figure 3-7).

Limitations of Virtual Reality Setup

Motor performance improvement during virtual reality training without perturbations was much lower than improvement during virtual reality training with perturbations and training with unaltered view (Table 3-1). There seems to be a decrement in short-term motor learning that occurs with virtual reality use compared to not using virtual reality at all, as expected from the literature. One contributing factor may be the field of view. Our virtual reality headset had a 100° field of view, whereas human field of view is at least 180° (Walker, Hall, & Hurst, 1976). Peripheral vision is important for maintaining stability (Amblard & Carblanc, 1980; Assaiante, Marchand, & Amblard, 1989); therefore decreased field of view could have impaired balance performance. Peripheral optic flow while wearing a headset can greatly reduce head and body sway during stance (Horiuchi, Ishihara, & Imanaka, 2017). Another possible factor is the refresh rate of the webcam (30 Hz) and headset (75 Hz), which can affect unipedal stance stability (Kawamura & Kijima, 2016). In contrast, stability in virtual reality may remain impaired even when controlling for field of view and refresh rate (Kelly, Riecke, Loomis, & Beall, 2008), suggesting further research is needed. See Steinicke et al. for further discussion (Steinicke, Visell, Campos, & Lécuyer, 2013).

It is also worth noting that the perturbation timing affects improvement. During pilot testing, we randomized perturbations to occur throughout training, which actually led to worse improvement for the virtual reality perturbations group (mean: 30.7%, SD: 59.0%, n=3) compared to the

virtual reality without perturbations group (mean: -16.4%, SD: 24.9%, n=3). By timing perturbations to consistently occur shortly after subjects stepped onto the beam, we appear to have maximized their impact. Future studies should also consider larger sample size per group and testing for longer learning and retention effects across days.

Conclusions

We used a novel visual rotation perturbation paradigm to overcome the negative effects of immersive virtual reality during a beam-walking balance task. These perturbations induced distinct electrocortical responses in parietal, occipital, and cingulate areas due to conflicts between sensory input during balance. Power spectra differences between virtual reality training groups showed increased theta power and decreased alpha power when training with perturbations compared to virtual training without perturbations across multiple cortical regions, indicating that the perturbations induced a change in cortical activity. The beam-walking improvements we found could not be explained as adaptation effects, suggesting short-term motor learning improvements in balance control. Such perturbation training may be useful in future immersive virtual reality paradigms to minimize the negative effects of virtual reality on short-term motor learning.

Chapter 4: Differentiation in Theta and Beta Electrocortical Activity between Visual and Physical Perturbations to Walking and Standing Balance[3]

Abstract

Human balance is a complex process in healthy adults, requiring precisely-timed coordination between sensory information, cognitive processing, and motor control. It has been difficult to quantify brain dynamics during human balance control due to limitations in brain imaging modalities. The goal of this study was to determine if by using high-density electroencephalography (EEG) and independent component analysis, we can identify common cortical responses to visual and physical balance perturbations during walking and standing. We studied the responses of 30 healthy young adults to sensorimotor perturbations that challenged their balance. Subjects performed four 10-minute trials of beam-walking and tandem stance while either being mediolaterally pulled at the waist or viewing brief 20° field-of-view rotations in virtual reality. We recorded high-density EEG, motion capture, lower leg electromyography (EMG), and neck EMG. We hypothesized that both physical pull and visual rotation perturbations would elicit time-frequency fluctuations in theta (4-8 Hz) and beta (13-30 Hz) bands, with increased occipito-parietal activity during visual rotations compared to pull perturbations. Our results confirmed this hypothesis. For both perturbations, we found early theta synchronization and late alpha-beta (8-30 Hz) desynchronization following perturbation onset. This pattern was strongest in occipito-parietal areas during visual perturbations and strongest in sensorimotor areas during pull perturbations. These results suggest a similar time-frequency

[3] This chapter has been accepted for publication in *eNeuro* (Peterson & Ferris, 2018).

electrocortical pattern when humans respond to sensorimotor conflict, but with substantive differences in the brain areas involved for visual vs. physical perturbations. Our findings may have important implications for assessing and training balance in individuals with and without motor disabilities.

Introduction

In the real world, humans must constantly make postural adjustments to avoid losing balance. Such adjustments require precise coordination between sensory input, cognitive processing, and motor control (Macpherson & Horak, 2012). Dual-tasking studies have highlighted the importance of human supraspinal centers for maintaining balance during walking and standing (Rankin, Woollacott, Shumway-Cook, & Brown, 2000; Woollacott & Shumway-Cook, 2002). Despite this, our current understanding of real-world human cortical activity in response to balance perturbations is limited (Varghese, McIlroy, & Barnett-Cowan, 2017). Traditional neuroimaging methods, such as functional magnetic resonance imaging (fMRI) and functional near-infrared spectroscopy (fNIRS), are limited by stationary subjects and low temporal resolution.

High-density, source-localized EEG is currently the most promising method to noninvasively assess human cognitive activity during balance. The strengths of EEG are its portability and high temporal resolution (Gramann, Ferris, Gwin, & Makeig, 2014; Gramann, et al., 2011). High temporal resolution is essential for quantifying brief cortical balance responses. EEG is typically limited by its low spatial resolution and susceptibility to artifact contamination (Urigüen & Garcia-Zapirain, 2015). However, blind-source separation techniques such as independent component analysis can separate out cortical activity from artifacts, both reducing the effects of artifacts and enhancing spatial resolution (Makeig, Bell, Jung, & Sejnowski, 1996; Gwin,

Gramann, Makeig, & Ferris, 2010). Independent component analysis also allows researchers to draw stronger conclusions about specific brain regions compared to channel data which contains activity from multiple regions due to volume conduction.

Healthy adult EEG balance studies have focused on theta (4-8 Hz) and beta (13-30 Hz) frequency bands (Varghese, McIlroy, & Barnett-Cowan, 2017). EEG recordings show decreased electrocortical beta power associated with active gait control (Wagner, Solis-Escalante, Scherer, Neuper, & Müller-Putz, 2014) and more challenging balance tasks (Sipp, Gwin, Makeig, & Ferris, 2013). Beta power in parietal and central cortical regions has been shown to decrease following sudden changes in gait patterns, indicating that beta power in these areas is involved in motor inhibition (Wagner, Makeig, Gola, Neuper, & Müller-Putz, 2016). In addition, brief EEG theta oscillations occur when subjects lose their balance (Sipp, Gwin, Makeig, & Ferris, 2013) or are exposed to external perturbations (Varghese, et al., 2014). Other healthy adult EEG studies have indicated that theta may be related to changes in balance performance (Hülsdünker, Mierau, & Strüder, 2015; Slobounov, Teel, & Newell, 2013). It seems likely that increased theta and decreased beta power are involved during active balance control and may fluctuate as balance difficulty changes.

In addition to physical manipulations such as pushing the subject or suddenly translating the support surface (Adkin, Campbell, Chua, & Carpenter, 2008; Duckrow, Abu-Hasaballah, Whipple, & Wolfson, 1999), manipulated sensory information can provide insight into cortical sensory integration during balance control. In contrast to physical perturbations, sensory manipulations such as restricted vision, altered surface firmness, and auditory feedback target specific sensory input (Pirini, Mancini, Farella, & Chiari, 2011; Tse, et al., 2013). Sensory perturbations are advantageous for EEG experiments because they do not directly move the

subject in a consistent manner, unlike physical perturbations, reducing the effects of motion artifact (Kline, Huang, Snyder, & Ferris, 2015).

In particular, visual manipulations can greatly impact healthy adult electrocortical dynamics and balance control by inducing conflict among visual, vestibular, and proprioceptive inputs. Blindfolded walking in healthy adults has shown increased EEG spectral power in somatosensory areas (Oliveira, Schlink, Hairston, König, & Ferris, 2017a), indicating that visual manipulations can substantially alter electrocortical dynamics. Similarly, visual rotations using prism goggles can increase mediolateral sway during stance due to sensory conflict caused by inaccurate visual input (Cauquil, Bessou, Dupui, & Bessou, 1998). Also, perturbed optical flow can increase healthy adult parietal theta power (Slobounov, Teel, & Newell, 2013). Understanding visual processing during balance control is important because over-reliance on vision is a cause of increased falls in older adults (Franz J. R., Francis, Allen, O'Connor, & Thelen, 2015).

The purpose of our study was to identify similarities and differences in healthy adult electrocortical activity between physical pull and visual rotation perturbations during beam walking and tandem stance. We used a mediolateral pull to the subject's waist to physically challenge balance. For the visual perturbation, subjects wore a virtual reality head-mounted display that induced a 20° visual field rotation during beam walking and tandem stance. We hypothesized that both the physical pull and visual perturbations would transiently increase theta power (4-8 Hz) and decrease beta power (13-30 Hz), indicating cortical detection of perturbed balance and decreased motor inhibition, respectively. We also expected that visual rotations would increase fluctuations in occipito-parietal areas based on the prominent cortical areas for visual processing whereas physical pull perturbations would increase cortical activity in central

sensorimotor areas due to large EEG event-related potentials seen in these areas during physical perturbations, likely indicating planning of a motor response (Marlin, Mochizuki, Staines, & McIlroy, 2014).

Materials & Methods

Subjects

We tested 30 healthy, young adults [15 females-15 males, age 22.5±4.8 years (mean±standard deviation (SD))] for this study. All subjects identified themselves as right hand and right foot dominant, with normal or corrected vision. We screened subjects for any neurological, orthopedic, or cardiac conditions and injuries. All subjects provided written informed consent. Our protocol was approved by the University of Michigan Health Sciences and Behavioral Sciences Institutional Review Board for the protection of human subjects.

Before each experiment, we screened subjects for motion sickness in virtual reality. Subjects stood in place for a 5 minute activity while wearing a virtual reality headset (Oculus Rift DK2, Oculus VR, Irvine, CA). Subjects walked and jumped around a virtual environment using body gestures tracked by a Microsoft Kinect v2 (Microsoft, Redmond, WA). We included a disconnect between real and virtual movements to be more disorienting than our main testing protocol. Subjects participated in the main experiment if both the subject and experimenter agreed that they did not exhibit any symptoms of motion sickness. Two potential subjects exhibited motion sickness symptoms and did not participate in the experiment; 30 subjects passed this screening.

Experiment Design

Subjects either walked at 0.22 m/s or stood on a 2.5 cm tall by 12.7 cm wide balance beam mounted to a treadmill. Subjects wore a body-support harness for safety, with extended support

straps to allow for unrestricted mediolateral movement. The beam was designed to be wide enough for a single foot to enforce tandem gait and tandem stance. We gave subjects specific instruction to look straight ahead and to avoid looking at their feet. We instructed subjects to only move their hips side-to-side to balance when on the balance beam, avoiding rotations across their body's longitudinal axis. Subjects also crossed their arms and walked heel-to-toe during the walking conditions. These instructions followed previous studies (Domingo & Ferris, 2009; Domingo & Ferris, 2010). We had subjects cross their arms while walking so that subjects avoided swinging their arms to stabilize themselves. It made the task more difficult and also conformed with previous studies on treadmill balance beam walking (Domingo & Ferris, 2009; Domingo & Ferris, 2010; Sipp, Gwin, Makeig, & Ferris, 2013). Crossed arms can also reduce inter-subject variability during the task because there is no variation in arm movement.

We used two types of perturbations during testing: a visual field rotation and a mediolateral pull to one side (Figure 4-1). We randomly selected half of the subjects to perform visual rotations first while the other half performed the pull perturbations first. The visual field rotation was presented with an Oculus Rift virtual reality headset. Subjects saw the view of a webcam mounted to the headset. This view was digitally rotated 20° clockwise or counterclockwise for 0.5 sec. For the pull perturbation, subjects were physically pulled by one of two electromechanical motors [Chiaphua Industries Motor (CIM)] placed on either side of the treadmill. When commanded (dSPACE GmbH, Paderborn, Germany), one motor rotated an attached bar 90° away from the subject, which pulled on a steel cable connected to the subject's safety harness. The motor rotated back 1 sec after the initial rotation. Tensile load cells (LCM703, OMEGA Engineering, INC., Norwalk, CT) were attached in series with the steel cable on either side to record pull force and onset. Both perturbation types were presented using

predefined pseudo-random sequences. Subjects were exposed to each perturbation for 10 minute conditions of 150 perturbations each (75 per side). We had subjects exposed to each of these perturbations while standing and while walking (4 trials total). Subjects were asked to stand in tandem stance, with their right foot in front of the left. Subjects walked at a speed of 0.22 m/s to enable subjects to maintain balance consistently on the balance beam.

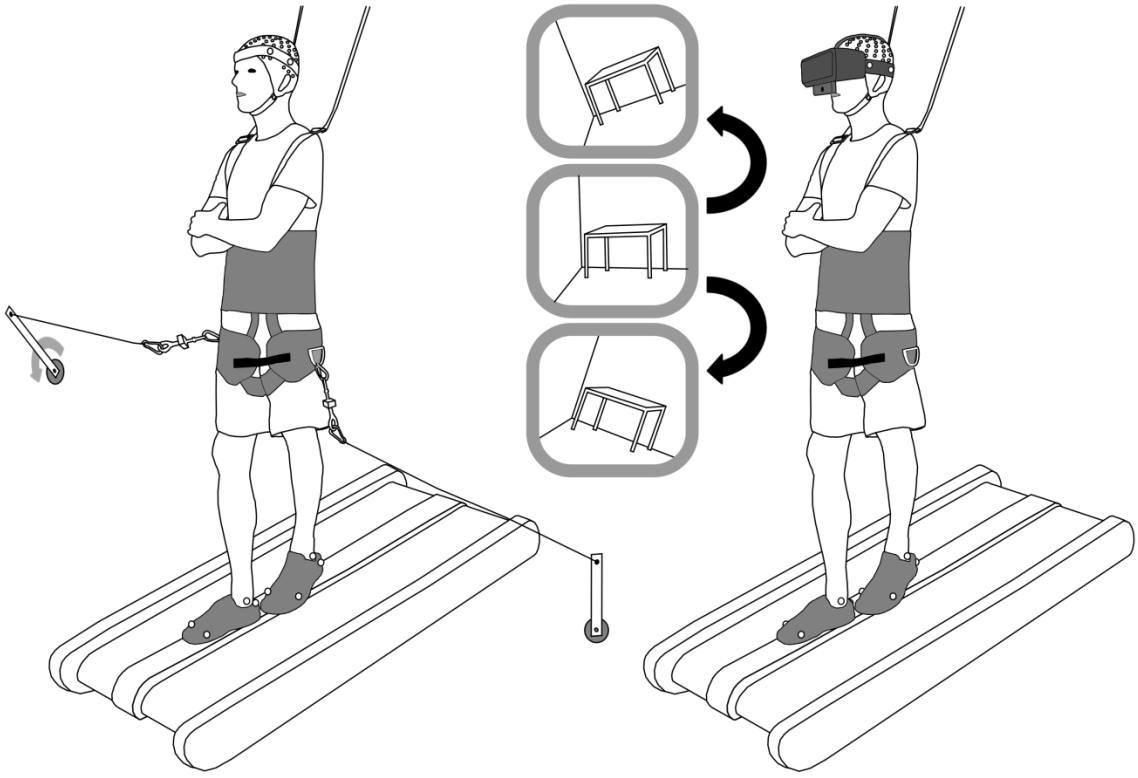

Figure 4-1: Experiment setup. A sketch of a subject walking on the beam, exposed to pull (left) and visual rotation (right) perturbations. Subjects wore a body-support harness for all conditions. The inset sketches show example 20° perturbations in counterclockwise (top) and clockwise (bottom) directions. Subjects were exposed to pull and visual rotation perturbations during separate 10-minute trials of standing and walking, leading to 4 total trials per subject.

We recorded EEG using a 136-channel system (BioSemi Active II, BioSemi, Amsterdam, NL), sampled at 512 Hz. Two of the EEG electrodes were used to record left and right neck muscle activity. EEG electrode positions were measured using a Zebris ELPOS digitizer (Zebris Medical GmbH, Isny, Germany). We also recorded motion capture from 16 reflective markers on the feet,

sacrum, neck, and head (Vicon, Los Angeles, CA). We recorded EMG from 4 lower leg muscles of each leg (tibialis anterior, soleus, medial gastrocnemius, and peroneus longus), sampled at 1000 Hz (Biometrics, Ladysmith, VA). We used a 0.5 Hz square pulse to synchronize the recording systems.

To analyze perturbation-evoked activity, we needed to determine perturbation onset events. For visual perturbations, we programmed keyboard button presses on the virtual reality computer keyboard to correspond with perturbation onset, using Windows Input Simulator. This keyboard input was recorded and synchronized with the EEG data using Lab Streaming Layer (Delorme, et al., 2011). Pull perturbation events were determined by finding peaks in detrended load cell data. We estimated the pull onset events by finding when the load cell voltage first went 3 standard deviations above baseline voltage prior to each peak and manually inspected each to ensure accuracy. We used these onset times as the final pull perturbation events.

Behavioral and Physiological Measures

We used cleaned, mediolateral motion capture marker trajectories from the head and sacrum to estimate perturbation-evoked changes in stability and overall stability during each trial. We estimated body and head sway during each trial with mediolateral standard deviation of the sacrum and head markers. We ran a 2x2 repeated measure ANOVA to test for main effects of perturbation type (pull vs. rotate) and physical task (standing vs. walking). Post-hoc pairwise comparisons were performed using t-tests with false discovery rate correction ($p<0.05$) (Benjamini & Yekutieli, 2001). We also analyzed the perturbation-evoked head and sacrum mediolateral displacement. Marker trajectories were detrended, 6 Hz low-pass filtered, and fully rectified. We epoched the result around each perturbation onset, subtracted baseline motion for the half-second before perturbation onset, and averaged the result for each perturbation type.

Peak load cell voltages were used to determine if pull forces differed due to the physical task (standing vs. walking) or pull direction (left vs. right). We converted peak detrended load cell voltages to pull forces (in N) based on prior calibration of the load cells with known weights. A 2x2 repeated measure ANOVA analyzed main effects of physical task and pull direction on peak pull force.

We also analyzed perturbation-evoked EMG activity in the lower leg. EMG data were detrended, 20 Hz high-pass filtered, and full-wave rectified (Sipp, Gwin, Makeig, & Ferris, 2013). We used 3 minutes of 0.22 m/s baseline tandem walking to normalize the EMG activity for each muscle electrode. Baseline walking occurred without perturbations and without the virtual reality headset. EMG activity during baseline walking was detrended, 20 Hz high-pass filtered, and full-wave rectified. We then time-warped the baseline EMG to the gait cycle (beginning and ending at right heel strike) and averaged across gait cycles for each EMG electrode. We found 45.9±18.9 baseline gait cycles per subject (mean±SD). The maximum value of the average time-warped gait cycle for each EMG electrode was used for normalization. Such peak gait cycle normalization has been shown to reduce inter-subject variability compared to using maximum voluntary contractions (Yang & Winter, 1984). We epoched the normalized EMG activity around each perturbation onset, subtracted baseline activity during the half-second before perturbation onset, and averaged across trials for each perturbation type. Based on these results, we averaged the perturbation-evoked EMG over a 0.3 sec time window (0.2-0.5 after perturbation onset) for each subject to statistically compare peak EMG activity. 2x4 repeated measure ANOVA tests analyzed intra-condition main effects of muscle type (tibialis anterior, soleus, gastrocnemius, peroneus longus) and body side (left vs. right). We also used a 2x2

repeated measure ANOVA to test for inter-condition main effects of physical task and perturbation type. Post-hoc pairwise comparisons were performed using t-tests, corrected for multiple comparisons using false discovery rate.

To test for the presence of adaptation effects during each trial, we calculated the pull force, peak EMG amplitude, and mediolateral marker position for the head and sacrum during the first and last minute of each trial. We performed 2x4 repeated measure ANOVA tests to look for significant main effects of trial type and adaptation (first minute vs. last minute). Post-hoc pairwise comparisons were performed using t-tests with false discovery rate correction. All non-EEG statistics were calculated in R (R Core Team, 2017), with statistical significance determined if $p<0.05$.

EEG Data Processing

We processed all EEG data using custom EEGLAB scripts (Delorme & Makeig, 2004). EEG data was downsampled to 256 Hz, 1 Hz high-pass filtered, merged across all conditions, and referenced to the common median of all channels. We reduced 60 Hz line noise using Cleanline (Mullen T. R., 2014). We rejected bad channels that had high standard deviation, had kurtosis above 5 standard deviations, or were uncorrelated for more than 1% of the time (Kline, Huang, Snyder, & Ferris, 2015; Luu, Brantley, Nakagome, Zhu, & Contreras-Vidal, 2017c). We retained 111±7 channels (mean±SD).

We further denoised the remaining EEG channels. To remove large mechanical artifacts, we used artifact subspace reconstruction (Mullen, et al., 2013) with a threshold of 20 standard deviations, which has been used in a previous mobile EEG study (Artoni, et al., 2017). We also performed selective low-pass filtering using ensemble empirical mode decomposition (Al-

Subari, et al., 2015; Wu & Huang, 2009) and canonical correlation analysis (Hotelling, 1936), similar to Roy et al. (Roy, Shukla, Shukla, & Rawat, 2017). This specifically targeted large high-frequency activity with low autocorrelation such as muscle activity and line noise (Safieddine, et al., 2012). We then re-referenced the data to the common average and interpolated the rejected channels to maintain a consistent montage across the head.

Next, we ran independent component analysis on the data using adaptive mixture independent component analysis (AMICA) (Palmer, Kreutz-Delgado, & Makeig, 2006; Palmer, Makeig, Kreutz-Delgado, & Rao, 2008). Prior to this, we ran principal component analysis to ensure that the data sent into independent component analysis was full rank. We reduced down to 90 principal components for all subjects to maximize the ratio of data points to channels, which helps ensure that independent component analysis can properly separate sources of activity (Särelä & Vigário, 2003).

After independent component analysis, we fit each independent component to an equivalent dipole using DIPFIT2, retaining components that explained greater than 85% of the scalp variance (Oostenveld & Oostendorp, 2002). We removed non-cortical components based on visual inspection of dipole location and power spectra, retaining 240 total dipoles. These remaining cortical dipoles were clustered using k-means, with weights of 10 for dipole locations, 2 for power spectra, and 1 for scalp maps. Dipoles greater than 3 standard deviations from the final clusters were placed in an outlier cluster. We analyzed clusters containing dipoles from more than half of the subjects (>15), which resulted in 8 clusters (Figure 4-2). These clusters were located in left occipital (18 subjects, 25 dipoles), right occipital (16 subjects, 22 dipoles), posterior parietal (23 subjects, 29 dipoles), anterior parietal (18 subjects, 23 dipoles), left

sensorimotor (23 subjects, 25 dipoles), right sensorimotor (22 subjects, 30 dipoles), supplementary motor (27 subjects, 48 dipoles), and anterior cingulate (16 subjects, 18 dipoles).

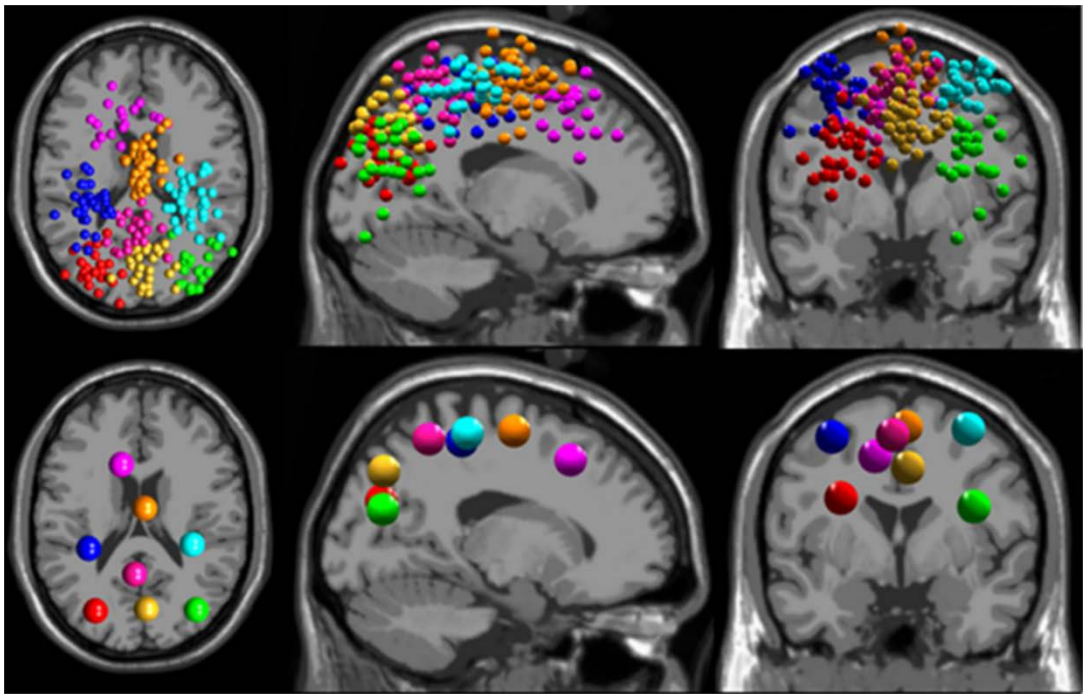

Figure 4-2: Source-localized dipole clusters across subjects. The resulting cortical dipoles corresponding to independent components are shown (top) for all subjects (n=30), colored according to its corresponding cluster. Cluster centroids are shown (bottom) in axial (left), sagittal (middle), and coronal (right) views. Cluster coloring is: left occipital (red), right occipital (green), posterior parietal (yellow), anterior parietal (pink), left sensorimotor (blue), right sensorimotor (cyan), supplementary motor (orange), and anterior cingulate (purple).

To analyze electrocortical activity during each trial, we calculated average EEG log power spectra. We compared spectral differences across trials by averaging spectral power into 4 frequency bands: theta (4-8 Hz), alpha (8-13 Hz), beta (13-30 Hz), and gamma (30-100 Hz). 2x2 nonparametric permutation test repeated measure ANOVAs were used to analyze main effects of perturbation type and physical task for each frequency band, with 2000 permutations for each test. Further pairwise comparisons were performed using Wilcoxon rank-sum tests, corrected for multiple comparisons using false discovery rate. These statistics were performed in MATLAB (MATLAB 2013a, Mathworks, Natick, MA), with significance if $p<0.05$ for all tests.

We assessed perturbation-evoked electrocortical activity with EEG log time-frequency activity averaged across epochs, known as event-related spectral perturbations (ERSPs). We split the data into 2-sec epochs (0.5 sec before to 1.5 sec after perturbation onset), resulting in 150±1 epochs for stand pull, 145±22 epochs for walk pull, 148±7 epochs for stand rotate, and 149±0 epochs for walk pull (mean±SD). We subtracted baseline activity for the half-second preceding perturbation onset. We used bootstrap statistics in MATLAB to determine significant differences from baseline, with a significant difference if $p<0.05$. Non-significant values were set to 0. When calculating ERSPs, we took the median across trials instead of the mean to ensure that any large power fluctuations from a single trial did not skew the final ERSP results.

Because of the consistent spectral pattern across clusters, we were able to quantify the onset of each perturbation-evoked synchronization and desynchronization. We chose the largest contiguous region between 200 ms before and 500 ms after the perturbation onset, specifying frequency bands of 4-13 Hz for the synchronization and 8-30 Hz for the desynchronization. These bands were chosen based on the frequencies of the major ERSP fluctuations for both perturbation types. We defined the onset latency as the first time bin when the ERSP was outside of ±1 dB. This was performed on significance masked ERSPs for every dipole within each cluster. For each cluster, we performed one-way Kruskal-Wallis tests to test for a significant effect of synchronization vs. desynchronization onsets. We also performed two separate Kruskal-Wallis tests for significant effects of perturbation type (rotations vs. pulls) and physical task (standing vs. walking) for each of the synchronization and desynchronization onsets (5 total tests per cluster). We performed these statistics in R, with significance if $p<0.05$.

We also assessed neck muscle EMG recorded from two EEG external electrodes placed on the back of the neck, approximately 5 cm above the seventh cervical vertebrae (C7) and 1 cm to either side. We referenced these externals to the EEG common-average reference and use artifact subspace reconstruction to remove any gross artifact. We epoched the muscle activity into the same 2-sec epochs as the EEG data, calculating average EEG log power spectra and ERSPs using the same methods as the EEG data. We performed the same ERSP significance masking and 2x2 nonparametric permutation test repeated measure ANOVAs for the power spectra, with significance if $p<0.05$. We have included statistical tables summarizing all statistical tests performed (Table 4-1, Table 4-2, Table 4-3). Note that all pairwise comparisons used a false discovery rate correction (Benjamini & Yekutieli, 2001), and all p-values presented for these comparisons are adjusted to keep the false positive (alpha) threshold at 0.05.

Table 4-1: Statistical table for behavioral analyses

Measure	Data Structure	Type of test	Power (parametric) or 95% confidence interval (non-parametric)
Pull force	Normal	2x2 repeated measure ANOVA	Pull direction: 0.568, physical task: 0.360, interaction: 0.059
Sacrum marker SD (Fig. 4A)	Normal	2x2 repeated measure ANOVA	Perturbation type: 1.00, physical task: 0.997, interaction: 0.358
Head marker SD (Fig. 4B)	Normal	2x2 repeated measure ANOVA	Perturbation type: 1.00, physical task: 0.998, interaction: 0.378
EMG intra-conditions (Fig. 5)	Normal	2x4 repeated measure ANOVA	Stand Pull (Muscle type: 1.00, body side: 1.00, interaction: 0.730), Walk Pull (Muscle type: 1.00, body side: 0.054, interaction: 0.228), Stand Rotate (Muscle type: 0.206, body side: 0.088, interaction: 0.153), Walk Rotate (Muscle type: 0.217, body side: 0.233, interaction: 0.123)
EMG inter-conditions (Fig. 5)	Normal	2x2 repeated measure ANOVA	Perturbation type: 0.950, physical task: 1.00, interaction: 0.988
Behavioral adaptation (Fig. 6)	Normal	2x2 repeated measure ANOVA	Pull force (trial type: 0.698, adaptation: 0.589, interaction: 0.052), peak EMG (trial type: 1.00, adaptation: 0.379, interaction: 0.196), head marker SD (trial type: 1.00, adaptation: 0.111, interaction: 0.896), sacrum marker SD (trial type: 1.00, adaptation: 0.263, interaction: 0.174)

The data structure, type of statistical test used, and statistical power are shown for all behavioral statistical tests performed. We calculated two-way repeated measure ANOVA power using the anova_stats() function from the sjstats library in R.

Table 4-2: Statistical table for event-related spectral perturbation (ERSP) onsets

Measure	Data Structure	Type of test	95% confidence interval
EEG ERSP onset latencies between synchronization/ desynchronization (Fig. 10)	Non-normal	One-way Kruskal-Wallis test	Left occipital (sync: 52.7-105, desync: 182-242), right occipital (sync: 54.7-114, desync: 160-203), posterior parietal (sync: 23.4-70.3, desync: 176-234), anterior parietal: (sync: 54.7-145, desync: 188-250), left sensorimotor (sync: 39.1-113, desync: 137-203), right sensorimotor (sync: 82.0-145, desync: 195-250), supplementary motor area (sync: 54.7-97.7, desync: 160-258), anterior cingulate (sync: 137-203, desync: 129-234)
EEG ERSP synchronization onset (Fig. 10)	Non-normal	2 one-way Kruskal-Wallis tests	**Stand** (Left occipital: 39.1-105, right occipital: 54.7-112, posterior parietal: 7.81-54.7, anterior parietal: 7.81-97.7, left sensorimotor: 7.81-76.2, right sensorimotor: 31.2-113, supplementary motor area: 39.1-84, anterior cingulate: 113-211), **walk** (Left occipital: 39.1-189, right occipital: 54.7-129, posterior parietal: 54.7-113, anterior parietal: 97.7-188, left sensorimotor: 82.0-176, right sensorimotor: 97.7-188, supplementary motor area: 82.0-121, anterior cingulate: 113-256), **pull perturbation** (Left occipital: 70.3-189, right occipital: 70.3-152, posterior parietal: 54.7-152, anterior parietal: 23.4-160, left sensorimotor: 15.6-89.8, right sensorimotor: 70.3-145, supplementary motor area: 7.81-39.1, anterior cingulate: 82.0-174), **rotation perturbation** (Left occipital: 23.4-70.3, right occipital: 26.8-105, posterior parietal: 7.81-54.7, anterior parietal: 37.9-143, left sensorimotor: 39.1-160, right sensorimotor: 70.3-160, supplementary motor area: 113-176, anterior cingulate: 176-242)
EEG ERSP desynchronization onset (Fig. 10)	Non-normal	2 one-way Kruskal-Wallis tests	**Stand** (Left occipital: 182-281, right occipital: 160-219, posterior parietal: 176-234, anterior parietal: 197-266, left sensorimotor: 145-219, right sensorimotor: 188-250, supplementary motor area: 176-309, anterior cingulate: 97.7-266), **walk** (Left occipital: 137-219, right occipital: 145-227, posterior parietal: 176-234, anterior parietal: 129-281, left sensorimotor: 113-211, right sensorimotor: 160-273, supplementary motor area: 70.3-234, anterior cingulate: 54.7-266), **pull perturbation** (Left occipital: 82.0-273, right occipital: 84.0-219, posterior parietal: 105-234, anterior parietal: 189-316, left sensorimotor: 121-195, right sensorimotor: 160-250, supplementary motor area: 145-309, anterior cingulate: 99.8-281), **rotation perturbation** (Left occipital: 188-242, right occipital: 188-219, posterior parietal: 196-234, anterior parietal: 176-250, left sensorimotor: 145-250, right sensorimotor: 188-258, supplementary motor area: 113-242, anterior cingulate: 54.7-242)

Data structure, type of statistical test used, and 95% confidence intervals are shown for ERSP onset. We calculated 95% confidence intervals using bootstrap statistics with 5000 replicates.

Table 4-3: Statistical table for EEG power analyses

Measure	Data Structure	Type of test	95% confidence interval
EEG power spectra (Fig. 7)	Non-normal	2x2 permutation repeated measure ANOVA	-
EEG ERSPs (Figs. 8 & 9)	Non-normal	Bootstrap statistics	-
Neck power spectra (Fig. 11)	Non-normal	2x2 permutation repeated measure ANOVA	-
Neck muscle ERSPs (Fig. 11)	Non-normal	Bootstrap statistics	-

The data structure and type of statistical test used are shown for EEG event-related spectral power (ERSP) and power spectra statistical comparisons performed. We did not include power or confidence intervals due to the high number of comparisons performed.

Results

Marker Standard Deviation & Perturbation Response

Pull perturbations induced rapid mediolateral displacements in the subject's head and torso, but visual perturbations led to a delayed head mediolateral displacement that was more prominent for walking compared to standing (Figure 4-3). Mediolateral head and sacrum position changed starting at approximately 400 ms after perturbation onset. In contrast, visual perturbations during standing induced no noticeable displacements in head and sacrum. Average head and sacrum displacements following perturbation onset were small, indicating that minimal motion artifact is present in the EEG (Figure 4-3). Marker displacements were primarily under 1 cm, suggesting little head and sacrum motion immediately following perturbation onset. The walk rotate trial appears to induce the largest deviation of the head, which is most pronounced approximately 1

sec after perturbation onset. This suggests a lack of consistent head motion immediately following perturbation onset. Based on this, we would expect minimal motion artifact in the EEG data.

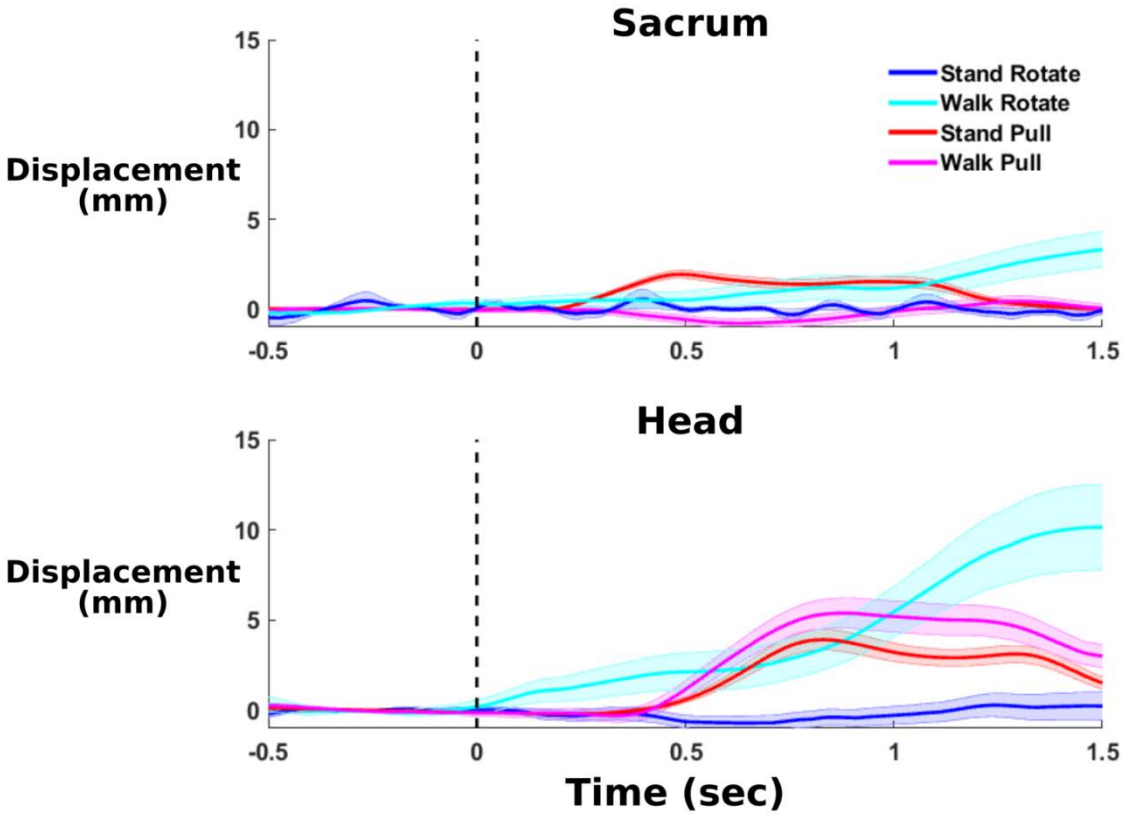

Figure 4-3: Motion capture marker perturbation-evoked displacement. Average sacrum (top) and head (bottom) mediolateral displacement is shown for all conditions (n=30), time-locked to the perturbation onset at 0 sec (shading shows standard error). We rectified displacements to quantify average mediolateral movements away from the beam in either direction. We subtracted off baseline activity during the half-second prior to perturbation onset. Displacements of both markers stayed near or below 0.5 cm for the first second after the perturbation onset, indicating little consistent head or body mediolateral movement to the perturbation. This suggests that there is likely minimal motion artifact in the EEG data.

Across each entire trial, estimated sacrum and head mediolateral sway was notably increased during walk rotate and decreased during stand pull (Figure 4-4). Our 2x2 repeated measure ANOVA test found significant main effects of perturbation type (sacrum: p=1.62e-7, head: p=1.09e-12) and physical task (sacrum: p=8.08e-6, head: p=3.47e-6) for both markers. The

interaction terms were not significant. Pairwise comparisons for both markers found that walk rotate had significantly increased standard deviation compared to stand pull (sacrum: p=2e-16, head: p=2.1e-12), walk pull (sacrum: p=2.7e-12, head: p=1.1e-9), and stand rotate (sacrum: p=0.004, head: p=0.003). Marker standard deviation was also significantly decreased during stand pull compared to walk pull (sacrum: p=4.5e-11, head: p=1.2e-8) and stand rotate (sacrum: p=0.047, head: p=1.7e-3). We found no other significant differences. Note that this estimated sway is the average across the entire trial and does not reflect the perturbation-evoked displacement responses shown in Figure 4-3.

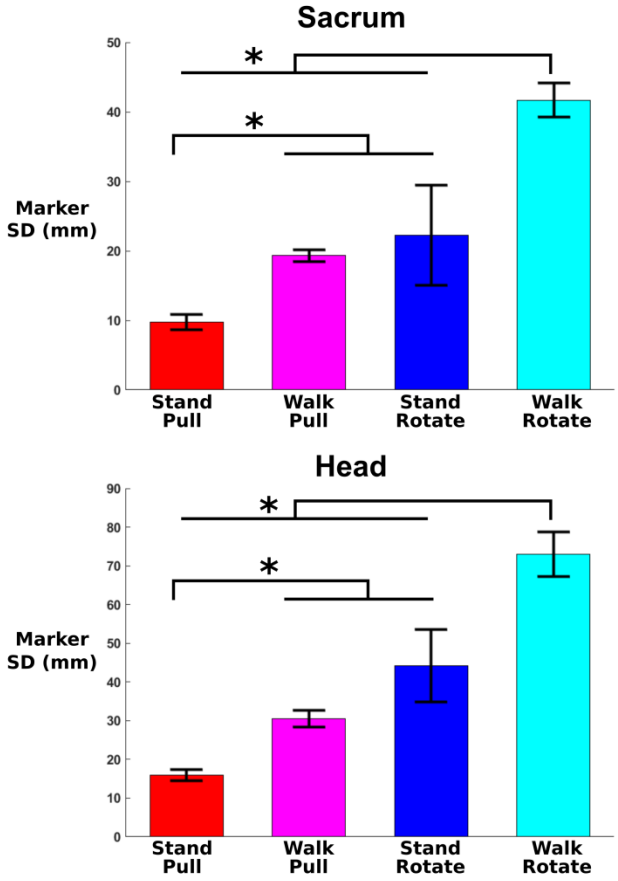

Figure 4-4: Mean mediolateral marker standard deviation across trials. The average sacrum (top) and head (bottom) mediolateral standard deviation for each entire trial is shown (n=30; error bars show standard error). Asterisks indicate significant pairwise differences ($p<0.05$). Both head and sacrum mediolateral sway indicate that subjects had the least side-to-side movement to pull perturbations during stance and the most movement to visual rotations during walking.

Pull Force Results

We found no differences in pull perturbation force between walking and standing trials, and between right and left pulls. Pull forces to the subject's left side were 16.73±6.56 N during standing and 15.76±6.23 N during walking (mean±SD). Pull forces to the subject's right side were 15.38±2.15 N during standing and 14.00±2.54 N during walking. While we found a significant main effect of pull direction (p=0.035), we found no significant pairwise differences in pull direction during standing (p=0.420) and walking (p=0.420). We found no significant main effect of physical task (p=0.112), and the interaction term was also not significant (p=0.778).

EMG Perturbation Response

We found substantial differences in peak EMG activity across muscles following perturbation onset, along with notably increased left leg EMG compared to right leg during stand pull. The average EMG perturbation response is shown in Figure 4-5. The 2x4 repeated measure ANOVA test for stand pull found significant main effects for muscle type (p=3.68e-9), body side (p=2e-16), and their interaction (p=0.027). Pairwise comparisons showed significant increases in all left side muscles compared to right muscles (tibialis anterior: p=0.0087, gastrocnemius: p=5.17e-11, peroneus longus: p=5.58e-7), except for soleus (p=0.065). Across muscles, we found significantly decreased soleus activity compared to tibialis anterior (p=6.94e-6) and peroneus longus (0.021). Gastrocnemius peak EMG was also significantly decreased compared to tibialis anterior (p=1.32e-6) and peroneus longus (p=0.002). Tibialis anterior peak EMG was also significantly greater than peak peroneus longus EMG (p=0.039). No other significant pairwise comparisons were found. For walk pull, we found a significant main effect of muscle type (p=4.38e-14), with significantly decreased soleus and gastrocnemius EMG compared to tibialis anterior (soleus: p=7.12e-6, gastrocnemius: p=3.17e-13) and peroneus longus (soleus: p=3.66e-5,

gastrocnemius: p=8.26e-13). Peak gastrocnemius EMG was significantly decreased compared to soleus (p=1.65e-8). No other comparisons were significant. ANOVA tests for stand rotate and walk rotate found no significant effects.

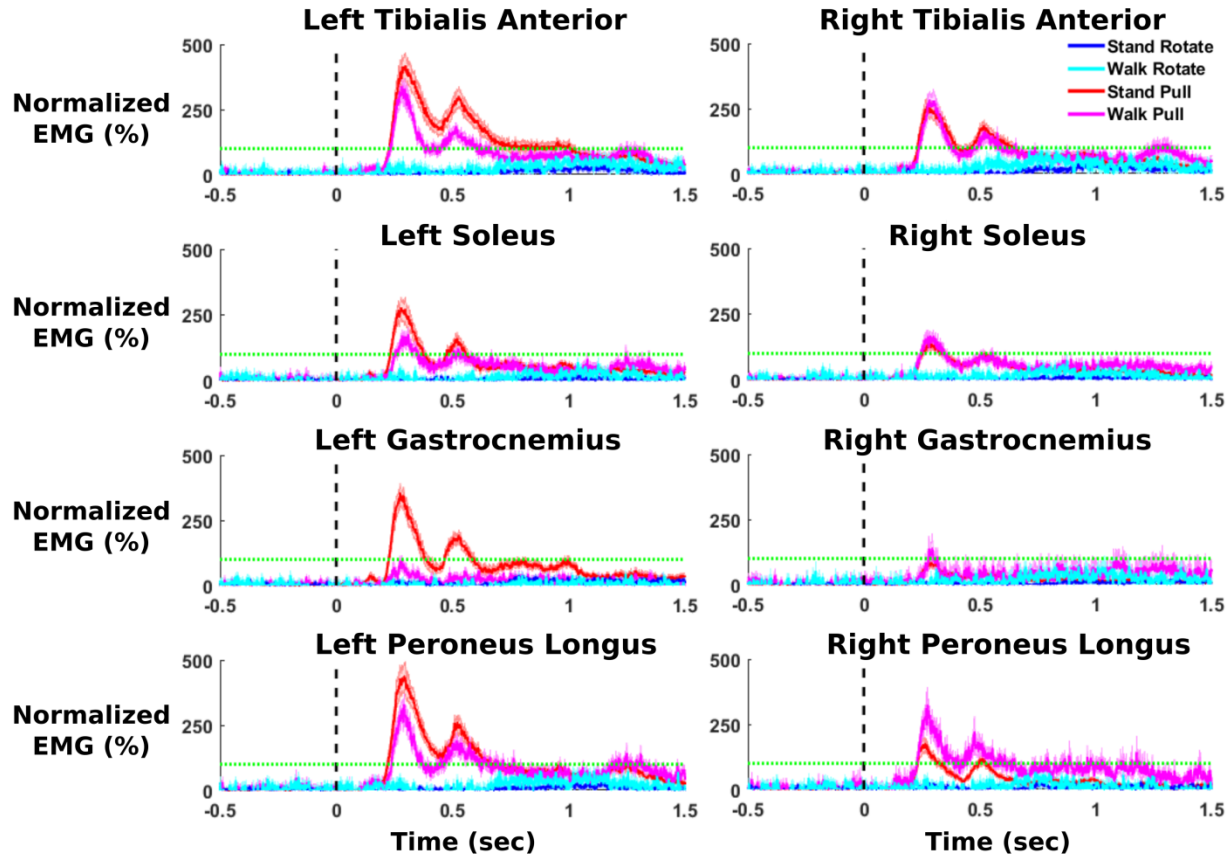

Figure 4-5: EMG perturbation-evoked activity. Average rectified EMG activity is shown for 8 lower leg muscles across all trials (n=30), time-locked to the perturbation onset at 0 sec (shading shows standard error). Each muscle's activity was normalized to peak EMG activity during the 15 seconds of walking prior to perturbation onset during the walk pull condition. The horizontal green line indicates this 100% peak EMG activity during walking. We subtracted off the baseline activity during the half-second before perturbation onset. Pull perturbations show clear increases in muscle activity following perturbation onset, with substantially increased left leg muscle activity to pull perturbations administered during standing. This is especially noticeable between the left and right medial gastrocnemius.

For EMG across all 4 conditions, pull perturbations substantially increased peak EMG compared to visual perturbations, with notable differences in muscle activity between standing and walking. Our 2x2 repeated measure ANOVA across all 4 conditions showed a significant main

effect of physical task (p=3.32e-4), a significant main effect of perturbation type (p=2e-16), and a significant interaction term (p=2.53e-5). For pairwise comparisons, we found significantly increased peak EMG activity between the pull and rotate conditions for almost all muscles. The only exception was that the right gastrocnemius muscle did not significantly differ between walk pull and both stand rotate (p=0.077) and walk rotate (p=0.171). We found significantly increased EMG during stand pull compared with walk pull for left tibialis anterior (p=0.008), left soleus (p=0.025), left gastrocnemius (p=2.17e-11), and left peroneus longus (p=0.003). In contrast, we found significantly increased right peroneus longus (p=0.002) EMG during walk pull compared to stand pull.

Behavioral Adaptation during Each Trial

There was no notable adaptation in any behavioral measure from the first to last minute of each trial. Comparing the first minute to the last minute of each 10-minute trial showed no statistical differences in standard deviation of sacrum (p=0.187) and head (p=0.474) marker mediolateral position or pooled EMG amplitude across muscles (p=0.099), as shown in Figure 4-6. We did find a significant adaptation of pull force (p=0.031), but no pairwise comparisons were significant (p=0.200 for walk pull early vs. stand pull late; p=0.410 for all other comparisons). There was also a significant interaction between trial and adaptation effects for the head mediolateral standard deviation (p=0.004). Post-hoc pairwise t-tests found no significant adaptation effects for head mediolateral standard deviation during stand pull (p=0.208), walk pull (p=0.141), stand rotate (p=0.118), and walk rotate (p=0.118). Adaptation effects appeared minimal during each trial, indicating that each trial can be considered reasonably consistent from beginning to end.

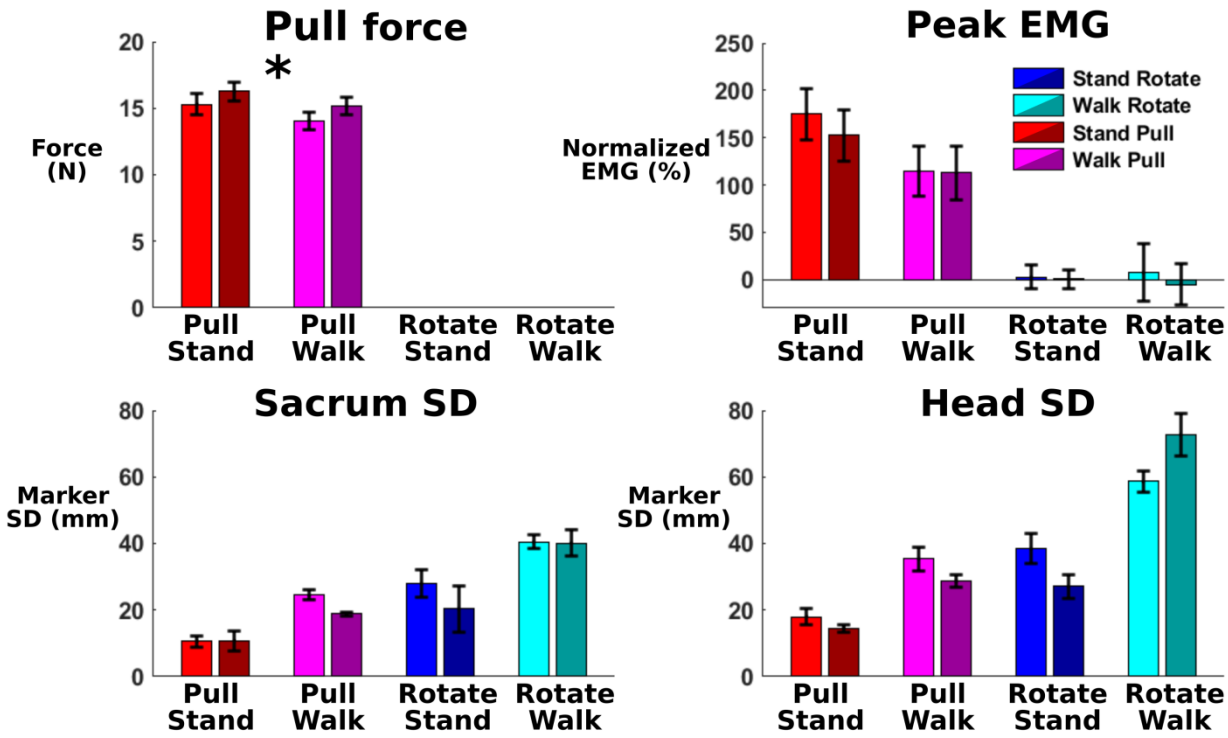

Figure 4-6: Adaptation results for behavioral measures. The average and standard error of the first (lighter color) and last (darker color) minute of each 10-minute trial are shown for behavioral measures (n=30). Because pull force could only be calculated during the pull perturbation, there are no values during the rotation perturbations. We only found a significant difference between the first and last minute for pull force (denoted by asterisk; repeated measure ANOVA p=0.031), although no pairwise comparisons were significant. We found no other significant adaptation effects for the other measures. Our results indicate that minimal adaptation effects were present.

EEG Power Spectra

We found significantly increased theta spectral power during walk rotate compared to all other conditions across multiple areas (Figure 4-7). Walk rotate showed significantly increased theta power in right occipital, left occipital, anterior parietal, and anterior cingulate compared to all other conditions (p=5.0e-4 for all).

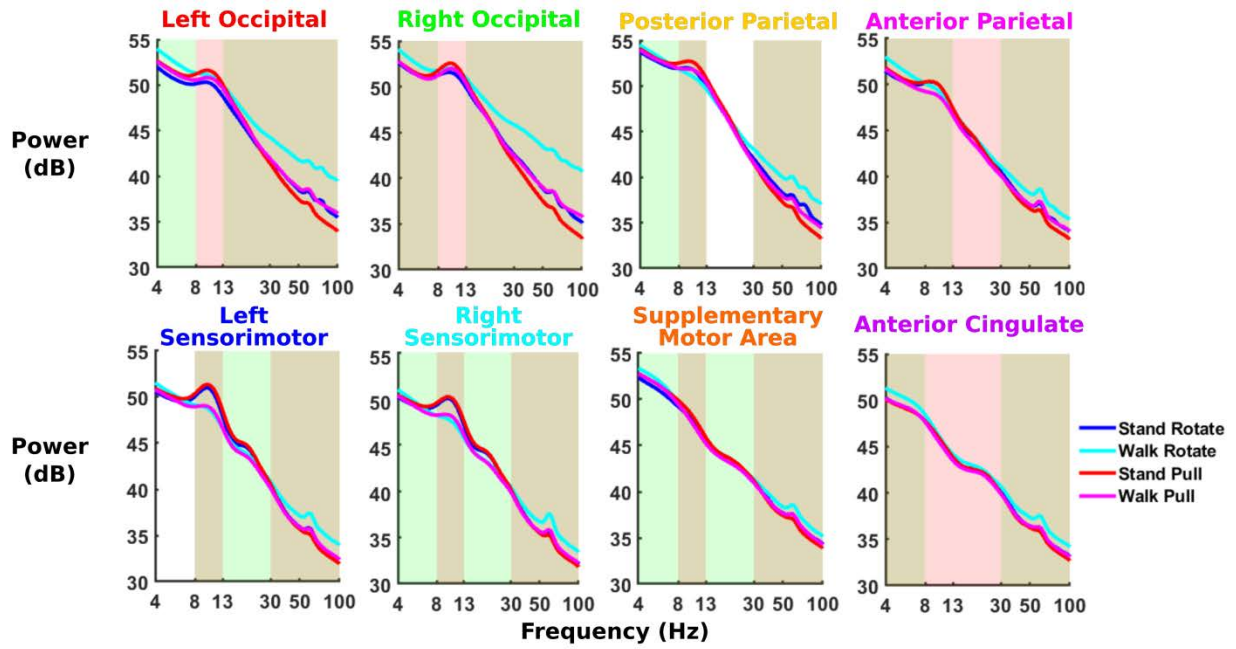

Figure 4-7: EEG cluster power spectra for each trial. The average EEG power spectra is shown for each trial (n=30), with log scaling along the x-axis. Shading reflects significant 2x2 ANOVA main effects. Green shading indicates a significant main effect of physical task (standing vs. walking), red shading indicates a significant main effect of perturbation type (rotation vs. pull), and brown shading indicates both main effects are significant. We found significant increases in theta and gamma power during walk rotate compared to the other three conditions, primarily in occipito-parietal areas. We also found significant increases in alpha and beta power during standing compared with walking in sensorimotor areas.

Alpha and beta power were substantially increased during standing conditions compared to walking in several cortical areas. Left and right sensorimotor areas showed significantly increased alpha and beta spectral power during stand pull and stand rotate compared to walk pull and walk rotate, respectively (p=5.0e-4 for all). We also found significantly increased alpha power during both standing conditions compared to their corresponding walking conditions in posterior parietal (p=5.0e-4 for both). In addition, we found significantly increased alpha and beta power in supplementary motor area during stand pull compared to walk pull (p=5.0e-4), but no significant difference between conditions with the visual rotation.

In gamma band, we primarily found increased spectral power during walk rotate and decreased spectral power during stand pull. Across all clusters, walk rotate had significantly increased gamma power compared to all other conditions (p=5.0e-4 for all). We also found significantly decreased gamma power for stand pull compared to all other conditions in left occipital, right occipital, and posterior parietal (p=5.0e-4 for all).

EEG ERSPs

ERSP plots for visual perturbations show theta synchronization immediately after perturbation onset followed by alpha-beta desynchronization (Figure 4-8). A similar pattern of time-frequency activity occurs immediately following perturbation termination. This pattern is strongest in the left occipital, right occipital, and posterior parietal areas, with weaker patterns of synchronization and desynchronization seen in other cortical clusters.

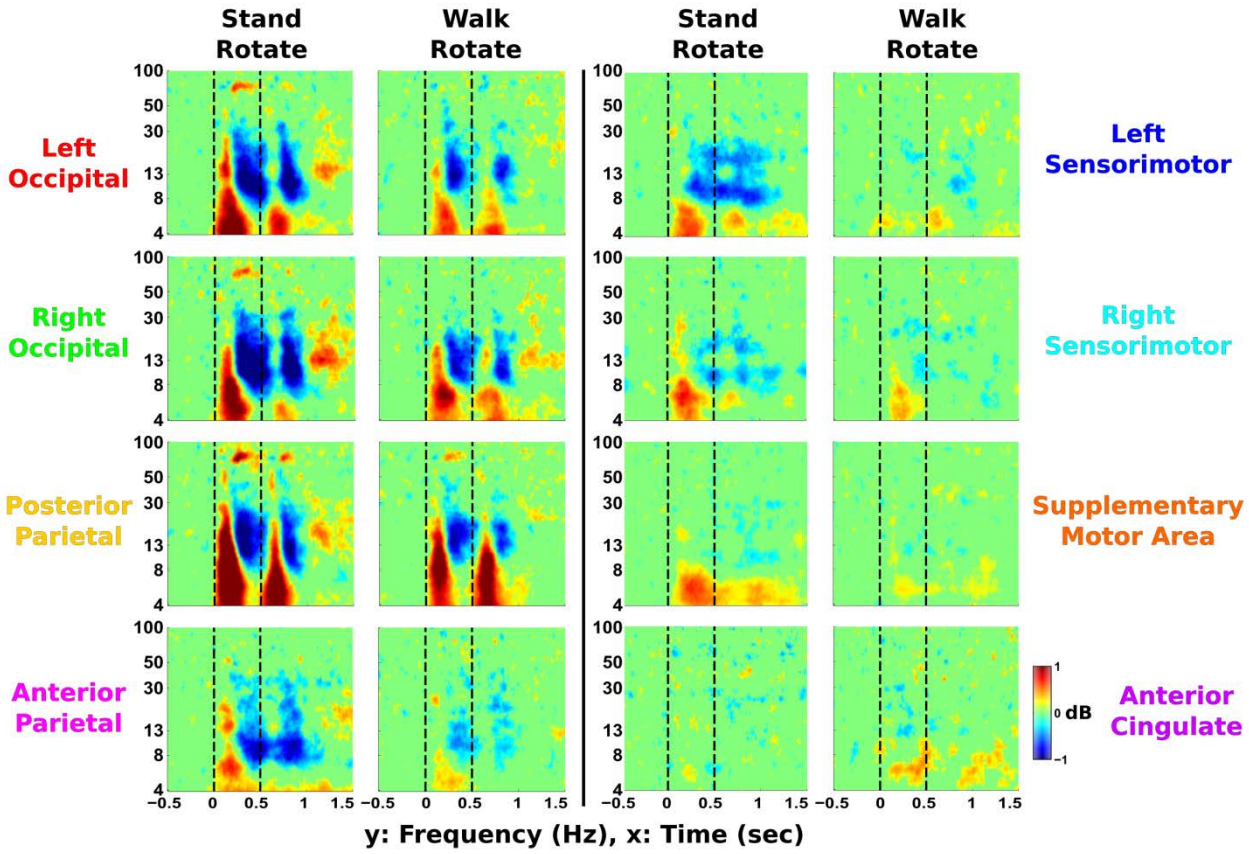

Figure 4-8: EEG event-related spectral perturbation (ERSP) plots for visual rotations. EEG ERSPs are shown for the visual rotation perturbations during standing and walking (n=30). Significant increases in spectral power relative to baseline (the 500 ms before perturbation onset) are shown in red, referred to as synchronization. Significant decreases in power relative to baseline are displayed in blue and are referred to as desynchronization. Vertical lines indicate perturbation onset and termination at 0 sec and 0.5 sec, respectively. Non-significant differences from baseline (bootstrap statistics $p \geq 0.05$) were set to 0 dB (green). Occipito-parietal areas showed the largest spectral fluctuations, while anterior cingulate had little changes in spectral power.

Pull perturbation ERSPs show a similar pattern of theta synchronization followed by alpha-beta desynchronization during perturbation onset and termination (Figure 4-9), but primarily located in different cortical areas compared to the visual perturbation. Theta synchronization appears in sensorimotor and anterior cingulate areas, with the strongest activity in the supplementary motor area. Large alpha-beta desynchronization also occurs in these areas, with strongest activity in left

and right sensorimotor areas. Similar time-frequency patterns with weaker strength were seen in occipito-parietal areas.

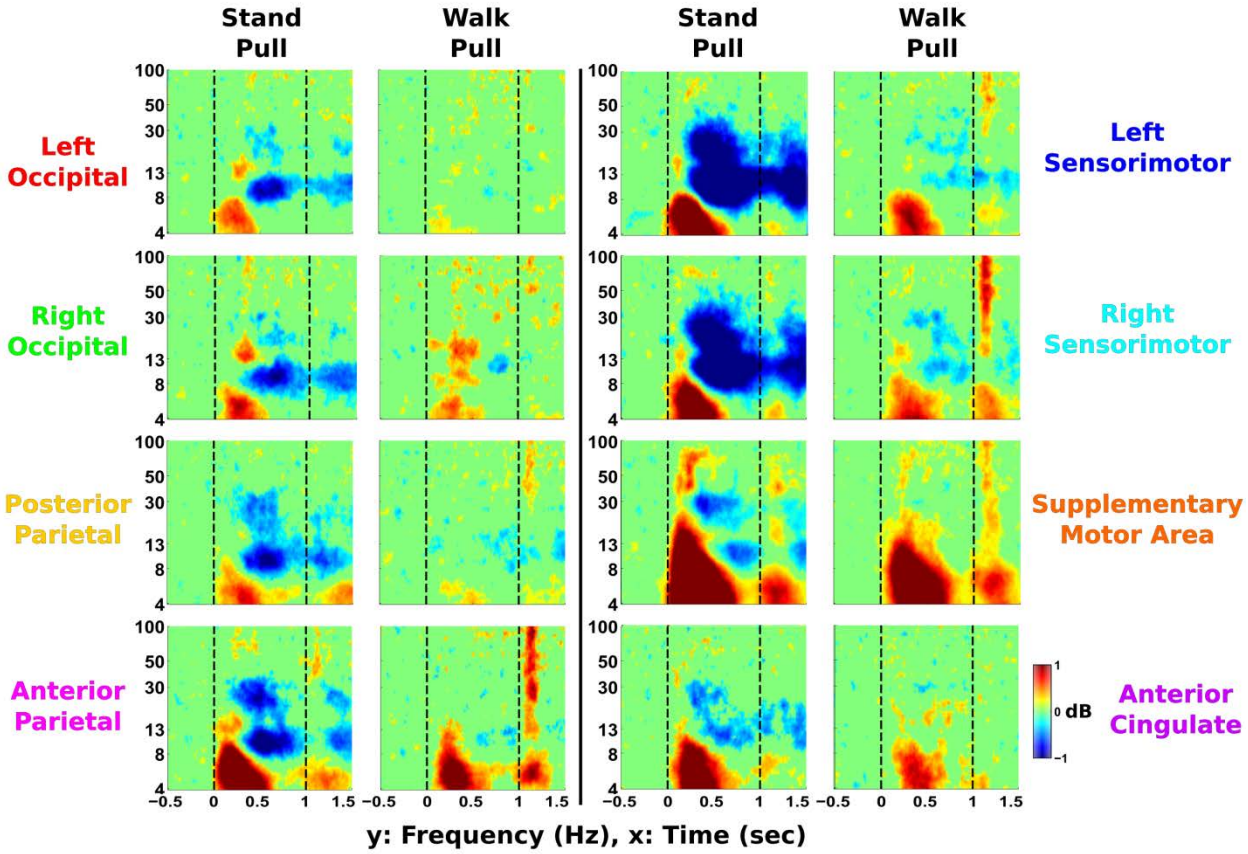

Figure 4-9: EEG event-related spectral perturbation (ERSP) plots for pull perturbations. EEG ERSPs are shown for the pull perturbations during standing and walking (n=30). Significantly increased spectral power compared to baseline (the 500 ms before perturbation onset) is displayed in red, known as synchronization. Significantly decreased power compared to baseline is shown in blue, referred to as desynchronization. Vertical lines indicate perturbation onset and termination at 0 sec and 1 sec, respectively. Non-significant differences from baseline (bootstrap statistics $p \geq 0.05$) have been set to 0 dB (green). Centro-frontal motor areas show large fluctuations in spectral power following perturbation onset, with the greatest theta synchronization in supplementary motor area. Alpha-beta desynchronization (8-30 Hz) is most prominent in left and right sensorimotor clusters.

ERSP synchronization onset occurred notably before desynchronization in most cortical clusters, with differences in synchronization onset across trials in multiple sensorimotor areas (Figure 4-10). In all clusters except the anterior cingulate ($p=0.615$), we found significantly earlier

synchronization onset compared with desynchronization onset (left occipital: p=5.85e-5, right occipital: p=6.04e-5, posterior parietal: p=7.56e-10, anterior parietal: p=1.14e-5, left sensorimotor: p=2.70e-4, right sensorimotor: p=1.30e-6, supplementary motor area: p=1.24e-5). In addition, we found a significant effect of perturbation type during synchronization onset in posterior parietal (p=0.019), supplementary motor area (p=4.18e-11), and anterior cingulate (p=0.024). We also found a significant effect of physical task during synchronization onset in posterior parietal (p=0.006), anterior parietal (p=0.008), left sensorimotor (p=0.005), and right sensorimotor (p=1.88e-4). For desynchronization onset, we found no significant main effects of perturbation type or physical task.

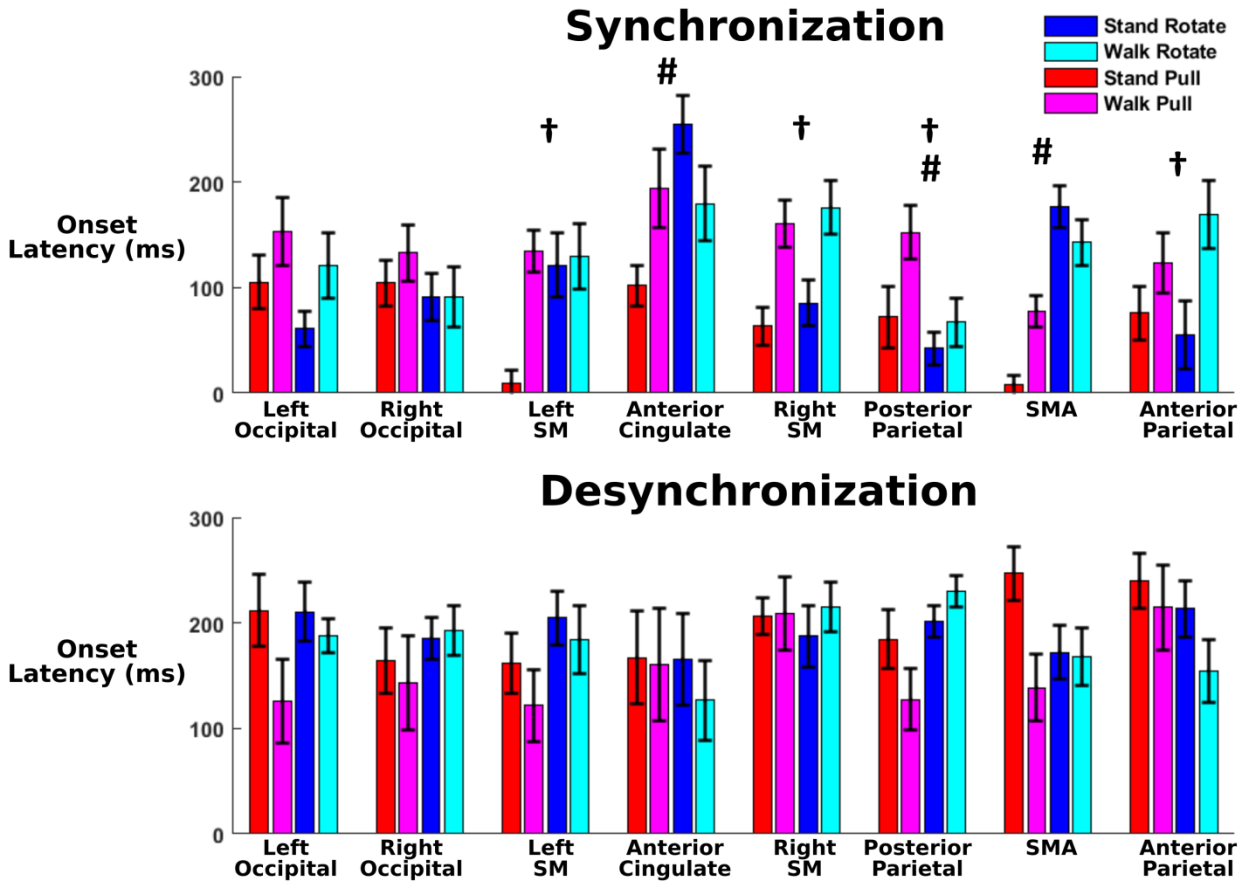

Figure 4-10: Event-related spectral perturbation (ERSP) onset latencies. The onset latencies of ERSP's across each cluster are shown for the theta-alpha synchronization (top) and alpha-beta desynchronization (bottom), with error bars showing standard error. We have indicated significant one-way Kruskal-Wallis main effects of perturbation type (#, rotation vs. pull) and physical task (†, standing vs. walking). Left and right SM indicate left and right sensorimotor areas, and SMA indicates supplementary motor area. Most significant effects were found in centro-frontal motor areas during synchronization onset. We found significantly increased desynchronization onset latency compared with synchronization onset latency in all clusters except anterior cingulate.

Neck Muscle EMG

Neck muscles showed substantially increased spectral power in the walk rotate condition and perturbation-evoked power increased only during the pull perturbations (Figure 4-11). We found significantly increased beta and gamma power during walk rotate compared to the other conditions and significantly decreased beta and gamma power for stand pull compared to all other conditions (p=5.0e-4 for all). ERSP plots show significantly increased neck muscle power

immediately following pull perturbation onsets, primarily in beta and gamma frequency bands. In contrast, we found little power fluctuations during the visual rotation perturbations.

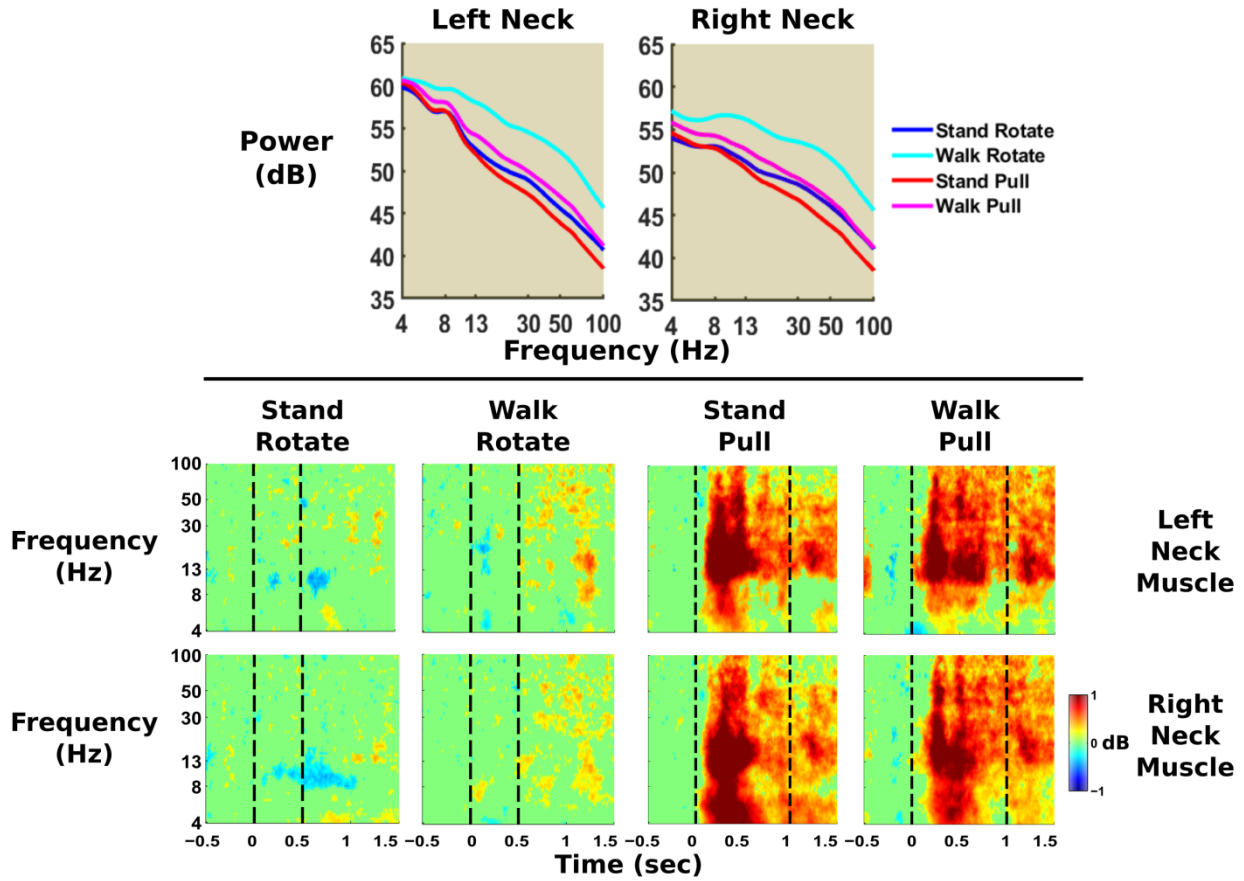

Figure 4-11: Neck muscle spectral power activity. Average power spectra (top) and median event-related spectral perturbation (ERSP) plots (bottom) are shown for left and right neck muscle EEG electrode locations (n=30). Power spectra shading indicates that there were significant 2x2 repeated measure ANOVA effects of perturbation type and physical task across all frequency bands. The neck muscle power spectra for the Walk Rotate condition was noticeably higher than the other 3 conditions for both neck electrodes. Significantly increased spectral power compared to baseline (the 500 ms before perturbation onset) is displayed in red and significantly decreased power compared to baseline is shown in blue. Vertical lines indicate perturbation onset at 0 sec and perturbation termination at 0.5 or 1 sec, depending on the perturbation type. We set non-significant differences from baseline (bootstrap statistics $p \geq 0.05$) to 0 dB (green). Based on the ERSPs, only the pull perturbations appear to immediately increase neck muscle activity. Neck muscle activity only showed up as increased synchronization on the ERSP, and not decreased synchronization.

Discussion

We were able to identify robust electrocortical fluctuations in response to perturbations that challenged balance. We found transient theta synchronization and alpha-beta desynchronization following perturbation onset, as hypothesized. This spectral activity increased in occipito-parietal areas following visual perturbations, whereas physical pulls increased activity in sensorimotor areas, as hypothesized. Surprisingly, we found little activity in the anterior cingulate following visual perturbations. This study demonstrates that analysis of spectral power fluctuations in clusters of electrocortical sources can provide considerable insight into the networks and functional activity related to sensorimotor tasks (Gramann, et al., 2011; Makeig S. , 2002).

Body Sway and Muscle Response

Body and head sway notably increased during walking and during virtual reality use, indicating reduced stability (Figure 4-4). We expected to find increased body and head sway during walking compared to standing because walking involves dynamic balance. In addition, body and head motion increased when subjects wore the virtual reality headset for the visual perturbations compared to unaltered viewing during the pull perturbations. Based on previous studies, this may indicate decreased stability when wearing a head-mounted display (Kelly, Riecke, Loomis, & Beall, 2008; Robert, Ballaz, & Lemay, 2016). In our virtual reality setup, reduced stability could have been caused by a reduced field of view, low latency, or the location of the webcam below eye level.

Our lower leg EMG results showed that physical pull perturbations induced a robust muscle response while visual perturbations did not elicit a consistent muscle response (Figure 4-5). This is not surprising because the pull perturbations physically attempt to move the subject mediolaterally, necessitating a muscular response. The visual perturbation does not physically

alter each subject's movement, instead relying on disruption of visual input to require a balance response. Physical mediolateral perturbations induce a reflex response, where the ankle muscles attempt to brake side-to-side motion by co-contracting (Hof & Duysens, 2018). This quick muscle response to physical pull perturbations highlights the importance of sufficient muscle strength to maintain stability (Papa, Garg, & Dibble, 2015).

During the pull perturbations, muscle activity was greatest in the peroneus longus and tibialis anterior, with a notable asymmetry between left and right leg muscles during standing. The tibialis anterior, peroneus longus, and medial gastrocnemius have been shown to be important in mediolateral body stabilization, while soleus activity may be more active during posterior perturbations (Henry, Fung, & Horak, 1998). Interestingly, muscle activity during stand pull was notably asymmetrical, with left leg muscle activity higher than the corresponding right leg muscles, especially for the medial gastrocnemius. Subjects stood with their left leg in back, suggesting that the back leg was more involved in stabilization. The large increase in the left gastrocnemius muscle may indicate recruitment of larger leg muscles to help stabilize the body during balance. It would be interesting to see if this asymmetrical muscle response also occurs between the front and back foot during walking, but this would require timing the perturbation to occur during double support phase.

EEG Power Spectra

Electrocortical spectral power showed increased alpha power during standing compared with walking, likely reflecting differences in motor readiness (Figure 4-7). We found this increased alpha power during standing compared to walking in left/right occipital, left/right sensorimotor, anterior parietal, posterior parietal, and supplementary motor area, with the largest differences in sensorimotor areas. Alpha power has been shown to decrease when walking compared to

standing (Presacco, Goodman, Forrester, & Contreras-Vidal, 2011; Youssofzadeh, Zanotto, Wong-Lin, Agrawal, & Prasad, 2016). Alpha power can also decrease when performing cognitively engaging tasks such as walking in an interactive virtual environment (Wagner, Solis-Escalante, Scherer, Neuper, & Müller-Putz, 2014) and closed-loop brain-computer interface control of a virtual avatar while walking (Luu, Nakagome, He, & Contreras-Vidal, 2017b).

In addition, we found significantly increased theta power across multiple clusters when subjects were exposed to visual perturbations while walking, possibly indicating a cognitive response to challenging balance conditions. Body and head sway substantially increased during walk rotate compared to all other conditions, suggesting that this condition challenged balance the most. Increased theta power has been seen during tasks requiring balance (Sipp, Gwin, Makeig, & Ferris, 2013; Slobounov, Cao, Jaiswal, & Newell, 2009) and can correspond to more challenging balance tasks (Hülsdünker, Mierau, & Strüder, 2015; Youssofzadeh, Zanotto, Wong-Lin, Agrawal, & Prasad, 2016). Increased theta power during walk rotate seems to provide a cognitive indicator that balance difficulty increased.

In the gamma band, we found increased power during walking visual rotations and decreased power during standing physical pull perturbations for most brain areas. Gamma power differences appeared most pronounced in left occipital, right occipital, and posterior parietal. These power spectra differences align quite well to the head and body sway estimates (Figure 4-4), with stand pull having the lowest sway and walk rotate having the highest. Gamma power has been implicated in active cortical processing (Başar, Başar-Eroglu, Karakaş, & Schürmann, 2001) and can increase with greater instability (Slobounov, Cao, Jaiswal, & Newell, 2009). It is possible that neck muscle activity contaminated the occipital and posterior parietal clusters as they are closest to the back of the head where the neck muscles are located. However, there was

virtually no neck muscle activation in response to the visual rotation and very strong neck muscle activation in response to the physical pull perturbation (Figure 4-11). In contrast, the visual rotation had the greatest gamma power in occipital and posterior parietal clusters, and physical pull perturbations had low gamma power in occipital and posterior parietal clusters. These observations strongly suggest that our signal processing adequately removed neck muscle activity from the brain sources. Even for the physical pull perturbations when there was clear neck muscle activity, the neck ERSP showed frequencies primarily above 13 Hz and it remained fairly consistent after perturbation onset. The brain source synchronizations of interest were all below 13 Hz and occurred within the first half-second after perturbation onset. For these reasons, it does not seem likely that the neck muscle electrical activity affected our results.

Perturbation-evoked EEG

During the pull perturbations, large theta synchronization was seen in sensorimotor and supplementary motor areas (Figure 4-9). This initial synchronization has been shown to be similar to the N1 peak seen during averaged event-related EEG activity following balance perturbations (Varghese, et al., 2014). This N1 activity tends to be widespread, with strongest activity localized to the supplementary motor area (Marlin, Mochizuki, Staines, & McIlroy, 2014), which also shows the greatest theta synchronization in our study. N1 activity has been shown to be present despite changes in task (Quant, Adkin, Staines, Maki, & McIlroy, 2004). Similarly, theta synchronization in our data appears to show up in most clusters for both perturbation types and is well-conserved between standing and walking. In addition, theta synchronization onset latency was notably altered in centro-frontal motor areas based on the type of perturbation and whether subjects stood or walked. Previous research has shown that the brain uses an internal model and identifies loss of balance if body motion diverges too many standard

deviations from the previous behavior (Ahmed, 2005). Walking involves more baseline movement than standing, which could notably increase this standard deviation threshold used by the brain and potentially result in the delayed theta synchronization seen during walking. This increased threshold may be due to the increased mediolateral sway seen during walking. Interestingly, the single N1 EEG peak in young adults has been found to be delayed and more prolonged in older adults, especially in older adults with reduced mobility (Duckrow, Abu-Hasaballah, Whipple, & Wolfson, 1999). This suggests that theta band synchronization may be useful for studying cognitive deterioration in balance performance.

Although the pull perturbations during standing elicited a asymmetrical electrocortical onset times and leg muscle response amplitude, these are likely unrelated to each other. We found a substantial increase in left leg muscle response compared to the right leg during pull perturbations while standing, likely due to greater use of the back leg for maintaining balance. Similarly, the EEG synchronization onset during this trial (Figure 4-10) showed a notable decrease in onset latency in left sensorimotor compared with right sensorimotor. Previous research during loss of balance showed that the left sensorimotor area was more active than right sensorimotor, regardless of the direction in which balance was lost and even though leg muscle activity differed based on direction (Sipp, Gwin, Makeig, & Ferris, 2013). The authors concluded that the left sensorimotor was the earliest electrocortical indicator that balance is lost, which agrees with our findings. In another study, beta power in left premotor area was modulated during stabilized vs. unaltered walking, while remaining unaffected in the right premotor area (Bruijn, Van Dieën, & Daffertshofer, 2015). Diffusion tensor imaging of older adults found significant correlations between stability measures and left hemisphere corticospinal tracts, with no significant correlations for right corticospinal tracts, suggesting corticospinal lateralization

when maintaining stability (Bruijn, Van Impe, Duysens, & Swinnen, 2014). This may be explained by left hemisphere dominance in right-handed humans during a variety of skilled movements (Serrien, Ivry, & Swinnen, 2006), potentially implicating subjects' handedness in inducing asymmetrical cortical results. These studies suggest that our subjects' asymmetrical electrocortical onset times are likely influenced by brain laterality during balance control, not stance position, but further research is needed to verify this.

We also found large alpha-beta desynchronization in sensorimotor areas following the pull perturbation while standing, likely reflecting changes in motor readiness and decreased motor inhibition. This is further evidenced by the largest alpha-beta desynchronization during standing occurring in sensorimotor areas, which also showed the large increases in alpha-beta spectral power during standing compared to walking. Similar transient alpha-beta desynchronization has been shown previously (Luu, Nakagome, He, & Contreras-Vidal, 2017b; Seeber, Scherer, Wagner, Solis-Escalante, & Müller-Putz, 2014). It has also been suggested that beta desynchronization may reflect the brain detecting a change from the status quo (Engel & Fries, 2010). During the visual rotations, beta desynchronization may indicate a change in the status quo due to conflict between visual and vestibular inputs and conflict between visual and proprioceptive inputs. Such alpha-beta frequency fluctuations may not readily correspond to averaged event-related activity, indicating that time-frequency decomposition can provide useful additional information.

The similarity in time-frequency patterns between visual and physical perturbations suggests a common electrocortical signature due to sensorimotor conflict (Figure 4-8 and Figure 4-9). We were able to determine that low-frequency synchronization consistently occurred before higher-frequency desynchronization in most cortical areas, suggesting a similar pattern to sensorimotor

perturbations. This pattern in our data is similar to that seen during visual conflict tasks using EEG (Jiang, Bailey, & Xiao, 2018) and local field potential recordings in the subthalamic nucleus (Hell, Taylor, Mehrkens, & Bötzel, 2018; Zavala, et al., 2016). All three of these studies recorded similar theta and beta oscillations in the cortex, indicating an important connection between the subthalamic nucleus and cortex during conflict. This seems to warrant further exploration, especially due to the importance of the subthalamic nucleus in Parkinson's disease (Collomb-Clerc & Welter, 2015). Based on the similar patterns elicited by visual and pull perturbations, one might expect notable differences in electrocortical activity using visual conflicts on patients with Parkinson's disease compared to healthy adults, especially if they have freezing of gait symptoms (Gilat, et al., 2013; Matar, Shine, Naismith, & Lewis, 2013). Despite our study being limited to healthy, young adults, there seems to be enough evidence to suggest that similar time-frequency, perturbation-evoked EEG activity should be studied in patient populations. While Parkinson's disease has been primarily associated with basal ganglia dysfunction (Blandini, Nappi, Tassorelli, & Martignoni, 2000), dual-task studies have indicated that cortical activity is also affected (Salazar, et al., 2017; Yogev, et al., 2005), making EEG a potentially relevant recording site. It is also interesting to note similarities between our perturbation time-frequency pattern and the gait-related time-frequency pattern seen in other studies during foot-ground contact and initial stance (Gwin, Gramann, Makeig, & Ferris, 2011; Seeber, Scherer, Wagner, Solis-Escalante, & Müller-Putz, 2014). Gait time-frequency patterns usually show theta synchronization during heel-strikes, which is similar to the synchronization we found after perturbation onset. This theta synchronization during foot-ground contact may indicate increased sensorimotor processing due to increased instability during stepping.

We were surprised by the lack of spectral fluctuations in anterior cingulate following the visual rotation (Figure 4-8). We had hypothesized that there would be large occipito-parietal spectral fluctuations for the visual rotation condition, but we still expected some spectral fluctuations in the anterior cingulate based on past balance studies (Sipp, Gwin, Makeig, & Ferris, 2013; Slobounov, Cao, Jaiswal, & Newell, 2009) and gait (Luu, Nakagome, He, & Contreras-Vidal, 2017b; Gwin, Gramann, Makeig, & Ferris, 2011). We did see anterior cingulate activity during pull perturbations, which was likely a more similar match to the previous studies. One interpretation for the lack of anterior cingulate spectral fluctuations after the visual rotations is that the anterior cingulate is primarily focused on maintaining balance and changes to physical posture. The posterior parietal and occipital areas may be primarily responsible for resolving visual conflict, so no further processing by the anterior cingulate is needed. The anterior cingulate has been shown to be active during error-monitoring to visual conflicts (Gehring & Knight, 2000; van Veen & Carter, 2002), but it may depend on how the anterior cingulate defines errors (Carter, et al., 1998). It is also worth noting that most visual flanker or Stroop tasks to analyze anterior cingulate activity require a motor response, whereas our visual perturbation did not necessitate a physical response. If the visual perturbations led to a step-off from the beam, we would expect to see anterior cingulate activity. Further research is needed, but this highlights the importance of measuring electrocortical activity during more real-world movements.

While we did not find consistent cortical sources in the prefrontal area, this should not necessarily be interpreted that prefrontal areas are uninvolved with the perturbation response. On the contrary, multiple fNIRS studies have found increased prefrontal oxygenation during challenging balance tasks (Basso Moro, et al., 2014; Ferrari, et al., 2013) and dual-tasking

(Mahoney, et al., 2016; Mirelman, et al., 2014). It is possible that artifact from eye movements and blinks in the EEG may have made it more challenging for independent component analysis to separate out prefrontal sources.

Perturbation Magnitude

A limitation of the study is the use of only one perturbation magnitude for the visual rotation and physical pull perturbations. In an ideal world, we could have conducted a range of different magnitudes of visual rotation (e.g., 5°, 10°, 20°, 40°, and 90° of rotation) and physical pull forces (e.g. 5 N, 10 N, 15 N, 25 N, and 50 N). This would have provided information about the relationship between perturbation size and the electrocortical dynamics timing and amplitude. Previous studies examining scalp EEG during perturbations to standing have found that either increasing the perturbation magnitude or shortening the perturbation duration can increase the low-frequency electrocortical response, with no differences in electrocortical timing (Dietz, Quintern, Berger, & Schenck, 1985; Mochizuki, Boe, Marlin, & McIlRoy, 2010; Staines, McIlroy, & Brooke, 2001). While these studies did show some scaling of electrocortical responses with perturbation magnitude, the relationship was less than proportional. Given that there was no effect on electrocortical timing in the previous studies, it suggests that measuring only one perturbation magnitude per condition was not a major weakness to our results. It may also be worth conducting future studies at faster walking speeds than 0.22 m/s. We did not include faster gait speeds because we did not want to add an extra confound into the experiment. Faster speeds increase the inter-subject variability in balance performance as the task is more difficult. Choosing 0.22 m/s also makes it easier to compare our results to previous studies that have used the same speed (Domingo & Ferris, 2009; Domingo & Ferris, 2010; Sipp, Gwin, Makeig, & Ferris, 2013). However, previous studies have found no difference in cortical and

muscular responses to cognitive dual-tasking at various gait speeds, so the effect of gait speed may be minimal (Kline, Poggensee, & Ferris, 2014; Meester, Al-Yahya, Dawes, Martin-Fagg, & Piñon, 2014). Future studies that examine patient population will likely want to examine scaling of the perturbation magnitude as they can have reductions in sensorimotor function that make detection of the perturbation different from neurologically intact subjects.

EEG Motion Artifact

While any EEG study during human movement includes concerns of artifact contamination, motion artifact appeared to have minimal effect on our results. Motion artifact has been shown to have differential effects across the head during walking (Kline, Huang, Snyder, & Ferris, Isolating gait-related movement artifacts in electroencephalography during human walking, 2015). In contrast, our EEG ERSPs and power spectra were quite consistent between left and right clusters in occipital and sensorimotor areas (Figure 4-8 and Figure 4-9). Such symmetry provides strong evidence against motion artifact being present. In addition, we do not see broadband activity during perturbation onset, which is a hallmark of motion artifact during EEG gait experiments (Oliveira, Schlink, Hairston, König, & Ferris, 2017b). We also validated our EEG hardware and signal processing techniques against motion artifacts using an electrical head phantom and motion platform as done in previous published work (Oliveira, Schlink, Hairston, König, & Ferris, 2016). We are very confident that the EEG is not affected by motion artifacts given this validation. Furthermore, the visual rotations do not elicit consistent head movement, especially during standing (Figure 4-3). While some motion from the pull perturbations was expected, the head movement immediately following perturbation onset was at most 0.5 cm on average. Little consistent head motion appeared to be present, and the effects of inconsistent motion artifacts were likely reduced by averaging. In addition, taking the median across trials for

the ERSPs instead of the mean likely prevented any inconsistent artifacts skewing the resulting ERSP. Using the median may be useful in future EEG studies, especially if motion artifact is a concern.

Conclusions

By testing subjects with brief visual rotation and physical pull perturbations, we were able to identify a highly conserved electrocortical time-frequency pattern but in different brain regions. This pattern was strongest in occipito-parietal areas during visual perturbations and strongest in sensorimotor areas during pull perturbations. Such a common time-frequency signature may be important in assessing balance dysfunction and improving our understanding of balance control in individuals with mobility disorders.

Chapter 5: Combined Head Phantom and Neural Mass Model Validation of Effective Connectivity Measures[4]

Abstract

Objective Due to its high temporal resolution, electroencephalography (EEG) has become a promising tool for quantifying cortical dynamics and effective connectivity in a mobile setting. While many connectivity estimators are available, the efficacy of these measures has not been rigorously validated in real-world scenarios. The goal of this study was to quantify the accuracy of independent component analysis and multiple connectivity measures on ground-truth connections while exposed real-world volume conduction and head motion. *Approach* We collected high-density EEG from a phantom head with embedded antennae, using neural mass models to generate transiently interconnected signals. The head was mounted upon a motion platform that mimicked recorded human head motion at various walking speeds. We used cross-correlation and signal to noise ratio to determine how well independent recovered the original antenna signals. For connectivity measures, we computed the average and standard deviation across frequency of each estimated connectivity peak. *Main results* Independent component analysis recovered most antenna signals, as evidenced by cross-correlations primarily above 0.8, and maintained consistent signal to noise ratio values near 10 dB across walking speeds compared to scalp channel data, which had decreased signal to noise ratio to ~2 dB at fast walking speeds. The various connectivity measures were generally able to identify the true interconnections, but some measures were susceptible to spurious high-frequency connections

[4] This chapter will be submitted for publication in *Journal of Neural Engineering*.

inducing large standard deviations of ~10 Hz. *Significance* Our results indicate that independent component analysis and some connectivity measures can be effective at recovering underlying connections among brain areas. These results highlight the utility of validating EEG processing techniques with a combination of complex signals, phantom head use, and realistic head motion.

Introduction

A recent thrust of neuroimaging research has been to measure brain activity during mobile real-world scenarios (Ladouce, Donaldson, Dudchenko, & Ietswaart, 2017). Traditional neuroimaging methods, such as functional magnetic resonance imaging (fMRI) and positron emission tomography (PET), require stationary subjects, limiting their use for real-world recordings. In contrast, high-density EEG is a promising method for recording real-world brain dynamics due to its portability and high temporal resolution (Gramann, Ferris, Gwin, & Makeig, 2014; Gramann, et al., 2011). EEG is affected by low spatial resolution and artifact contamination, making it challenging to extract meaningful cortical information (Urigüen & Garcia-Zapirain, 2015). Blind source separation using independent component analysis can separate out cortical and artefactual sources, reducing the impact of artifact contamination and improving spatial resolution (Gwin, Gramann, Makeig, & Ferris, 2010; Makeig, Bell, Jung, & Sejnowski, 1996). Such high-density, source-localized experiments have been performed during mobile tasks such as treadmill walking, stair stepping, and balance-beam walking (Bradford, Lukos, & Ferris, 2016; Peterson, Furuichi, & Ferris, 2018; Luu, Brantley, Nakagome, Zhu, & Contreras-Vidal, 2017c).

While many EEG studies analyze frequency-domain spectral power, understanding the flow of information amongst brain areas using connectivity analysis can provide a more complete understanding of the brain by quantifying interactions amongst cortical regions. However, there

are many connectivity measures to choose from. One class of measures originated from Granger causality, which states that one signal causes activity in another if information from the past of the cause signal provides information that helps predict the future of the effect signal (Granger, 1969). This idea was developed for 2 signals only, but has since been extended to multichannel data use a multivariate autoregressive modelling (Lütkepohl, 2007). One extension was directed transfer function (Kaminski & Blinowska, 1991), which was based on the transfer function of the autoregressive model. This was corrected using normalization to be frequency independent and sensitive only to direct connections, leading to full-frequency directed transfer function (ffDTF) and direct directed transfer function (dDTF), respectively (Korzeniewska, Mańczak, Kamiński, Blinowska, & Kasicki, 2003). Another extension of Granger Causality is partial directed coherence, which was based on the model coefficients in the frequency domain (Baccalá & Sameshima, 2001). Corrections to make this measure less dependent on scaling and later scale-free have resulted in generalized partial directed coherence (gPDC) and renormalized partial directed coherence (rPDC), respectively (Baccala, Sameshima, & Takahashi, 2007; Schelter, Timmer, & Eichler, 2009). In additions to these extensions of Granger causality, there is also Granger-Geweke Causality (GGC) (Geweke, 1982). Additionally, other connectivity measures, such as weighted phase lag index (WPLI) and phase locking value (PLV), do not use multivariate autoregressive models. PLV measures the relative phase between two sources (Lachaux, Rodriguez, Martinerie, & Varela, 1999), but can include spurious, instantaneous connections due to volume conduction. In contrast, WPLI is based on imaginary coherence, which ignores these instantaneous connections and increases sensitivity to true connections (Vinck, Oostenveld, van Wingerden, Battaglia, & Pennartz, 2011). For our study, we used the debiased WPLI-square estimator from Vinck et al. (Vinck, Oostenveld, van Wingerden,

Battaglia, & Pennartz, 2011). Because PLV and WPLI do not act on model-fit EEG activity, they take advantage of averaging results across multiple trials.

Due to the abundance of connectivity measures, several studies have attempted to validate these measures. Previous research has used simulated data to generate connection patterns with a known ground truth (Wang, et al., 2014). This has been used to verify connectivity during walking (Snyder, Vindiola, Vettel, & Ferris, 2013) and to show that connectivity measures can be affected by volume conduction (Brunner, Billinger, Seeber, Mullen, & Makeig, 2016). The downside of such modelling is that it usually avoids the non-linearities of the real world, which could potentially violate the assumptions of the measure being validated. Another way to compare measures is by recording EEG from human subjects and then using various metrics for validation (Mahjoory, et al., 2017), but this leads to assumptions about the underlying connectivity pattern in the absence of a ground truth. There is currently a need to validate connectivity measures on real-world ground truth signals.

In addition, there is ongoing debate as to whether connectivity estimation should be performed at the channel or source level (Brunner, Billinger, Seeber, Mullen, & Makeig, 2016; Kaminski & Blinowska, The Influence of Volume Conduction on DTF Estimate and the Problem of Its Mitigation, 2017; Van de Steen, et al., 2016). The concern with source-level connectivity is that it impairs the channel data's correlative structure, removing important information (Kaminski & Blinowska, Directed Transfer Function is not influenced by volume conduction inexpedient pre-processing should be avoided, 2014). On the other hand, source-level connectivity is less influenced by volume conduction and involves a specific cortical area (Brunner, Billinger, Seeber, Mullen, & Makeig, 2016). In addition to the volume conduction, motion artifact becomes a concern in mobile settings (Kline, Huang, Snyder, & Ferris, 2015). There is also a need to

determine if independent component analysis preprocessing can result in accurate connectivity estimation in the presence of real-world volume conduction and motion artifact.

One way to provide a real-world testing with ground truth signals is to use a phantom head with embedded antennae. Head phantoms have long been used in fMRI research to test methods (Kneeland, Knowles, & Cahill, 1984) and have also validated EEG source estimation techniques (Baillet, et al., 2001; Chowdhury, Mullinger, Glover, & Bowtell, 2014). EEG phantom heads mounted upon a moving platform have quantified the effects of head motion and cable sway (Oliveira, Schlink, Hairston, König, & Ferris, 2016; Symeonidou, Nordin, Hairston, & Ferris, 2018). However, no phantom head studies have validated connectivity estimation techniques. In order to test connectivity measures using complex, multi-frequency signals, we used a neural mass model. Neural mass models are based on the oscillatory properties of neuronal networks, which can be used to generate oscillations at various physiological frequency ranges (David & Friston, 2003). By summing the results of multiple neural mass models, complex waveforms can be created (Ma, 2018). Additionally, interconnections can be created between neural mass model signals to analyze EEG connectivity (Gordon, Franaszczuk, Hairston, Vindiola, & McDowell, 2013; Vindiola, Vettel, Gordon, Franaszczuk, & McDowell, 2014; Snyder, Vindiola, Vettel, & Ferris, 2013). However, these previous studies involved computer simulation and did not account for the real-world effects as a phantom head might.

The purpose of this study was to determine the efficacy of independent component analysis and connectivity measures on signals of varying complexity exposed to real-world volume conduction and motion artifact. We hypothesized that independent component analysis would be able to recover the antennae sources and separate out motion artifact as measured by signal to noise ratio and cross-correlation of the resulting independent components. In addition, we

hypothesized that the connectivity estimation measures we used would be able to find the true causal interactions based on the peak frequency for each measure.

Materials & Methods

Phantom Head Setup and Antenna Signals

Our phantom head consisted of a mannequin head with 8 exposed wire pairs, around which we used a combination of dental plaster, sodium propionate, and water to simulate realistic tissue conductance. See Oliveira et al. for a more complete description (Oliveira, Schlink, Hairston, König, & Ferris, 2016). We sent predefined signals into each antenna using an input/output interface (MicroLabBox, dSPACE GmbH, Paderborn, Germany). We used 6 of the 8 antennae due to memory constraints (Figure 5-1). 3 antenna signals contained intermittent connections, while the other 3 were distractor signals to see how well independent component analysis and connectivity measures performed in the presence of other signals.

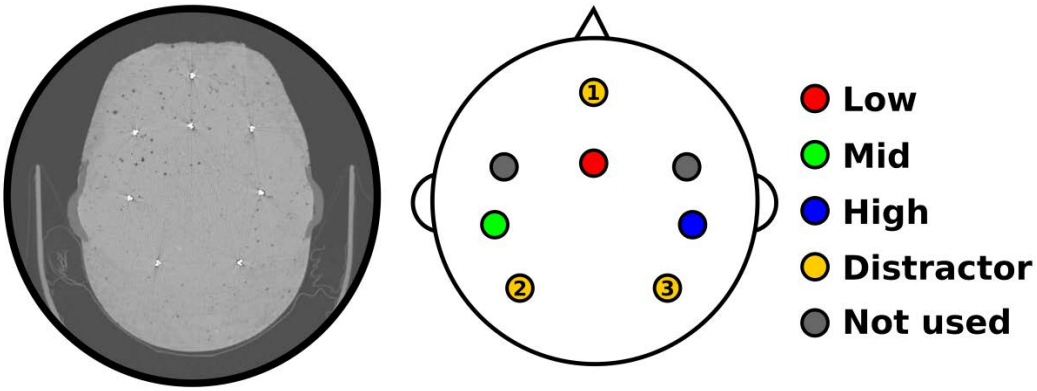

Figure 5-1: Phantom head antennae locations. A CT scan (left) and diagram (right) of the antennae locations within the phantom head are shown, using an axial view. The low, mid, and high antennae were used to generate the signals of interest that contained intermittent connections. These names are based on the peak frequency content of each antenna, with the low signal containing the lowest peak frequency while the high signal included the highest peak frequency of the 3 signals. In addition, we used 3 distractor signals at the antenna locations marked in yellow, which are numbered for later reference. Two other antennae were not used for this study due to technological constraints.

The 3 non-distractor signals were classified as low, mid, and high based on the main frequency component of the signal, as shown in Figure 5-2. The low signal's peak frequency was at 6.5 Hz, corresponding to the EEG theta band. Peak frequency for the mid signal was at 10 Hz, corresponding to the EEG alpha band. For the high signal, the peak frequency was at 41 Hz, which corresponded to the EEG gamma band. The experiment included 3 conditions with different antenna signals: 1) signals with a single peak frequency, 2) signals with a smeared, single peak frequency, and 3) signals with two frequency peaks.

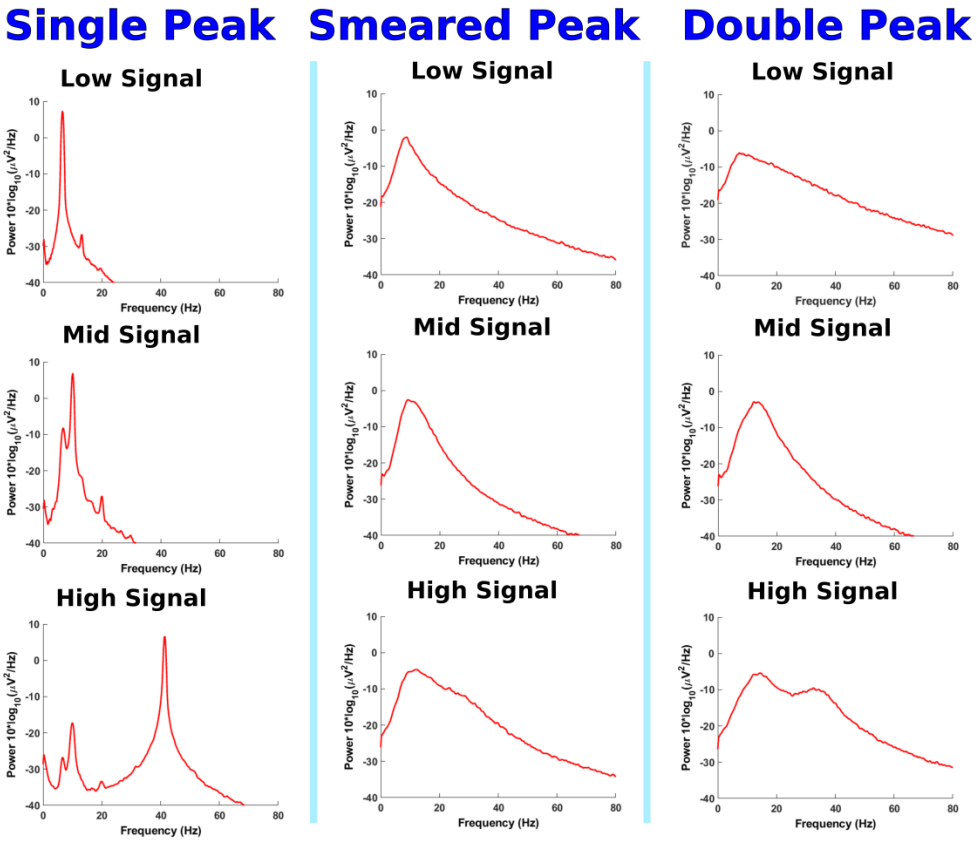

Figure 5-2: Antenna signals of interest power spectra. The power spectra for the 3 signals of interest (low, mid, high) are shown for each condition. Signals in the single peak condition have a single sharp frequency peak, indicating one dominant frequency (the smaller peaks in the mid and high signals are from intermittent connections throughout each condition). The power spectra during the smeared peak condition are less sharp, reflecting a more complex signal. For the double peak condition, each signal had two frequency peaks, which is best exemplified by the high signal power spectra.

We generated complex and physiologically-relevant signals for each antenna using a neural mass model based on previous research (David & Friston, 2003; Vindiola, Vettel, Gordon, Franaszczuk, & McDowell, 2014). We used the neural mass model to generate 6 separate sources with peak frequencies in different EEG bands (delta, theta, alpha, beta, low gamma, and high gamma). These sources were summed together to create each final antenna signal, using the different weightings shown in Table 5-1.

Table 5-1: Neural mass model frequency weightings

		Delta (4 Hz)	Theta (6.5 Hz)	Alpha (10 Hz)	Beta (23 Hz)	Low gamma (41 Hz)	High gamma (47 Hz)
Low Signal	Single Peak	0	1	0	0	0	0
	Smeared Peak	0.1	0.5	0.25	0.1	0.05	0
	Double Peak	0	0.7	0	0	0.3	0
Mid Signal	Single Peak	0	0	1	0	0	0
	Smeared Peak	0.1	0.1	0.5	0.25	0.05	0
	Double Peak	0	0	0.7	0.3	0	0
High Signal	Single Peak	0	0	0	0	1	0
	Smeared Peak	0.1	0.1	0.25	0.05	0.5	0
	Double Peak	0	0.3	0	0	0.7	0
Distractor 1	Single Peak	1	0	0	0	0	0
	Smeared Peak	0.5	0.1	0	0	0.2	0.2
	Double Peak	0.7	0	0	0	0	0.3
Distractor 2	Single Peak	0	0	0	1	0	0
	Smeared Peak	0.1	0	0	0.5	0.2	0.2
	Double Peak	0	0	0.3	0.7	0	0
Distractor 3	Single Peak	0	0	0	0	0	1
	Smeared Peak	0.2	0	0	0.1	0.2	0.5
	Double Peak	0.3	0	0	0	0	0.7

Values show the relative weighting of each source generated from the neural mass model (column headers), with weights adding up to 1. The single peak condition used one neural mass model source for each antenna, while the smeared peak condition distributed weights to neural mass model sources with nearby peak frequencies. The double peak condition used unequal weightings of only 2 neural mass model sources.

For each condition, we induced periodic connections between the 3 antenna signals of interest, using the pattern shown in Figure 5-3. The 6 pre-defined signals lasted for 20 minutes total for each signal condition, with intermittent connections every 2 seconds. We recorded 20 minutes of 128-channel EEG (BioSemi Active II, BioSemi, Amsterdam, NL) from these signals sent through the phantom head, resulting in 100 trials for each type of periodic connection.

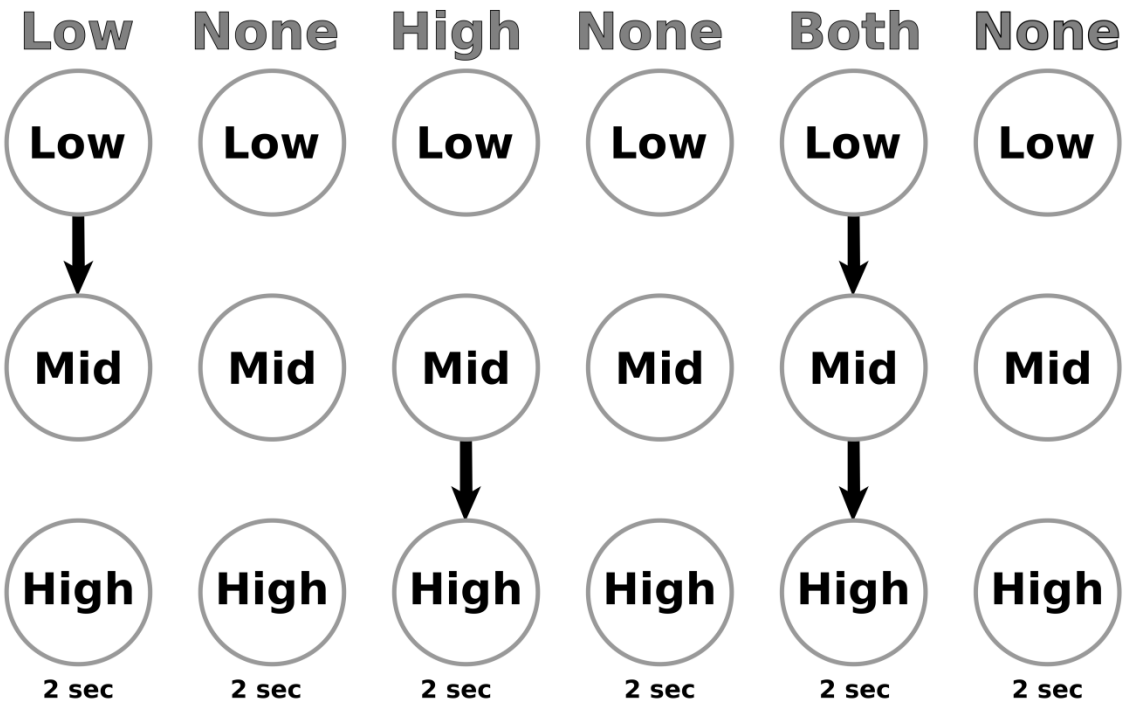

Figure 5-3: Connectivity protocol between 3 antennae of interest. The pattern for each connectivity trial is shown. Circles indicate the 3 antenna signals of interest, with low/mid/high referring to each signal's relative peak frequency. Arrows signify when a connection between signals was present, with titles at the top indicating what type of connection was present during each 2 second period. Each trial lasted 12 seconds total. We included 100 trials (20 minutes total) for each motion condition.

It should be noted that for the single dominant frequency condition, we found that the front-most low-frequency distractor signal (peak frequency of 4 Hz) resulted in suboptimal independent component analysis decomposition. When we analyzed the correlation for each antenna signal between 12 sec trials, we found a much higher autocorrelation for this low-frequency distractor

signal (0.42) than any of the other signals, including the low signal (0.01). This suggests that independent component analysis performs better with some data variability. We used a 3.25-4.75 Hz notch filter to remove this signal only for the single dominant frequency condition, which improved the independent component analysis decomposition.

We collected real-world human head motion during gait from one young healthy subject (male), using an inertial measurement unit (APDM, Portland, OR) strapped to his forehead. This subject provided written informed consent, and our protocol was approved by the University of Michigan Health Sciences and Behavioral Sciences Institutional Review Board for the protection of human subjects. We recorded 20-minute conditions each of standing and walking at 0.5 m/s, 1.0 m/s, 1.5 m/s, and 2.0 m/s. This data was converted into trajectories that were replicated by our Notus hexapod (Symétrie, Nimes, FR), similar to a previous study (Symeonidou, Nordin, Hairston, & Ferris, 2018). By mounting the phantom head on top of the hexapod, we could simulate realistic human motion during phantom head recordings. Due to electromagnetic noise from the hexapod motors when using the MicroLabBox, all EEG recordings with the antenna signals turned on were performed with the motors off. We recorded EEG motion data separately on the same testing day and added the motion data to the signal data during post-processing.

EEG Analysis

EEG data were processed in EEGLAB using custom Matlab 2013a scripts (Delorme & Makeig, 2004). We high-pass filtered the data at 1 Hz to remove baseline drift. We performed bad channel rejection by identifying channels with notably large standard deviation, a kurtosis above 5 standard deviations, or with uncorrelated activity for more than 1% of the trial time (Peterson, Furuichi, & Ferris, 2018). No channels matched these criteria, so all channels were retained. We referenced the data to the common channel average. For the motion-only data, we performed a

fast Fourier transform using Welch's method to characterize the frequency content of motion artifact at different walking speeds. We then added the motion and signal data, creating separate motion trials for each signal condition. In addition, we added simulated pink noise to maintain a similar 1/f power result to standard EEG studies (Linkenkaer-Hansen, Nikouline, Palva, & Ilmoniemi, 2001). We also increased the 60 Hz noise by adding uniform random noise that was bandpass filtered between 59-61 Hz. We then re-referenced to the common average across channels and ran adaptive mixture independent component analysis (AMICA) (Palmer, Makeig, Kreutz-Delgado, & Rao, 2008; Palmer, Kreutz-Delgado, & Makeig, 2006), using principal component analysis reduction to 60 components beforehand.

After running independent component analysis, we used the maximum cross-correlation between independent components and the original antenna signals to identify the component associated with each antenna. It is important to note that the sign of each independent component time series can be arbitrary based on the component weights, leading to inverted component data compared to the original signals (Makeig & Onton, 2009). This is less of an issue for single-frequency sinusoidal signals, where lagging the component signal can remove the inversion effect. Because we dealt with complex frequencies, we selected the maximum cross-correlation between each the inverted and non-inverted component time series. We also calculated the power spectra of the 3 antenna signals of interest (low, mid, high) and their corresponding components in order to quantify similarity in frequency content. We also computed scalp maps for each component to visually determine the spatial similarity between the antenna and its corresponding component. In addition to cross-correlation, we calculated signal to noise ratio by using the independent component analysis weights that map channels to components and applying them separately to the signal data and to the motion and pink noise data because we collected the

signal and noise data separately. Signal to noise ratio was calculated as the mean square of the signal data divided by the mean square of the noise data, converted to decibels.

Connectivity was performed using the Source Information Flow Toolbox (SIFT) (Delorme, et al., 2011). We retained the 5 components that best aligned with the 5 antenna signals used (excluding the front-most distractor components for consistency across conditions). These 5 components were processed in SIFT, using a 500 ms sliding window and 25 ms step size. Each window was detrended. Each connection type had 100 trials per condition. We fit separate multivariate autoregressive models to our data for each motion and signal condition (and connection type), using Hannan-Quinn information criterion to determine the optimal model order (Lütkepohl, 2007). After fitting and validating the model, connectivity was estimated using dDTF, ffDTF, gPDC, rPDC, GGC, WPLI, PLV (Figure 5-4). We also performed phase-randomized surrogate statistics to determine significantly nonzero connectivity estimates (Theiler, Eubank, Longtin, Galdrikian, & Doyne Farmer, 1992). This uses the same model fitting and connectivity estimation techniques, but applied to phase-randomized data, creating a null distribution. Non-significant values were set to 0.

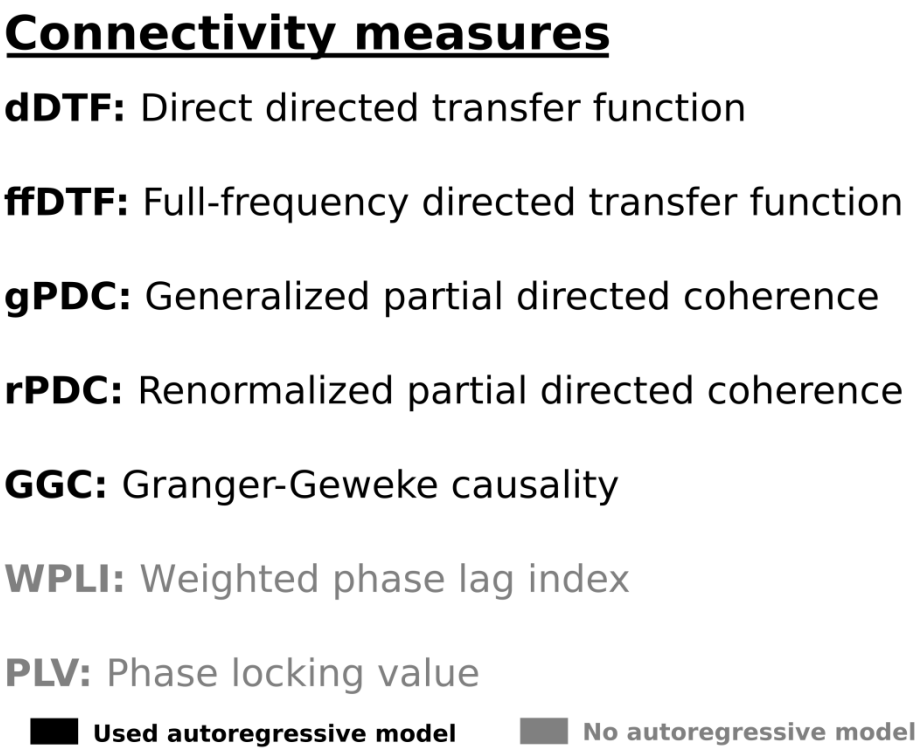

Figure 5-4: Connectivity measure abbreviations. The abbreviations for the connectivity measures used in this study are provided for reference. We have used different colors to indicate measures that used an autoregressive model (black) and ones that were applied directly to the independent component data (gray).

To reduce the dimensionality of our connectivity data, we averaged the resulting time-frequency connectivity values across the first second of connectivity onset, as shown in Figure 5-5. We then normalized the averaged results to the maximum value for each condition, allowing comparisons across different measures. We plotted this averaged, normalized connectivity together for all connectivity measures during the stationary condition. To quantify relative accuracy and precision, we computed an average frequency and standard deviation during the stationary condition, weighted by the connectivity strengths at each frequency. We also used the maximum value across frequency bins for each connection to determine how strong each estimated connection was. We compared the stationary condition to the motion conditions using correlation of the time-averaged, significance-masked connectivity. This included a comparison

between the connectivity results from the stationary condition and from the signals that were sent into each antenna, which helped determine the effect of the phantom head. While we did use surrogate statistics, we were unable to use statistics to compare across conditions and measures because there is no inter-subject variability. We feel that it is reasonable to not have statistics because we have a ground truth to compare to. Similar studies attempting to validate EEG processing and connectivity measures have also not used statistics (Mahjoory, et al., 2017; Oliveira, Schlink, Hairston, König, & Ferris, 2016).

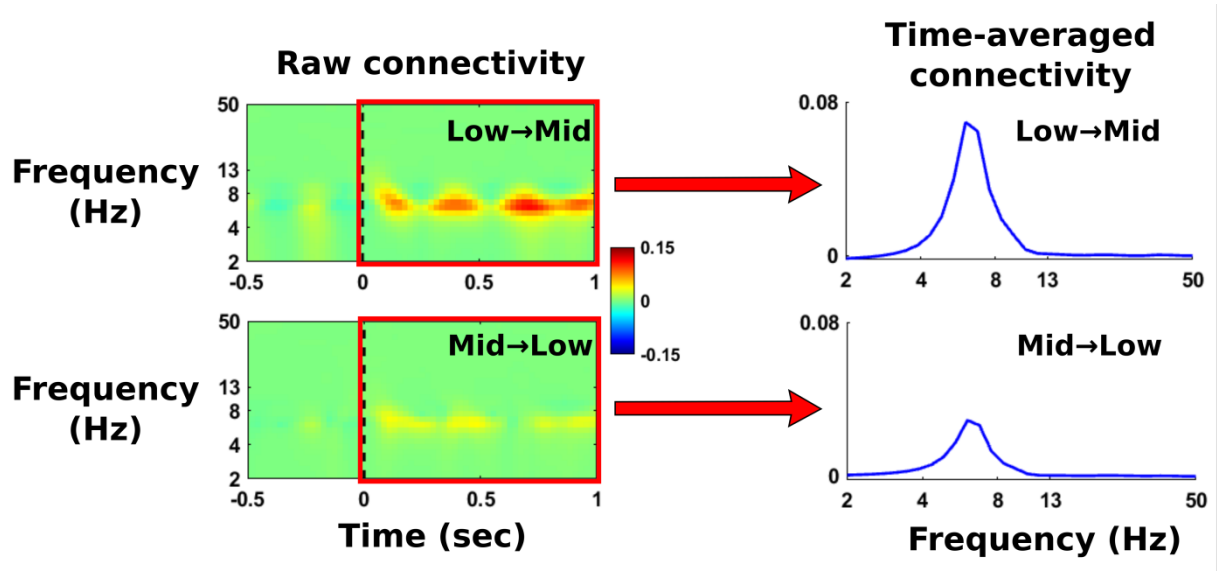

Figure 5-5: Example of time-averaged connectivity. An example of how the time-averaged connectivity is obtained from the time-frequency connectivity results from SIFT. We averaged the 1 second following connection onset, which is at time 0. This results in a one-dimensional trace that shows the average frequency connectivity that measure found. Using this, we were able to plot connectivity results across all measures of interest on a single plot.

Results

The EEG motion artifact noise from head motion during walking was concentrated at frequencies below 4 Hz (Figure 5-6). Each walking speed contained different frequency peaks. As walking speed increased, EEG noise data power peaks increased in power and shifted

towards higher frequencies. This can be seen in the raw data traces, where faster speeds have larger peak amplitudes and faster oscillatory behavior. At faster walking speeds of 1.5-2.0 m/s, large harmonic frequency peaks can be seen near 2 and 3 Hz.

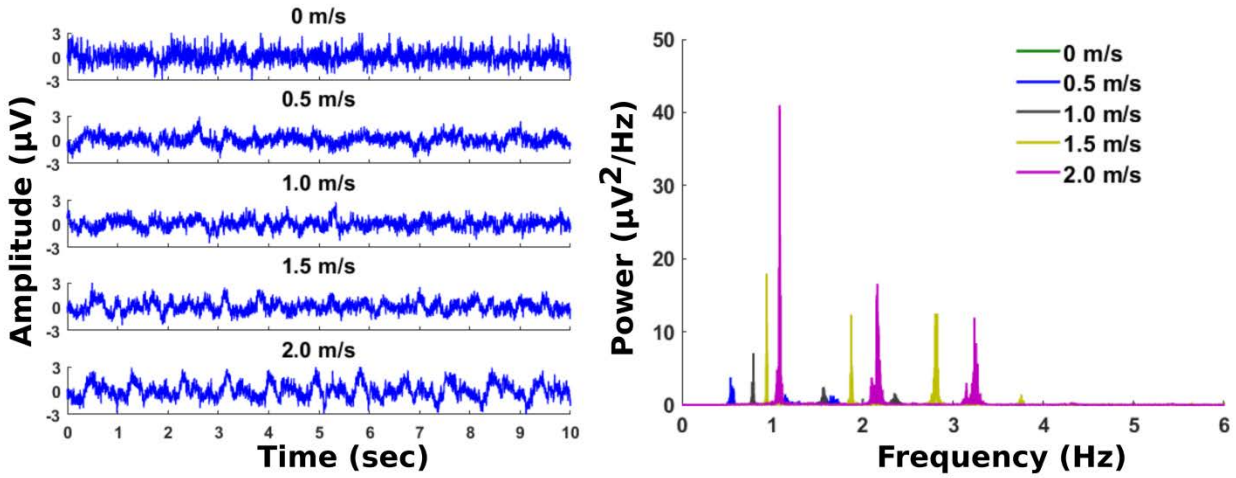

Figure 5-6: Real walking noise effect on EEG. The time courses (left) and power spectra (right) of just the head motion artifact recorded with the EEG system are shown. We recorded head motion during 5 different walking speeds, from stationary (0 m/s) to 2.0 m/s, and used a motion platform to play back this head motion while recording EEG from the phantom head. Peak frequency power increases at faster walking speeds, along with each peak shifting towards a higher frequency. This can be seen in the time courses, as the rhythmic motion artifact becomes more pronounced and oscillates quicker as walking speed increases.

Independent component analysis performed well in finding the 3 signals of interest in each condition (Figure 5-7 and Figure 5-8). The only exception was the low signal during the double peak condition, which was not well-recovered based on the difference in power spectra and low signal to noise ratio. Otherwise, independent components had high signal to noise ratio values ~10 dB or higher that remained consistent at fast movement speeds. In contrast, the signal to noise ratio of the Cz channel started near 10 dB during the stationary condition, but decreased to ~2 dB at the fastest walking speed. Visual inspection of the independent component power and original antenna signal power spectra indicated that volume conduction, head motion, and pink

noise mostly added power to the delta (1-4 Hz) and gamma (>30 Hz) power bands. Cross-correlation was above 0.9 for the single peak condition, above 0.8 for the mid and high signals for the other conditions. Based on the decreased signal to noise ratios and cross-correlations for the low signals compared to the other signals in the smeared peak and double peak conditions, independent component analysis seemed to have the greatest difficulty recovering low-frequency signals.

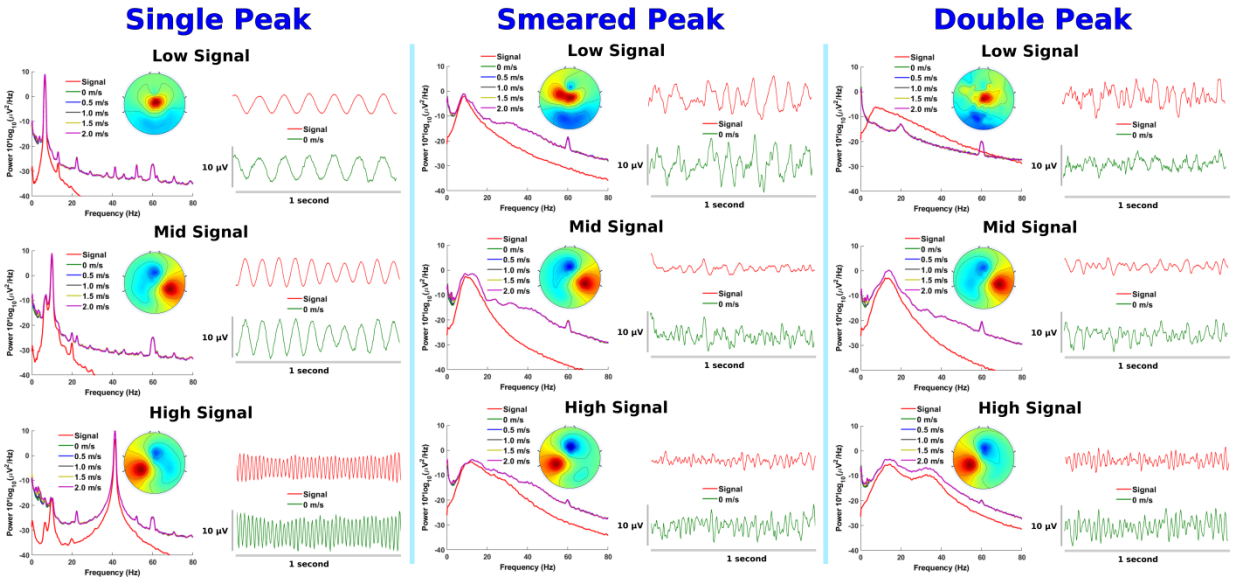

Figure 5-7: Antennae signals and recovered independent components. The results of each independent component decomposition are shown for the 3 conditions. Power spectra results for each movement speed are displayed along with the power spectra of the original signals sent through each antenna in red. We visually compared the time course for each signal before being sent through the phantom (red) to the reconstructed signal from independent component analysis during the stationary condition (green). Additionally, the channel weightings for each independent component are visualized by the inset scalp maps, which match well with the true locations of the antenna that generated the corresponding signal.

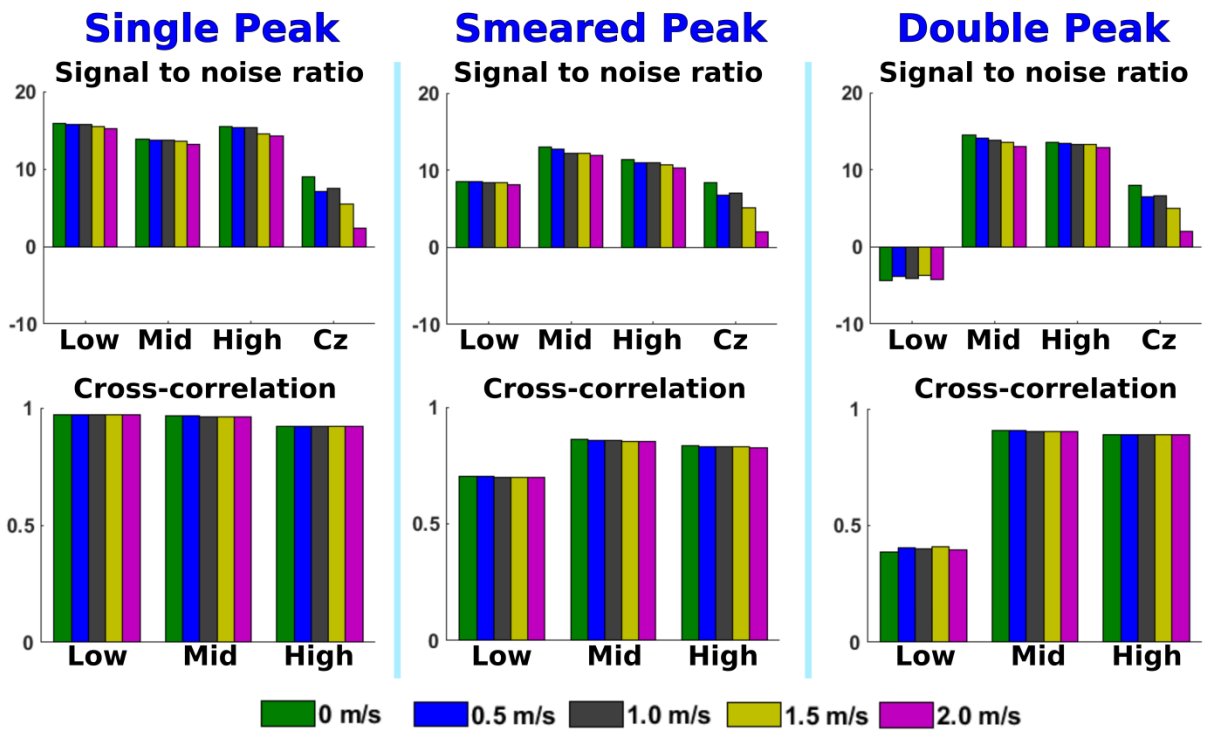

Figure 5-8: Component signal to noise ratio and cross-correlation. Plots are shown of recovered component signal to noise ratio and cross-correlation between the component and original antenna signal. Signal to noise ratio remained consistent across walking speeds for the components, while the signal to noise ratio of a representative channel (Cz) is notably affected. Additionally, cross-correlation indicated which independent components best match with their respective original signals. With the exception of the low signal for the double peak condition, independent component analysis appeared to recover the original signals well.

Autoregressive model validation prior to connectivity estimation showed reasonable model fits to the data, as shown in Table 5-2. All models across signal and motion conditions had low parameter to datapoint ratios (<0.1), indicating that overfitting was unlikely. Interestingly, the model orders increased slightly for the single peak condition compared to the other two conditions. For all conditions, the likelihood of the residuals being white and the consistency were below the desired levels of 0.95 and 85%, respectively, which likely indicates extra data structure not captured by the model. The negative stability index across all conditions indicated that all models were stable. Overall, the models were stable and appeared to avoid overfitting,

indicating that they fit the data well. In addition, we used the same model fit across different connectivity measures, meaning that the fit of each model should not have impacted inter-measure connectivity differences.

Table 5-2: Multivariate autoregressive model validation results

	Single Peak	Smeared Peak	Double Peak
Parameter to datapoint ratio	0.04 (0.00)	0.03 (0.00)	0.03 (0.00)
Model Order	9.4 (0.9)	7.8 (0.1)	7.8 (0.2)
Residual whiteness likelihood	0.82 (0.02)	0.90 (0.01)	0.90 (0.01)
Consistency (%)	75.7 (1.5)	74.6 (4.1)	75.9 (3.3)
Stability index	-0.03 (0.00)	-0.11 (0.02)	-0.10 (0.00)

Mean validation results from the fit models are shown, with standard deviation in parentheses. Optimal model order was determined using the Hannan-Quinn Criterion across all time windows. The models were stable and likely avoided overfitting due to negative stability indices and parameter to datapoint ratios below 0.1, respectively. The likelihood of the residuals being white and the model consistency were slightly lower than desired, indicating that the model may not have completely captured all of the data variance. We used the same model fit across different connectivity measures, which avoids differences in model fit from affecting inter-measure differences.

Time-averaged estimated connectivity varied among different connectivity measures for the stationary motion condition (Figure 5-9), with some measures containing frequent spurious results. Most connectivity measures were able to determine the mid signal to high signal connection, validating the use of such measures for estimating connectivity. However, there were clear differences across measures. Both PLV and WPLI frequently found spurious, high-frequency connections. They also correctly estimated connectivity in the low to mid connection during the double peak condition, even though independent component analysis did not recover

the original low signal. Both GGC and gPDC also had spurious high-frequency connections, with GGC identifying no true connectivity during the single peak condition. In addition, rPDC incorrectly estimated spurious low-frequency connectivity. While ffDTF and dDTF appeared to be robust to noise, we noticed that ffDTF can sometimes estimate the connection to be in the wrong direction, such as to both low to mid connections during the smeared peak condition. dDTF may sometimes show directional connections as bidirectional, but it does not appear to indicate incorrect connectivity direction. Still, this suggests caution when interpreting estimated connectivity direction.

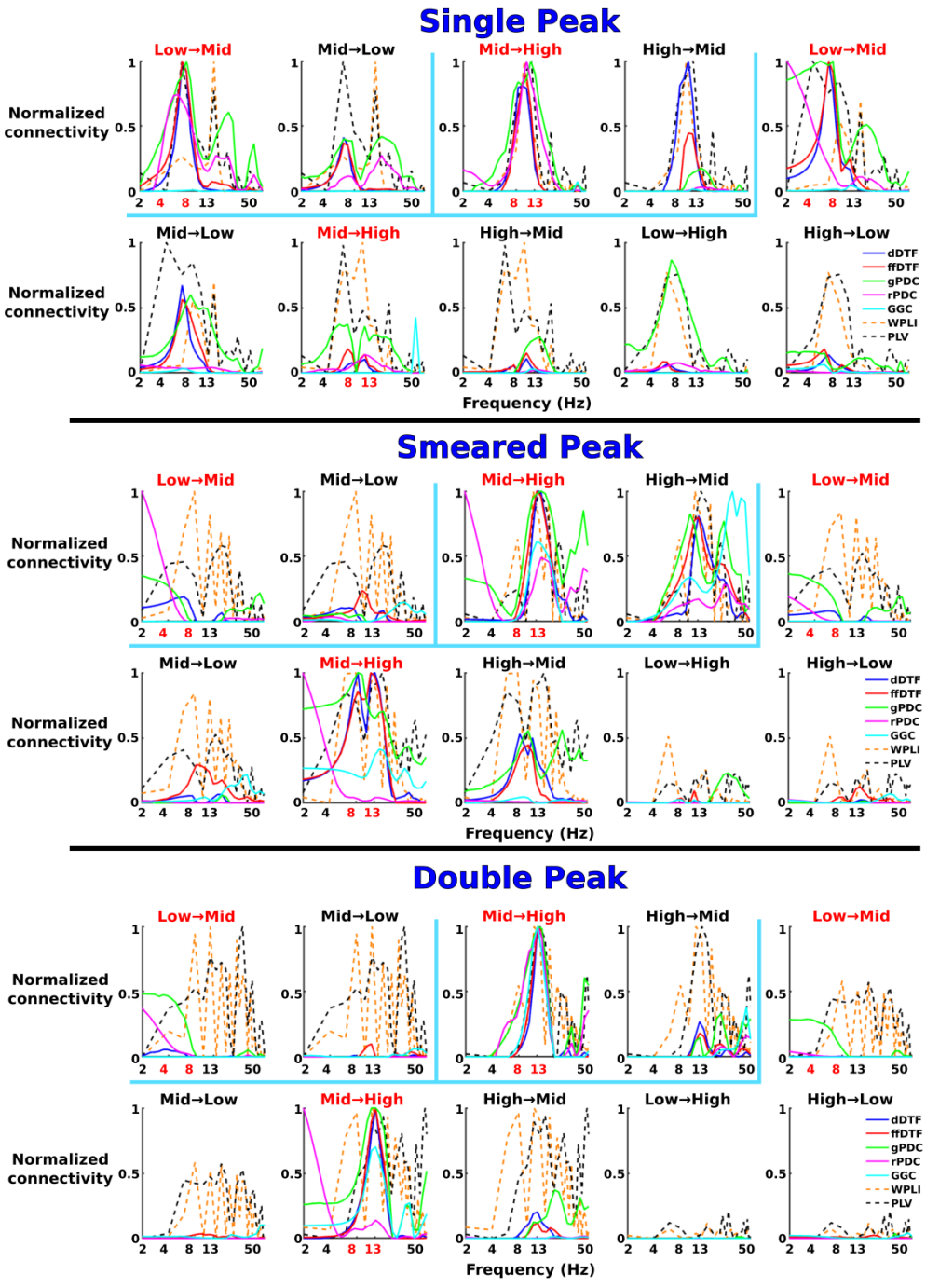

Figure 5-9: Time-averaged connectivity results. Time-averaged connectivity results are shown for our 8 measures of interest for the stationary motion speed only. Connectivity was tested for significance using phase-randomized surrogate statistics with 200 permutations. Non-significant connectivity results were set to 0, and the resulting connectivity was averaged across the 1 second after connection onset. Red titles indicate true connections, with red frequencies indicating the frequency range of the expected connection. Note that WPLI and PLV are undirected measures, so they show the same result regardless of connectivity direction.

The weighted average and standard deviation of the time-averaged connectivity highlighted differences in accuracy and precision across measures (Table 5-3). PLV, WPLI, and gPDC had consistently high average frequency and large standard deviations, reflecting their susceptibility to spurious high-frequency connectivity. GGC performed best when estimating the mid to high connections for the smeared peak and double peak conditions. Otherwise, it did not estimate much other connectivity, indicating that its performance can vary considerably based on experimental conditions and the underlying connections present. ffDTF performs well for the single peak condition, but did not find anything for the low to mid connections during the smeared peak condition. Both dDTF and rPDC appear to perform well, but rPDC appears biased towards low frequencies of 4-5 Hz during some mid to high connections when the low to mid connection is also present.

Table 5-3: Weighted mean and standard deviation of connectivity results

Table 3A: Single Peak weighted mean and standard deviation (Hz)

	Low → Mid	Mid → High	Low → Mid	Mid → High
dDTF	6.5 (2.7)	10.0 (3.9)	5.9 (2.3)	9.1 (2.1)
ffDTF	6.8 (4.1)	10.3 (3.8)	6.0 (2.8)	8.5 (2.5)
gPDC	11.4 (9.7)	11.4 (5.4)	8.2 (7.2)	10.4 (6.7)
rPDC	9.6 (7.9)	10.6 (4.7)	4.6 (4.3)	11.0 (5.0)
GGC	10.4 (9.0)	39.5 (4.0)	9.5 (4.6)	39.6 (3.5)
WPLI	15.3 (12.7)	12.9 (7.1)	15.2 (12.5)	12.2 (9.2)
PLV	16.2 (12.9)	22.5 (17.9)	14.8 (12.6)	18.8 (15.4)

Table 3B: Smeared Peak weighted mean and standard deviation (Hz)

	Low → Mid	Mid → High	Low → Mid	Mid → High
dDTF	5.1 (3.2)	16.0 (5.8)	5.3 (3.4)	10.0 (5.5)
ffDTF	-	14.3 (3.4)	-	9.5 (4.5)
gPDC	12.3 (15.2)	18.9 (13.6)	10.2 (12.6)	11.7 (7.2)
rPDC	3.9 (5.8)	13.9 (14.6)	3.7 (4.8)	4.0 (2.7)
GGC	2.5 (0.4)	15.0 (4.0)	3.4 (1.1)	13.4 (9.4)
WPLI	15.1 (8.9)	18.3 (10.6)	16.2 (9.5)	15.5 (9.1)
PLV	20.6 (14.7)	26.6 (16.5)	22.4 (15.8)	28.8 (17.1)

Table 3C: Double Peak weighted mean and standard deviation (Hz)

	Low → Mid	Mid → High	Low → Mid	Mid → High
dDTF	4.1 (2.2)	14.4 (4.7)	4.7 (1.8)	12.7 (4.2)
ffDTF	-	13.5 (2.6)	-	12.5 (3.2)
gPDC	4.6 (5.2)	17.9 (13.2)	5.0 (6.1)	13.8 (11.8)
rPDC	3.3 (3.3)	15.2 (11.1)	3.4 (4.2)	4.8 (6.4)
GGC	-	13.3 (4.4)	-	14.6 (10.5)
WPLI	21.3 (10.8)	21.4 (12.0)	24.0 (12.9)	21.3 (12.6)
PLV	23.3 (12.1)	35.3 (18.4)	24.6 (13.5)	35.2 (16.5)

For each time-averaged connectivity result with surrogate statistics applied, we computed a weighted mean and standard deviation to quantify the location and spread of the estimated connectivity. This is only shown for the stationary motion speed. In addition, green shading indicates the maximum value within that time-averaged connectivity result to determine how strong the result was.

Correlation between the stationary condition and motion conditions show a complex effect of motion on connectivity estimation (Figure 5-10). All measures were affected by motion, which may rely on the quality of the independent component decomposition for each condition. dDTF usually had high correlations close to 1 across motion conditions, except for the double connections for the single peak and smeared peak conditions where correlation dropped almost to 0. rPDC also had consistently high correlations near 1 across motion conditions, except during the smeared peak condition. Both WPLI and PLV only displayed correlations near 1 for the single peak condition, indicating that they may be more susceptible to motion effects for complex signals. It is important to note that these results must be interpreted in conjunction with the stationary condition results. For example, GGC was quite consistent for the single peak condition, but the stationary results show that GGC was consistently finding hardly any connectivity. In addition, the estimated connectivity using the raw antenna signals was consistently different from the stationary condition for all measures, highlighting the effect of real-world phantom head testing.

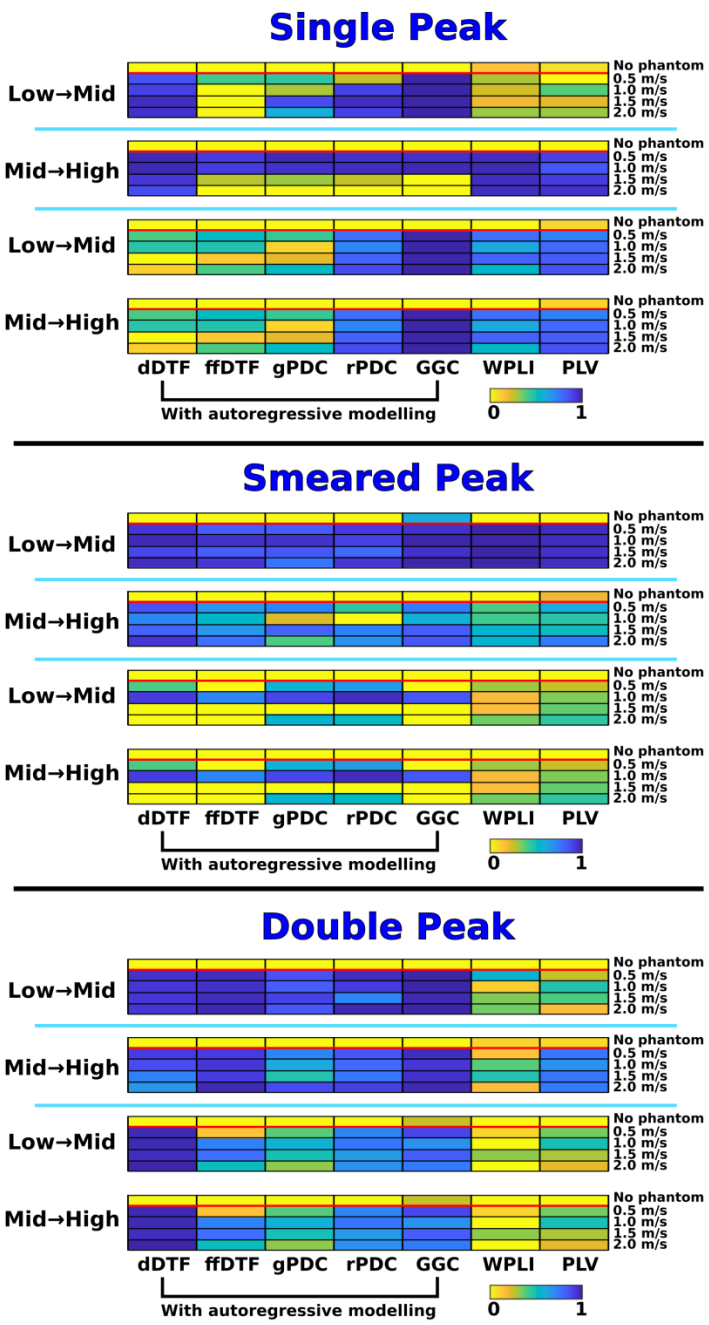

Figure 5-10: Correlation to original signals and motion conditions. The correlation between time-averaged connectivity of the stationary motion and all other head motions are shown. We also included connectivity results performed on the original signals that were sent into each antenna, designated as 'no phantom'. All motion speeds (and original signals) were fit to their own model, time-averaged, and masked using phase-randomized surrogate statistics with 200 permutations each. Both dDTF and rPDC appear to have high correlation across motion for most conditions. In addition, connectivity on the signals before they were sent through the antennae had consistently low correlation to the stationary condition, indicating the importance of using head phantoms for validating connectivity methods.

Discussion

We used a novel combination of complex neural mass model signals and a phantom head to validate independent component analysis and connectivity measures under realistic head motions. We found that independent component analysis primarily recovered the original signals of interest and separated out motion artifact. For connectivity estimation, we found variable results across measures and conditions, with most measures were able to correctly estimate the underlying connectivity. Measures applied directly to the data, instead of a fitted model, were susceptible to spurious high-frequency connections. In general, dDTF, ffDTF, and rPDC performed best for our experiments out of the measures we used.

Motion Artifact and Independent Component Analysis

The effect of walking on the EEG occurred mostly at low frequencies, indicating that slow walking speeds minimally affect EEG results, especially at most physiological frequencies. This has been indicated by other studies (Nathan & Contreras-Vidal, 2015; Snyder, Kline, Huang, & Ferris, 2015), but differences in cable sway across experimental setups can affect results (Symeonidou, Nordin, Hairston, & Ferris, 2018). We bundled the cables together for this study, which decreased the effect of motion artifact. As walking speed increased, the spectral power peaks of the noise data and the frequencies of these peaks increased. This highlights the challenge of computationally removing motion artifact during fast walking and running, where the motion artifact is large and can overlap with EEG frequencies of interest. Dual-layer EEG systems that can subtract out motion artifact appear to be a promising method to mitigate this issue (Nordin, Hairston, & Ferris, In press).

Independent component analysis performed well in mostly recovering the original signals. We expected this given the frequent use of independent component analysis in EEG research and its

ability to recover single-frequency, sinusoidal signals during similar phantom head validation (Oliveira, Schlink, Hairston, König, & Ferris, 2016). The consistent signal to noise ratio across motion speeds emphasizes the importance of using blind source separation to minimize the effects of motion, which is why such methods are used often during mobile tasks (Gwin, Gramann, Makeig, & Ferris, 2010; Sipp, Gwin, Makeig, & Ferris, 2013). The cross-correlation results aligned well with the signal to noise ratio results of the recovered independent components of interest. Based on the low-frequency profile of the motion artifact, it is perhaps not surprising that independent component analysis did not recover the low signal as well as the other signals in the smeared peak and double peak conditions. This may be an important concern when analyzing low-frequency EEG activity during motion. Still, all signals had consistent cross-correlations and signal to noise ratios across motion speeds, suggesting that robust motion separation did occur.

Connectivity Estimation Measures

Connectivity measures generally identified the true connections, especially the mid to high connection. This validates the use of independent component analysis and such measures for mobile EEG settings. However, there were substantial differences in performance across measures, especially with regards to finding false positives. We especially noticed this for PLV and WPLI, which estimated connectivity directly from the data instead of using a fitted model. Because these measures utilize trial averaging, their performance likely would have increased with more trials. In addition, many other factors could have altered connectivity estimation, such as choice of reference or type of source localization used (Mahjoory, et al., 2017). Still, multivariate autoregressive modelling may provide a more robust framework for connectivity estimation than trial averaging.

Out of the estimation techniques using multivariate autoregressive modelling, we found that dDTF, ffDTF, and rPDC appear to provide the most reliable estimates. GGC appeared unreliable, especially in the single peak and smeared peak conditions. Other techniques have been used for GGC besides multivariate autoregressive models (Dhamala, Rangarajan, & Ding, 2008), indicating that the methods used with GGC should be carefully considered beforehand (Dhamala, Liang, Bressler, & Ding, 2018). We also found that ffDTF estimated the true connectivity correctly in most cases, but some of its results would lead researchers to conclude that the connection occurred in the wrong direction. This makes ffDTF potentially problematic to use if directionality is of particular interest, such as analyzing the connectivity between the cortex and leg muscles. Directionality accuracy appears improved for dDTF and rPDC, but it still appears important to utilize statistical tests to firmly establish a specific directionality. Our results show that no one measure provides a completely clean picture of the true underlying connectivity, suggesting that using multiple connectivity measures may provide the most robust estimates of underlying connections.

Despite the consistent component signal to noise ratio values, connectivity estimation still was impacted by motion and real-world volume conduction. Correlations varied between motion conditions and the stationary condition for all measures, without a clear indication of one measure being most robust to motion in all cases. In general, rPDC and dDTF appear to be the most stable across walking speeds, despite varying estimates during the smeared peak condition. While GGC, WPLI, and PLV were fairly consistent in some conditions, it is important to note that their stationary connectivity estimations were not ideal results, even if they were maintained for different walking speeds. In addition, we found consistently low correlation between the estimated connectivity during the stationary condition and the estimated connectivity performed

on the original signals before being sent through the head. This effect was seen across all measures and conditions, indicating that volume conduction and noise from real-world recording at the scalp do consistently affect the resulting connectivity estimation (Brunner, Billinger, Seeber, Mullen, & Makeig, 2016).

Limitations

While we were able to validate connectivity under real-world scenarios, our study was limited to a subset of connectivity measures and motion artifact that did not consistently occur during the event of interest. There are many other available measures to estimate connectivity, including coherence, mutual information, and multivariate phase synchronization (Jalili, Barzegaran, & Knyazeva, 2014). We focused primarily on measures based on Granger causality that were available in the SIFT toolbox (Delorme, et al., 2011). In addition, there are many other source localization techniques, such as the various beamforming methods (Jonmohamadi, et al., 2014). We also did not look at motion artifact that consistently overlaps with connectivity onset, which would be applicable to EEG studies during locomotion. Any lingering motion artifact following independent component analysis may have had a notable effect on connectivity if time-locked to an event of interest. For this reason, it is important to consider the potential effects of motion artifact, even at slow walking speeds, if it is time-locked to the event of interest. The influence of motion artifact depends on a variety of factors, including the performance of blind source separation of motion and brain sources, the events of interest, and cable sway (Symeonidou, Nordin, Hairston, & Ferris, 2018; Snyder, Kline, Huang, & Ferris, 2015).

Conclusions

We validated that several connectivity measures can accurately estimate true connections between complex signals exposed to real-world volume conduction and head movement via a

head phantom. Independent component analysis recovered most of the original signals and appeared to separate out motion artifact. We were able to show that performing connectivity on sources from independent component analysis can find the true connections in a real-world scenario, but no one measure performed optimally in every condition. It may be beneficial to use multiple connectivity measures to increase confidence in the estimated connectivity results. Our technique opens up the ability to use complex, ground-truth signals in a real-world environment to validate EEG methods, improving our understanding of how well common EEG methods truly work.

Chapter 6: Group-level Corticomuscular Connectivity during Visual and Physical Perturbations to Walking and Standing Balance [5]

Abstract

Maintaining balance is a complex process requiring multisensory processing and coordinated muscle activation. Previous studies have indicated that the cortex is directly involved in balance control, we less information is known about cortical flow of signals for balance. We studied electrocortical dynamics of healthy young subjects (19 subjects: 7 male and 12 female) walking and standing with both visual and physical perturbations to their balance. Independent component analysis of electroencephalography (EEG) can provide rigorous single-subject connectivity information but extending such analysis to multiple subjects remains an open problem due to variations in computed components across subjects. The goal of this study was to estimate missing component data in order to quantify differences in group-level corticomuscular connectivity responses to sensorimotor perturbations during walking and standing. We hypothesized that our novel group-level connectivity method would result in a model that would fit the data well. We also hypothesized that cortical connectivity would be located primarily in occipito-parietal areas during visual rotations and primarily in central motor areas during physical pull perturbations. Our findings show that our estimation technique reasonably approximates independent components and our models were likely unaffected by overfitting. We also found the strongest cortical connections in similar parietal and occipital areas, regardless of the perturbation type. Results also indicated corticomuscular connectivity from supplementary

[5] This chapter has been submitted for publication in *NeuroImage*.

motor area to lower leg muscles, suggesting potential corticomuscular communication during perturbed balance. These results show that sensorimotor perturbations to balance alter cortical networks and that similar group-level connectivity analyses may be useful for future studies.

Introduction

In real world scenarios, humans frequently make postural adjustments to avoid losing balance. Such adjustments necessitate precise coordination between sensory input, cognitive processing, and motor control (Macpherson & Horak, 2012). Despite the cortex's involvement in maintaining balance (Bolton, 2015), our current understanding of real-world human cortical activity during perturbed balance remains limited (Varghese, McIlroy, & Barnett-Cowan, 2017). Stationary recordings and low temporal resolution have limited traditional neuroimaging methods, such as functional magnetic resonance imaging (fMRI) and functional near-infrared spectroscopy (fNIRS). In contrast, high-density, source-localized EEG is a promising method to assess human cortical dynamics during balance because of its high temporal resolution and portability (Gramann, Ferris, Gwin, & Makeig, 2014; Gramann, et al., 2011). While EEG can be limited by low spatial resolution and artifact contamination (Urigüen & Garcia-Zapirain, 2015), blind-source separation techniques such as independent component analysis can separate out cortical activity from artifacts, leading to enhanced spatial resolution and reduced artifact contamination (Makeig, Bell, Jung, & Sejnowski, 1996; Gwin, Gramann, Makeig, & Ferris, 2010).

In addition to analyzing dynamics of each cortical area individually, connectivity allows analysis of how these sources interact with each other. This is relevant during perturbed balance, where many brain regions are active due to sensorimotor integration (Sipp, Gwin, Makeig, & Ferris, 2013; Slobounov, Cao, Jaiswal, & Newell, 2009). A variety of measures can be used to quantify

connectivity, including undirected and directed measures (Blinowska, 2011). Such measures can be used on either channel data or independent components from blind-source separation, although component data is less susceptible to motion artifact and volume conduction (Snyder, Kline, Huang, & Ferris, 2015; Brunner, Billinger, Seeber, Mullen, & Makeig, 2016). We used direct Directed Transfer Function (dDTF) (Korzeniewska, Mańczak, Kamiński, Blinowska, & Kasicki, 2003), which is a modified form of Directed Transfer Function (Kaminski & Blinowska, 1991) that emphasizes direct connections. dDTF is an extension of Granger causality to multiple data channels and allows for quantification of directed connectivity. Granger causality is based on the assumption that one channel (Channel A) causes activity in another channel (Channel B) if A provides past information that helps predict B (Granger, 1969). A multivariate autoregressive model is often used to extend this principle to more than 2 channels. This model fits the time series data by predicting the next value in time by using a linear combination of past values (Harrison, Penny, & Friston, 2003). The number of past values used, referred to as the model order, must be carefully managed to avoid overfitting the model with too many past values (Lütkepohl, 2007). We chose dDTF to quantify connectivity based on its robust performance and ability to ignore indirect connections (Astolfi, et al., 2007; Höller, et al., 2017).

Despite several rigorous pipelines and toolboxes for single-subject connectivity estimation (Delorme, et al., 2011; He, et al., 2011; Oostenveld, Fries, Maris, & Schoffelen, 2011), analyzing group-level connectivity with independent components remains an open problem. Independent component analysis is primarily data-driven, with the experimenter not directly influencing where the resulting components will be located. While this is an advantage in many cases, this becomes a challenge for connectivity analysis because the locations of independent components vary across subjects. Ideally, every subject would have one component dipole in each group-

level cluster, as seen for example subject 1 in Figure 6-1. More likely, though, subjects will not have dipoles in all clusters, which greatly impacts the available connections to analyze. Despite missing dipoles in just one cluster, example subject 2 only has one connection between dipoles that we can analyze, instead of 3. Example subject 3 demonstrates another issue of having multiple dipoles in a single cluster. Due to this component location inconsistency across subjects, it has been challenging to develop an appropriate technique for addressing this issue. One currently available method for group analysis is disjoint clustering via the measure projection toolbox (Bigdely-Shamlo, Mullen, Kreutz-Delgado, & Makeig, 2013). This projects each dipole into common regions of interest which can then be averaged across subjects, resulting in an estimation for group-level connectivity. The downside to this method is that it does not specifically address any missing dipoles, and the results can be substantially different based on parameter selection and the connectivity measure used (Lee C. , 2016). Another method uses a hierarchical Bayesian model to infer group-level connectivity using a Monte Carlo algorithm (Mullen T. R., 2014). This method includes the uncertainty from missing dipoles to generate more robust statistical analyses, but is complex and remains under development. There is a need to estimate the missing data for group connectivity analysis, ideally by combining group-level and subject-specific information.

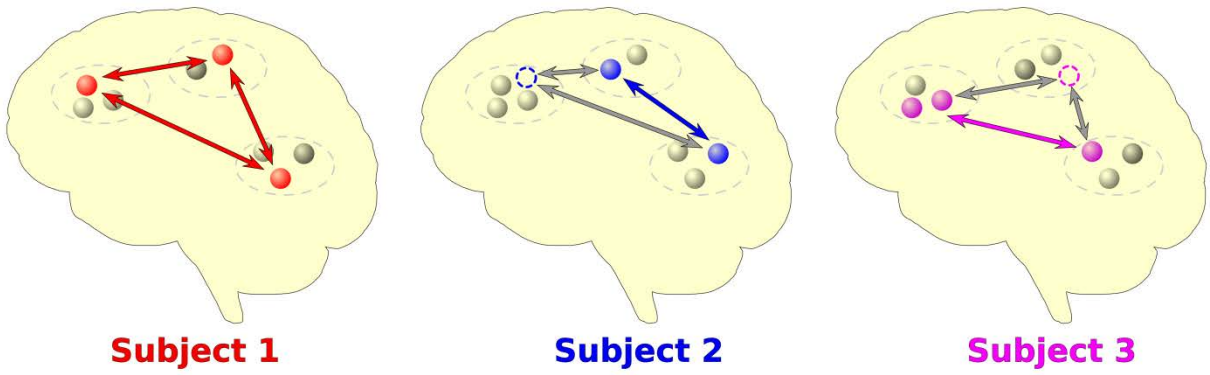

Figure 6-1: Example of group-level connectivity missing data problem. Example subject independent components are shown to illustrate the group-level connectivity issue with missing data. Dashed gray circles indicate 3 cortical clusters in the brain. Ideally, all subjects would have a single dipole in each cluster (subject 1). However, independent component analysis is data-driven, so group-level clusters are unlikely to contain dipoles from all subjects or can contain multiple dipoles from a single subject, as can be seen for subjects 2 and 3. Because connectivity is interested in the interaction between sources (shown with double-sided arrows), missing a single component for subjects 2 and 3 eliminates two connections between clusters. There is a need to estimate this missing data in order to perform group-level connectivity analyses.

Connectivity has been studied during gait and perturbed balance, with different motor actions altering cortical and corticomuscular connections. Connectivity has been shown to increase during standing compared to treadmill walking as well as decrease when performing a cognitive task during standing, potentially indicating increased focus during stationary balance control (Lau, Gwin, & Ferris, 2014). In addition, connectivity responses to expected and unexpected balance perturbations were found to be similar, although unexpected perturbations elicited increased connectivity strengths (Varghese J. P., 2016). For healthy adults performing recumbent stepping, it was found that connectivity was greatly increased during arm movements compared to leg movements, likely reflecting greater cortical involvement with upper-limb movements (Kline, Huang, Snyder, & Ferris, 2016). In addition to cortical connections, multiple studies have shown potential corticomuscular connections during gait (Artoni, et al., 2017; Petersen, Willerslev-Olsen, Conway, & Nielsen, 2012; Roeder, Boonstra, Smith, & Kerr, 2018). While

gait may involve more anticipatory balance responses, similar connectivity responses between unexpected and expected balance perturbations seen by Varghese (2016) suggest that the cortex may be involved in muscles responses to unexpected perturbations, in addition to subcortical structures (Jacobs & Horak, Cortical control of postural responses, 2007). In general, many aspects of connectivity during perturbed balance remain unexplored (Varghese, McIlroy, & Barnett-Cowan, 2017). Assessing group-level connectivity during perturbed balance could improve understanding of cortical network activity during balance as well as electrocortical dynamics in mobile, real-world scenarios.

The purpose of this study was to quantify differences in group-level corticomuscular connectivity responses to sensorimotor perturbations and during walking. We estimated missing component data by balancing group-level and subject-specific information, enabling group connectivity analysis of independent components. We hypothesized that our group-level connectivity model would fit the data well and produce connectivity results robust to parameter selection and choice of connectivity measure. We also hypothesized that cortical connectivity would be located primarily in occipito-parietal areas during visual rotations based on the prominent visual processing cortical areas and primarily in central motor areas during physical pull perturbations, based on previous perturbation-evoked EEG activity found in these areas (Sipp, Gwin, Makeig, & Ferris, 2013; Varghese, et al., 2014). For corticomuscular connectivity, we were unsure if there would be any interaction during the perturbations because they are reactionary, but we hypothesized that the most likely connection would be between the tibialis anterior and supplementary motor area, based on previous corticomuscular connectivity during gait (Artoni, et al., 2017; Petersen, Willerslev-Olsen, Conway, & Nielsen, 2012).

Materials and Methods

We tested 30 healthy, young adults [15 females and 15 males, age 22.5±4.8 years (mean±SD {standard deviation})]. All subjects identified themselves as right hand and right foot dominant, with normal or corrected vision. We screened subjects for any neurological, orthopedic, or cardiac conditions and injuries. All subjects provided written informed consent. The University of Michigan Health Sciences and Behavioral Sciences Institutional Review Board approved our protocol for the protection of human subjects. Prior to testing, we prescreened all subjects for motion sickness in virtual reality.

During the experiment, subjects either walked at 0.22 m/s or stood on a 2.5 cm tall by 12.7 cm wide balance beam mounted to a treadmill. The beam was only wide enough for one foot to enforce tandem gait and tandem stance. Subjects wore a body-support harness for safety, which had extended support straps to allow unrestricted mediolateral movement. We specifically instructed subjects to look straight ahead and to avoid looking down at their feet. We also instructed subjects to cross their arms to increase the difficulty of the task and to decrease inter-subject variability because there is no variation in arm movement. Subjects were also told to walk heel-to-toe and to move their hips side-to-side to balance, avoiding rotations across their body's longitudinal axis. These instructions align with previous treadmill balance beam walking studies (Domingo & Ferris, 2009; Domingo & Ferris, 2010; Sipp, Gwin, Makeig, & Ferris, 2013).

We presented subjects with two types of sensorimotor perturbations: a side-to-side pull at the waist and a 20 degree field-of-view rotation. The side-to-side pull was performed using rotational motors on either side of the subject. During perturbation onset, one motor rotates a bar away from the subject. This bar is fixed to a wire that is attached to the subject, pulling the

subject mediolaterally to one side. This perturbation lasted for 1 second before the motor rotated back to its starting position. We used tensile load cells in series with the wire connected to the subject in order to determine the onset of the pull perturbation. The field-of-view rotation was performed using a virtual reality headset (Oculus Rift DK2, Oculus, Redmond, WA). We attached a webcam (Logitech c930e, Logitech) below the virtual reality headset. The webcam view was displayed on the virtual reality headset, providing subjects a pass-through virtual reality experience. We performed perturbations by digitally rotating the virtual reality view 20 degrees clockwise or counterclockwise. This perturbation lasted for a half second before the virtual reality view digitally rotated back to its starting position.

We recorded 136-channel EEG (BioSemi Active II, BioSemi, Amsterdam, NL) and 8 lower-leg EMG channels (Vicon, Los Angeles, CA). EEG was sampled at 512 Hz and synced with visual perturbation events using Lab Streaming Layer (Delorme, et al., 2011). EEG electrode positions were determined using a Zebris ELPOS digitizer (Zebris Medical GmbH, Isny, Germany). EMG was sampled at 1000 Hz and was recorded with the load cell data. We synced the EMG and EEG data using a 0.5 Hz square wave. To determine pull perturbation onset, we detrended the load cell data (LCM703, OMEGA Engineering, INC., Norwalk, CT) and used a 3-standard deviation threshold from baseline activity that was visually inspected.

We used custom EEGLAB scripts to process the EEG data (Delorme & Makeig, 2004). EEG data was downsampled to 256 Hz, high-pass filtered at 1 Hz, merged across all conditions, and referenced to the median channel value for each timepoint. We reduced 60 Hz line noise using the Cleanline plugin for EEGLAB (Mullen T. R., 2014). We rejected bad channels that had high standard deviation, had kurtosis above 5 standard deviations, or were uncorrelated for more than 1% of the total time (Peterson, Furuichi, & Ferris, 2018). We retained 111±7 channels

(mean±SD) across all subjects. These remaining channels were further denoised. We removed large mechanical artifacts using artifact subspace reconstruction (Mullen, et al., 2013), setting a threshold of 20 standard deviations (Artoni, et al., 2017). We also performed selective low-pass filtering by combining ensemble empirical mode decomposition (Al-Subari, et al., 2015; Wu & Huang, 2009) and canonical correlation analysis (Hotelling, 1936). This targeted large high-frequency activity with low autocorrelation, such as muscle activity and line noise (Safieddine, et al., 2012). We then performed a common average reference and interpolated the rejected channels to maintain a consistent head montage.

We performed adaptive mixture independent component analysis (Palmer, Kreutz-Delgado, & Makeig, 2006; Palmer, Makeig, Kreutz-Delgado, & Rao, 2008), reducing down to 80 principal components prior to independent component analysis. We performed dipole fitting on each resulting independent component, retaining only those components that were well fit by the model (residual model variance less than 15%). We visually inspected the remaining dipoles, removing components contaminated with muscle artifact, eye movements, and line noise based on power spectra and dipole location. The final cortical components were pooled across all subjects and grouped with k-means clustering. We retained clusters containing more than half of the subjects (>15), resulting in 8 cortical clusters of activity. We split the data into epochs of -1 to 2 sec, centered around perturbation onset, resulting in 146±1 epochs for stand pull, 145±5 epochs for walk pull, 144±9 epochs for stand rotate, and 146±1 epochs for walk rotate (mean±SD).

Before calculating connectivity, we determined how many clusters each subject had at least one dipole in (Figure 6-2). Subjects with fewer dipoles across all clusters had more missing information, which was undesirable. We only retained subjects with dipoles in more than half

(>4) of the total clusters, resulting in 19 subjects (7 male and 12 female, age 22.1±5.1 years [mean±SD]) with 175 total dipoles. We then estimated the missing information in these subjects using each cluster's average scalp map, which was computed from the dipoles of the 19 subjects retained (Figure 6-3). These cluster scalp map provide an average mapping of EEG channels to that particular cluster across the group and tend to be highly dipolar, meaning that they can be well explained by a single equivalent dipole in the brain. High dipolarity is thought to be an indication that independent components reflect true EEG sources (Delorme, Palmer, Onton, Oostenveld, & Makeig, 2012). For each subject that had missing data for a particular cluster, we warped that cluster's scalp map to the subject's specific channel locations, based on their head coordinate transform calculated by DIPFIT2 (Oostenveld & Oostendorp, 2002). We then used the subject's channel locations to estimate the inverse weight matrix using the cluster scalp map. This inverse weight matrix provides a mapping from each subject's channel data to the estimated group-level cluster activity. It is important to note that our estimated data does not directly result from independent component analysis, which minimizes mutual information to maximize independence between components. Instead, our estimation method is indirectly reliant on ICA because it uses information from the group clusters, which are averaged across independent components from other subjects. It also uses the subject-specific data, which is critical in keeping group comparisons consistent. In addition to estimating missing data, if a subject had multiple dipoles in one cluster, we retained the dipole whose activity had the highest variance. This resulted in every subject having exactly 8 dipoles corresponding to each of the group-level clusters.

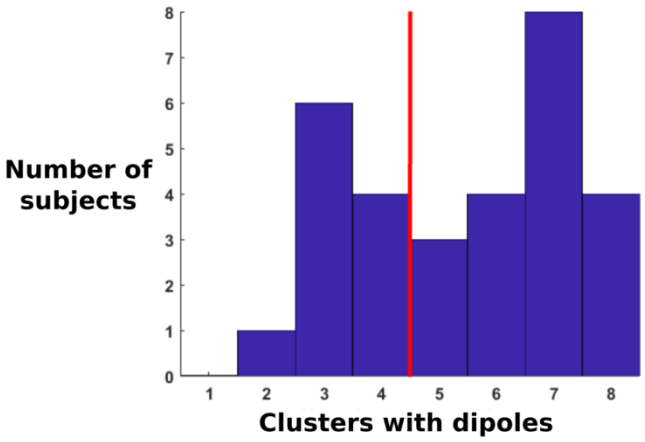

Figure 6-2: Clusters with dipoles per subject. A histogram of the number of clusters (out of 8) with at least one dipole for each subject. The red line indicates the cutoff of a subject having dipoles in more than half of the total clusters (>4). To minimize data estimation, we retained the 19 subjects to the right of the red line. This reduced the amount of estimated data by ~68%.

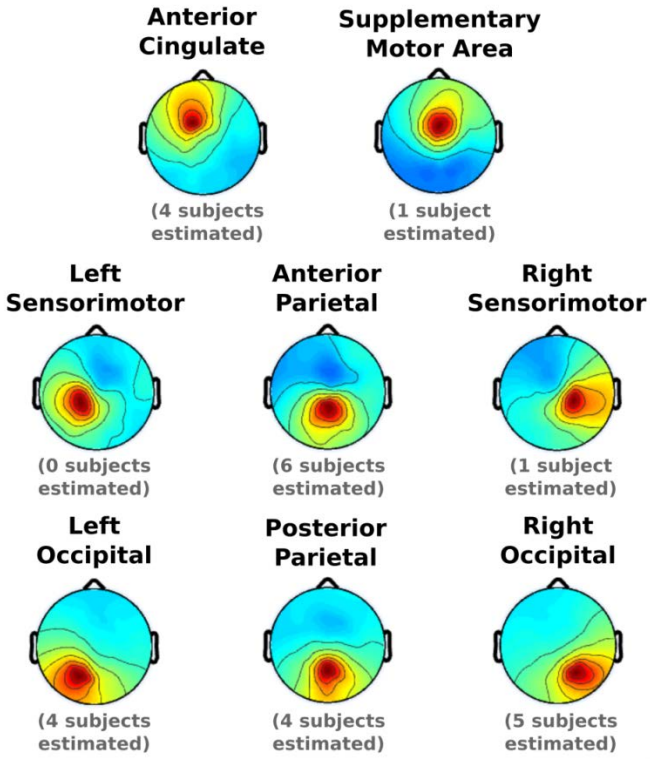

Figure 6-3: Group cluster scalp maps. Average scalp maps across all 19 subjects are shown for the 8 cortical clusters prior to data estimation. Scalp maps show the mapping of channels to average cluster activity. These scalp maps were interpolated to each subject's channel locations to estimate missing subject components for each cluster (number of estimated subjects for each cluster shown in parentheses).

To test how well our data estimation performs, we compared pairwise mutual information and dipole fitting residual variance for our estimated data and independent components. Both measures are used as quality measures to determine how well ICA performed (Artoni, Menicucci, Delorme, Makeig, & Micera, 2014; Delorme, Palmer, Onton, Oostenveld, & Makeig, 2012). Mutual information quantifies statistical independence between two variables, with a lower value indicating less dependence between the two sources. A mutual information value of 0 indicates that the two signals are completely independent (Cover & Thomas, 2006). We looked at the 8 cortical cluster sources for each subject following data estimation and calculated mutual information between all pairs (excluding self-pairs). We separated pairs of non-estimated independent components from all pairs that included at least one estimated component. We also computed the pairwise mutual information of the channel data for comparison. Due to volume conduction, we would expect the channel data to have many more high-valued mutual information pairs than either component set. Exponential probability distributions were fit to each group (components, estimated data, channels), scaled by the number of comparisons in each group. We chose an exponential distribution based on visual inspection of each group's histogram. In addition to mutual information, we also performed dipole fitting on the estimated components to find the residual variance that the model was unable to explain. Lower residual variance indicates components that fit the model well and can be more indicative of true brain sources (Delorme, Palmer, Onton, Oostenveld, & Makeig, 2012). We performed the same scaled exponential fit as the pairwise mutual information, but we only compared components and estimated data because channels do not have scalp maps.

We also included data from the 8 lower leg EMG electrodes in our connectivity analysis. EMG data was 1 Hz high-pass filtered and half-wave rectified as has been done previously (Gwin &

Ferris, 2012). We also de-modulated the signal using the Hilbert transform to retain the phase component of the EMG signal while forcing the amplitude to be consistent. This has been used previously or corticomuscular connectivity estimation and can help reduce the effect of EMG bursts in amplitude on the final connectivity measure (Boonstra, et al., 2009; Roeder, Boonstra, Smith, & Kerr, 2018). We then downsampled the both the EEG and EMG data to 128 Hz and synced them together, using epochs of -1 to 2 sec, centered around perturbation onset. Adding the EMG data resulted in 16 total sources for each subject (8 cortical, 8 muscular).

Following missing data estimation, we randomly selected 100 trials from each subject to create one large EEG-EMG dataset that was balanced across subjects. Because both visual and pull perturbations were performed to two sides (left/right or clockwise/counterclockwise), we selected 50 trials in either direction for each subject to maintain consistency. We then used the source information flow toolbox (SIFT) to fit a multivariate autoregressive model to the data (Delorme, et al., 2011). One limitation of grouping multiple subjects into one for modelling is that it assumes that all subjects have the same model order, which is likely not the case. However, we are looking for group-level connectivity, and there are always assumptions that must be made to perform a coherent group-level analysis. We felt that a single model of the group could best capture the variability of the subjects and find the similarities between them. In addition, having a high number of trials (1900) across the group can help avoid overfitting by minimizing the ratio of parameters to data points. We used a sliding window of 400 ms with step size of 20 ms. We analyzed model orders of 1 to 20 and used Hannan-Quinn information criterion to determine the optimal model order (Lütkepohl, 2007), which tries to improve model fit while avoiding high model orders to avoid overfitting. We also validated our fitted model using tests for consistency, stability, and whiteness of residuals, provided by SIFT. Consistency

was determined by simulating data from the model and calculating the Euclidean norm between the real and simulated data correlation matrices (Ding, Bressler, Yang, & Liang, 2000). This value ranges from 0-100%. Higher consistency indicates that the model was able to adequately capture the correlation structure of the real data. Stability was determined checking the logarithm of the largest eigenvalue of the model coefficient matrix (Ding, Bressler, Yang, & Liang, 2000). If this value is less than 0, then the model is stable and the results are stationary across time. Whiteness of residuals was tested using an autocorrelation function test with confidence intervals, where the final value indicates the probability that the data is white. This value ranges from 0 to 1 and should be as high as possible to increase the confidence that the residuals are truly white. If the residuals are not white, then this would indicate that there is still some correlation structure in the data that is not captured by the model (Lütkepohl, 2007).

Next, we calculated connectivity using direct directed transfer function (dDTF). Directed transfer function can be considered an extension of Granger causality (Kamiński, Ding, Truccolo, & Bressler, 2001) that can determine directed information flow amongst multichannel data. To minimize the effects of indirect connections, dDTF involves multiplying full frequency directed transfer function by partial coherence, which is sensitive to only direct connections. We calculated dDTF across time-frequency bins ranging from 2-50 Hz and -0.5 to 1.5 seconds, with perturbation onset at 0 seconds. Because we were concerned that our model order may have been too low, we separately fit models for each condition using a model order of 30 and computed dDTF. We compared the dDTF results between our 2 models for each condition, using the R2 from a simple linear fit to determine how well the models compared. We used the lower model order fit for all subsequent analyses because lower model orders are less susceptible to overfitting the data.

Similar to EEG time-frequency analyses, we analyzed baseline and perturbation-evoked connectivity for each condition using non-parametric surrogate statistics to eliminate non-significant results. To analyze baseline activity, we applied phase randomization statistics to the dDTF connectivity results (Theiler, Eubank, Longtin, Galdrikian, & Doyne Farmer, 1992), using 250 samples and setting non-significant differences to 0. This statistical test randomizes the phase of the data and then performs model fitting and connectivity estimation, creating a null distribution. The connectivity results with non-randomized phase can be compared with this null distribution to determine how likely they reflect true connectivity. After phase randomization statistics, we then averaged the results across time (-0.5 sec before perturbation onset to 1.5 sec after) and frequency, using 3 frequency bands of interest: theta (4-8 Hz), alpha (8-13 Hz), and beta (13-30 Hz). For perturbation-evoked connectivity, we applied bootstrap statistics (250 samples) to determine significantly different connectivity from the half second of activity prior to perturbation onset (Efron & Tibshirani, 1993). This half-second of baseline activity was then subtracted off and all non-significant differences from baseline were set to 0. In contrast to phase randomization, bootstrapping samples the data with replacement before fitting a model and estimating connectivity, creating a null distribution to use for the baseline connectivity. We plotted the significance-masked, time-frequency plots for the perturbation-evoked connectivity to avoid averaging out transient activity.

We analyzed cortical connectivity for all 4 perturbation conditions. Baseline connectivity results were plotted in a bidirectional graph for each condition and frequency band. Edge widths in this bidirectional graph indicate baseline connectivity strength, with larger widths indicating increased baseline connectivity. We thresholded visible connections at one-fifth of the maximum baseline cortico-cortical connection across conditions. This provides a clearer view of the largest

cortico-cortical connections. For perturbation-evoked activity, we plotted the time-frequency maps for each of the 4 conditions, using the bootstrap significance masking procedure described previously. Because we were uninterested in self-interactions, we plotted spectral density along the diagonal of the time-frequency plots for each condition. Spectral density was computed based on the fit model and bootstrap significance-masked in the same way as the dDTF results. This spectral density measure is equivalent to event-related spectral perturbations (ERSPs), but uses the model-fitted results instead of the data directly.

In addition to cortical connectivity, we were also interested in quantifying differences in intermuscular connectivity and corticomuscular connectivity. To simplify our analysis, we only focused on the 2 pull perturbation conditions, as we found that these elicited a consistent time-frequency muscle response, whereas the visual perturbations did not (Peterson & Ferris, 2018). We analyzed baseline connectivity between muscles for the 2 conditions, plotting the results using a bidirectional graph for each condition and frequency band. We then looked at the significance-masked, perturbation-evoked connectivity between muscles and between cortical and muscular sources using surrogate bootstrap statistics. Because dDTF is a directional measure of connectivity, it can be used to determine if corticomuscular connectivity occurs only from the brain to muscles and not in the other direction. For corticomuscular connectivity we significance masked for both significant differences from baseline and significant differences from muscle-to-brain connectivity. We did not plot baseline corticomuscular connectivity because visual inspection of significance-masked connectivity using phase randomization was nearly identical to the significance-masked, perturbation-evoked connectivity using bootstrap statistics, indicating that the estimated corticomuscular activity from our models did not have a baseline.

Results

Missing Data Estimation

The estimated components generated from the group-averaged scalp maps appear quite similar to components generated from ICA, based on mutual information and residual variance (Figure 6-4). Pairwise mutual information showed a similar exponential fit between the independent components and the estimated components. There is a larger tail for the estimated components, but this is expected because Infomax ICA is designed minimize mutual information. The exponential fit for the channels is qualitatively different than both component fits. For residual variance (or dipolarity), the estimated components show decreased residual variance on average than the independent components, indicating that they can be better modelled by DIPFIT2. This was expected because the estimated components are generated from the average group scalp maps (Figure 6-3), which appear tightly located in one region of the scalp. While the estimated components may not be as statistically independent as components from ICA, they are more dipolar and appear to be a reasonable estimation of subject-specific, group-level activity.

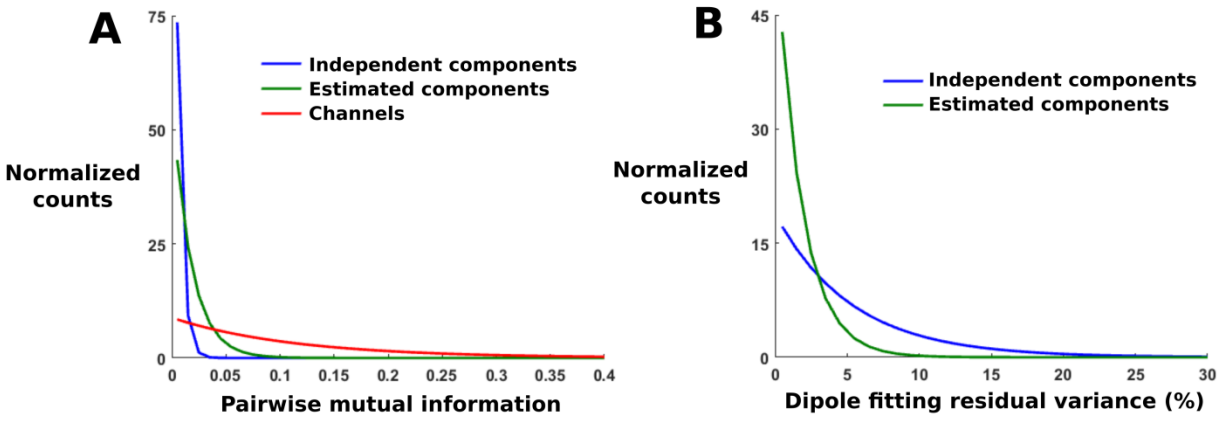

Figure 6-4: Pairwise mutual information of estimated components. Pairwise mutual information (A) and dipole fitting residual variance (B) are shown for the clustered independent components (blue), estimated components (green), and channel data (red). Estimated component pairwise mutual information includes all component pairs with at least one estimated component. Lines show a normalized exponential fit to histogram data. Decreased pairwise mutual information indicates greater statistical independence. As expected, components from independent component analysis show the lowest pairwise mutual information. While the estimated components have increased pairwise mutual information compared to the independent components, they still have much lower pairwise mutual information than the channel data. Also, the estimated components have higher dipolarity on average than the independent components, likely due to the high dipolarity of the group scalp maps.

Model Validation

Our model validation metrics indicate that the multivariate autoregressive model for each condition fits the group data well and is unlikely to be overfitted to the data (Table 6-1). The model order for all conditions was 6. This was the optimal model order for all time windows and even across other information measures besides Hannan-Quinn information criterion, including Bayesian information criterion, Akaike information criterion, and Akaike's final prediction error (Lütkepohl, 2007). Because model order, number of epochs, and number of components were consistent across conditions, they all had the same parameter to datapoint ratio of 0.02, which is below the target value of 0.1 to avoid overfitting. The residual whiteness likelihood was 0.89 for all conditions, indicating that there is an 11% chance that the residuals are not white. While this would ideally be 95% or higher, we were unable to increase this likelihood by using higher

model orders, indicating that this is likely the most optimal fit. Consistency was ~55-60% across conditions, likely reflecting the difficulty of capturing inter-subject variability. In addition, all conditions had model stability index values below 0, indicating that the models were stable and stationary. These model validation results suggest that the fitted models reflect group-level activity reasonably well.

Table 6-1: Model fitting results

	Stand Pull	Walk Pull	Stand Rotate	Walk Rotate
Parameter to datapoint ratio	0.02	0.02	0.02	0.02
Model Order	6	6	6	6
Residual whiteness likelihood	0.89 (0.00)	0.89 (0.00)	0.89 (0.01)	0.89 (0.00)
Consistency (%)	58.3 (3.7)	56.2 (3.6)	60.5 (3.8)	54.9 (3.9)
Stability index	-0.19 (0.01)	-0.19 (0.00)	-0.18 (0.01)	-0.19 (0.01)

Average validation results from model fitting are shown for all 4 conditions, with standard deviation in parentheses. We selected the average optimal model order determined by the Hannan-Quinn Criterion across all 400 ms windows used. Residual whiteness was tested using the autocorrelation function test for significance. Consistency indicates how well the model can generate data that correlates to the original data, with 100% being a perfect match. Stability index looks at how stationary the model is across time. The model can be considered stable if the stability index is less than 0.

Our higher-order models are highly similar to the lower-order models, indicating that the neither model seems to overfit or underfit the data too much. For the higher-order model, the optimal model order was 30 across all conditions, time windows, and information criteria. All model

validation metrics were nearly identical between the two model orders. We plotted the lower- and higher-order model dDTF results against each other to determine how much of an effect the model order had on the results (Figure 6-5). The linear fit R2 value ranged from 0.73-0.85 across the perturbation conditions, indicating that such a drastic change in the model order did not alter the resulting connectivity analysis much. Overall, the model order does not appear to have a large effect on the subsequent connectivity result, potentially because the parameter to data point ratio was only 0.08 due to the large number of trials used. Additionally, we computed a linear fit on just the lower order model between dDTF and renormalized partial directed (rPDC) as well as dDTF and Granger-Geweke causality (GGC), which are other common connectivity measures. The linear fit R2 value ranged from 0.40-0.50 across conditions between dDTF and rPDC (Schelter, Timmer, & Eichler, 2009) and from 0.58-0.68 across conditions between dDTF and GGC (Geweke, 1982). While this does indicate differences across measures, the results are quite consistent and showed qualitatively similar results.

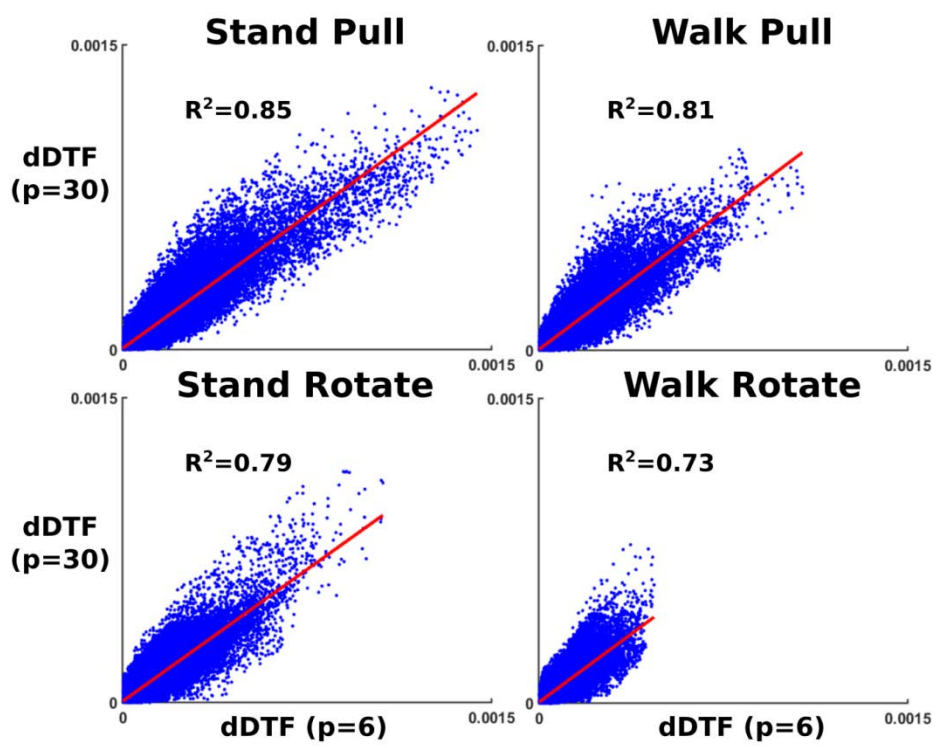

Figure 6-5: Linear fit of different model orders. To determine if the model was underfitting the data, we fit the data to a separate model with much higher model order (30) and compared the connectivity results to our 6th-order model (computed using dDTF). We found that the connectivity results for both models aligned with each other for all 4 conditions. Using a linear fit, we found R2 values greater than 0.7 for all conditions, indicating that both models seem to be relatively free of overfitting/underfitting.

Cortical Connectivity

Baseline cortical connectivity was primarily focused in parietal and occipital areas, with consistent connections between occipital and posterior parietal areas and from sensorimotor to occipital areas (Figure 6-6). This may reflect sensorimotor integration when performing the task. The strongest connections were in theta and alpha bands. Few connections went across hemispheres, with the only exception being between left and right occipital areas. Interestingly, we found similar theta band connections during both standing conditions, with notably fewer during walking. In contrast, alpha connections seemed to vary more between pull and rotation perturbations.

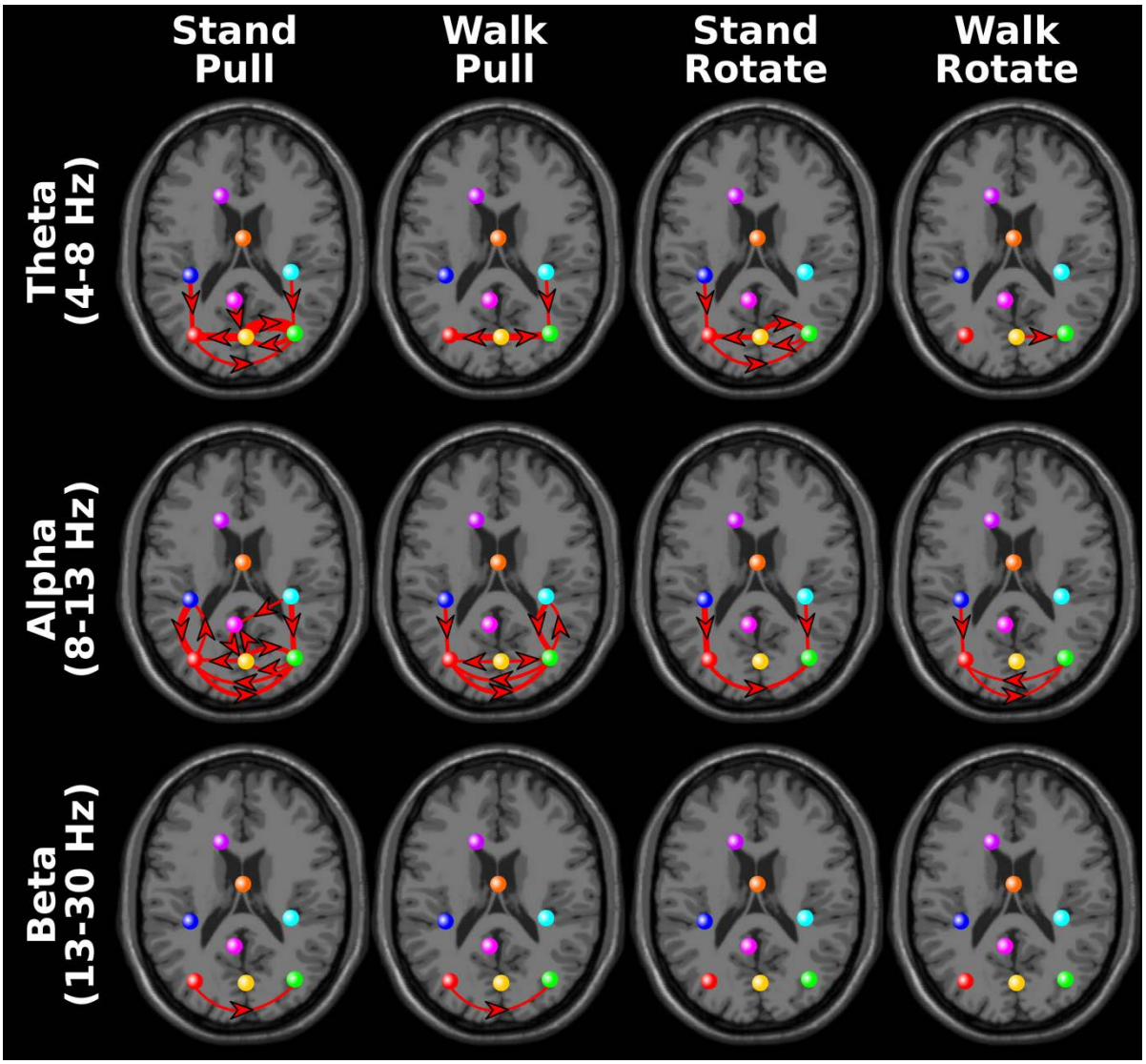

Figure 6-6: Baseline cortical connectivity results. Baseline cortical connectivity results are shown using dDTF. Cortical areas are designated with each cluster centroid: left occipital (red), right occipital (green), posterior parietal (yellow), anterior parietal (magenta), left sensorimotor (blue), right sensorimotor (cyan), supplementary motor area (orange), and anterior cingulate (purple). Non-significant differences from a phase-randomized null distribution were set to 0, and the resulting connectivity was averaged across time for each frequency band. The maximum connection was in the theta band from posterior parietal to right occipital during stand pull. We are only showing connections that are greater than one-fifth of this maximum connection. Baseline connectivity is focused primarily in parietal and occipital areas in theta and alpha bands, with consistent baseline connectivity between occipital and posterior parietal areas, along with connections from sensorimotor to occipital areas.

For perturbation-evoked connectivity, we found transient theta connectivity from supplementary motor area to left sensorimotor, right sensorimotor, and posterior parietal areas during pull perturbations while standing (Figure 6-7). These transient connections were not present during pull perturbations while walking. Interestingly, the theta spectral density was strongest in supplementary motor area, left sensorimotor, and right sensorimotor area for stand pull. In contrast, we found a transient theta connectivity increase during walk pull between anterior parietal and left sensorimotor that was not present during stand pull. We also found some alpha connectivity decreases from posterior parietal to left/right occipital after pull perturbation onset, especially during stand pull. For the visual perturbation, we found a large decrease in alpha connectivity from left sensorimotor to left occipital. This was strongest during standing, but still present during walking.

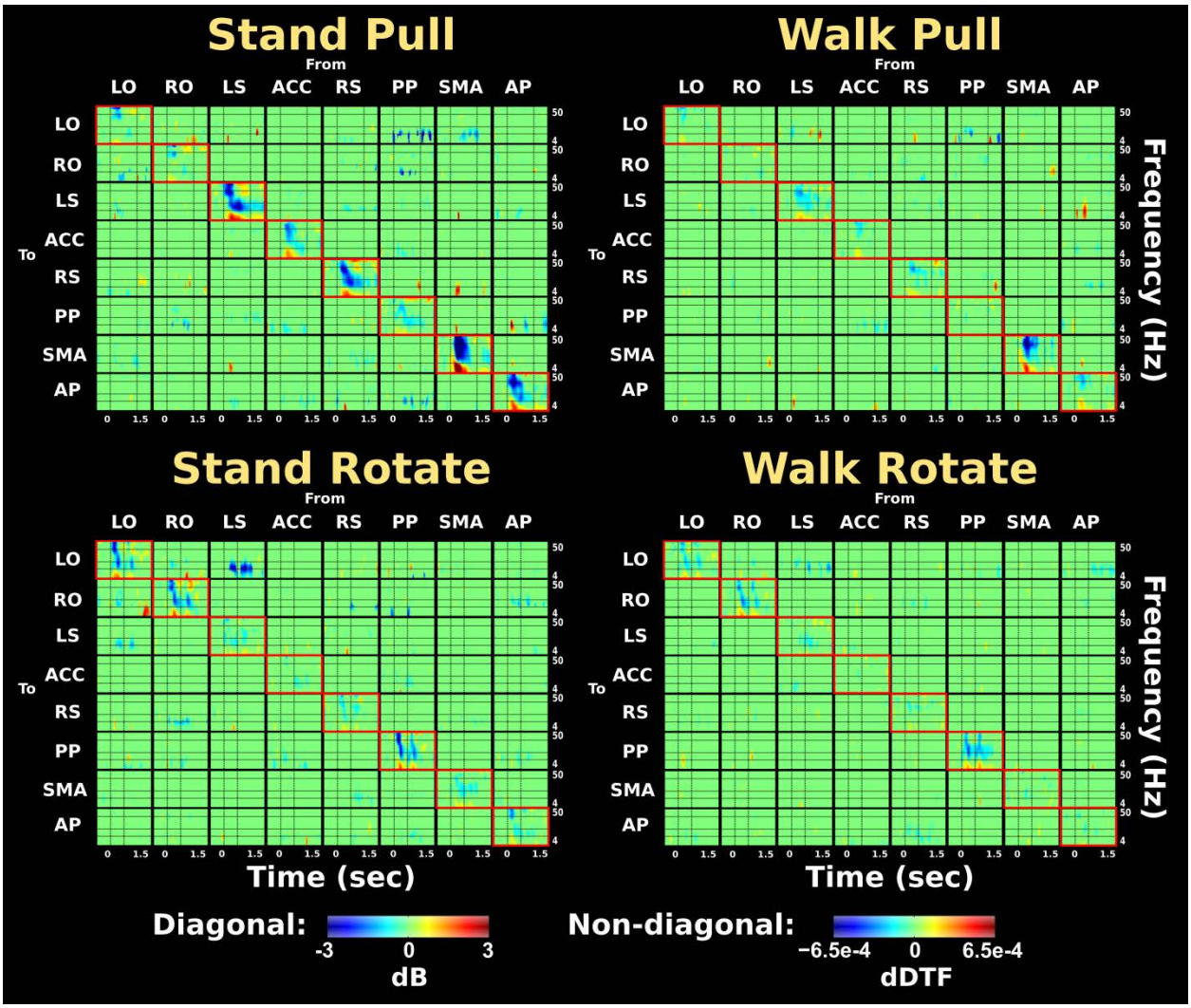

Figure 6-7: Perturbation-evoked cortico-cortical connectivity. The perturbation-evoked connectivity between cortical areas using dDTF is shown with event-related spectral perturbation (ERSP) plots along the diagonal (boxed in red). Cortical area abbreviations are: left occipital (LO), right occipital (RO), left sensorimotor (LS), anterior cingulate (ACC), right sensorimotor (RS), posterior parietal (PP), supplementary motor area (SMA), and anterior parietal (AP). We subtracted baseline activity from the half-second before the perturbation onset and set non-significant differences from baseline to 0 using bootstrap surrogate statistics ($p>0.05$). ERSPs show low frequency power increase (synchronization) and higher frequency power decrease (desynchronization), both of which are stronger in the standing conditions compared to walking. Stand pull shows decreased connectivity from posterior parietal to left/right occipital areas and increased connectivity between supplementary motor area and left/right sensorimotor areas. Stand rotate shows a large decrease in left sensorimotor to left occipital connectivity, which is weaker during walk rotate.

Intermuscular and Corticomuscular Connectivity during Pull Perturbations

For baseline intermuscular connectivity, we found 3 consistent bidirectional connections for both pull conditions, with no large connections between legs (Figure 6-8). We found bidirectional connections between tibialis anterior and peroneus longus, soleus and peroneus longer, and soleus and medial gastrocnemius. The overall connections during walking appeared more symmetrical than during stance. This indicates an asymmetrical EMG response during stance, where the back leg (left leg) appears more active than the front leg (right leg). Importantly, we did not find large baseline connections between muscles on different legs, which suggests that our results reflect true intermuscular connections.

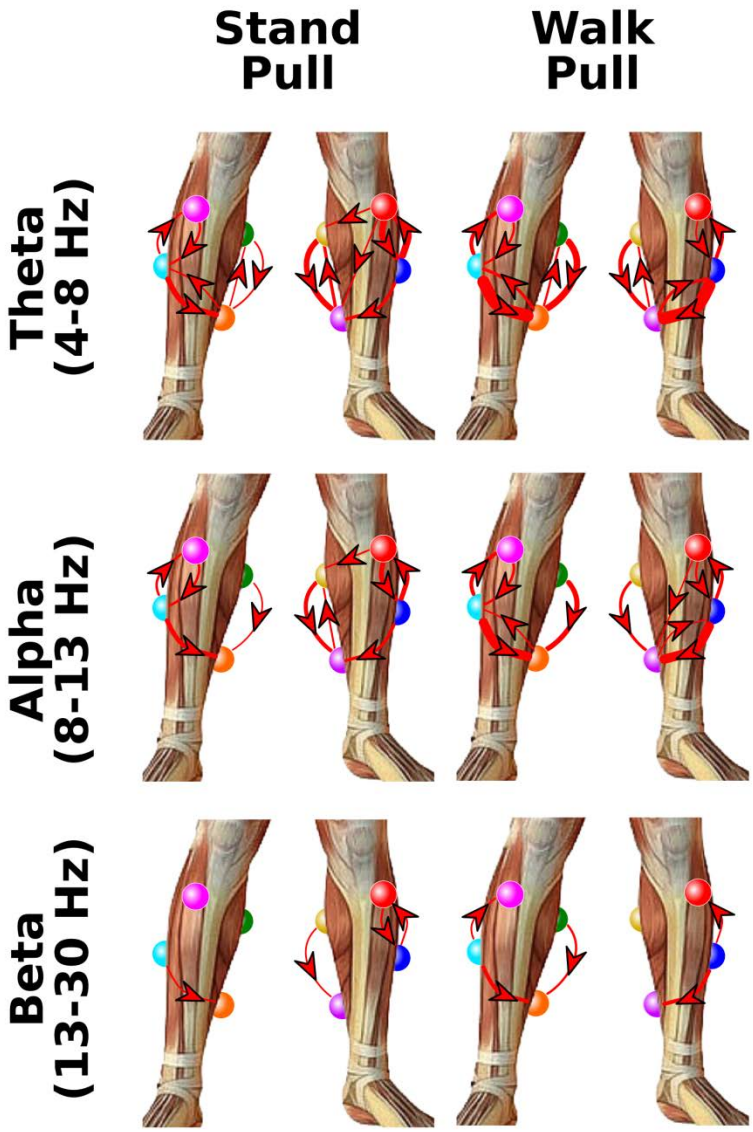

Figure 6-8: Baseline intermuscular connectivity results. The baseline connectivity strengths among lower leg muscles are shown for both pull perturbation conditions, using average significance-masked dDTF. Arrows designate the direction of each connection. Leg muscles are designated using spheres as: left tibialis anterior (red), left soleus (purple), left medial gastrocnemius (yellow), left peroneus longus (blue), right tibialis anterior (magenta), right soleus (orange), right medial gastrocnemius (green), right peroneus longus (cyan). All results are to the same scale, with the maximum connection in the theta band from left peroneus longus to left soleus during walk pull. Only connections with a value greater than one-tenth this maximum value are shown. Peroneus longus is shown slightly below the muscle belly for visual purposes. Both conditions show bidirectional connectivity between tibialis anterior and peroneus longus, peroneus longus and soleus, and soleus and medial gastrocnemius, especially across lower frequency bands.

For perturbation-evoked intermuscular connectivity, we found increased 4-13 Hz connectivity following perturbation onset (Figure 6-9, top row). Similar to baseline intermuscular connectivity, the perturbation-evoked connectivity pattern appears to be more symmetrical between legs during walking pull perturbations compared to stance pull perturbations. During walking the 4-13 Hz increase in connectivity occurs primarily between peroneus longus and both tibialis anterior and soleus. In contrast, intermuscular connectivity during stance pull perturbations shows a notable 4-13 Hz connectivity increase between left tibialis anterior and both left peroneus longus and left medial gastrocnemius that were not seen in the right leg. Muscle spectral fluctuations for each condition show a similar pattern that is much stronger during standing. This pattern is an increase in low-frequency (4-13 Hz) spectral power and a decrease in high-frequency (30-50 Hz) spectral power. As with baseline intermuscular connectivity, we found little perturbation-evoked connectivity effects between muscles on different legs.

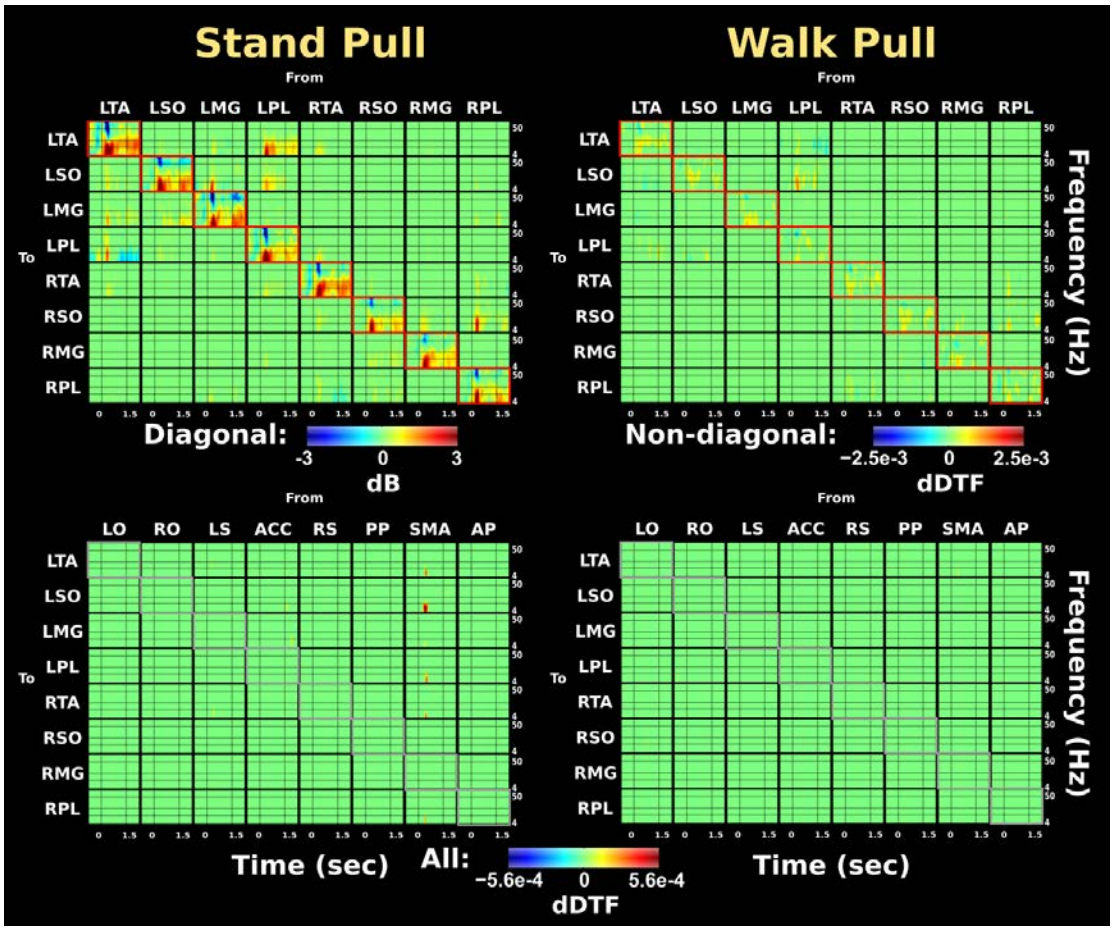

Figure 6-9: Intermuscular and corticomuscular connectivity. The perturbation-evoked intermuscular (top row) and corticomuscular (bottom row) connectivity are shown for both pull perturbation conditions, using dDTF. Cortical area abbreviations are left occipital (LO), right occipital (RO), left sensorimotor (LS), anterior cingulate (ACC), right sensorimotor (RS), posterior parietal (PP), supplementary motor area (SMA), and anterior parietal (AP). Muscle abbreviations are left/right tibialis anterior (LTA/RTA), left/right soleus (LSO/RSO), left/right medial gastrocnemius (LMG/RMG), and left/right peroneus longus (LPL/RPL). Intermuscular connectivity plots show baseline-subtracted event-related spectral perturbation (ERSP) plots along the diagonal, boxed in red. Non-significant differences from baseline have been set to 0 for all plots. ERSPs for both conditions show low frequency power increase with high frequency power decrease, but power fluctuations are stronger for stand pull. Both conditions show transient connectivity between peroneus long and tibialis anterior as well as peroneus longus and soleus for both legs, but stand pull has stronger connectivity between left peroneus longus and left tibialis anterior and from left medial gastrocnemius to left soleus, potentially reflecting asymmetrical muscle response between legs during standing pull perturbations. For corticomuscular connectivity, we set non-significant differences from baseline to 0, along with non-significant differences from the muscles to the brain to remove potential motion artifact. We only found significant theta band activity from the supplementary motor area primarily to left leg muscles during pull perturbations during stance. This was not present during walk pull or any other brain areas for stand pull, suggesting that it may indicate some sort of true connection.

For corticomuscular connectivity, we found significant 4-8 Hz connectivity from supplementary motor area to left leg muscles following pull perturbations during standing (Figure 6-9, bottom row). This corticomuscular connectivity was significant from the supplementary motor area to left/right tibialis anterior, left soleus, and left peroneus longus. This low-frequency connectivity increase agrees with the intermuscular results and only come from the cortical region that appears to have the strongest theta band synchronization following perturbation onset. Most of the muscles that had significant corticomuscular connectivity were in the left leg, which had asymmetrically increased activation compared to the right leg. Corticomuscular connectivity was not present, when the muscle responses were weaker and more symmetrical. In addition, this connectivity was significantly different compared to connections from each muscle to the supplementary motor area, indicating that this may be true corticomuscular connectivity.

Discussion

We developed a novel group-level connectivity analysis for quantifying differences in information flow between cortical areas for different sensorimotor perturbations. This group-level analysis modelled the data well and was robust to parameter selection and the connectivity measure used, as hypothesized. Baseline cortical connectivity was strongest in occipital and parietal areas for both perturbation types, which partially agrees with our hypothesis. There was also a large decrease in alpha connectivity from left sensorimotor to left occipital following the visual perturbation. We found consistent bidirectional intermuscular connections between lower leg muscles following pull perturbation onset. For corticomuscular connectivity, we found significant 4-8 Hz connectivity from supplementary motor area to most left leg muscles and right

tibialis anterior, as hypothesized, which may reflect direct cortical influence on the asymmetrical standing postural response.

Group-level Connectivity Analysis

Our missing data estimation technique performed comparably to the cortical components from independent component analysis, indicating that this is a reasonable method. It should be noted that our data estimation technique is not equivalent to independent component analysis, as can be seen by the slightly increased pairwise mutual information for these estimated components compared to the independent components. Our estimation technique also removes inter-subject differences in dipole location because it assumes that the best approximation is based on the group. However, we limited the effects of this estimation by removing subjects with few dipoles across clusters. For studies with fewer subjects, it may be preferable to remove certain clusters instead of subjects to reduce the amount of data estimation performed.

In addition, our multivariate autoregressive model fits across pooled subject data for each group produced reliable and reasonable results (Lütkepohl, 2007). Our low parameter to datapoint ratio suggests that our model avoided overfitting. It should be noted that our model validation results indicate that the model is not as stationary and consistent as desired. This was unaffected by a higher model order, but may have been marginally improved by a smaller window size. We avoided window sizes below 400 ms because we wanted appropriate frequency resolution for our results and lower time windows can degrade low-frequency connectivity results. While the stationary and consistency below their desired values, the models were stable and did not appear affected by overfitting or underfitting of the model, based on low parameter to data point ratio and similarity between dDTF at low and high model orders. Additionally, the model-fitted cortical spectral density results during the pull perturbations closely match the cortical cluster

ERSPs from previous studies, with low-frequency power increase primarily in supplementary motor area (Sipp, Gwin, Makeig, & Ferris, 2013; Varghese, et al., 2014). The higher-frequency power decrease also matches desynchronization seen following perturbed stepping speed during walking (Wagner, Makeig, Gola, Neuper, & Müller-Putz, 2016). This gives us confidence that our model reasonably captured group-level activity.

Cortical Connectivity

Baseline cortical connectivity was located in parietal and occipital areas and mostly avoiding crossovers between hemispheres. Similar theta and alpha connectivity in occipital and parietal areas was found during single leg balance in healthy adults (Mierau, et al., 2017). Connectivity in frontal areas has been shown to increase in older adults and in young adults when the postural task becomes more challenging (Huang, Lin, & Hwang, 2017). Our postural task may have been fairly easy to perform because it did not induce stepping, which may explain the lack of fronto-central clusters and connectivity. We also found increased theta connections during standing conditions compared with walking conditions, which agrees with a previous study using Granger causality (Lau, Gwin, & Ferris, 2014). Additionally, alpha connections increased during the pull perturbation compared to the visual rotation, which may reflect differences in the motor response required between perturbation types.

Perturbation-evoked cortical connectivity showed few substantive results, despite similar model-fitted cortical spectral density patterns across multiple cortical regions. We found a notable decrease in connectivity from left sensorimotor to left occipital during visual rotations, likely reflecting unreliable visual input. The left sensorimotor area has been shown to be more active during loss of balance than the right sensorimotor area (Sipp, Gwin, Makeig, & Ferris, 2013), which may reflect a left hemisphere bias in responding to perturbations, at least in right-handed

healthy adults (Bruijn, Van Impe, Duysens, & Swinnen, 2014). We also found brief theta connectivity between left sensorimotor and supplementary motor area during pull perturbations while standing and between left sensorimotor and anterior parietal during pull perturbations while walking, agreeing with previous research showing that pull perturbations only briefly alter cortical connectivity (Varghese J. P., 2016). Interestingly, we found little beta band baseline or perturbation-evoked connectivity, despite large beta desynchronization in spectral density for all conditions. Based on the delayed onset of alpha desynchronization compared to beta desynchronization for our spectral density plots, it seems likely that these reflect two separate processes. This alpha desynchronization appears mostly absent during walking with pull perturbations, which likely reflects a change in motor readiness (Wagner, Solis-Escalante, Scherer, Neuper, & Müller-Putz, 2014). With connectivity analysis, it is clear that the alpha and beta desynchronization reflect two distinct processes, highlighting the importance of using connectivity analysis in conjunction with spectral information.

Intermuscular and Corticomuscular Connectivity during Pull Perturbations

We found primarily low frequency connectivity among muscles, which is surprising because EMG and corticomuscular connectivity are usually analyzed primarily at higher frequencies (Gwin & Ferris, 2012). In contrast, intermuscular coherence during balance control has been seen to be strongest at low frequencies (Boonstra, et al., 2015; Boonstra, et al., 2008) and is thought to reflect that the activity in different muscles are changing at the same time (Mochizuki, Semmler, Ivanova, & Garland, 2006). While this could be motion artifact, we primarily see baseline and perturbation-evoked connectivity within each leg, instead of between legs, indicating that this likely reflects true linkages amongst muscles. It has also been suggested that surface EMG recordings are low-pass filtered due to volume conduction by the skin (Farina &

Holobar, 2016), which could lead to important information being located mostly at low frequencies.

Despite finding several intracortical and intermuscular connections following the perturbation, we only found significant corticomuscular connectivity from the supplementary motor area primarily to left leg muscles. Repeated transcranial magnetic stimulation of the supplementary motor area has been shown to affect anticipatory postural response duration in both healthy adults and individuals with Parkinson's disease, indicating that the supplementary motor area is important during balance control (Jacobs, Lou, Kraakevik, & Horak, 2009). While our experiment was a reactive response and not an anticipatory response, it has been shown that both types of responses result in similar cortical connectivity patterns (Varghese J. P., 2016). The supplementary motor area also has strong spectral fluctuations and has been shown to be one of the most prominent electrocortical areas during perturbed balance responses (Marlin, Mochizuki, Staines, & McIlroy, 2014). It seems likely that this transient increase in 4-8 Hz corticomuscular connectivity may reflect the cortical input into the timing of the postural response.

Limitations and Considerations

Despite the promising results of our group-level connectivity method, it is important to note the limitations of this approach. Firstly, our method does not account for inter-subject variability in estimated component locations, instead forcing the group-level location on it because there is no other scalp map to use for the missing data. This reduces inter-subject variability, which is further reduced when data from all subjects are pooled and fit to one group-level model. This reduction in inter-subject variability is not ideal, but appears to produce reasonable and informative group-level results. We would prefer to explore the information flow in each subject's cortical areas, but variations in number of dipoles, dipole location, and model fitting

parameters make it difficult to tease apart what effects are only due to each subject's data, and not variations in analysis parameters. Additionally, the group-level scalp maps used to estimate missing component data may act as a suboptimal spatial filter given the true variation in inter-subject dipole locations. However, we are taking advantage of the low spatial resolution of EEG and the model attempting to find common activity across all subjects. We are assuming that if the true missing dipole is located nearby, our estimated group-level scalp map is close enough and that any unwanted activity from this estimation is ignored by the final fitted model. This may be a valid assumption for mobile EEG data, where the resulting clusters tend to be quite separate in space from each other, but may not apply to EEG data where cortical areas of interest are spatially close together. It is worth noting that we also removed 11 subjects' data for this study to limit the amount of data estimation performed. Such subject removal may be infeasible for studies with smaller numbers of total subjects.

In addition, it is also possible that spurious connectivity results are generated due to high number of estimated sources between 2 cortical areas. This would be expected if the estimated sources were not statistically independent from each other and the independent components and contained common information. If this were the case, we would have expected to see strong connections between anterior parietal and posterior parietal due to their close proximity and high number of estimated sources. Because we did not see this, our results seem to have been unaffected by such spurious connectivity.

Conclusions

We used a novel group-level connectivity analysis technique to analyze source-localized information flow between brain regions during sensorimotor perturbations. Our analysis modelled the data well, producing reasonable connectivity results. We found that sensorimotor

perturbations to walking and standing balance led to strong baseline cortical connectivity in parietal and occipital areas, which may reflect sensory integration performed to consistently maintain balance. We also found corticomuscular connectivity from the supplementary motor area primarily to lower leg muscles, which may indicate cortical assistance with response timing. Our group-level connectivity analysis may useful for future connectivity studies to enhance our understanding of group-level neuromuscular interactions.

Chapter 7: Discussion

The purpose of this dissertation was to quantify the effects of sensorimotor perturbations on electrocortical dynamics and short-term balance learning in virtual reality. In chapter 2, I examined the effects of high heights exposure in virtual reality on balance performance and electrocortical dynamics. In chapter 3, I compared the use of transient visual perturbations during balance training to virtual reality and real world control groups, analyzing differences in balance performance and EEG activity. In chapters 4 and 6, I identified similarities and differences in electrocortical activity and group-level connectivity between physical pull and visual rotation perturbations during beam walking and tandem stance. In chapter 5, I validated independent component analysis and standard connectivity techniques when exposed to real-world head motion and volume conduction with ground-truth signals. These studies have expanded the understanding of perturbed sensory input during balance while also providing novel techniques and research questions for future EEG studies.

Main Findings

The main finding for chapter 2 was that virtual reality headset use is immersive but impairs balance performance and cognitive loading compared to unaltered viewing without the headset. I found significantly increased response times to a secondary task while beam walking during virtual reality at low heights compared to unaltered view. This was corroborated by significantly decreased EEG event-related peak activity in the anterior cingulate in virtual reality. Decreased EEG event-related peak activity has been seen for a similar secondary task during increasingly challenging cognitive tasks (Shaw, et al., 2018). The anterior cingulate plays an important role in

maintaining balance and detecting errors (Sipp, Gwin, Makeig, & Ferris, 2013; Gehring & Knight, 2000), so I was not surprised to find this area the most affected by virtual reality use during beam-walking.

In chapter 3, I showed that a brief visual perturbation during virtual reality balance training can boost short-term motor learning to remove the negative learning effects of virtual reality. Virtual reality training with perturbations led to equivalent pretest-to-posttest improvement compared to unaltered viewing without the headset. Both groups had significantly increased improvement compared to virtual reality training without perturbations. The perturbations did not induce after-effects, suggesting that perturbation training altered short-term motor learning through repeated adaptation (Bastian, 2008; Krakauer, Ghez, & Ghilardi, 2005). Repeated adaptation to perturbed visual input can improve the ability to adapt to novel visual perturbations, known as adaptive generalization (Welch, Bridgeman, Anand, & Browman, 1993). Such adaptive generalization can occur during upper-limb and lower-limb training (Seidler, 2004; Shadmehr & Moussavi, 2000; Batson, et al., 2011).

Based on our findings, perturbations training appeared to primarily induce a cognitive change. The perturbation-evoked EEG response matched previous EEG event-related dynamics during perturbed balance (Varghese, et al., 2014), with strongest perturbation responses in parietal, occipital, and cingulate regions. Power spectral analysis indicated that virtual reality with perturbations training significantly increased theta power in frontal occipital, and cingulate regions compared to the control groups, likely indicating altered sensorimotor processing during perturbations training (Hülsdünker, Mierau, & Strüder, 2015; Youssofzadeh, Zanotto, Wong-Lin, Agrawal, & Prasad, 2016). I also found decreases in alpha power for the virtual reality perturbations group in multiple cortical regions compared to the virtual reality without

perturbations group. This suggests that perturbations training may improve mental engagement, as has been shown in other lower-limb tasks (Wagner, Solis-Escalante, Scherer, Neuper, & Müller-Putz, 2014; Luu, Nakagome, He, & Contreras-Vidal, 2017b). Taken together, this study shows that brief visual perturbations can be used to substantially improve virtual reality balance training by altering cortical dynamics.

In chapter 4, I identified a similar electrocortical time-frequency pattern for both physical pull and visual rotation perturbations but in notably different areas of the brain. The time-frequency pattern involved an initial theta synchronization followed by alpha-beta desynchronization, matching previous research into perturbed lower limb movements (Varghese, et al., 2014; Seeber, Scherer, Wagner, Solis-Escalante, & Müller-Putz, 2014). Theta-band synchronization appears to be a hallmark of perturbed balance (Sipp, Gwin, Makeig, & Ferris, 2013), while beta desynchronization may be the cortical response to a change in the status quo (Engel & Fries, 2010). This time-frequency pattern appears in other research, including magnetoencephalography recordings in auditory cortex during repetitive tone presentation (Fujioka, Trainor, Large, & Ross, 2012) and local field potential recordings in the subthalamic nucleus during visual conflict (Hell, Taylor, Mehrkens, & Bötzel, 2018).

In chapter 5, I used ground truth signals exposed to the real-world effects of volume conduction and motion artifact to perform novel validation of effective connectivity measures. I found that independent component analysis can separate out motion artifact well (Snyder, Kline, Huang, & Ferris, 2015). The potential for motion artifact to generate spurious connectivity results highlights the need to use independent component analysis, instead of scalp channel data, when performing connectivity analysis on mobile EEG data. My phantom head validation technique highlighted the prevalence of false positive results for several popular connectivity measures,

which could be caused by the nonlinearities of the real-world EEG recording. Such phantom heads embedded with complex antenna signals will allow future validation of our EEG processing methods, improving the robustness of EEG analyses.

In chapter 6, I used a novel group-level connectivity analysis which found occipito-parietal patterns of cortical connectivity and evidence of corticomuscular connectivity during balance control. For cortical connectivity, I found increased theta connections during standing compared to walking, agreeing with previous research (Lau, Gwin, & Ferris, 2014). In addition, the pull perturbations increased alpha connections compared to the visual rotations, indicating potential inter-perturbation differences in the motor cortex's response. I found low-frequency corticomuscular connectivity from the supplementary motor area primarily to left leg muscles during pull perturbations. Low-frequency coherence between muscles has been seen during balance control (Boonstra, et al., 2008; Boonstra, et al., 2015) and may indicate muscle coactivation (Mochizuki, Semmler, Ivanova, & Garland, 2006). The supplementary motor area makes sense as the cortical area as it had the largest pull perturbation response, agreeing with previous studies (Marlin, Mochizuki, Staines, & McIlroy, 2014; Varghese, et al., 2014). Transcranial magnetic stimulation of the supplementary motor area can disrupt the physical perturbation response, indicating its importance during balance control (Jacobs, Lou, Kraakevik, & Horak, 2009). This study showed the utility of group-level connectivity analysis to uncover information about the brain network dynamics during perturbed balance.

Limitations

While these studies provide novel insights and techniques into the field, there were several limitations of these experiments, most notably with the virtual reality setup. Virtual reality use negatively impacted stability and short-term motor learning (Peterson, Rios, & Ferris, 2018;

Peterson, Furuichi, & Ferris, 2018). One factor may have been the 100° field of view of our virtual reality headset, which was below typical human field of view of 180° (Walker, Hall, & Hurst, 1976). Several studies have demonstrated the importance of peripheral vision in maintaining stability (Amblard & Carblanc, 1980; Assaiante, Marchand, & Amblard, 1989). Another factor may have been the low refresh rate of the headset and webcam, which were 75 Hz and 30 Hz, respectively. Low refresh rates can impair stability (Kawamura & Kijima, 2016). Future studies should consider constructing virtual reality setups that improve upon these limitations to minimize its negative effects on stability.

In addition, the EEG analyses and results used in my studies may have been limited by artifact contamination. Because there is not ground truth for most of my studies, I could not verify that the EEG data is completely free from artifact contamination. However, I used head motion and neck EMG to determine the likely impact of the most prominent artefactual signals. I also found similar electrocortical patterns in symmetrical cortical areas, which differs from the asymmetrical motion artifact patterns seen across the head during walking (Kline, Huang, Snyder, & Ferris, 2015). In addition, several of my events of interest were not time-locked to a consistent motion event, as is the case when studying gait. Because of these factors, I feel confident that my EEG results contain little, if any, motion artifact that would not affect the conclusions of each study. Still, EEG recordings typically do not include ground-truth validation, which is why phantom head testing seems important for future experiments.

Despite the increased realism provided by phantom head testing, there were limitations for my connectivity validation approach. The signals sent through the phantom were assumed to reasonably approximate true cortical signals, especially in the way that transient connections occurred. This approach seemed optimal compared to using independent component results from

recorded human data because it provides no guarantee that independent component analysis will be able to separate the signals, whereas it may be biased in separating out previous independent components. In addition, the phantom head only contains a single material, without skin or a skull. I partially compensated for the lack of skin by computationally adding pink noise to the data. However, the realism of the phantom head should be improved in future studies to contain more realistic layers of varying conductances for enhanced validation accuracy.

Even though my group-level connectivity method showed promising results, it was limited by not taking into account inter-subject variability and applying potentially suboptimal estimates for missing component data. Ideally, this method would include inter-subject variability, but model fitting parameters and inter-subject differences in the number of dipoles can greatly affect connectivity estimation, making it challenging to tease apart which differences in estimated connectivity are due to true inter-subject cortical differences. In addition, my estimation technique assumed that the group-level dipole locations were the best choice for each subject's missing data, even though inter-subject dipole locations tend to vary. This assumption took advantage of the low spatial resolution of EEG and how clusters tend to be spatially spread out for mobile recordings. Because of this, my group-level connectivity method may not be suitable for EEG studies where the group-level clusters are packed tightly in space.

Conclusions

Throughout this dissertation, I have shown the importance of using high-density, source-localized EEG analysis to understand the cortical effects of sensorimotor balance perturbations. In addition, my dissertation highlights the usefulness of considering cortical dynamics for improving motor learning. It is important to consider cortical activity in conjunction with behavior because each provides extra information to facilitate understanding of the other. I also

developed new EEG analysis methods, including a selective low-pass filter to remove muscle activity and a group-level analysis method in source space. As new techniques are developed, it will become important to validate them using realistic head phantoms, similar to my assessment of connectivity measures. Such methodology should improve future mobile EEG experimental findings, while also providing new avenues for exploration in human balance control and sensorimotor integration.

Bibliography

Adamovich, S. V., Fluet, G. G., Tunik, E., & Merians, A. S. (2009). Sensorimotor training in virtual reality: a review. *NeuroRehabilitation, 25*(1), 29-44. doi:10.3233/NRE-2009-0497

Adkin, A. L., Campbell, A. D., Chua, R., & Carpenter, M. G. (2008). The influence of postural threat on the cortical response to unpredictable and predictable postural perturbations. *Neurosci. Lett., 435*(2), 120-125. doi:10.1016/j.neulet.2008.02.018

Adkin, A. L., Quant, S., Maki, B. E., & McIlroy, W. E. (2006). Cortical responses associated with predictable and unpredictable compensatory balance reactions. *Exp. Brain Res., 172*(1), 85-93. doi:10.1007/s00221-005-0310-9

Ahmed, A. A. (2005). *A theory for identifying loss of balance: analysis of control error and compensatory responses in healthy adults.* University of Michigan.

Akizuki, H., Uno, A., Arai, K., Morioka, S., Ohyama, S., Nishiike, S., . . . Takeda, N. (2005). Effects of immersion in virtual reality on postural control. *Neurosci. Lett., 379*(1), 23-26. doi:10.1016/j.neulet.2004.12.041

Allum, J. H., Gresty, M., Keshner, E., & Shupert, C. (1997). The control of head movements during human balance corrections. *J. Vestib. Res., 7*(2-3), 189-218.

Al-Subari, K., Al-Baddai, S., Tomé, A. M., Goldhacker, M., Faltermeier, R., & Lang, E. W. (2015). EMDLAB: A toolbox for analysis of single-trial EEG dynamics using empirical mode decomposition. *J. Neurosci. Methods, 253*, 193-205. doi:10.1016/j.jneumeth.2015.06.020

Amblard, B., & Carblanc, A. (1980). Role of foveal and peripheral visual information in maintenance of postural equilibrium in man. *Percept. Mot. Skills, 51*(3 Pt 1), 903-912. doi:10.2466/pms.1980.51.3.903

Anglin, J. M., Sugiyama, T., & Liew, S.-L. (2017). Visuomotor adaptation in head-mounted virtual reality versus conventional training. *Sci. Rep., 7*, 45469. doi:10.1038/srep45469

Anguera, J. A., Seidler, R. D., & Gehring, W. J. (2009). Changes in performance monitoring during sensorimotor adaptation. *J. Neurophysiol., 102*(3), 1868-1879. doi:10.1152/jn.00063.2009

Artoni, F., Fanciullacci, C., Bertolucci, F., Panarese, A., Makeig, S., Micera, S., & Chisari, C. (2017). Unidirectional brain to muscle connectivity reveals motor cortex control of leg muscles during stereotyped walking. *Neuroimage, 159*, 403-416. doi:10.1016/j.neuroimage.2017.07.013

Artoni, F., Menicucci, D., Delorme, A., Makeig, S., & Micera, S. (2014). RELICA: a method for estimating the reliability of independent components. *Neuroimage, 103*, 391-400. doi:10.1016/j.neuroimage.2014.09.010

Assaiante, C., Marchand, A. R., & Amblard, B. (1989). Discrete visual samples may control locomotor equilibrium and foot positioning in man. *J. Mot. Behav., 21*(1), 72-91.

Assländer, L., & Peterka, R. J. (2014). Sensory reweighting dynamics in human postural control. *J. Neurophysiol., 111*(9), 1852-1864. doi:10.1152/jn.00669.2013

Astolfi, L., Cincotti, F., Mattia, D., Grazia Marciani, M., Baccala, L. A., de Vico Fallani, F., . . . Babiloni, F. (2007). Comparison of different cortical connectivity estimators for high-resolution EEG recordings. *Hum. Brain Mapp., 28*(2), 143-157. doi:10.1002/hbm.20263

Baccalá, L. A., & Sameshima, K. (2001). Partial directed coherence: a new concept in neural structure determination. *Biol. Cybern., 84*(6), 463-474. doi:10.1007/PL00007990

Baccala, L. A., Sameshima, K., & Takahashi, D. Y. (2007). Generalized Partial Directed Coherence. *2007 15th International Conference on Digital Signal Processing.* doi:10.1109/icdsp.2007.4288544

Bai, Y., Wan, X., Zeng, K., Ni, Y., Qiu, L., & Li, X. (2016). Reduction hybrid artifacts of EMG-EOG in electroencephalography evoked by prefrontal transcranial magnetic stimulation. *J. Neural Eng., 13*(6), 066016. doi:10.1088/1741-2560/13/6/066016

Baillet, S., Riera, J. J., Marin, G., Mangin, J. F., Aubert, J., & Garnero, L. (2001). Evaluation of inverse methods and head models for EEG source localization using a human skull phantom. *Phys. Med. Biol., 46*(1), 77-96.

Başar, E., Başar-Eroglu, C., Karakaş, S., & Schürmann, M. (2001). Gamma, alpha, delta, and theta oscillations govern cognitive processes. *Int. J. Psychophysiol., 39*(2-3), 241-248.

Basso Moro, S., Bisconti, S., Muthalib, M., Spezialetti, M., Cutini, S., Ferrari, M., . . . Quaresima, V. (2014). A semi-immersive virtual reality incremental swing balance task activates prefrontal cortex: a functional near-infrared spectroscopy study. *Neuroimage, 85 Pt 1*, 451-460. doi:10.1016/j.neuroimage.2013.05.031

Bastian, A. J. (2008). Understanding sensorimotor adaptation and learning for rehabilitation. *Curr. Opin. Neurol., 21*(6), 628-633. doi:10.1097/WCO.0b013e328315a293

Batson, C. D., Brady, R. A., Peters, B. T., Ploutz-Snyder, R. J., Mulavara, A. P., Cohen, H. S., & Bloomberg, J. J. (2011). Gait training improves performance in healthy adults exposed to novel sensory discordant conditions. *Exp. Brain Res., 209*(4), 515-524. doi:10.1007/s00221-011-2574-6

Benedek, M., & Kaernbach, C. (2010a). A continuous measure of phasic electrodermal activity. *J. Neurosci. Methods, 190*(1), 80-91. doi:10.1016/j.jneumeth.2010.04.028

Benedek, M., & Kaernbach, C. (2010b). Decomposition of skin conductance data by means of nonnegative deconvolution. *Psychophysiology, 47*(4), 647-658. doi:10.1111/j.1469-8986.2009.00972.x

Benjamini, Y., & Yekutieli, D. (2001). The control of the false discovery rate in multiple testing under dependency. *Ann. Stat., 29*(4), 1165-1188.

Bernier, P.-M., Chua, R., & Franks, I. M. (2005). Is proprioception calibrated during visually guided movements? *Exp. Brain Res., 167*(2), 292-296. doi:10.1007/s00221-005-0063-5

Bigdely-Shamlo, N., Mullen, T., Kreutz-Delgado, K., & Makeig, S. (2013). Measure projection analysis: a probabilistic approach to EEG source comparison and multi-subject inference. *Neuroimage, 72*, 287-303. doi:10.1016/j.neuroimage.2013.01.040

Blandini, F., Nappi, G., Tassorelli, C., & Martignoni, E. (2000). Functional changes of the basal ganglia circuitry in Parkinson's disease. *Prog. Neurobiol., 62*(1), 63-88. doi:10.1016/s0301-0082(99)00067-2

Blinowska, K. J. (2011). Review of the methods of determination of directed connectivity from multichannel data. *Med. Biol. Eng. Comput., 49*(5), 521-529. doi:10.1007/s11517-011-0739-x

Boesch, M., Sefidan, S., Ehlert, U., Annen, H., Wyss, T., Steptoe, A., & La Marca, R. (2014). Mood and autonomic responses to repeated exposure to the Trier Social Stress Test for

Groups (TSST-G). *Psychoneuroendocrinology, 43*, 41-51. doi:10.1016/j.psyneuen.2014.02.003
Bogost, M. D., Burgos, P. I., Little, C. E., Woollacott, M. H., & Dalton, B. H. (2016). Electrocortical Sources Related to Whole-Body Surface Translations during a Single- and Dual-Task Paradigm. *Front. Hum. Neurosci., 10*, 524. doi:10.3389/fnhum.2016.00524
Bolton, D. A. (2015). The role of the cerebral cortex in postural responses to externally induced perturbations. *Neurosci. Biobehav. Rev., 57*, 142-155. doi:10.1016/j.neubiorev.2015.08.014
Boonstra, T. W., Daffertshofer, A., Roerdink, M., Flipse, I., Groenewoud, K., & Beek, P. J. (2009). Bilateral motor unit synchronization of leg muscles during a simple dynamic balance task. *Eur. J. Neurosci., 29*(3), 613-622. doi:10.1111/j.1460-9568.2008.06584.x
Boonstra, T. W., Danna-Dos-Santos, A., Xie, H.-B., Roerdink, M., Stins, J. F., & Breakspear, M. (2015). Muscle networks: Connectivity analysis of EMG activity during postural control. *Sci. Rep., 5*, 17830. doi:10.1038/srep17830
Boonstra, T. W., Roerdink, M., Daffertshofer, A., van Vugt, B., van Werven, G., & Beek, P. J. (2008). Low-alcohol doses reduce common 10- to 15-Hz input to bilateral leg muscles during quiet standing. *J. Neurophysiol., 100*(4), 2158-2164. doi:10.1152/jn.90474.2008
Booth, V., Masud, T., Connell, L., & Bath-Hextall, F. (2013). The effectiveness of virtual reality interventions in improving balance in adults with impaired balance compared with standard or no treatment: a systematic review and meta-analysis. *Clinical Rehabilitation, 28*(5), 419-431. doi:10.1177/0269215513509389
Boudraa, A.-O., & Cexus, J.-C. (2007). EMD-Based Signal Filtering. *IEEE Trans. Instrum. Meas., 56*(6), 2196-2202. doi:10.1109/tim.2007.907967
Bradford, J. C., Lukos, J. R., & Ferris, D. P. (2016). Electrocortical activity distinguishes between uphill and level walking in humans. *J. Neurophysiol., 115*(2), 958-966. doi:10.1152/jn.00089.2015
Brown, L. A., Polych, M. A., & Doan, J. B. (2006). The effect of anxiety on the regulation of upright standing among younger and older adults. *Gait & Posture, 24*(4), 397-405. doi:10.1016/j.gaitpost.2005.04.013
Bruijn, S. M., Van Dieën, J. H., & Daffertshofer, A. (2015). Beta activity in the premotor cortex is increased during stabilized as compared to normal walking. *Front. Hum. Neurosci., 9*, 593. doi:10.3389/fnhum.2015.00593
Bruijn, S. M., Van Impe, A., Duysens, J., & Swinnen, S. P. (2014). White matter microstructural organization and gait stability in older adults. *Front. Aging Neurosci., 6*, 104. doi:10.3389/fnagi.2014.00104
Brunner, C., Billinger, M., Seeber, M., Mullen, T. R., & Makeig, S. (2016). Volume Conduction Influences Scalp-Based Connectivity Estimates. *Front. Comput. Neurosci., 10*, 121. doi:10.3389/fncom.2016.00121
Calogiuri, G., Litleskare, S., Fagerheim, K. A., Rydgren, T. L., Brambilla, E., & Thurston, M. (2017). Experiencing Nature through Immersive Virtual Environments: Environmental Perceptions, Physical Engagement, and Affective Responses during a Simulated Nature Walk. *Front. Psychol., 8*, 2321. doi:10.3389/fpsyg.2017.02321
Carpenter, M. G., Frank, J. S., & Silcher, C. P. (1999). Surface height effects on postural control: a hypothesis for a stiffness strategy for stance. *Journal of Vestibular Research, 9*(4), 277-286.

Carter, C. S., Braver, T. S., Barch, D. M., Botvinick, M. M., Noll, D., & Cohen, J. D. (1998). Anterior cingulate cortex, error detection, and the online monitoring of performance. *Science, 280*(5364), 747-749.

Carter, N. D., Kannus, P., & Khan, K. M. (2001). Exercise in the prevention of falls in older people: a systematic literature review examining the rationale and the evidence. *Sports Med., 31*(6), 427-438.

Castermans, T., Duvinage, M., Cheron, G., & Dutoit, T. (2014). About the cortical origin of the low-delta and high-gamma rhythms observed in EEG signals during treadmill walking. *Neurosci. Lett., 561*, 166-170. doi:10.1016/j.neulet.2013.12.059

Cauquil, A. S., Bessou, M., Dupui, P., & Bessou, P. (1998). Lateral dynamic balance reactions to circular translation of the visual field. *C. R. Acad. Sci. III, 321*(4), 289-294.

Chang, C.-J., Yang, T.-F., Yang, S.-W., & Chern, J.-S. (2016). Cortical Modulation of Motor Control Biofeedback among the Elderly with High Fall Risk during a Posture Perturbation Task with Augmented Reality. *Front. Aging Neurosci., 8*, 80. doi:10.3389/fnagi.2016.00080

Chen, X., He, C., & Peng, H. (2014). Removal of Muscle Artifacts from Single-Channel EEG Based on Ensemble Empirical Mode Decomposition and Multiset Canonical Correlation Analysis. *J. Appl. Math., 2014*, 1-10. doi:10.1155/2014/261347

Chiarovano, E., de Waele, C., MacDougall, H. G., Rogers, S. J., Burgess, A. M., & Curthoys, I. S. (2015). Maintaining Balance when Looking at a Virtual Reality Three-Dimensional Display of a Field of Moving Dots or at a Virtual Reality Scene. *Front. Neurol., 6*. doi:10.3389/fneur.2015.00164

Chowdhury, M. E., Mullinger, K. J., Glover, P., & Bowtell, R. (2014). Reference layer artefact subtraction (RLAS): a novel method of minimizing EEG artefacts during simultaneous fMRI. *Neuroimage, 84*, 307-319. doi:10.1016/j.neuroimage.2013.08.039

Clays, E., De Bacquer, D., Crasset, V., Kittel, F., de Smet, P., Kornitzer, M., . . . De Backer, G. (2011). The perception of work stressors is related to reduced parasympathetic activity. *Int. Arch. Occup. Environ. Health, 84*(2), 185-191. doi:10.1007/s00420-010-0537-z

Clemson, L., Fiatarone Singh, M. A., Bundy, A., Cumming, R. G., Manollaras, K., O'Loughlin, P., & Black, D. (2012). Integration of balance and strength training into daily life activity to reduce rate of falls in older people (the LiFE study): randomised parallel trial. *BMJ, 345*, e4547. doi:10.1136/bmj.e4547

Cleworth, T. W., Horslen, B. C., & Carpenter, M. G. (2012). Influence of real and virtual heights on standing balance. *Gait Posture, 36*(2), 172-176. doi:10.1016/j.gaitpost.2012.02.010

Collomb-Clerc, A., & Welter, M.-L. (2015). Effects of deep brain stimulation on balance and gait in patients with Parkinson's disease: A systematic neurophysiological review. *Neurophysiol. Clin., 45*(4-5), 371-388. doi:10.1016/j.neucli.2015.07.001

Corbetta, D., Imeri, F., & Gatti, R. (2015). Rehabilitation that incorporates virtual reality is more effective than standard rehabilitation for improving walking speed, balance and mobility after stroke: a systematic review. *J. Physiother., 61*(3), 117-124. doi:10.1016/j.jphys.2015.05.017

Cover, T. M., & Thomas, J. A. (2006). *Elements of Information Theory.* Wiley-Interscience.

Critchley, H. D. (2002). Electrodermal responses: what happens in the brain. *Neuroscientist, 8*(2), 132-142. doi:10.1177/107385840200800209

Darekar, A., McFadyen, B. J., Lamontagne, A., & Fung, J. (2015). Efficacy of virtual reality-based intervention on balance and mobility disorders post-stroke: a scoping review. *J. Neuroeng. Rehabil., 12*, 46. doi:10.1186/s12984-015-0035-3

David, O., & Friston, K. J. (2003). A neural mass model for MEG/EEG: coupling and neuronal dynamics. *Neuroimage, 20*(3), 1743-1755.

Del Percio, C., Brancucci, A., Bergami, F., Marzano, N., Fiore, A., Di Ciolo, E., . . . Eusebi, F. (2007). Cortical alpha rhythms are correlated with body sway during quiet open-eyes standing in athletes: a high-resolution EEG study. *Neuroimage, 36*(3), 822-829. doi:10.1016/j.neuroimage.2007.02.054

Delorme, A., & Makeig, S. (2004). EEGLAB: an open source toolbox for analysis of single-trial EEG dynamics including independent component analysis. *J. Neurosci. Methods, 134*(1), 9-21. doi:10.1016/j.jneumeth.2003.10.009

Delorme, A., Mullen, T., Kothe, C., Akalin Acar, Z., Bigdely-Shamlo, N., Vankov, A., & Makeig, S. (2011). EEGLAB, SIFT, NFT, BCILAB, and ERICA: new tools for advanced EEG processing. *Comput. Intell. Neurosci., 2011*, 130714. doi:10.1155/2011/130714

Delorme, A., Palmer, J., Onton, J., Oostenveld, R., & Makeig, S. (2012). Independent EEG sources are dipolar. *PLoS One, 7*(2), e30135. doi:10.1371/journal.pone.0030135

Dhamala, M., Liang, H., Bressler, S. L., & Ding, M. (2018). Granger-Geweke causality: Estimation and interpretation. *Neuroimage, 175*, 460-463. doi:10.1016/j.neuroimage.2018.04.043

Dhamala, M., Rangarajan, G., & Ding, M. (2008). Analyzing information flow in brain networks with nonparametric Granger causality. *Neuroimage, 41*(2), 354-362. doi:10.1016/j.neuroimage.2008.02.020

Dietz, V., Quintern, J., Berger, W., & Schenck, E. (1985). Cerebral potentials and leg muscle e.m.g. responses associated with stance perturbation. *Exp. Brain Res., 57*(2). doi:10.1007/bf00236540

Ding, M., Bressler, S. L., Yang, W., & Liang, H. (2000). Short-window spectral analysis of cortical event-related potentials by adaptive multivariate autoregressive modeling: data preprocessing, model validation, and variability assessment. *Biol. Cybern., 83*(1), 35-45. doi:10.1007/s004229900137

Domingo, A., & Ferris, D. P. (2009). Effects of physical guidance on short-term learning of walking on a narrow beam. *Gait Posture, 30*(4), 464-468. doi:10.1016/j.gaitpost.2009.07.114

Domingo, A., & Ferris, D. P. (2010). The effects of error augmentation on learning to walk on a narrow balance beam. *Exp. Brain Res., 206*(4), 359-370. doi:10.1007/s00221-010-2409-x

Duckrow, R. B., Abu-Hasaballah, K., Whipple, R., & Wolfson, L. (1999). Stance perturbation-evoked potentials in old people with poor gait and balance. *Clin. Neurophysiol., 110*(12), 2026-2032.

Duque, G., Boersma, D., Loza-Diaz, G., Hassan, S., Suarez, H., Geisinger, D., . . . Demontiero, O. (2013). Effects of balance training using a virtual-reality system in older fallers. *Clin. Interv. Aging, 8*, 257-263. doi:10.2147/CIA.S41453

Efron, B., & Tibshirani, R. J. (1993). *An Introduction to the Bootstrap.* doi:10.1007/978-1-4899-4541-9

Emmelkamp, P. M., Bruynzeel, M., Drost, L., & van der Mast, C. A. (2001). Virtual reality treatment in acrophobia: a comparison with exposure in vivo. *Cyberpsychol. Behav., 4*(3), 335-339. doi:10.1089/109493101300210222

Engel, A. K., & Fries, P. (2010). Beta-band oscillations—signalling the status quo? *Curr. Opin. Neurobiol., 20*(2), 156-165. doi:10.1016/j.conb.2010.02.015

Epure, P., Gheorghe, C., Nissen, T., Toader, L.-O., Nicolae, A., Nielsen, S. S., . . . Petersson, E. (2014). Effect of the Oculus Rift head mounted display on postural stability. In P. Sharkey, L. Pareto, J. Broeren, & M. Rydmark (Ed.), *The 10th International Conference on Disability Virtual Reality & Associated Technologies* (pp. 119-127). Reading University Press.

Farina, D., & Holobar, A. (2016). Characterization of Human Motor Units From Surface EMG Decomposition. *Proc. IEEE, 104*(2), 353-373. doi:10.1109/jproc.2015.2498665

Ferrari, M., Bisconti, S., Spezialetti, M., Moro, S. B., Di Palo, C., Placidi, G., & Quaresima, V. (2013). Prefrontal Cortex Activated Bilaterally by a Tilt Board Balance Task: A Functional Near-Infrared Spectroscopy Study in a Semi-Immersive Virtual Reality Environment. *Brain Topogr., 27*(3), 353-365. doi:10.1007/s10548-013-0320-z

Fortis, P., Goedert, K. M., & Barrett, A. M. (2011). Prism adaptation differently affects motor-intentional and perceptual-attentional biases in healthy individuals. *Neuropsychologia, 49*(9), 2718-2727. doi:10.1016/j.neuropsychologia.2011.05.020

Franz, J. R., Francis, C. A., Allen, M. S., O'Connor, S. M., & Thelen, D. G. (2015). Advanced age brings a greater reliance on visual feedback to maintain balance during walking. *Hum. Mov. Sci., 40*, 381-392. doi:10.1016/j.humov.2015.01.012

Franz, J. R., Francis, C., Allen, M., & Thelen, D. G. (2016). Visuomotor Entrainment and the Frequency-Dependent Response of Walking Balance to Perturbations. *IEEE Trans. Neural Syst. Rehabil. Eng.* doi:10.1109/TNSRE.2016.2603340

Friman, O., Borga, M., Lundberg, P., & Knutsson, H. (2002). Exploratory fMRI analysis by autocorrelation maximization. *Neuroimage, 16*(2), 454-464. doi:10.1006/nimg.2002.1067

Fujioka, T., Trainor, L., Large, E., & Ross, B. (2012). Internalized Timing of Isochronous Sounds Is Represented in Neuromagnetic Beta Oscillations. *J Neurosci, 32*(5), 1791-1802. doi:10.1523/JNEUROSCI.4107-11.2012

Gehring, W. J., & Knight, R. T. (2000). Prefrontal-cingulate interactions in action monitoring. *Nat. Neurosci., 3*(5), 516-520. doi:10.1038/74899

Gentili, R. J., Rietschel, J. C., Jaquess, K. J., Lo, L.-C., Prevost, M., Miller, M. W., . . . Hatfield, B. D. (2014). Brain biomarkers based assessment of cognitive workload in pilots under various task demands. *Conf. Proc. IEEE Eng. Med. Biol. Soc., 2014*, 5860-5863. doi:10.1109/EMBC.2014.6944961

Geweke, J. (1982). Measurement of Linear Dependence and Feedback Between Multiple Time Series. *J. Am. Stat. Assoc., 77*(378), 304. doi:10.2307/2287238

Gianaros, P. J., Muth, E. R., Mordkoff, J. T., Levine, M. E., & Stern, R. M. (2001). A questionnaire for the assessment of the multiple dimensions of motion sickness. *Aviat. Space Environ. Med., 72*(2), 115-119.

Gibbons, J. D., & Chakraborti, S. (2011). Nonparametric Statistical Inference. In *International Encyclopedia of Statistical Science* (pp. 977-979). doi:10.1007/978-3-642-04898-2_420

Gilat, M., Shine, J. M., Bolitho, S. J., Matar, E., Kamsma, Y. P., Naismith, S. L., & Lewis, S. J. (2013). Variability of Stepping during a Virtual Reality Paradigm in Parkinson's Disease Patients with and without Freezing of Gait. *PLoS One, 8*(6), e66718. doi:10.1371/journal.pone.0066718

Giromini, L., Ando', A., Morese, R., Salatino, A., Di Girolamo, M., Viglione, D. J., & Zennaro, A. (2016). Rorschach Performance Assessment System (R-PAS) and vulnerability to

stress: A preliminary study on electrodermal activity during stress. *Psychiatry Res., 246*, 166-172. doi:10.1016/j.psychres.2016.09.036
Gonzalez-Franco, M., & Lanier, J. (2017). Model of Illusions and Virtual Reality. *Front. Psychol., 8*, 1125. doi:10.3389/fpsyg.2017.01125
González-Franco, M., Peck, T. C., Rodríguez-Fornells, A., & Slater, M. (2014). A threat to a virtual hand elicits motor cortex activation. *Exp. Brain Res., 232*(3), 875-887. doi:10.1007/s00221-013-3800-1
Gordon, S. M., Franaszczuk, P. J., Hairston, W. D., Vindiola, M., & McDowell, K. (2013). Comparing parametric and nonparametric methods for detecting phase synchronization in EEG. *J. Neurosci. Methods, 212*(2), 247-258. doi:10.1016/j.jneumeth.2012.10.002
Gramann, K., Ferris, D. P., Gwin, J., & Makeig, S. (2014). Imaging natural cognition in action. *Int. J. Psychophysiol., 91*(1), 22-29. doi:10.1016/j.ijpsycho.2013.09.003
Gramann, K., Gwin, J. T., Ferris, D. P., Oie, K., Jung, T.-P., Lin, C.-T., . . . Makeig, S. (2011). Cognition in action: imaging brain/body dynamics in mobile humans. *Rev. Neurosci., 22*(6), 593-608. doi:10.1515/RNS.2011.047
Granger, C. W. (1969). Investigating Causal Relations by Econometric Models and Cross-spectral Methods. *Econometrica, 37*(3), 424. doi:10.2307/1912791
Gutekunst, M., Geuss, M., Rauhoeft, G., Stefanucci, J. K., Kloos, U., & Mohler, B. (2014). Short Paper: A Video Self-avatar Influences the Perception of Heights in an Augmented Reality Oculus Rift. *ICAT-EGVE 2014*, 9-12.
Gwin, J. T., & Ferris, D. P. (2012). Beta- and gamma-range human lower limb corticomuscular coherence. *Front. Hum. Neurosci., 6*, 258. doi:10.3389/fnhum.2012.00258
Gwin, J. T., Gramann, K., Makeig, S., & Ferris, D. P. (2010). Removal of movement artifact from high-density EEG recorded during walking and running. *J. Neurophysiol., 103*(6), 3526-3534. doi:10.1152/jn.00105.2010
Gwin, J. T., Gramann, K., Makeig, S., & Ferris, D. P. (2011). Electrocortical activity is coupled to gait cycle phase during treadmill walking. *Neuroimage, 54*(2), 1289-1296. doi:10.1016/j.neuroimage.2010.08.066
Harrison, L., Penny, W. D., & Friston, K. (2003). Multivariate autoregressive modeling of fMRI time series. *Neuroimage, 19*(4), 1477-1491. doi:10.1016/s1053-8119(03)00160-5
He, B., Dai, Y., Astolfi, L., Babiloni, F., Yuan, H., & Yang, L. (2011). eConnectome: A MATLAB toolbox for mapping and imaging of brain functional connectivity. *J. Neurosci. Methods, 195*(2), 261-269. doi:10.1016/j.jneumeth.2010.11.015
Hell, F., Taylor, P. C., Mehrkens, J. H., & Bötzel, K. (2018). Subthalamic stimulation, oscillatory activity and connectivity reveal functional role of STN and network mechanisms during decision making under conflict. *Neuroimage, 171*, 222-233. doi:10.1016/j.neuroimage.2018.01.001
Hellhammer, D. H., Wüst, S., & Kudielka, B. M. (2009). Salivary cortisol as a biomarker in stress research. *Psychoneuroendocrinology, 34*(2), 163-171. doi:10.1016/j.psyneuen.2008.10.026
Henry, S. M., Fung, J., & Horak, F. B. (1998). EMG responses to maintain stance during multidirectional surface translations. *J. Neurophysiol., 80*(4), 1939-1950. doi:10.1152/jn.1998.80.4.1939
Héroux, M. E., Law, T. C., Fitzpatrick, R. C., & Blouin, J.-S. (2015). Cross-Modal Calibration of Vestibular Afference for Human Balance. *PLoS One, 10*(4), e0124532. doi:10.1371/journal.pone.0124532

Hjortskov, N., Rissén, D., Blangsted, A. K., Fallentin, N., Lundberg, U., & Søgaard, K. (2004). The effect of mental stress on heart rate variability and blood pressure during computer work. *Eur. J. Appl. Physiol., 92*(1-2), 84-89. doi:10.1007/s00421-004-1055-z

Hof, A. L., & Duysens, J. (2018). Responses of human ankle muscles to mediolateral balance perturbations during walking. *Hum. Mov. Sci., 57*, 69-82. doi:10.1016/j.humov.2017.11.009

Hoffman, H. G., Meyer 3rd, W. J., Ramirez, M., Roberts, L., Seibel, E. J., Atzori, B., . . . Patterson, D. R. (2014). Feasibility of articulated arm mounted Oculus Rift Virtual Reality goggles for adjunctive pain control during occupational therapy in pediatric burn patients. *Cyberpsychol. Behav. Soc. Netw., 17*(6), 397-401. doi:10.1089/cyber.2014.0058

Hoffman, H. G., Patterson, D. R., Seibel, E., Soltani, M., Jewett-Leahy, L., & Sharar, S. R. (2008). Virtual reality pain control during burn wound debridement in the hydrotank. *Clin. J. Pain, 24*(4), 299-304. doi:10.1097/AJP.0b013e318164d2cc

Höller, Y., Uhl, A., Bathke, A., Thomschewski, A., Butz, K., Nardone, R., . . . Trinka, E. (2017). Reliability of EEG Measures of Interaction: A Paradigm Shift Is Needed to Fight the Reproducibility Crisis. *Front. Hum. Neurosci., 11*, 441. doi:10.3389/fnhum.2017.00441

Horiuchi, K., Ishihara, M., & Imanaka, K. (2017). The essential role of optical flow in the peripheral visual field for stable quiet standing: Evidence from the use of a head-mounted display. *PLoS One, 12*(10), e0184552. doi:10.1371/journal.pone.0184552

Horlings, C. G., Carpenter, M. G., Küng, U. M., Honegger, F., Wiederhold, B., & Allum, J. H. (2009). Influence of virtual reality on postural stability during movements of quiet stance. *Neurosci. Lett., 451*(3), 227-231. doi:10.1016/j.neulet.2008.12.057

Hotelling, H. (1936). Relations Between Two Sets of Variates. *Biometrika, 28*(3/4), 321. doi:10.2307/2333955

Howell, D. R., Osternig, L. R., & Chou, L.-S. (2016). Consistency and cost of dual-task gait balance measure in healthy adolescents and young adults. *Gait Posture, 49*, 176-180. doi:10.1016/j.gaitpost.2016.07.008

Huang, C.-Y., Lin, L. L., & Hwang, I.-S. (2017). Age-Related Differences in Reorganization of Functional Connectivity for a Dual Task with Increasing Postural Destabilization. *Front. Aging Neurosci., 9*, 96. doi:10.3389/fnagi.2017.00096

Huang, N. E., Shen, Z., Long, S. R., Wu, M. C., Shih, H. H., Zheng, Q., . . . Liu, H. H. (1998). The empirical mode decomposition and the Hilbert spectrum for nonlinear and non-stationary time series analysis. *Proceedings of the Royal Society A: Mathematical, Physical and Engineering Sciences, 454*(1971), 903-995. doi:10.1098/rspa.1998.0193

Hülsdünker, T., Mierau, A., & Strüder, H. K. (2015). Higher Balance Task Demands are Associated with an Increase in Individual Alpha Peak Frequency. *Front. Hum. Neurosci., 9*, 695. doi:10.3389/fnhum.2015.00695

Huppert, D., Grill, E., & Brandt, T. (2013). Down on heights? One in three has visual height intolerance. *J. Neurol., 260*(2), 597-604. doi:10.1007/s00415-012-6685-1

Iandolo, R., Bellini, A., Saiote, C., Marre, I., Bommarito, G., Oesingmann, N., . . . Inglese, M. (2018). Neural correlates of lower limbs proprioception: An fMRI study of foot position matching. *Hum. Brain Mapp.* doi:10.1002/hbm.23972

Ibrahim, M. S., Mattar, A. G., & Elhafez, S. M. (2016). Efficacy of virtual reality-based balance training versus the Biodex balance system training on the body balance of adults. *J. Phys. Therapy Sci., 28*(1), 20-26. doi:10.1589/jpts.28.20

Jacobs, J. V., & Horak, F. B. (2007). Cortical control of postural responses. *J. Neural Transm., 114*(10), 1339-1348. doi:10.1007/s00702-007-0657-0

Jacobs, J. V., Lou, J. S., Kraakevik, J. A., & Horak, F. B. (2009). The supplementary motor area contributes to the timing of the anticipatory postural adjustment during step initiation in participants with and without Parkinson's disease. *Neuroscience, 164*(2), 877-885. doi:10.1016/j.neuroscience.2009.08.002

Jaffe, D. L., Brown, D. A., Pierson-Carey, C. D., Buckley, E. L., & Lew, H. L. (2004). Stepping over obstacles to improve walking in individuals with poststroke hemiplegia. *J. Rehabil. Res. Dev., 41*(3A), 283-292.

Jalili, M., Barzegaran, E., & Knyazeva, M. G. (2014). Synchronization of EEG: bivariate and multivariate measures. *IEEE Trans. Neural Syst. Rehabil. Eng., 22*(2), 212-221. doi:10.1109/TNSRE.2013.2289899

Jiang, J., Bailey, K., & Xiao, X. (2018). Midfrontal Theta and Posterior Parietal Alpha Band Oscillations Support Conflict Resolution in a Masked Affective Priming Task. *Front. Hum. Neurosci., 12*. doi:10.3389/fnhum.2018.00175

Jonmohamadi, Y., Poudel, G., Innes, C., Weiss, D., Krueger, R., & Jones, R. (2014). Comparison of beamformers for EEG source signal reconstruction. *Biomed. Signal Process. Control, 14*, 175-188. doi:10.1016/j.bspc.2014.07.014

Jung, J., Yu, J., & Kang, H. (2012). Effects of Virtual Reality Treadmill Training on Balance and Balance Self-efficacy in Stroke Patients with a History of Falling. *J. Phys. Therapy Sci., 24*(11), 1133-1136. doi:10.1589/jpts.24.1133

Kalron, A., Fonkatz, I., Frid, L., Baransi, H., & Achiron, A. (2016). The effect of balance training on postural control in people with multiple sclerosis using the CAREN virtual reality system: a pilot randomized controlled trial. *J. Neuroeng. Rehabil., 13*, 13. doi:10.1186/s12984-016-0124-y

Kaminski, M. J., & Blinowska, K. J. (1991). A new method of the description of the information flow in the brain structures. *Biol. Cybern., 65*(3), 203-210. doi:10.1007/bf00198091

Kaminski, M., & Blinowska, K. J. (2014). Directed Transfer Function is not influenced by volume conduction inexpedient pre-processing should be avoided. *Front. Comput. Neurosci., 8*. doi:10.3389/fncom.2014.00061

Kaminski, M., & Blinowska, K. J. (2017). The Influence of Volume Conduction on DTF Estimate and the Problem of Its Mitigation. *Front. Comput. Neurosci., 11*, 36. doi:10.3389/fncom.2017.00036

Kamiński, M., Ding, M., Truccolo, W. A., & Bressler, S. L. (2001). Evaluating causal relations in neural systems: granger causality, directed transfer function and statistical assessment of significance. *Biol. Cybern., 85*(2), 145-157. doi:10.1007/s004220000235

Kanekar, N., & Aruin, A. S. (2014). The effect of aging on anticipatory postural control. *Exp. Brain Res., 232*(4), 1127-1136. doi:10.1007/s00221-014-3822-3

Kang, H.-K., Kim, Y., Chung, Y., & Hwang, S. (2012). Effects of treadmill training with optic flow on balance and gait in individuals following stroke: randomized controlled trials. *Clin. Rehabil., 26*(3), 246-255. doi:10.1177/0269215511419383

Kannus, P., Sievänen, H., Palvanen, M., Järvinen, T., & Parkkari, J. (2005). Prevention of falls and consequent injuries in elderly people. *Lancet, 366*(9500), 1885-1893. doi:10.1016/S0140-6736(05)67604-0

Kawamura, S., & Kijima, R. (2016). Effect of head mounted display latency on human stability during quiescent standing on one foot. *2016 IEEE Virtual Reality (VR).* doi:10.1109/vr.2016.7504722

Kelly, J. W., Riecke, B., Loomis, J. M., & Beall, A. C. (2008). Visual control of posture in real and virtual environments. *Percept. Psychophys., 70*(1), 158-165.

Kerns, J. G. (2004). Anterior Cingulate Conflict Monitoring and Adjustments in Control. *Science, 303*(5660), 1023-1026. doi:10.1126/science.1089910

Kline, J. E., Huang, H. J., Snyder, K. L., & Ferris, D. P. (2015). Isolating gait-related movement artifacts in electroencephalography during human walking. *J. Neural Eng., 12*(4), 046022. doi:10.1088/1741-2560/12/4/046022

Kline, J. E., Huang, H. J., Snyder, K. L., & Ferris, D. P. (2016). Cortical Spectral Activity and Connectivity during Active and Viewed Arm and Leg Movement. *Front. Neurosci., 10*, 91. doi:10.3389/fnins.2016.00091

Kline, J. E., Poggensee, K., & Ferris, D. P. (2014). Your brain on speed: cognitive performance of a spatial working memory task is not affected by walking speed. *Front. Hum. Neurosci., 8*. doi:10.3389/fnhum.2014.00288

Kneeland, J. B., Knowles, R. J., & Cahill, P. T. (1984). Magnetic resonance imaging systems: optimization in clinical use. *Radiology, 153*(2), 473-478. doi:10.1148/radiology.153.2.6484181

Kolasinski, E. M. (1995). *Simulator sickness in virtual environments.* Retrieved from https://books.google.com/books/about/Simulator_sickness_in_virtual_environmen.html?hl=&id=7qwrAAAAYAAJ

Korzeniewska, A., Mańczak, M., Kamiński, M., Blinowska, K. J., & Kasicki, S. (2003). Determination of information flow direction among brain structures by a modified directed transfer function (dDTF) method. *J. Neurosci. Methods, 125*(1-2), 195-207.

Krakauer, J. W., Ghez, C., & Ghilardi, M. F. (2005). Adaptation to visuomotor transformations: consolidation, interference, and forgetting. *J. Neurosci., 25*(2), 473-478. doi:10.1523/JNEUROSCI.4218-04.2005

Kurz, I., Gimmon, Y., Shapiro, A., Debi, R., Snir, Y., & Melzer, I. (2016). Unexpected perturbations training improves balance control and voluntary stepping times in older adults - a double blind randomized control trial. *BMC Geriatr., 16*, 58. doi:10.1186/s12877-016-0223-4

Lach, H. W. (2005). Incidence and risk factors for developing fear of falling in older adults. *Public Health Nurs., 22*(1), 45-52. doi:10.1111/j.0737-1209.2005.22107.x

Lachaux, J. P., Rodriguez, E., Martinerie, J., & Varela, F. J. (1999). Measuring phase synchrony in brain signals. *Hum. Brain Mapp., 8*(4), 194-208.

Ladouce, S., Donaldson, D. I., Dudchenko, P. A., & Ietswaart, M. (2017). Understanding Minds in Real-World Environments: Toward a Mobile Cognition Approach. *Front. Hum. Neurosci., 10*. doi:10.3389/fnhum.2016.00694

Lau, T. M., Gwin, J. T., & Ferris, D. P. (2014). Walking reduces sensorimotor network connectivity compared to standing. *J. Neuroeng. Rehabil., 11*, 14. doi:10.1186/1743-0003-11-14

Lawrence, C. A., & Barry, R. J. (2010). Cognitive processing effects on auditory event-related potentials and the evoked cardiac response. *Int. J. Psychophysiol., 78*(2), 100-106. doi:10.1016/j.ijpsycho.2010.06.027

Lee, C. (2016). Group-Level Analysis of Source-Resolved Event Related Potential and Brain Connectivity.

Lee, T. W., Girolami, M., & Sejnowski, T. J. (1999). Independent component analysis using an extended infomax algorithm for mixed subgaussian and supergaussian sources. *Neural Comput., 11*(2), 417-441.

Lim, C. L., Rennie, C., Barry, R. J., Bahramali, H., Lazzaro, I., Manor, B., & Gordon, E. (1997). Decomposing skin conductance into tonic and phasic components. *Int. J. Psychophysiol., 25*(2), 97-109.

Linkenkaer-Hansen, K., Nikouline, V. V., Palva, J. M., & Ilmoniemi, R. J. (2001). Long-range temporal correlations and scaling behavior in human brain oscillations. *J. Neurosci., 21*(4), 1370-1377.

Little, C. E., & Woollacott, M. (2015). EEG measures reveal dual-task interference in postural performance in young adults. *Exp. Brain Res., 233*(1), 27-37. doi:10.1007/s00221-014-4111-x

Lott, A., Bisson, E., Lajoie, Y., McComas, J., & Sveistrup, H. (2003). The effect of two types of virtual reality on voluntary center of pressure displacement. *Cyberpsychol. Behav., 6*(5), 477-485. doi:10.1089/109493103769710505

Luck, S. J. (2014). *An Introduction to the Event-related Potential Technique.* Bradford Book. Retrieved from https://books.google.com/books/about/An_Introduction_to_the_Event_related_Pot.html?hl=&id=8GD1jgEACAAJ

Lütkepohl, H. (2007). *New Introduction to Multiple Time Series Analysis.* Springer Science & Business Media.

Luu, T. P., Brantley, J. A., Nakagome, S., Zhu, F., & Contreras-Vidal, J. L. (2017c). Electrocortical correlates of human level-ground, slope, and stair walking. *PLoS One, 12*(11), e0188500. doi:10.1371/journal.pone.0188500

Luu, T. P., He, Y., Nakagome, S., Nathan, K., Brown, S., Gorges, J., & Contreras-Vidal, J. L. (2017a). Multi-Trial Gait Adaptation of Healthy Individuals during Visual Kinematic Perturbations. *Front. Hum. Neurosci., 11*. doi:10.3389/fnhum.2017.00320

Luu, T. P., Nakagome, S., He, Y., & Contreras-Vidal, J. L. (2017b). Real-time EEG-based brain-computer interface to a virtual avatar enhances cortical involvement in human treadmill walking. *Sci. Rep., 7*(1), 8895. doi:10.1038/s41598-017-09187-0

Ma, Z. (2018). Neurophysiological Analysis of the Genesis Mechanism of EEG During the Interictal and Ictal Periods Using a Multiple Neural Masses Model. *Int. J. Neural Syst., 28*(1), 1750027. doi:10.1142/S0129065717500277

Macpherson, J. M., & Horak, F. B. (2012). Posture. In E. Kandel, J. Schwartz, T. Jessell, S. Siegelbaum, & A. J. Hudspeth, *Principles of Neural Science, Fifth Edition* (pp. 935-959). McGraw Hill Professional.

Mahjoory, K., Nikulin, V. V., Botrel, L., Linkenkaer-Hansen, K., Fato, M. M., & Haufe, S. (2017). Consistency of EEG source localization and connectivity estimates. *Neuroimage, 152*, 590-601. doi:10.1016/j.neuroimage.2017.02.076

Mahoney, J. R., Holtzer, R., Izzetoglu, M., Zemon, V., Verghese, J., & Allali, G. (2016). The role of prefrontal cortex during postural control in Parkinsonian syndromes a functional near-infrared spectroscopy study. *Brain Res., 1633*, 126-138. doi:10.1016/j.brainres.2015.10.053

Makeig, S. (2002). Dynamic Brain Sources of Visual Evoked Responses. *Science, 295*(5555), 690-694. doi:10.1126/science.1066168

Makeig, S., & Onton, J. (2009). ERP Features and EEG Dynamics: An ICA Perspective. In S. Luck, & E. Kappenman, *Oxford Handbook of Event-Related Potential Components.* New York: Oxford University Press.

Makeig, S., Bell, A. J., Jung, T. P., & Sejnowski, T. J. (1996). Independent component analysis of electroencephalographic data. *Adv Neur In, 8*, 145-151.

Maki, B. E., & McIlroy, W. E. (2007). Cognitive demands and cortical control of human balance-recovery reactions. *J. Neural Transm., 114*(10), 1279-1296. doi:10.1007/s00702-007-0764-y

Malik, M. (1996). Heart rate variability: standards of measurement, physiological interpretation and clinical use. Task Force of the European Society of Cardiology and the North American Society of Pacing and Electrophysiology. *Circulation, 93*(5), 1043-1065. Retrieved from https://www.ncbi.nlm.nih.gov/pubmed/8598068

Marlin, A., Mochizuki, G., Staines, W. R., & McIlroy, W. E. (2014). Localizing evoked cortical activity associated with balance reactions: does the anterior cingulate play a role? *J. Neurophysiol., 111*(12), 2634-2643. doi:10.1152/jn.00511.2013

Martin, T. A., Keating, J. G., Goodkin, H. P., Bastian, A. J., & Thach, W. T. (1996). Throwing while looking through prisms. I. Focal olivocerebellar lesions impair adaptation. *Brain, 119 (Pt 4)*, 1183-1198.

Matar, E., Shine, J. M., Naismith, S. L., & Lewis, S. J. (2013). Using virtual reality to explore the role of conflict resolution and environmental salience in freezing of gait in Parkinson's disease. *Parkinsonism Relat. Disord., 19*(11), 937-942. doi:10.1016/j.parkreldis.2013.06.002

McCraty, R., & Shaffer, F. (2015). Heart Rate Variability: New Perspectives on Physiological Mechanisms, Assessment of Self-regulatory Capacity, and Health risk. *Glob Adv Health Med, 4*(1), 46-61. doi:10.7453/gahmj.2014.073

Meehan, M., Insko, B., Whitton, M., & Brooks, F. P. (2002). Physiological measures of presence in stressful virtual environments. *Proceedings of the 29th annual conference on Computer graphics and interactive techniques - SIGGRAPH '02.* doi:10.1145/566570.566630

Meester, D., Al-Yahya, E., Dawes, H., Martin-Fagg, P., & Piñon, C. (2014). Associations between prefrontal cortex activation and H-reflex modulation during dual task gait. *Front. Hum. Neurosci., 8*, 78. doi:10.3389/fnhum.2014.00078

Mellman, T. A., Knorr, B. R., Pigeon, W. R., Leiter, J. C., & Akay, M. (2004). Heart rate variability during sleep and the early development of posttraumatic stress disorder. *Biol. Psychiatry, 55*(9), 953-956. doi:10.1016/j.biopsych.2003.12.018

Mierau, A., Pester, B., Hülsdünker, T., Schiecke, K., Strüder, H. K., & Witte, H. (2017). Cortical Correlates of Human Balance Control. *Brain Topogr., 30*(4), 434-446. doi:10.1007/s10548-017-0567-x

Mihara, M., Miyai, I., Hatakenaka, M., Kubota, K., & Sakoda, S. (2008). Role of the prefrontal cortex in human balance control. *Neuroimage, 43*(2), 329-336. doi:10.1016/j.neuroimage.2008.07.029

Miltner, W. H., Lemke, U., Weiss, T., Holroyd, C., Scheffers, M. K., & Coles, M. G. (2003). Implementation of error-processing in the human anterior cingulate cortex: a source

analysis of the magnetic equivalent of the error-related negativity. *Biol. Psychol., 64*(1-2), 157-166.
Mirelman, A., Maidan, I., Bernad-Elazari, H., Nieuwhof, F., Reelick, M., Giladi, N., & Hausdorff, J. M. (2014). Increased frontal brain activation during walking while dual tasking: an fNIRS study in healthy young adults. *J. Neuroeng. Rehabil., 11*, 85. doi:10.1186/1743-0003-11-85
Mirelman, A., Maidan, I., Herman, T., Deutsch, J. E., Giladi, N., & Hausdorff, J. M. (2011). Virtual reality for gait training: can it induce motor learning to enhance complex walking and reduce fall risk in patients with Parkinson's disease? *J. Gerontol. A Biol. Sci. Med. Sci., 66*(2), 234-240. doi:10.1093/gerona/glq201
Mochizuki, G., Boe, S., Marlin, A., & McIlRoy, W. E. (2010). Perturbation-evoked cortical activity reflects both the context and consequence of postural instability. *Neuroscience, 170*(2), 599-609. doi:10.1016/j.neuroscience.2010.07.008
Mochizuki, G., Semmler, J. G., Ivanova, T. D., & Garland, S. J. (2006). Low-frequency common modulation of soleus motor unit discharge is enhanced during postural control in humans. *Exp. Brain Res., 175*(4), 584-595. doi:10.1007/s00221-006-0575-7
Mognon, A., Jovicich, J., Bruzzone, L., & Buiatti, M. (2011). ADJUST: An automatic EEG artifact detector based on the joint use of spatial and temporal features. *Psychophysiology, 48*(2), 229-240. doi:10.1111/j.1469-8986.2010.01061.x
Mulavara, A. P., Cohen, H. S., & Bloomberg, J. J. (2009). Critical features of training that facilitate adaptive generalization of over ground locomotion. *Gait Posture, 29*(2), 242-248. doi:10.1016/j.gaitpost.2008.08.012
Mullen, T. R. (2014). *The Dynamic Brain: Modeling Neural Dynamics and Interactions From Human Electrophysiological Recordings.* Retrieved from https://books.google.com/books/about/The_Dynamic_Brain.html?hl=&id=APG4oQEACAAJ
Mullen, T., Kothe, C., Chi, Y. M., Ojeda, A., Kerth, T., Makeig, S., . . . Jung, T.-P. (2013). Real-time modeling and 3D visualization of source dynamics and connectivity using wearable EEG. *Conf. Proc. IEEE Eng. Med. Biol. Soc., 2013*, 2184-2187. doi:10.1109/EMBC.2013.6609968
Mullen, T., Kothe, C., Chi, Y. M., Ojeda, A., Kerth, T., Makeig, S., . . . Jung, T.-P. (2015). Real-time modeling and 3D visualization of source dynamics and connectivity using wearable EEG. *Conf. Proc. IEEE Eng. Med. Biol. Soc., 2015*, 2184-2187. doi:10.1109/EMBC.2013.6609968
Munoz, E., Sliwinski, M. J., Scott, S. B., & Hofer, S. (2015). Global perceived stress predicts cognitive change among older adults. *Psychol. Aging, 30*(3), 487-499. doi:10.1037/pag0000036
Nathan, K., & Contreras-Vidal, J. L. (2015). Negligible Motion Artifacts in Scalp Electroencephalography (EEG) During Treadmill Walking. *Front. Hum. Neurosci., 9*, 708. doi:10.3389/fnhum.2015.00708
Neelon, M. F., Williams, J., & Garell, P. C. (2006). The effects of attentional load on auditory ERPs recorded from human cortex. *Brain Res., 1118*(1), 94-105. doi:10.1016/j.brainres.2006.08.006
Nemanich, S. T., & Earhart, G. M. (2015). How do age and nature of the motor task influence visuomotor adaptation? *Gait Posture, 42*(4), 564-568. doi:10.1016/j.gaitpost.2015.09.001

Nordin, A., Hairston, W., & Ferris, D. (In press). Dual-electrode motion artifact cancellation for mobile electroencephalography. *J. Neural Eng.*

Ogaya, S., Ikezoe, T., Soda, N., & Ichihashi, N. (2011). Effects of balance training using wobble boards in the elderly. *J. Strength Cond. Res.*, *25*(9), 2616-2622. doi:10.1519/JSC.0b013e31820019cf

Oliveira, A. S., Schlink, B. R., Hairston, W. D., König, P., & Ferris, D. P. (2016). Induction and separation of motion artifacts in EEG data using a mobile phantom head device. *J. Neural Eng.*, *13*(3), 036014. doi:10.1088/1741-2560/13/3/036014

Oliveira, A. S., Schlink, B. R., Hairston, W. D., König, P., & Ferris, D. P. (2017a). Restricted vision increases sensorimotor cortex involvement in human walking. *J. Neurophysiol.*, *118*(4), 1943-1951. doi:10.1152/jn.00926.2016

Oliveira, A. S., Schlink, B. R., Hairston, W. D., König, P., & Ferris, D. P. (2017b). A Channel Rejection Method for Attenuating Motion-Related Artifacts in EEG Recordings during Walking. *Front. Neurosci.*, *11*, 225. doi:10.3389/fnins.2017.00225

Oostenveld, R., & Oostendorp, T. F. (2002). Validating the boundary element method for forward and inverse EEG computations in the presence of a hole in the skull. *Hum. Brain Mapp.*, *17*(3), 179-192. doi:10.1002/hbm.10061

Oostenveld, R., Fries, P., Maris, E., & Schoffelen, J.-M. (2011). FieldTrip: Open source software for advanced analysis of MEG, EEG, and invasive electrophysiological data. *Comput. Intell. Neurosci.*, *2011*, 156869. doi:10.1155/2011/156869

Padrao, G., Gonzalez-Franco, M., Sanchez-Vives, M. V., Slater, M., & Rodriguez-Fornells, A. (2016). Violating body movement semantics: Neural signatures of self-generated and external-generated errors. *Neuroimage*, *124*(Pt A), 147-156. doi:10.1016/j.neuroimage.2015.08.022

Palacios-Navarro, G., Albiol-Pérez, S., & García-Magariño García, I. (2016). Effects of sensory cueing in virtual motor rehabilitation. A review. *J. Biomed. Inform.*, *60*, 49-57. doi:10.1016/j.jbi.2016.01.006

Palmer, J. A., Kreutz-Delgado, K., & Makeig, S. (2006). Super-Gaussian Mixture Source Model for ICA. In *Lecture Notes in Computer Science* (pp. 854-861). doi:10.1007/11679363_106

Palmer, J. A., Makeig, S., Kreutz-Delgado, K., & Rao, B. D. (2008). Newton method for the ICA mixture model. *2008 IEEE International Conference on Acoustics, Speech and Signal Processing.* doi:10.1109/icassp.2008.4517982

Papa, E. V., Garg, H., & Dibble, L. E. (2015). Acute effects of muscle fatigue on anticipatory and reactive postural control in older individuals: a systematic review of the evidence. *J. Geriatr. Phys. Ther.*, *38*(1), 40-48. doi:10.1519/JPT.0000000000000026

Parijat, P., Lockhart, T. E., & Liu, J. (2015). Effects of perturbation-based slip training using a virtual reality environment on slip-induced falls. *Ann. Biomed. Eng.*, *43*(4), 958-967. doi:10.1007/s10439-014-1128-z

Petersen, T. H., Willerslev-Olsen, M., Conway, B. A., & Nielsen, J. B. (2012). The motor cortex drives the muscles during walking in human subjects. *J. Physiol.*, *590*(10), 2443-2452. doi:10.1113/jphysiol.2012.227397

Peterson, S. M., & Ferris, D. P. (2018). Differentiation in theta and beta electrocortical activity between visual and physical perturbations to walking and standing balance. *eNeuro*. doi:10.1523/ENEURO.0207-18.2018

Peterson, S. M., Furuichi, E., & Ferris, D. P. (2018). Effects of virtual reality high heights exposure during beam-walking on physiological stress and cognitive loading. *PLoS One, 13*(7), e0200306. doi:10.1371/journal.pone.0200306

Peterson, S. M., Rios, E., & Ferris, D. P. (2018). Transient visual perturbations boost short-term balance learning in virtual reality by modulating electrocortical activity. *J. Neurophysiol.* doi:10.1152/jn.00292.2018

Picard, R. W., Fedor, S., & Ayzenberg, Y. (2015). Multiple Arousal Theory and Daily-Life Electrodermal Activity Asymmetry. *Emot. Rev., 8*(1), 62-75. doi:10.1177/1754073914565517

Pirini, M., Mancini, M., Farella, E., & Chiari, L. (2011). EEG correlates of postural audio-biofeedback. *Hum. Mov. Sci., 30*(2), 249-261. doi:10.1016/j.humov.2010.05.016

Poh, M.-Z., Swenson, N. C., & Picard, R. W. (2010). A wearable sensor for unobtrusive, long-term assessment of electrodermal activity. *IEEE Trans. Biomed. Eng., 57*(5), 1243-1252. doi:10.1109/TBME.2009.2038487

Presacco, A., Goodman, R., Forrester, L., & Contreras-Vidal, J. L. (2011). Neural decoding of treadmill walking from noninvasive electroencephalographic signals. *J. Neurophysiol., 106*(4), 1875-1887. doi:10.1152/jn.00104.2011

Proteau, L., Marteniuk, R. G., & Lévesque, L. (1992). A sensorimotor basis for motor learning: evidence indicating specificity of practice. *Q. J. Exp. Psychol. A, 44*(3), 557-575.

Quant, S., Adkin, A. L., Staines, W. R., Maki, B. E., & McIlroy, W. E. (2004). The effect of a concurrent cognitive task on cortical potentials evoked by unpredictable balance perturbations. *BMC Neurosci., 5*, 18. doi:10.1186/1471-2202-5-18

R Core Team. (2017). *R: A language and environment for statistical computing.* R Foundation for Statistical Computing, Vienna, Austria. Retrieved from http://www.R-project.org/

Rankin, J. K., Woollacott, M. H., Shumway-Cook, A., & Brown, L. A. (2000). Cognitive Influence on Postural Stability: A Neuromuscular Analysis in Young and Older Adults. *J. Gerontol. A Biol. Sci. Med. Sci., 55*(3), M112-M119. doi:10.1093/gerona/55.3.m112

Regenbogen, C., De Vos, M., Debener, S., Turetsky, B. I., Mössnang, C., Finkelmeyer, A., . . . Kellermann, T. (2012). Auditory processing under cross-modal visual load investigated with simultaneous EEG-fMRI. *PLoS One, 7*(12), e52267. doi:10.1371/journal.pone.0052267

Reinhardt, T., Schmahl, C., Wüst, S., & Bohus, M. (2012). Salivary cortisol, heart rate, electrodermal activity and subjective stress responses to the Mannheim Multicomponent Stress Test (MMST). *Psychiatry Res., 198*(1), 106-111. doi:10.1016/j.psychres.2011.12.009

Robert, M. T., Ballaz, L., & Lemay, M. (2016). The effect of viewing a virtual environment through a head-mounted display on balance. *Gait Posture, 48*, 261-266. doi:10.1016/j.gaitpost.2016.06.010

Roeder, L., Boonstra, T. W., Smith, S. S., & Kerr, G. K. (2018). Dynamics of corticospinal motor control during overground and treadmill walking in humans. *J. Neurophysiol.* doi:10.1152/jn.00613.2017

Roy, V., Shukla, S., Shukla, P. K., & Rawat, P. (2017). Gaussian Elimination-Based Novel Canonical Correlation Analysis Method for EEG Motion Artifact Removal. *J. Healthc. Eng., 2017*, 9674712. doi:10.1155/2017/9674712

Sabri, M., Humphries, C., Verber, M., Liebenthal, E., Binder, J. R., Mangalathu, J., & Desai, A. (2014). Neural effects of cognitive control load on auditory selective attention. *Neuropsychologia, 61*, 269-279. doi:10.1016/j.neuropsychologia.2014.06.009

Safieddine, D., Kachenoura, A., Albera, L., Birot, G., Karfoul, A., Pasnicu, A., . . . Merlet, I. (2012). Removal of muscle artifact from EEG data: comparison between stochastic (ICA and CCA) and deterministic (EMD and wavelet-based) approaches. *EURASIP J. Adv. Signal Process., 2012*. doi:10.1186/1687-6180-2012-127

Salazar, R. D., Ren, X., Ellis, T. D., Toraif, N., Barthelemy, O. J., Neargarder, S., & Cronin-Golomb, A. (2017). Dual tasking in Parkinson's disease: Cognitive consequences while walking. *Neuropsychology, 31*(6), 613-623. doi:10.1037/neu0000331

Sanchez-Vives, M. V., & Slater, M. (2005). From presence to consciousness through virtual reality. *Nat. Rev. Neurosci., 6*(4), 332-339. doi:10.1038/nrn1651

Särelä, J., & Vigário, R. (2003). Overlearning in marginal distribution-based ICA: analysis and solutions. *J. Mach. Learn. Res., 4*, 1447-1469.

Schelter, B., Timmer, J., & Eichler, M. (2009). Assessing the strength of directed influences among neural signals using renormalized partial directed coherence. *J. Neurosci. Methods, 179*(1), 121-130. doi:10.1016/j.jneumeth.2009.01.006

Schlink, B. R., Peterson, S. M., Hairston, W. D., König, P., Kerick, S. E., & Ferris, D. P. (2017). Independent Component Analysis and Source Localization on Mobile EEG Data Can Identify Increased Levels of Acute Stress. *Front. Hum. Neurosci., 11*, 310. doi:10.3389/fnhum.2017.00310

Schmidt, R. A. (1991). Frequent Augmented Feedback Can Degrade Learning: Evidence and Interpretations. In *Tutorials in Motor Neuroscience* (pp. 59-75). doi:10.1007/978-94-011-3626-6_6

Schmidt, R. A., Young, D. E., Swinnen, S., & Shapiro, D. C. (1989). Summary knowledge of results for skill acquisition: support for the guidance hypothesis. *J. Exp. Psychol. Learn. Mem. Cogn., 15*(2), 352-359.

Schmidt, S., & Walach, H. (2000). Electrodermal activity (EDA) – state-of-the-art measurement and techniques for parapsychological purposes. *J. Parapsychol., 64*(2), 139-163.

Schniepp, R., Kugler, G., Wuehr, M., Eckl, M., Huppert, D., Huth, S., . . . Brandt, T. (2014). Quantification of gait changes in subjects with visual height intolerance when exposed to heights. *Front. Hum. Neurosci., 8*, 963. doi:10.3389/fnhum.2014.00963

Seeber, M., Scherer, R., Wagner, J., Solis-Escalante, T., & Müller-Putz, G. R. (2014). EEG beta suppression and low gamma modulation are different elements of human upright walking. *Front. Hum. Neurosci., 8*, 485. doi:10.3389/fnhum.2014.00485

Seidler, R. D. (2004). Multiple motor learning experiences enhance motor adaptability. *J. Cogn. Neurosci., 16*(1), 65-73. doi:10.1162/089892904322755566

Seidler, R. D. (2010). Neural correlates of motor learning, transfer of learning, and learning to learn. *Exerc. Sport Sci. Rev., 38*(1), 3-9. doi:10.1097/JES.0b013e3181c5cce7

Seinfeld, S., Bergstrom, I., Pomes, A., Arroyo-Palacios, J., Vico, F., Slater, M., & Sanchez-Vives, M. V. (2015). Influence of Music on Anxiety Induced by Fear of Heights in Virtual Reality. *Front. Psychol., 6*, 1969. doi:10.3389/fpsyg.2015.01969

Serrien, D. J., Ivry, R. B., & Swinnen, S. P. (2006). Dynamics of hemispheric specialization and integration in the context of motor control. *Nat. Rev. Neurosci., 7*(2), 160-166. doi:10.1038/nrn1849

Shadmehr, R., & Moussavi, Z. M. (2000). Spatial generalization from learning dynamics of reaching movements. *J. Neurosci., 20*(20), 7807-7815.

Shattuck, D. W., Mirza, M., Adisetiyo, V., Hojatkashani, C., Salamon, G., Narr, K. L., . . . Toga, A. W. (2008). Construction of a 3D probabilistic atlas of human cortical structures. *Neuroimage, 39*(3), 1064-1080. doi:10.1016/j.neuroimage.2007.09.031

Shaw, E. P., Rietschel, J. C., Hendershot, B. D., Pruziner, A. L., Miller, M. W., Hatfield, B. D., & Gentili, R. J. (2018). Measurement of attentional reserve and mental effort for cognitive workload assessment under various task demands during dual-task walking. *Biol. Psychol., 134*, 39-51. doi:10.1016/j.biopsycho.2018.01.009

Sherrington, C., Whitney, J. C., Lord, S. R., Herbert, R. D., Cumming, R. G., & Close, J. C. (2008). Effective Exercise for the Prevention of Falls: A Systematic Review and Meta-Analysis. *J. Am. Geriatr. Soc., 56*(12), 2234-2243. doi:10.1111/j.1532-5415.2008.02014.x

Simeonov, P. I., Hsiao, H., Dotson, B. W., & Ammons, D. E. (2005). Height effects in real and virtual environments. *Hum. Factors, 47*(2), 430-438. doi:10.1518/0018720054679506

Sipp, A. R., Gwin, J. T., Makeig, S., & Ferris, D. P. (2013). Loss of balance during balance beam walking elicits a multifocal theta band electrocortical response. *J. Neurophysiol., 110*(9), 2050-2060. doi:10.1152/jn.00744.2012

Slater, M., Usoh, M., & Steed, A. (1994). Depth of Presence in Virtual Environments. *Presence: Teleoperators and Virtual Environments, 3*(2), 130-144. doi:10.1162/pres.1994.3.2.130

Slobounov, S. M., Teel, E., & Newell, K. M. (2013). Modulation of cortical activity in response to visually induced postural perturbation: combined VR and EEG study. *Neurosci. Lett., 547*, 6-9. doi:10.1016/j.neulet.2013.05.001

Slobounov, S., Cao, C., Jaiswal, N., & Newell, K. M. (2009). Neural basis of postural instability identified by VTC and EEG. *Exp. Brain Res., 199*(1), 1-16. doi:10.1007/s00221-009-1956-5

Snyder, K. L., Kline, J. E., Huang, H. J., & Ferris, D. P. (2015). Independent Component Analysis of Gait-Related Movement Artifact Recorded using EEG Electrodes during Treadmill Walking. *Front. Hum. Neurosci., 9*, 639. doi:10.3389/fnhum.2015.00639

Snyder, K. L., Vindiola, M., Vettel, J. M., & Ferris, D. P. (2013). Cortical connectivity during uneven terrain walking. *2013 6th International IEEE/EMBS Conference on Neural Engineering (NER).* doi:10.1109/ner.2013.6695914

Soffel, F., Zank, M., & Kunz, A. (2016). Postural stability analysis in virtual reality using the HTC vive. *Proceedings of the 22nd ACM Conference on Virtual Reality Software and Technology - VRST '16.* doi:10.1145/2993369.2996341

Staines, W. R., McIlroy, W. E., & Brooke, J. D. (2001). Cortical representation of whole-body movement is modulated by proprioceptive discharge in humans. *Exp. Brain Res., 138*(2), 235-242.

Steinicke, F., Visell, Y., Campos, J., & Lécuyer, A. (2013). *Human Walking in Virtual Environments: Perception, Technology, and Applications.* Springer. Retrieved from https://books.google.com/books/about/Human_Walking_in_Virtual_Environments.html?hl=&id=rtUiswEACAAJ

Steinman, S. A., & Teachman, B. A. (2011). Cognitive processing and acrophobia: validating the Heights Interpretation Questionnaire. *J. Anxiety Disord., 25*(7), 896-902. doi:10.1016/j.janxdis.2011.05.001

Sterling, D. A., O'Connor, J. A., & Bonadies, J. (2001). Geriatric falls: injury severity is high and disproportionate to mechanism. *J. Trauma, 50*(1), 116-119.
Symeonidou, E.-R., Nordin, A. D., Hairston, W. D., & Ferris, D. P. (2018). Effects of Cable Sway, Electrode Surface Area, and Electrode Mass on Electroencephalography Signal Quality during Motion. *Sensors, 18*(4). doi:10.3390/s18041073
Tarvainen, M. P., Niskanen, J.-P., Lipponen, J. A., Ranta-Aho, P. O., & Karjalainen, P. A. (2014). Kubios HRV--heart rate variability analysis software. *Comput. Methods Programs Biomed., 113*(1), 210-220. doi:10.1016/j.cmpb.2013.07.024
Thayer, J. F., Ahs, F., Fredrikson, M., Sollers, J. J., & Wager, T. D. (2012). A meta-analysis of heart rate variability and neuroimaging studies: implications for heart rate variability as a marker of stress and health. *Neurosci. Biobehav. Rev., 36*(2), 747-756. doi:10.1016/j.neubiorev.2011.11.009
Thayer, J. F., Hansen, A. L., & Johnsen, B. H. (2010). The Non-invasive Assessment of Autonomic Influences on the Heart Using Impedance Cardiography and Heart Rate Variability. In *Handbook of Behavioral Medicine* (pp. 723-740). doi:10.1007/978-0-387-09488-5_47
Theiler, J., Eubank, S., Longtin, A., Galdrikian, B., & Doyne Farmer, J. (1992). Testing for nonlinearity in time series: the method of surrogate data. *Physica D, 58*(1-4), 77-94. doi:10.1016/0167-2789(92)90102-s
Tse, Y. Y., Petrofsky, J. S., Berk, L., Daher, N., Lohman, E., Laymon, M. S., & Cavalcanti, P. (2013). Postural sway and rhythmic electroencephalography analysis of cortical activation during eight balance training tasks. *Med. Sci. Monit., 19*, 175-186. doi:10.12659/MSM.883824
Urigüen, J. A., & Garcia-Zapirain, B. (2015). EEG artifact removal-state-of-the-art and guidelines. *J. Neural Eng., 12*(3), 031001. doi:10.1088/1741-2560/12/3/031001
Van de Steen, F., Faes, L., Karahan, E., Songsiri, J., Valdes-Sosa, P. A., & Marinazzo, D. (2016). Critical Comments on EEG Sensor Space Dynamical Connectivity Analysis. *Brain Topogr*. doi:10.1007/s10548-016-0538-7
van Veen, V., & Carter, C. S. (2002). The anterior cingulate as a conflict monitor: fMRI and ERP studies. *Physiol. Behav., 77*(4-5), 477-482.
Varghese, J. P. (2016). Cortical activations underlying human bipedal balance control.
Varghese, J. P., Marlin, A., Beyer, K. B., Staines, W. R., Mochizuki, G., & McIlroy, W. E. (2014). Frequency characteristics of cortical activity associated with perturbations to upright stability. *Neurosci. Lett., 578*, 33-38. doi:10.1016/j.neulet.2014.06.017
Varghese, J. P., McIlroy, R. E., & Barnett-Cowan, M. (2017). Perturbation-evoked potentials: Significance and application in balance control research. *Neurosci. Biobehav. Rev., 83*, 267-280. doi:10.1016/j.neubiorev.2017.10.022
Vinck, M., Oostenveld, R., van Wingerden, M., Battaglia, F., & Pennartz, C. M. (2011). An improved index of phase-synchronization for electrophysiological data in the presence of volume-conduction, noise and sample-size bias. *Neuroimage, 55*(4), 1548-1565. doi:10.1016/j.neuroimage.2011.01.055
Vindiola, M. M., Vettel, J. M., Gordon, S. M., Franaszczuk, P. J., & McDowell, K. (2014). Applying EEG phase synchronization measures to non-linearly coupled neural mass models. *J. Neurosci. Methods, 226*, 1-14. doi:10.1016/j.jneumeth.2014.01.025

Wagner, J., Makeig, S., Gola, M., Neuper, C., & Müller-Putz, G. (2016). Distinct β Band Oscillatory Networks Subserving Motor and Cognitive Control during Gait Adaptation. *J. Neurosci., 36*(7), 2212-2226. doi:10.1523/JNEUROSCI.3543-15.2016

Wagner, J., Solis-Escalante, T., Scherer, R., Neuper, C., & Müller-Putz, G. (2014). It's how you get there: walking down a virtual alley activates premotor and parietal areas. *Front. Hum. Neurosci., 8*. doi:10.3389/fnhum.2014.00093

Walker, H. K., Hall, W. D., & Hurst, J. W. (1976). *Clinical methods: the history, physical, and laboratory examinations.* Retrieved from https://books.google.com/books/about/Clinical_methods.html?hl=&id=7xcEAQAAIAAJ

Wang, H. E., Bénar, C. G., Quilichini, P. P., Friston, K. J., Jirsa, V. K., & Bernard, C. (2014). A systematic framework for functional connectivity measures. *Front. Neurosci., 8*, 405. doi:10.3389/fnins.2014.00405

Welch, R. B., Bridgeman, B., Anand, S., & Browman, K. E. (1993). Alternating prism exposure causes dual adaptation and generalization to a novel displacement. *Percept. Psychophys., 54*(2), 195-204.

Witmer, B. G., & Singer, M. J. (1998). Measuring Presence in Virtual Environments: A Presence Questionnaire. *Presence: Teleoperators and Virtual Environments, 7*(3), 225-240. doi:10.1162/105474698565686

Wolpert, D. M., Goodbody, S. J., & Husain, M. (1998). Maintaining internal representations: the role of the human superior parietal lobe. *Nat. Neurosci., 1*(6), 529-533. doi:10.1038/2245

Woollacott, M., & Shumway-Cook, A. (2002). Attention and the control of posture and gait: a review of an emerging area of research. *Gait Posture, 16*(1), 1-14. doi:10.1016/s0966-6362(01)00156-4

Wright, W. G. (2014). Using virtual reality to augment perception, enhance sensorimotor adaptation, and change our minds. *Front. Syst. Neurosci., 8*, 56. doi:10.3389/fnsys.2014.00056

Wu, Z., & Huang, N. E. (2009). Ensemble empirical mode decomposition: a noise-assisted data analysis method. *Adv. Adapt. Data Anal., 01*(01), 1-41. doi:10.1142/s1793536909000047

Xu, P., Xiong, X. C., Xue, Q., Tian, Y., Peng, Y., Zhang, R., . . . Yao, D. Z. (2014). Recognizing mild cognitive impairment based on network connectivity analysis of resting EEG with zero reference. *Physiol. Meas., 35*(7), 1279-1298. doi:10.1088/0967-3334/35/7/1279

Yang, J. F., & Winter, D. A. (1984). Electromyographic amplitude normalization methods: improving their sensitivity as diagnostic tools in gait analysis. *Arch. Phys. Med. Rehabil., 65*(9), 517-521.

Yogev, G., Giladi, N., Peretz, C., Springer, S., Simon, E. S., & Hausdorff, J. M. (2005). Dual tasking, gait rhythmicity, and Parkinson's disease: which aspects of gait are attention demanding? *Eur. J. Neurosci., 22*(5), 1248-1256. doi:10.1111/j.1460-9568.2005.04298.x

Youssofzadeh, V., Zanotto, D., Wong-Lin, K., Agrawal, S. K., & Prasad, G. (2016). Directed Functional Connectivity in Fronto-Centroparietal Circuit Correlates With Motor Adaptation in Gait Training. *IEEE Trans. Neural Syst. Rehabil. Eng., 24*(11), 1265-1275. doi:10.1109/TNSRE.2016.2551642

Zavala, B., Tan, H., Ashkan, K., Foltynie, T., Limousin, P., Zrinzo, L., . . . Brown, P. (2016). Human subthalamic nucleus-medial frontal cortex theta phase coherence is involved in conflict and error related cortical monitoring. *Neuroimage, 137*, 178-187. doi:10.1016/j.neuroimage.2016.05.031

Zeni, J. A., Richards, J. G., & Higginson, J. S. (2008). Two simple methods for determining gait events during treadmill and overground walking using kinematic data. *Gait Posture, 27*(4), 710-714. doi:10.1016/j.gaitpost.2007.07.007